

Cover illustration: Top: Seed-based functional connectivity maps with left posterior parietal cortex as seed region in control rats (left), Poly I:C WG offspring (middle) and Poly I:C WL offspring (right) (overlayed on a study-specific anatomical MRI template). Increased functional connectivity in the default mode-like network can be observed in Poly I:C WL offspring compared to controls. Right: Brain inflammation in the lesion, perilesional cortex, ipsilesional hippocampus and thalamus of a Controlled Cortical Impact-injured rat. From top to bottom: a PET image with the TSPO radiotracer [¹⁸F]PBR111 (overlayed on an MR image), an *in vitro* autoradiograph with the TSPO radiotracer [³H]PK11195 and a histological image of a section immunohistochemically stained for CD11b (a marker of microglia). Bottom: EEG signal of an epileptic seizure in a rat in the chronic period following Controlled Cortical Impact-injury.

Printed by: D. Provo NV, Brulens 30 Unit 23, 2275 Gierle

Copyright © 2018 by Stephan Missault. All rights reserved, except published chapters for which copyright lies with the publishers of the corresponding research papers.



Faculty of Medicine and Health Sciences

Medical Sciences

In vivo imaging correlates of long-term behavioural
outcome following different brain insults

In vivo beeldvormingscorrelaten van chronische
gedragsveranderingen na verschillende vormen van
hersenschade

Dissertation for the degree of
doctor in Medical Sciences

at the University of Antwerp to be defended by

Stephan MISSAULT

Supervisors

Prof. Dr. Stefanie Dedeurwaerdere

Prof. Dr. Marleen Verhoye

Antwerp, 2018

Promotors

Prof. Dr. Stefanie Dedeurwaerdere

Laboratory of Experimental Hematology

Vaccine & Infectious Disease Institute (VAXINFECTIO)

Prof. Dr. Marleen Verhoye

Bio-Imaging Lab

Internal jury members

Prof. Dr. Patrick Cras

Neurology

Prof. Dr. Sebastiaan Engelborghs

Reference Center for Biological Markers of Dementia (BIODEM)

Laboratory of Neurochemistry and Behavior

Institute Born-Bunge

External jury members

Prof. Dr. Mathias Hoehn

In-Vivo Nuclear Magnetic Resonance Laboratory, Max Planck

Institute for Metabolism Research, Cologne, Germany

Dr. Nadja Van Camp

Preclinical PET Imaging Platform, Molecular Imaging Research

Center (MIRCen), CEA, Fontenay-aux-Roses, France

<i>Abstract</i>	i
<i>Samenvatting</i>	v
<i>List of abbreviations</i>	ix
Chapter 1. Rationale and objectives	1
Chapter 2. Introduction	11
1. Epilepsy	13
1.1. Definition and epidemiology	13
1.2. Aetiology	14
1.3. ECM and epilepsy	14
1.3.1. Introduction to the ECM	14
1.3.1.1. General properties of the ECM	14
1.3.1.2. Perineuronal nets	15
1.3.1.3. ECM proteases	16
1.3.2. ECM and epilepsy	20
1.4. Need for novel treatment targets, prognostic and predictive biomarkers	23
2. Traumatic brain injury	24
2.1. Definition, aetiology, epidemiology and classification	24
2.2. Pathophysiology of TBI	26
2.2.1. Neuronal damage	26
2.2.2. Altered perfusion	27
2.2.3. Blood-brain barrier disruption	28
2.2.4. Oedema	29
2.2.5. Inflammation	30
2.3. Need for more specific prognostic biomarkers	32
3. Schizophrenia	34
3.1. Definition, epidemiology and course of the disorder	34
3.2. Aetiology	35
3.2.1. Genetic risk factors	35
3.2.2. Environmental risk factors	36
3.2.3. Interplay of genetic and environmental risk factors	37
3.3. Pathophysiology of schizophrenia	38
3.3.1. Abnormalities in neurotransmission	38
3.3.2. Neuroanatomical abnormalities	41
3.3.3. Dysconnectivity	41

3.3.4.	Immune system abnormalities.....	43
3.4.	Need for prognostic and predictive biomarkers	44
4.	References.....	45
Chapter 3. Animal models.....		55
1.	Epilepsy.....	57
2.	Traumatic brain injury	59
2.1.	Weight-drop injury	59
2.2.	Fluid percussion injury	60
2.3.	Controlled Cortical Impact injury	61
3.	Schizophrenia	62
3.1.	Neurodevelopmental models	63
3.1.1.	Gestational MAM	63
3.1.2.	Social isolation rearing	64
3.1.3.	Maternal or prenatal immune activation models.....	64
3.1.4.	Miscellaneous neurodevelopmental models.....	66
3.2.	Two-hit models.....	66
4.	References.....	68
Chapter 4. <i>In vivo</i> imaging and related techniques.....		71
1.	PET and SPECT imaging	73
1.1.	General principle and relative (dis)advantages	73
1.2.	PET	74
1.3.	SPECT	75
2.	<i>In vitro</i> and <i>ex vivo</i> autoradiography	76
2.1.	<i>In vitro</i> autoradiography	76
2.2.	<i>Ex vivo</i> autoradiography.....	78
3.	Radioisotopes employed in this PhD thesis.....	79
3.1.	[¹¹¹ In]MICA-401	79
3.2.	[¹⁸ F]BR351 and [¹⁸ F]BR420	80
3.3.	[¹⁸ F]PBR111	81
4.	MRI	83
4.1.	Diffusion MRI: Diffusion tensor imaging.....	83
4.1.1.	Diffusion MRI.....	83
4.1.2.	Diffusion-weighted imaging	85
4.1.3.	Diffusion tensor imaging	86

4.2.	BOLD contrast-based fMRI: pharmacological MRI and resting-state fMRI	89
4.2.1.	BOLD contrast-based fMRI	89
4.2.2.	Pharmacological MRI	90
4.2.3.	Resting-state fMRI	91
5.	References	93
PART 1. Brain insults during young adulthood		95

Chapter 5. Decreased levels of active uPA and KLK8 assessed by [¹¹¹In]MICA-401 binding correlate with the seizure burden in an animal model of temporal lobe epilepsy

1.	Abstract	99
2.	Introduction	100
3.	Methods	102
3.1.	Study design	102
3.2.	Animals	102
3.3.	Kainic acid-induced <i>status epilepticus</i> (KASE)	103
3.4.	Controlled Cortical Impact (CCI)-induced traumatic brain injury (TBI)	103
3.5.	Video-EEG	104
3.6.	Radiochemistry	105
3.7.	Inhibitory potential of the radiolabelling precursor for serine proteases in rat	105
3.8.	Autoradiography	106
3.9.	Immunohistochemistry	108
3.10.	Assessment of blood-brain barrier (BBB) permeability	109
3.11.	Statistics	110
4.	Results	110
4.1.	High affinity of UAMC-01162 for rat uPA and KLK8	110
4.2.	Decreased specific binding of [¹¹¹ In]MICA-401 in the KASE model	110
4.3.	Specific binding of [¹¹¹ In]MICA-401 is not correlated with neuronal loss	111
4.4.	Specific binding of [¹¹¹ In]MICA-401 correlated with epilepsy phenotype in KASE rats at 12 w post- <i>SE</i>	114

4.5.	Decreased specific binding of [¹¹¹ In]MICA-401 in the CCI-injury model	115
4.6.	<i>In vivo</i> uptake of [¹¹¹ In]MICA-401 after CCI-injury.....	115
5.	Discussion.....	117
5.1.	Decreased [¹¹¹ In]MICA-401 binding after epileptogenic insults	117
5.2.	Hippocampal decrease in [¹¹¹ In]MICA-401 binding is correlated with seizure outcome in a TLE model	119
5.3.	[¹¹¹ In]MICA-401 does not penetrate the intact blood-brain barrier	121
5.4.	Limitations of the study	122
6.	Conclusions.....	122
7.	References.....	125
Chapter 6. Neuroimaging of subacute brain inflammation and microstructural changes predicts long-term functional outcome after experimental traumatic brain injury.....		
		129
1.	Abstract	131
2.	Introduction.....	132
3.	Materials and methods	136
3.1.	Animals	136
3.2.	Study design	136
3.3.	Controlled Cortical Impact-induced Traumatic Brain Injury ..	137
3.4.	PET imaging with [¹⁸ F]PBR111.....	138
3.5.	<i>In vivo</i> MRI: DTI and 3D T ₂ -weighted anatomical MRI	140
3.6.	Long-term outcome.....	142
3.6.1.	Open field test.....	142
3.6.2.	Sucrose preference test	142
3.6.3.	Video-EEG: spontaneous recurrent seizures and seizure susceptibility.....	143
3.6.4.	Morris water maze test.....	145
3.7.	Statistics	146
4.	Results	147
4.1.	Subacute brain inflammation after CCI-injury	147
4.2.	Subacute microstructural alterations after CCI-injury.....	151

4.3.	TSPO binding correlates with DTI parameters in the lesion of CCI-injured rats.....	155
4.4.	Chronic deficits after CCI-injury	157
4.4.1.	Disinhibition	157
4.4.2.	Anhedonia	157
4.4.3.	Spontaneous epileptiform activity and seizures.....	160
4.4.4.	Seizure susceptibility.....	161
4.4.5.	Impaired visuospatial learning.....	163
4.5.	Correlation between subacute TSPO binding and microstructural changes and chronic deficits in CCI-injured rats	163
4.6.	ROC curve analysis	169
4.7.	Stepwise regression analysis.....	172
5.	Discussion.....	177
5.1.	Subacute brain inflammation and microstructural changes after TBI	177
5.2.	Chronic sequelae of TBI.....	178
5.3.	Correlation between subacute brain inflammation and microstructural alterations and chronic TBI sequelae	181
5.4.	Prognostic biomarkers and models.....	184
6.	Conclusion	185
7.	References.....	187
PART 2. Brain insult during foetal development.....		193

Chapter 7. The risk for behavioural deficits is determined by the maternal immune response to prenatal immune challenge in a neurodevelopmental model

1.	Abstract	197
2.	Introduction.....	198
3.	Materials and Methods	200
3.1.	Animals	200
3.2.	Poly I:C dose-response study	201
3.3.	Behavioural study in MIA offspring.....	202
3.4.	Follow-up of MIA induction.....	203
3.5.	Behavioural analysis.....	203
3.5.1.	Prepulse inhibition (PPI).....	203
3.5.2.	Locomotor activity (LMA).....	204

3.5.3.	Sucrose preference test	204
3.6.	Histological analysis in MIA offspring	205
3.7.	Statistical analysis.....	205
4.	Results	207
4.1.	Poly I:C dose-response study	207
4.2.	Behavioural analysis in MIA offspring	211
4.2.1.	Follow-up of MIA induction.....	211
4.2.2.	Prepulse inhibition (PPI).....	212
4.2.3.	Locomotor activity (LMA).....	213
4.2.4.	Sucrose preference	214
4.2.5.	Histological analysis in MIA offspring	216
5.	Discussion.....	216
6.	References.....	225

Chapter 8. Hypersynchronicity in the default mode-like network is correlated with behavioural outcome in a neurodevelopmental model with relevance for schizophrenia..... 231

1.	Abstract	233
2.	Introduction.....	234
3.	Material and methods.....	236
3.1.	Animals	236
3.2.	Study design	237
3.3.	Maternal immune activation (MIA) and response.....	238
3.4.	Magnetic resonance imaging (MRI)	239
3.4.1.	Acquisition	239
3.4.2.	Data preprocessing.....	242
3.4.3.	Data analysis.....	243
3.5.	Behaviour	245
3.5.1.	Prepulse inhibition of the acoustic startle reflex	245
3.5.2.	Spontaneous locomotor activity	246
3.5.3.	Open field test.....	246
3.5.4.	Sucrose preference test	246
3.5.5.	MK-801 induced locomotor activity.....	246
3.6.	Histology: GluN1.....	247
3.7.	Statistics	248
4.	Results	249

4.1.	Maternal response to MIA	249
4.2.	Increased FC in DMN of adult Poly I:C WL offspring	250
4.3.	No microstructural changes in adult MIA offspring.....	253
4.4.	Attenuated response to NMDAR antagonist in adult MIA offspring	254
4.5.	Subtle behavioural deficits in adult MIA offspring	256
4.6.	No altered GluN1 protein levels in MIA offspring.....	258
4.7.	FC in DMN correlates with behaviour in MIA offspring	258
5.	Discussion.....	260
5.1.	Maternal response to MIA	260
5.2.	Increased FC in DMN of MIA offspring in the absence of microstructural changes.....	261
5.3.	Attenuated response to NMDAR antagonist in MIA offspring, but no change in NMDAR levels.....	262
5.4.	Subtle behavioural deficits in MIA offspring.....	263
5.5.	Hypersynchronicity in the DMN is related to behaviour in MIA offspring	264
6.	Conclusions and future perspectives	265
7.	References.....	268
Chapter 9. Discussion and future perspectives		279
1.	uPA/KLK8 activity correlates with seizure burden in a TLE model	283
2.	MMP-9 following TBI.....	285
3.	TSPO & DTI metrics as prognostic biomarkers for TBI outcome	287
4.	Chronic inflammation after prenatal immune activation	295
5.	Functional connectivity in the DMN correlates with behaviour in the MIA model.....	298
6.	Changes in extracellular proteases in schizophrenia	300
7.	Future perspectives.....	301
8.	References.....	302
<i>Acknowledgments/Dankwoord</i>		311
<i>Curriculum vitae</i>		317

Abstract

A single brain insult can have major, long-lasting consequences on a person's life. The identification of non-invasive *in vivo* imaging prognostic biomarkers that would allow an accurate prognosis of the long-term outcome after a brain insult would be of major value. In addition, such biomarkers may reveal new insights into the underlying neurobiological mechanisms that lead to a poor outcome following a brain insult and may open up new avenues towards novel treatments and preventive strategies. Discovering predictive biomarkers that allow to identify the patients that will benefit from a certain treatment and that allow to follow-up the treatment response would also be of great value.

In this PhD thesis we set out to identify *in vivo* imaging correlates of the long-term behavioural outcome following different brain insults, which could pave the way towards the identification of novel prognostic and predictive biomarkers. First of all, we investigated extracellular matrix proteases as possible biomarkers of epileptogenesis following a brain insult. A single photon emission computed tomography (SPECT) radiotracer with high affinity for active urokinase-type plasminogen activator (uPA) and kallikrein-related peptidase 8 (KLK8) was implemented in an *in vitro* autoradiography study of two different animal models of acquired epilepsy. A decreased activity of the extracellular proteases uPA/KLK8 was observed in relevant brain regions in the subacute phase following both kainic acid-induced *status epilepticus* (SE) and controlled cortical impact (CCI)-induced traumatic brain injury (TBI) during young adulthood. The decrease in uPA/KLK8 activity was even more pronounced and widespread in the chronic phase following SE, when rats had developed spontaneous recurrent epileptic seizures.

Moreover, the hippocampal decrease in uPA/KLK8 activity was correlated with the seizure burden in the animal model of temporal lobe epilepsy. However, *ex vivo* autoradiography with the SPECT probe in the TBI model revealed that the radiotracer was incapable of crossing the intact blood-brain barrier. This thwarted implementation of the SPECT tracer in an *in vivo* imaging study to investigate the potential prognostic value of early decreases in uPA/KLK8 activity regarding long-term outcome following brain injury. Secondly, we investigated the prognostic value of changes in brain inflammation and alterations in brain microstructure during the subacute phase for the long-term outcome following CCI-injury during young adulthood. Neuroinflammation was assessed by positron emission tomography (PET) imaging with a radioligand for translocator protein (TSPO), a marker of brain inflammation. Alterations in brain microstructure were assessed with diffusion tensor imaging (DTI). Subacute changes in brain inflammation and DTI metrics were able to predict different chronic TBI sequelae, including disinhibition, increased seizure susceptibility and impaired visuospatial learning/memory. In addition, we studied the impact of maternal immune activation (MIA), a risk factor for schizophrenia, on the offspring's brain and behaviour. First, we investigated whether there was microglial activation in the brain of adult rats that were exposed to prenatal immune activation (using the viral mimetic Poly I:C). No microglial activation was observed in this study. Interestingly, in adult offspring, behavioural outcome was dependent on the maternal response to the immune challenge. In the final study, we investigated whether adult MIA offspring had alterations in functional connectivity, brain microstructure and NMDA receptor function using respectively resting-state functional magnetic resonance imaging (MRI), DTI and pharmacological MRI with an NMDA

receptor antagonist. Increased functional connectivity was observed in the default mode-like network of adult MIA offspring of dams that lost weight following the immune challenge during pregnancy. No changes in brain microstructure were observed. An altered response to the NMDA receptor antagonist was observed in MIA offspring, indicative of altered NMDA receptor function. This was most pronounced in offspring of dams that gained weight following the immune stimulus. Hence, it seems that MIA offspring exhibited a different pathophysiology dependent on the maternal response to the immune activation. Finally, functional connectivity in the default mode-like network correlated with behaviour in the MIA offspring, as has been observed in schizophrenia patients. Future studies are warranted to investigate whether functional connectivity in the default mode-like network is a predictive biomarker in this neurodevelopmental animal model with relevance for schizophrenia. If so, it could be used in future studies for the identification of novel treatments instead of the behavioural read-out, which is quite variable in this model. It would also be interesting to investigate if hypersynchronicity in the default mode-like network is present early in life following MIA and may be a prognostic biomarker of the long-term behavioural outcome. Taken together, we have identified several relevant imaging correlates of chronic outcome following different brain insults.

Samenvatting

Eén enkel hersenletsel kan ernstige en langdurige gevolgen hebben op een persoons leven. De identificatie van niet-invasieve *in vivo* beeldvorming prognostische biomerkers die een accurate prognose zouden toelaten van de lange termijn effecten van een hersenletsel zou van onschatbare waarde zijn. Bovendien zouden zulke biomerkers nieuwe inzichten kunnen geven in de onderliggende neurobiologische mechanismen die tot een slechte prognose leiden na een hersenletsel en nieuwe wegen kunnen openen naar innovatieve therapieën en preventie strategieën. De ontdekking van predictieve biomerkers die toelaten om de patiënten te identificeren die baat hebben van een bepaalde behandeling en die toelaten om de respons op de behandeling op te volgen zou ook van ontelbare waarde zijn.

In deze doctoraatsthesis hadden we als doel om *in vivo* beeldvormingscorrelaten van de chronische gedragsveranderingen na verschillende soorten hersenschade te identificeren, welke de weg zouden kunnen banen naar nieuwe prognostische en predictieve biomerkers. Allereerst hebben we extracellulaire matrix proteasen onderzocht als mogelijke biomerkers van epileptogenese na een hersenletsel. Een SPECT radiotracer met hoge affiniteit voor actief urokinase-type plasminogen activator (uPA) en kallikrein-gerelateerd peptidase 8 (KLK8) werd geïmplementeerd in een *in vitro* autoradiografie studie van twee verschillende diermodellen van verworven epilepsie. Een verminderde activiteit van de extracellulaire proteasen uPA/KLK8 werd geobserveerd in relevante hersenregio's in de subacute fase na kainaat-geïnduceerde *status epilepticus* (SE) en gecontroleerde corticale impact (CCI)-geïnduceerd hersentrauma tijdens jongvolwassen leven. De vermindering in uPA/KLK8

activiteit was nog sterker uitgesproken en wijdverspreid in de chronische fase na *SE*, wanneer ratten spontane epileptische aanvallen ontwikkeld hadden. Bovendien was de afname in uPA/CLK8 activiteit in hippocampus gecorreleerd met de frequentie van epileptische aanvallen in het diermodel van temporale kwab epilepsie. *Ex vivo* autoradiografie met de SPECT tracer in het hersentrauma model toonde echter aan dat de radiotracer niet in staat was om de intacte bloed-hersenbarrière te passeren. Dit verhinderde implementatie van de SPECT tracer in een *in vivo* beeldvormingsstudie om de potentiële prognostische waarde van vroege afname in uPA/CLK8 activiteit te evalueren met betrekking tot de lange termijn gevolgen na hersenschade. Vervolgens onderzochten we de prognostische waarde van veranderingen in herseninflammatie en veranderingen in de microstructuur van de hersenen tijdens de subacute fase voor de lange termijn gevolgen na CCI-geïnduceerd hersentrauma tijdens jongvolwassen leven. Herseninflammatie werd gemeten met behulp van PET beeldvorming met een radioligand voor TSPO, een merker voor herseninflammatie. Veranderingen in de microstructuur van de hersenen werd gemeten met behulp van diffusie tensor beeldvorming (DTI). Subacute veranderingen in herseninflammatie en DTI metingen waren in staat om verschillende chronische gevolgen van hersentrauma te voorspellen waaronder disinhibitie, verhoogde gevoeligheid om epileptische aanvallen te ontwikkelen, en problemen in leren/geheugen. Hiernaast bestudeerden we ook de impact van maternale immuun activatie (MIA), een risicofactor voor schizofrenie, op de hersenen en het gedrag van de nakomelingen. Allereerst onderzochten we of er microglia activatie was in de hersenen van volwassen ratten die blootgesteld waren geweest aan prenatale immuun activatie (gebruik makende van het viraal mimeticum Poly I:C). In deze studie werd

geen microglia activatie geobserveerd. Een interessante observatie was dat de gedragsveranderingen in volwassen nakomelingen afhankelijk waren van de maternale respons op de immuun stimulus. In de finale studie onderzochten we of volwassen MIA nakomelingen veranderingen hadden in functionele connectiviteit, microstructuur van de hersenen en NMDA receptor functie, gebruik makende van respectievelijk functionele magnetische resonantie beeldvorming (MRI) tijdens rust, DTI en farmacologische MRI met een NMDA receptor antagonist. Verhoogde functionele connectiviteit werd geobserveerd in het “default mode-achtig netwerk” van volwassen MIA nakomelingen van moeders die gewicht verloren na de immuun stimulus tijdens de zwangerschap. Er werden geen veranderingen in microstructuur van de hersenen geobserveerd. Een veranderde respons op de NMDA receptor antagonist werd waargenomen in MIA nakomelingen, wat een veranderde NMDA receptor functie suggereert. Dit was het meest uitgesproken in nakomelingen van moeders die gewicht bijkwamen na de immuun stimulus. Het lijkt erop dat MIA nakomelingen een verschillende pathofysiologie vertoonden afhankelijk van de maternale respons op de immuun activatie. Functionele connectiviteit in het “default mode-achtig netwerk” correleerde met gedrag in de MIA nakomelingen, zoals geobserveerd werd in schizofrenie patiënten. Toekomstige studies zijn nodig om te onderzoeken of functionele connectiviteit in het “default mode-achtig netwerk” een predictieve biomarker is in dit neuro-ontwikkelingsmodel met relevantie voor schizofrenie. Als dit het geval is, zou dit gebruikt kunnen worden in toekomstige studies voor de identificatie van nieuwe therapieën in plaats van het gedrag, welke tamelijk variabel is in dit diermodel. Het zou ook interessant zijn om te onderzoeken of hypersynchroniciteit in het “default

mode-achtig netwerk” al vroeg aanwezig is in het leven na MIA en een prognostische biomerker zou kunnen zijn van de chronische gedragsveranderingen. Samengevat hebben we verschillende relevante beeldvormingscorrelaten geïdentificeerd van de chronische gevolgen na verschillende soorten hersenletsels.

List of abbreviations

AChE	acetylcholine esterase
AD	axial diffusivity
ADAM	a disintegrin and metalloproteinase
ADAMT	a disintegrin and metalloproteinase with thrombospondin motif
ADC	apparent diffusion coefficient
AMPA	α -amino-3-hydroxy-5-methyl-4-isoxazolepropionic acid
AMPH	amphetamine
ARG	autoradiography
ASR	acoustic startle reflex
ATP	adenosine triphosphate
Au1	primary auditory cortex
AUC	area under the curve
BBB	blood-brain barrier
BOLD	blood-oxygen level dependent
BSP1	brain serine protease 1
CA	cornu ammonis
CB	cannabinoid receptor
CBR	central benzodiazepine receptor
CCI	controlled cortical impact
CCL	chemokine (C-C motif) ligand
CD	cluster of differentiation
CEST	chemical exchange saturation transfer
Cg	cingulate cortex
ChABC	chondroitinase ABC

CNS	central nervous system
COX	cyclooxygenase
CSPG	chondroitin sulphate proteoglycan
CT	computed tomography
Ct	threshold cycle
C-terminal	carboxy(l)-terminal
CXCL10	C-X-C motif chemokine 10
DA	dopamine
DAB	3,3'-diaminobenzidine
DAMP	damage-associated molecular pattern
deoxyHb	deoxygenated haemoglobin
DG	dentate gyrus
dH ₂ O	distilled water
DISC1	disrupted-in-schizophrenia 1
DMN	default mode network
DNA	deoxyribonucleic acid
DOTA	tetraazacyclododecane-1,4,7,10-tetraacetic acid
DTI	diffusion tensor imaging
DW	diffusion-weighted
DWI	diffusion-weighted imaging
ECM	extracellular matrix
ED	epileptiform discharge
EEG	electroencephalography
EPI	echo planar imaging
ETL	extrahippocampal temporal lobe
FA	fractional anisotropy
FC	functional connectivity

FDG	fluorodeoxyglucose
fMRI	functional magnetic resonance imaging
FOV	field of view
FPI	fluid percussion injury
FWE	family wise error
FWHM	full width at half maximum
FXa	factor Xa
GABA	γ -aminobutyric acid
GAG	glycosaminoglycan
GD	gestational day
GE	gradient-echo
GFAP	glial fibrillary acidic protein
Glu	glutamate
HNE	hydroxynonenal
HRP	horseradish peroxidase
HVRS	high-voltage rhythmic spike
Iba1	ionized calcium-binding adapter molecule 1
IFN	interferon
Ig	immunoglobulin
IL	interleukin
iNOS	inducible nitric oxide synthase
i.p.	intraperitoneal
IP-10	interferon- γ inducible protein 10
i.v.	intravenous
KA	kainic acid
KASE	kainic acid-induced <i>status epilepticus</i>
KLK	kallikrein-related peptidase

LGI1	Leucine-rich, glioma inactivated 1
LMA	locomotor activity
LPS	lipopolysaccharide
M1	primary motor cortex
MAM	methylazoxymethanol acetate
MAO	monoamine oxidase
MCP-1	monocyte chemotactic protein 1
MD	mean diffusivity
MIA	maternal immune activation
MMP	matrix metalloproteinase
MPFC	medial prefrontal cortex
MR(I)	magnetic resonance (imaging)
MRS	magnetic resonance spectroscopy
mRNA	messenger ribonucleic acid
MWM	Morris water maze
NAA	N-acetyl-aspartate
NDS	normal donkey serum
NeuN	neuronal nuclei
NMDA	N-methyl-D-aspartate
NMDAR	N-methyl-D-aspartate receptor
NRG1	neuregulin-1
NDAID	nonsteroidal anti-inflammatory drug
N-terminal	amino-terminal
OFT	open field test
oxyHb	oxygenated haemoglobin
PAI	plasminogen activator inhibitor
PBR	peripheral benzodiazepine receptor

PBS	phosphate buffered saline
PCC	posterior cingulate cortex
PEG	polyethylene glycol
PET	positron emission tomography
phMRI	pharmacological magnetic resonance imaging
PND	postnatal day
PNN	perineuronal net
PNW	postnatal week
Poly I:C	polyinosinic:polycytidylic acid
PPI	prepulse inhibition
PtA	parietal association cortex
PTE	posttraumatic epilepsy
PtP	posterior parietal cortex
PTZ	pentylentetrazole
qPCR	quantitative polymerase chain reaction
RANTES	regulated on activation, normal T cell expressed and secreted
RARE	Rapid Acquisition with Relaxation Enhancement
RD	radial diffusivity
RF	radiofrequency
RLU	Relative Luminescence Unit
RNA	ribonucleic acid
ROC	receiver operating characteristic
ROI	region of interest
RS	retrosplenial cortex
rsfMRI	resting-state functional magnetic resonance imaging
S1	primary somatosensory cortex

s.c.	subcutaneous
<i>SE</i>	<i>status epilepticus</i>
SE	spin-echo
SEM	standard error of the mean
Serpin	serine protease inhibitor
SPECT	single photon emission tomography
SPT	sucrose preference test
SRPX2	Sushi Repeat-containing Protein, X-linked 2
SRS	spontaneous recurrent seizures
SUV	standardised uptake value
SWD	spike-wave discharge
TBI	traumatic brain injury
TE	echo time
TeA	temporal association cortex
TGF	transforming growth factor
TIMP	tissue inhibitor of metalloproteinases
TLE	temporal lobe epilepsy
TLR	Toll-like receptor
TNF	tumour necrosis factor
TR	repetition time
TSPO	translocator protein
tPA	tissue-type plasminogen activator
uPA	urokinase-type plasminogen activator
uPAR	urokinase-type plasminogen activator receptor
V1	primary visual cortex
vEEG	video-electroencephalography
WG	weight gain

WL

weight loss

1

Rationale and objectives

A single brain insult can have a dramatic, long-lasting impact on a person's life. Injury to the brain (e.g. due to a traumatic brain injury) induces coordinated responses including neurodegeneration, neuroplasticity and inflammation, and can result in various chronic sequelae, such as cognitive and psychiatric deficits and epilepsy. A brain insult early in life (e.g. during prenatal development) can alter the normal development of the brain and also result in various brain and behavioural abnormalities later in life.

Prognostic biomarkers that can predict the precise long-term outcome of brain insults are currently lacking. Such biomarkers would be extremely useful, not only for the prognosis, but also because they may provide insight into the underlying neurobiological mechanisms and put forward novel targets for treatment and possibly prevention of the chronic consequences. Non-invasive *in vivo* imaging brain biomarkers would be ideally suited for such purpose since they can provide a direct assessment of altered brain structure or function and allow longitudinal follow-up of patients. *In vivo* imaging correlates of the symptomatic presentation could also be potential predictive biomarkers, i.e. they might allow to predict which individuals may benefit from a certain treatment. In addition, they might be useful as a non-invasive read-out of therapeutic response.

Brain insults affect all components of the brain: neurons, glia, vasculature and the extracellular matrix. Brain structure and function is altered and different processes are triggered, which can be divided into three main responses: neurodegeneration, neuroplasticity and inflammation. The **main aim** of this PhD thesis was to identify *in vivo* imaging correlates of chronic behavioural outcome following discrete brain insults in experimental animal models. As potential candidates we investigated several molecular targets

including the extracellular matrix proteases urokinase-type plasminogen activator (uPA) and kallikrein-related peptidase 8 (KLK8/neuropsin), translocator protein (TSPO, a marker of brain inflammation) and NMDA receptor function, as well as brain microstructure and functional connectivity in the brain.

The PhD thesis is divided into two parts. In the first part (objectives 1 & 2), the impact of two different brain insults during young adulthood is investigated, i.e. *status epilepticus* (SE) and traumatic brain injury (TBI). In the second part (objectives 3 & 4), we investigated the impact of a brain insult during prenatal development, i.e. maternal immune activation (MIA).

Hypotheses and objectives

Since the extracellular matrix proteases uPA and KLK8 are upregulated by glial cells following brain injury and have been implicated in synaptic plasticity, we hypothesised that they are involved in epileptogenesis and are related to epilepsy outcome following epileptogenic brain insults such as SE and TBI. The **first objective** of this thesis was to evaluate a novel single photon emission computed tomography (SPECT) radiotracer, i.e. [¹¹¹In]MICA-401, which binds with high affinity to active uPA and KLK8, in both normal and injured rat brain (SE, TBI). Additionally, we investigated whether changes in [¹¹¹In]MICA-401 binding correlated with chronic epileptic seizure burden following SE. Due to the incapacity of this radiotracer to cross the intact blood-brain barrier, we decided to shift our focus towards another target.

Previous research from our lab has shown that subacute positron emission tomography (PET) imaging with the TSPO radioligand [¹⁸F]PBR111 in rats

following *SE* can predict the chronic seizure burden and is also related to psychiatric comorbidities of epilepsy. Other studies have shown that subacute alterations in brain microstructure can predict chronic seizure susceptibility and cognitive impairment following fluid percussion injury (an experimental model of mixed focal and diffuse TBI). Based on these observations, we hypothesised that subacute brain inflammation and microstructural alterations can predict various chronic TBI sequelae. The **second objective** of this thesis was to set-up a Controlled Cortical Impact (CCI) injury rat model (an experimental model of focal TBI) in our lab and to evaluate whether subacute TSPO expression and changes in brain microstructure could predict chronic functional deficits in this model, including psychiatric and cognitive abnormalities, seizure susceptibility and posttraumatic epilepsy.

Prenatal immune challenge is an important risk factor for several neuropsychiatric disorders, including schizophrenia. During the past 15 years, maternal immune activation (MIA) models have frequently been used to model schizophrenia. Since schizophrenic patients have been shown to exhibit immunological disturbances, we hypothesised that adult MIA offspring have chronic brain inflammation. The **third objective** of this thesis was to implement a MIA rat model (using the viral mimetic Poly I:C) in our lab and to evaluate whether adult MIA offspring display microglial activation in the brain.

Patients with schizophrenia display aberrant functional connectivity in the brain, especially in the default mode network. Additionally, there is a lot of evidence for NMDA receptor hypofunction in both patients and MIA models. Hence, we hypothesised that there is altered functional connectivity in the

default mode-like network and altered NMDA receptor function in MIA offspring, which correlate with behavioural outcome. The **fourth and final objective** of this PhD dissertation was to evaluate functional and structural brain connectivity, as well as NMDA receptor function, and their relationship to behaviour in adult MIA offspring.

Specific research questions

1. Are alterations in extracellular matrix proteases uPA/KLK8 (assessed by *in vitro* autoradiography with the novel SPECT radiotracer [¹¹¹In]MICA-401) related to chronic seizure burden following *SE*? Can the SPECT probe [¹¹¹In]MICA-401 be implemented for *in vivo* brain imaging?
2. Can subacute neuroinflammation (assessed with the PET TSPO radioligand [¹⁸F]PBR111) and changes in brain microstructure (assessed by diffusion tensor imaging (DTI)) predict long-term outcome following TBI?
3. Does prenatal immune challenge lead to persistent neuroinflammation in adulthood? Is the behavioural outcome and microglial activation in adult MIA offspring dependent on the maternal response to the immune challenge?
4. Does prenatal immune challenge result in altered functional connectivity in the default mode-like network (assessed by resting-state functional magnetic resonance imaging (fMRI)) and altered NMDA receptor function (assessed by pharmacological fMRI with the NMDA receptor antagonist MK-801) during adulthood and are they related to behavioural outcome? Are changes in functional connectivity and NMDA

receptor function in adult offspring depending on the maternal response to the immune challenge?

General outline of the dissertation

Chapter 2 is a general introduction, providing a brief description of the disorders modelled in this thesis (i.e. epilepsy, traumatic brain injury and schizophrenia). Epidemiology, aetiology and the need for biomarkers for these three disorders is described. The role of extracellular matrix in epilepsy and general pathophysiology of traumatic brain injury and schizophrenia are presented.

Chapter 3 provides an overview of rodent models of epilepsy, traumatic brain injury and schizophrenia.

Chapter 4 describes the principles of the *in vivo* imaging and related techniques used in this thesis (PET and SPECT, *in vitro* and *ex vivo* autoradiography, diffusion tensor imaging, pharmacological MRI and resting-state fMRI) and their relative advantages and limitations.

PART 1

Chapter 5 is an evaluation of the novel SPECT radioligand [¹¹¹In]MICA-401 and its capacity to assess alterations in extracellular matrix proteases uPA and KLK8 in the brain following epileptogenic insults (*SE* and *TBI*) using *in vitro* autoradiography. We investigated whether changes in [¹¹¹In]MICA-401 binding correlated with chronic seizure burden following *SE* and if [¹¹¹In]MICA-401 can be used for *in vivo* neuroimaging purposes. This chapter was published as “Missault S, Peeters L et al.: Decreased levels of active uPA and KLK8 assessed by [¹¹¹In]MICA-401 binding correlate with the seizure

burden in an animal model of temporal lobe epilepsy. *Epilepsia*. 2017 Sep;58(9):1615-1625.”

Chapter 6 is a thorough investigation of the potential of subacute *in vivo* imaging of TSPO (PET) and brain microstructure (DTI) to predict long-term functional outcome (behavioural and EEG deficits) following CCI injury. This chapter has been submitted to *Journal of Neurotrauma* as “Missault S, Anckaerts C et al.: Neuroimaging of subacute brain inflammation and microstructural changes predicts long-term functional outcome after experimental traumatic brain injury.”

PART 2

Chapter 7 is a general description of the MIA model as implemented in our lab and investigates the hypothesis that chronic microglial activation is present in adult MIA offspring. In addition, we investigated whether MIA offspring displayed differential behavioural deficits depending on the maternal weight response to the immune challenge (weight gain vs. loss), as was previously reported by one research group, and whether maternal weight response was associated with a differential immune response. This chapter was published as “Missault S, Van den Eynde K et al.: The risk for behavioural deficits is determined by the maternal immune response to prenatal immune challenge in a neurodevelopmental model. *Brain Behav Immun*. 2014 Nov;42:138-46.”

Chapter 8 is an investigation of functional connectivity, brain microstructure and NMDA receptor function in adult MIA offspring, and their relationship with behavioural outcome. Based on the previous work outlined in chapter 7, we hypothesised that MIA offspring exhibit a differential pathophysiology

depending on the maternal response to the immune challenge. This chapter will be submitted as “Missault S, Anckaerts C et al.: Increased functional connectivity in the default mode-like network is related to behavioural outcome in a neurodevelopmental model with relevance for schizophrenia.”

Chapter 9 is a general discussion of the obtained results and observations in relation to the literature. Finally, future perspectives are discussed.

2

Introduction

A single brain insult can have a devastating, long-lasting impact on a person's brain and behaviour. Brain insults such as traumatic brain injury can give rise to several deficits, including cognitive and psychiatric abnormalities and epilepsy. In addition, brain insults during early life can disrupt normal development of the brain and increase the risk for several neurodevelopmental disorders such as autism and schizophrenia. In this PhD thesis, several different brain insults in experimental animal models were used to model epilepsy, traumatic brain injury, and schizophrenia. This general introduction contains a brief description of epilepsy, traumatic brain injury and schizophrenia (including epidemiology and aetiology), the role of the extracellular matrix in epilepsy, general pathophysiology of traumatic brain injury and schizophrenia, as well as the need for biomarkers for these disorders.

1. Epilepsy

1.1. Definition and epidemiology

The word epilepsy is derived from the ancient Greek ἐπιλαμβάνειν, meaning “to seize upon”, “to attack”. Epilepsy is defined as a disorder characterised by an enduring predisposition of the brain to generate epileptic seizures. A patient is considered epileptic if 1) at least two unprovoked seizures occurred more than 24 h apart, 2) one unprovoked seizure occurred and the probability of further seizures is estimated to be similar to the general recurrence risk after two unprovoked seizures, occurring over the next ten years, or 3) an epilepsy syndrome is diagnosed (1). In addition, epilepsy is associated with several cognitive, psychological and social consequences (2).

Approximately 50 million people worldwide are currently living with epilepsy, making it one of the most common neurological disorders. The global annual incidence of epilepsy is estimated to be 2.4 million people (WHO, 2017). Incidence is high in early childhood (especially in neonates), stabilises after adolescence, is lowest during adulthood and increases again in older age groups (3).

1.2. Aetiology

Epilepsies fall within six different categories, based on the underlying cause. These are 1) genetic, 2) structural, 3) metabolic, 4) infectious, 5) immune and 6) unknown cause. In genetic epilepsy, the epilepsy is the direct result of a genetic defect. In structural epilepsy, there is a distinct other structural condition or disease present that has been associated with an increased risk for epilepsy, such as head trauma, stroke and brain tumour (4). In metabolic epilepsy, a metabolic disorder is present that is associated with epilepsy. In infectious and immune epilepsies, the epilepsy is the result of respectively an infection or immune disorder (5). Often, the cause is unknown (WHO, 2017).

1.3. ECM and epilepsy

1.3.1. Introduction to the ECM

1.3.1.1. General properties of the ECM

The extracellular matrix (ECM) in the brain is composed of molecules secreted by neurons and glia, which form stable aggregates in the extracellular space. The ECM fulfils many functions in the brain, both during neurodevelopment and in the adult brain. The quantity and composition of

the ECM change significantly during development. The final and most striking change, i.e. the formation of perineuronal nets, coincides with the end of the critical period, a time of enhanced plasticity in which the brain is especially sensitive to environmental stimuli (6). In the mature brain, the ECM has a slow turnover and mainly restricts structural plasticity, while still supporting many physiological processes (7). While most studies indicate a restricting role for ECM in structural plasticity during adulthood, many ECM components are beneficial for growth and regeneration. A balance between growth promoting and repellent cues may determine the net effect of ECM on structural plasticity (6, 7).

1.3.1.2. Perineuronal nets

With the closure of the critical period, perineuronal nets (PNNs) are formed, a process which is dependent on neuronal activity during a critical developmental period. PNNs are a unique structure in the ECM and are most prominently displayed around parvalbumin-expressing GABAergic interneurons. They surround cell bodies, proximal dendrites and axon initial segments in a mesh-like structure, interdigitating with synaptic contacts and astrocytic processes. While the exact function of PNNs is unknown, they are likely involved in the stabilisation of existing synapses, prevention of new synapses on mature neurons, linkage of the ECM to the cytoskeleton, and facilitation of neuron-astrocyte interactions. Experimental degradation of PNNs and ECM in general using chondroitinase ABC and hyaluronidase has been shown to reinstate plasticity in adult animals, which is usually only seen during the critical period (8) (Fig.2-1).

Degradation of PNNs has been shown in several animal models of epilepsy, which is at least partly due to the increased activity of extracellular matrix

proteases (such as matrix metalloproteinases) following epileptogenic insults (8, 9). Breakdown of the PNNs and the ECM in general allows renewed plasticity, which may contribute to epileptogenesis following brain injury.

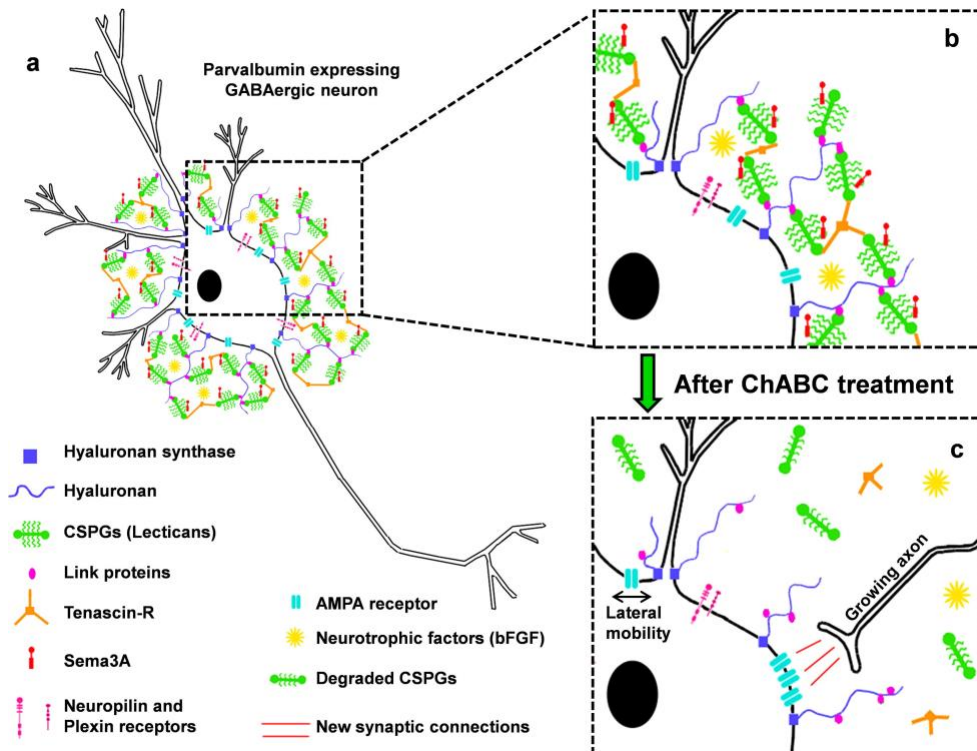


Fig.2-1. Restriction of structural plasticity by perineuronal nets (PNNs). **a.** PNNs enwrap cell bodies, proximal dendrites and axon initial segments of parvalbumin-expressing GABAergic interneurons in a mesh-like structure. **b.** Inhibitory components of PNNs act as a barrier against formation of new synapses, contribute to synapse stabilisation and trap neurotrophic factors. **c.** Disruption of PNNs can reactivate plasticity. Disruption of PNNs can be achieved experimentally using chondroitinase ABC (ChABC) or may occur due to increased activity of extracellular proteases following brain insults. (Soleman et al., 2013)

1.3.1.3. ECM proteases

Several extracellular proteases (or ECM proteases) are expressed in the central nervous system (Fig.2-2). Most of these are capable of degrading

various ECM components, and thus remodelling the ECM, in addition to other functions. For the purpose of this thesis, three of these proteases will be highlighted, i.e. the serine proteases urokinase-type plasminogen activator (uPA), kallikrein-related peptidase 8 (KLK8, also known as neuropsin), and matrix metalloproteinase-9 (MMP-9). These proteases are very interesting candidates for biomarkers of epileptogenesis. A cDNA profiling study that investigated many gene products, including gene products involved in neuronal plasticity, gliosis, organisation of the cytoskeleton or extracellular matrix, cell adhesion, signal transduction, regulation of cell cycle, and metabolism, revealed that uPA was one of the most highly upregulated gene products in the hippocampus during epileptogenesis following *status epilepticus* in rats (10). KLK8 has been shown to be involved in regulation of the excitation-inhibition balance, which is disturbed in epilepsy (11). Finally, an elegant study by Wilczynski et al. provided very convincing evidence for an important role of MMP-9 in epileptogenesis (12). While other MMPs (e.g. MMP-3) have also been suggested to be implicated in epilepsy, the most compelling evidence has been provided for MMP-9.

Urokinase-type plasminogen activator

uPA is part of the plasminogen activator/plasmin(ogen) system. It is secreted as an inactive zymogen (pro-uPA), which upon activation can convert inactive plasminogen into active plasmin. Hence, a proteolytic cascade is triggered that participates in extracellular matrix degradation and remodelling. Binding of uPA to its membrane-bound receptor uPAR ensures that proteolysis is restricted to the vicinity of the cell membrane. This leads to local amplification of the plasminogen cascade, since uPA-activated

plasmin can in turn activate pro-uPA. Activity of these proteases is tightly regulated by serine protease inhibitors, i.e. serpins, including neuroserpin and Plasminogen Activator Inhibitors PAI-1 and PAI-2. Moreover, uPA can activate several intracellular signalling pathways upon binding to its receptor, which is independent of its protease activity (13). uPA is involved in the regulation of many processes including cell adhesion, neuronal migration, neurite outgrowth, and angiogenesis (14-22).

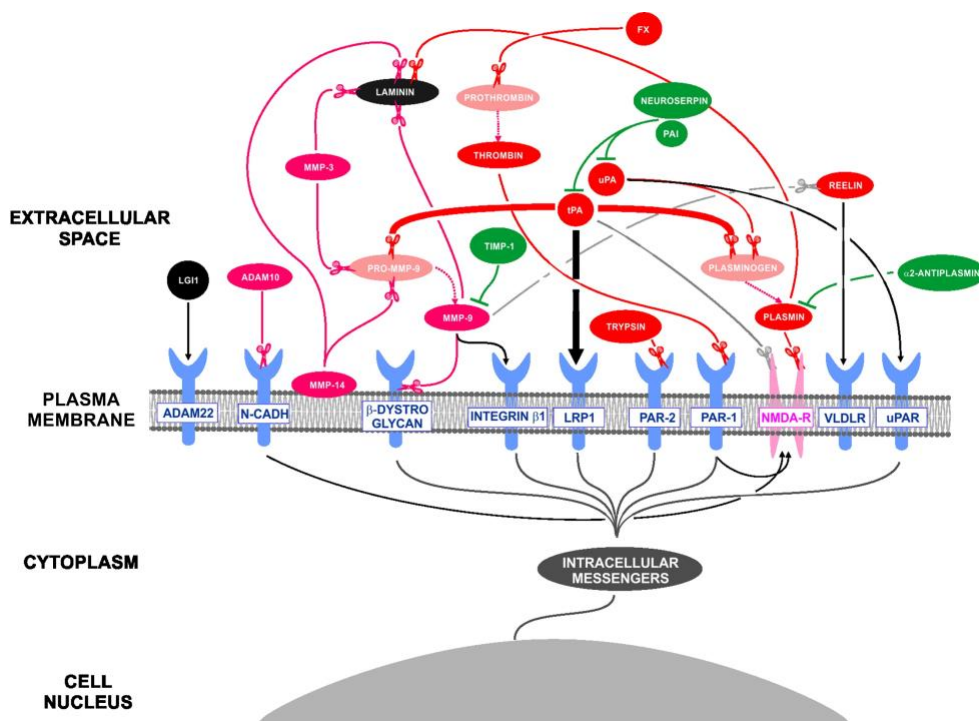


Fig.2-2. Simplified representation of the interaction network of extracellular proteases in the brain. Most of the proteases and receptors on which they act in this diagram have been implicated in brain injury, epileptogenesis and epilepsy. Red: serine proteases, dark pink: MMPs, green: enzyme inhibitors, black: extracellular matrix constituents, blue: receptors; light pink: NMDA receptor, red or dark pink arrows with scissors: proteolytic cleavage, green arrows with a dash: enzyme inhibition, black arrows: direct or indirect interaction other than cleavage or enzyme inhibition, grey arrows: putative or controversial interactions, red dashed arrows: transition from inactive to active state. (Lukasiuk et al., 2011)

Kallikrein-related peptidase 8

KLK8 or neuropsin is a trypsin-like serine protease that can degrade various ECM components and adhesion molecules. It is secreted as a zymogen (proneuropsin) and activation is dependent on neuronal activity in an NMDA receptor-dependent manner (23). It plays an important role in synaptic plasticity, including early-phase long-term potentiation, as well as in neurite outgrowth and fasciculation, and GABAergic neurotransmission (21, 24-32). Recently, it has been shown that neuropsin is involved in the regulation of the excitation-inhibition balance in hippocampus through its modulation of parvalbumin-expressing GABAergic interneuron activity via neuregulin-1 (NRG1) and ErbB4 signalling (11).

Matrix metalloproteinase-9

MMP-9 or gelatinase-B belongs to the family of the matrix metalloproteinases (MMPs), which are zinc- and calcium-dependent endopeptidases. It can degrade various ECM components, as well as cell adhesion molecules, growth factors and cytokines (33, 34). MMP-9 expression and activity is usually tightly regulated. MMP-9 expression is high during early development and decreases over time. While levels in the mature brain are low, MMP-9 activity can be induced in response to synaptic activity (35). MMP-9 is secreted as a zymogen (pro-MMP-9) and can be activated by other MMPs and components of the plasminogen activator/plasmin(ogen) system, depending on neuronal activity. Like other MMPs, MMP-9 is active very locally and transiently. MMP-9 is rapidly inactivated by co-released Tissue Inhibitor of Metalloproteinases 1 (TIMP1) (21). MMP-9 is involved in neurodevelopment and plasticity in the mature brain, playing roles in neurite outgrowth and migration, myelination,

synaptic plasticity, including late-phase long-term potentiation and dendritic spine remodelling and stabilisation, as well as in angiogenesis and neutrophil migration (35-38). Following brain injury, MMP-9 is also involved in blood-brain barrier breakdown and associated with neutrophil infiltration in the brain (39-41).

1.3.2. ECM and epilepsy

Several observations indicate a role of ECM in epilepsy (Fig.2-3).

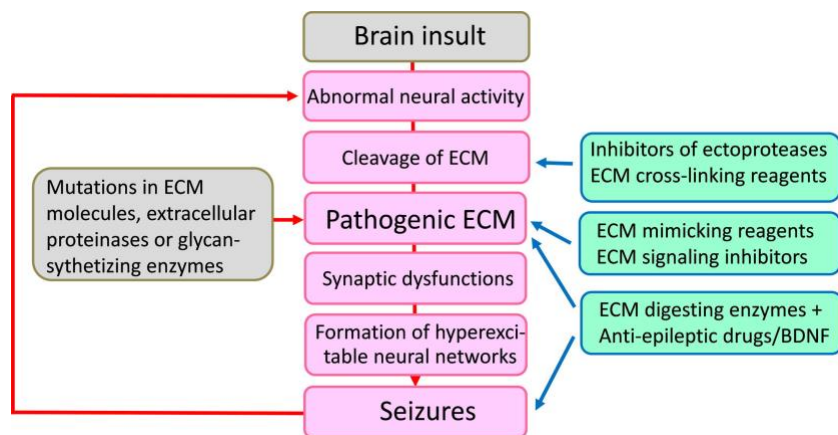


Fig.2-3. The extracellular matrix (ECM)-mediated mechanisms of epileptogenesis. A cascade of molecular and functional alterations (pink) is triggered either by mutations in ECM molecules or by acute brain insults (grey). Several potential ECM-based antiepileptogenic and antiepileptic treatment strategies (green) are envisaged but remain to be verified. (Soleman et al., 2013)

Seizures affect the composition of the ECM, upregulating and downregulating different components of the ECM, including components of PNNs and extracellular proteases (7, 8). Loss of PNNs and the appearance of degraded PNNs following *status epilepticus* (SE) could result in a more permissive environment that allows increased neurite outgrowth and synaptic plasticity, enhancing epileptogenesis. One possible explanation for the disorganisation of PNNs following SE is the loss of PNN support

structures, such as hyaluronan synthases and link proteins as was observed by McRae and colleagues (42). Another possible explanation could be the enzymatic degradation of PNNs by extracellular proteases (reviewed in (8)). Brain injury (including seizure activity) has been shown to increase expression of several extracellular proteases, including family members of the metzincin metalloproteinase superfamily: Matrix MetalloProteinases (MMPs), and A Disintegrin And Metalloproteinase with Thrombospondin motifs (ADAMTs), as well as various members of the plasminogen activator/plasmin(ogen) system (such as tissue-type plasminogen activators tPA). MMPs, zinc-dependent endopeptidases, can digest chondroitin sulphate proteoglycans (CSPGs), the organisational element within the PNNs. ADAMTS4 and ADAMTS5 are also capable of cleaving CSPGs. tPA can both directly and indirectly (through activation of MMPs) degrade CSPGs (8).

An altered expression and activity of uPA has been observed in several animal models of epilepsy (10, 43-46), as well as in human epilepsy (47), and after central nervous system (CNS) injury in general (48-53). Studies of animal models that have a deficiency in *Plau*, the gene encoding uPA, indicate that uPA might be neuroprotective. uPA knockout (uPA^{-/-}) mice exhibited more neurodegeneration and less neurogenesis after kainic acid-induced *status epilepticus* (KASE) compared to wild-type mice (46, 54). Similarly, uPA^{-/-} mice had a larger lesion volume following Controlled Cortical Impact (CCI) injury than their wild-type counterparts, as well as a worse behavioural outcome (55, 56). Investigation of uPA^{-/-} mice has also indicated a role of uPA in plasticity following CNS injury. uPA^{-/-} mice failed to show the structural remodelling of phrenic motor neuron synapses typical of the crossed phrenic phenomenon response following spinal cord injury, a

function dependent on the interaction between uPA and its receptor (57). Moreover, administration of a genetic construct that expresses uPA enhanced peripheral nerve regeneration after both traumatic and ischemic injury in wild-type mice (58). However, very recent studies have observed no difference in seizure susceptibility, epileptogenesis or worsening of epilepsy phenotype after KASE or CCI injury in uPA^{-/-} mice (56, 59). Mice deficient in uPA receptor (uPAR) were shown to have spontaneous seizures, which was attributed to a reduction in hepatocyte growth factor/scatter factor (60). Interestingly, one of the other ligands of the uPAR is Sushi Repeat-containing Protein, X-linked 2 (SRPX2), mutations of which cause epilepsy in humans. Epilepsy phenotype was more severe following *SE* in uPAR knockout mice compared to wild-types (61). There was however no significant difference in posttraumatic epilepsy outcome and chronic seizure susceptibility following Controlled Cortical Impact (CCI)-induced traumatic brain injury (TBI) between uPAR deficient mice and wild-type mice (62).

An altered expression of KLK8 has also been described in several animal models of epilepsy (25, 63-66), as well as after CNS injury in general (65, 67). KLK8 is involved in oligodendrocyte death, demyelination and axonal degeneration after CNS injury (67) and plays a role in epileptogenesis and seizure susceptibility. Inhibition of KLK8 markedly improved the epilepsy phenotype in partially kindled mice, but not fully kindled mice, suggesting a role in epileptogenesis (66). On the other hand, KLK8^{-/-} mice have been shown to exhibit increased hyperexcitability to seizure-evoking stimuli, and to have a disturbed excitation-inhibition balance with decreased GABAergic interneuron activity and increased pyramidal neuron activity following administration of the proconvulsant kainic acid (11, 68). Hence, it is likely

that a precise balance of KLK8 is required to maintain proper excitability (21).

MMP-9 expression and activity have also been shown to be markedly increased following epileptogenic insults (reviewed in (21)). This increase may exceed the physiological demands and possibly contribute to aberrant plasticity underlying epileptogenesis, as is suggested by studies in rats overexpressing MMP-9 (12). MMP-9 knockout mice showed decreased sensitivity to pentylenetetrazole (PTZ) kindling-induced epileptogenesis, while MMP-9 overexpressing rats had an increased susceptibility. In addition, MMP-9 deficiency resulted in diminished seizure-evoked pruning of dendritic spines and decreased aberrant synaptogenesis following mossy fiber sprouting, a form of hippocampal circuitry reorganisation that is thought to be related to epileptogenesis. (12). KLK8 deficient mice (11, 68).

1.4. Need for novel treatment targets, prognostic and predictive biomarkers

In approx. 70% of the cases, epilepsy can be treated with antiepileptic drugs. However, up to 30% of the patients do not respond well to pharmacological treatment (WHO, 2017). Hence, there is an urgent need for identification of novel treatment targets. Moreover, there are currently no preventive treatments, i.e. antiepileptogenic drugs, available to prevent epileptogenesis, i.e. the process by which a normal brain becomes epileptic. In the past 15 years, a lot of evidence has accumulated that points to an important role of extracellular matrix (ECM) remodelling during epileptogenesis and ictogenesis (i.e. the generation of seizures). Furthermore, due to its extracellular location, the ECM provides an attractive target for novel drugs.

A biomarker is defined as an objectively measured characteristic of a normal or pathological biological process. Three main types of biomarkers exist, i.e. diagnostic, prognostic, and predictive biomarkers. Diagnostic biomarkers can help in making a diagnosis of a disease. Prognostic biomarkers can help in predicting the prognosis of a patient, regardless of treatment. Predictive biomarkers can aid in identifying patients that will benefit from a certain treatment.

Prognostic biomarkers would be of extreme value in acquired epilepsy to identify the patients that will develop epilepsy following epileptogenic insults (such as traumatic brain injury). The identification of such biomarkers may also render insight into the underlying neurobiological mechanisms of epileptogenesis, providing new avenues for novel therapies that can delay or even prevent epileptogenesis. Finally, prognostic biomarkers can be used to enrich the trial population in clinical trials with patients with poor prognosis to evaluate novel drugs or other treatments, hence increasing the cost effectiveness of such studies. In addition, identification of predictive biomarkers would also be extremely useful in order to identify the patients that would benefit from a certain treatment and for follow-up of treatment response (69).

In this PhD thesis uPA and KLK8 were investigated as potential biomarkers of epilepsy.

2. Traumatic brain injury

2.1. Definition, aetiology, epidemiology and classification

Traumatic brain injury (TBI) (from the ancient Greek word τραυμα, meaning “wound”) can be defined as an injury to the brain, resulting from external

physical forces. There are many possible causes, such as motor vehicle accidents, falls, physical assaults (including firearms and knives), sports-related accidents, explosions, etc. TBI is a major cause of death and disability worldwide, and represents a serious global public health and socioeconomic problem. In 2013 for example, a total of approx. 2.8 million people with TBI were submitted to hospital care in the USA, of which approx. 56,000 people died (CDC, 2017). Lifelong disability is common in TBI survivors. It is estimated that in the USA 5.3 million people are living with a TBI-related disability, while in the European Union the estimate amounts to 7.7 million (70, 71). TBI often leads to cognitive deficits (e.g. attention deficit, inability to form visuospatial associations), psychiatric deficits (e.g. depression in 30-70% of TBI survivors) and impairments in self-regulatory behaviour (e.g. increased impulsivity, impulsive-aggressive behaviour) (72). TBI is often considered to be a 'silent epidemic', given the fact that public awareness of the magnitude of this problem is generally limited (70). The 30-year cumulative incidence of posttraumatic epilepsy has been shown to be respectively 2%, 4% and 17% after mild, moderate and severe TBI (73). Risk factors for posttraumatic epilepsy are brain contusion with subdural haematoma, skull fracture, loss of consciousness or amnesia for more than one day, an age of 65 years or older, as well as long-term increase in blood-brain barrier disruption (73, 74). Posttraumatic epilepsy accounts for approximately 10-20% of structural/metabolic epilepsies and 5% of all epilepsy (75). Mild injury (e.g. a concussion) can be defined as a TBI without skull fracture and a loss of consciousness or post-traumatic amnesia for less than 30 min. Moderate TBIs are characterised by loss of consciousness or post-traumatic amnesia lasting 30 min to 24 h or a skull fracture. Severe injury can be defined as having a brain contusion, intracranial haematoma,

or loss of consciousness or post-traumatic amnesia for more than 24 h (73). TBIs are also frequently subdivided into mild, moderate and severe categories based on the Glasgow Coma Scale score upon admission in the intensive care unit. The Glasgow Coma Scale consists of three components: eye opening, verbal and motor responses. A total score of 13-15 is defined as mild, 9-12 as moderate, and 3-8 as severe TBI. Young children, young adults and older adults (65+) are most likely to sustain a TBI (CDC, 2017).

2.2. Pathophysiology of TBI

Injury due to TBI can be divided into 1) primary injury, which represents the direct mechanical damage occurring at the moment of impact; and 2) secondary injury, which is the result of several pathological processes that are triggered following initial impact (Fig.2-4).

2.2.1. Neuronal damage

Following impact, there is direct tissue damage with excessive release of excitatory neurotransmitters (particularly glutamate), structural injury to neurons (including axons), glia and vasculature (due to shear, tensile and compressive forces), and impaired regulation of cerebral blood flow and metabolism, resulting in ischemia. Due to the impaired delivery of oxygen, cells switch to anaerobic metabolism, which is insufficient to maintain the cellular energy states. ATP depletion follows and failure of ATP-dependent ion pumps occurs. This results in membrane depolarisation along with secondary excessive release of excitatory neurotransmitters. AMPA receptors, NMDA receptors, and voltage-gated Na⁺ and Ca²⁺ channels are activated, resulting in Na⁺ and Ca²⁺ influx, which leads to self-digesting (catabolic) intracellular processes and mitochondrial Ca²⁺ overload, which

induces oxidative stress. Ca^{2+} activates lipid peroxidases, proteases, and phospholipases, which degrade membranes and increase the intracellular concentration of free fatty acids and free radicals. Oxidative stress leads to peroxidation of cellular and vascular structures, protein oxidation, DNA damage, and mitochondrial dysfunction. Additionally, Ca^{2+} -induced activation of caspases, translocases, and endonucleases triggers progressive structural changes of membranes and DNA, which leads to membrane degradation of vascular and cellular structures and ultimately necrosis or programmed cell death (apoptosis) (76, 77). Remaining cell debris is removed by inflammatory processes. Neuronal death due to excessive stimulation by excitatory neurotransmitters is known as excitotoxicity. This process plays an important role in the development of secondary injury following TBI, but also following other brain insults such as *status epilepticus*. Especially apoptotic cell death can explain delayed neuronal injury after brain injury.

2.2.2. Altered perfusion

Apart from neuronal injury, several other events occur following TBI. Cerebral blood flow (including autoregulation and CO_2 reactivity) and metabolism are impaired, resulting in either hypo- or hyperperfusion following TBI (76).

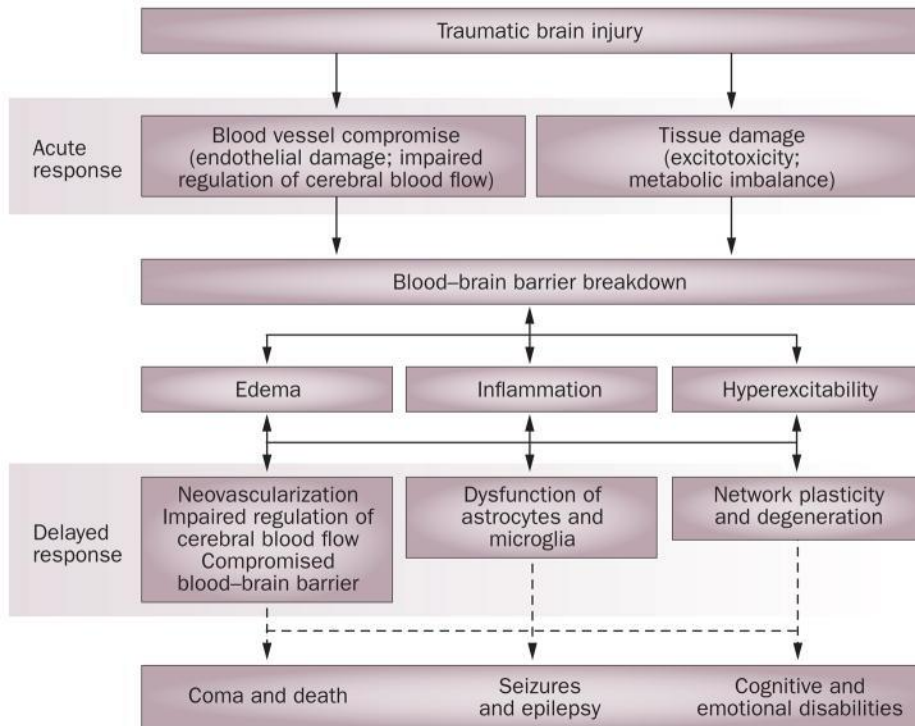


Fig.2-4. Simplified scheme of traumatic brain injury pathophysiology. (Shlosberg et al., 2010)

2.2.3. Blood-brain barrier disruption

Blood-brain barrier (BBB) disruption is another very important process that takes place after TBI and other brain insults such as *status epilepticus*. Impact-induced shearing stresses result in vascular damage, causing leakage of blood-borne proteins, including components of the coagulation cascade, and red blood cells. Extensive intravascular coagulation is set in motion, which reduces blood flow (known as the ‘no-reflow’ phenomenon), increasing the risk of ischemia. Extravasation of certain blood-borne proteins, including serum albumin, fibrinogen, and thrombin, can trigger activation of perivascular glia, especially microglia, and thus neuroinflammation. Activated astrocytes and microglia, as well as infiltrating neutrophils, produce and release multiple factors (including

cytokines such as transforming growth factor- β , tumour necrosis factor- α , interleukin-1 β ; reactive oxygen species; several MMPs such as MMP-9; vascular endothelial growth factor A; and glutamate) that can have a profound effect on BBB function. These factors can increase the paracellular permeability of endothelial cells via destruction or downregulation of tight junction proteins and hence contribute to BBB disruption. Several studies in rat TBI models have shown a biphasic opening of the BBB, with peaks at 4-6 hours and 2-3 days post-injury. The described events are thought to underlie the first peak in BBB permeability. The cause of the second peak is currently unknown (78, 79).

2.2.4. Oedema

Another important process following TBI is the formation of oedema. Several types of oedema can occur, most commonly vasogenic and cytotoxic oedema (80). Structural and functional impairment of the endothelial cell layer of the BBB results in extravasation of fluid and serum proteins, leading to an increase in extracellular/interstitial fluid, i.e. vasogenic oedema. Cytotoxic oedema is characterised by intracellular water accumulation in neurons, astrocytes and microglia, regardless of BBB integrity. Cell swelling is caused by increased cell membrane permeability for ions, ionic pump failure (due to ATP depletion), and uptake of osmotically active solutes. Cerebral oedema leads to an increase in intracranial pressure, which decreases cerebral perfusion pressure, hence promoting ischemia (76, 79, 80).

2.2.5. Inflammation

Brain inflammation is a major part of the pathophysiology of TBI and affects many of the aforementioned processes, including neuronal death, BBB injury, and oedema (Fig.2-5). Both primary and secondary injury trigger through the release of damage-associated molecular patterns (DAMPs) the induction of cellular mediators from brain parenchymal cells (neurons, microglia and astrocytes), including pro-inflammatory cytokines, vasoactive prostaglandins, free radicals, and complement, followed by induction of chemokines (i.e. chemotactic cytokines) and increased expression of cell adhesion molecules on the surface of cerebrovascular endothelium. The brain resident microglia and astrocytes are activated and peripheral immune cells are recruited. Polymorphonuclear leukocytes adhere to defective endothelium or intact endothelium that expresses cell adhesion molecules. The first wave of peripheral immune cells to enter the brain are the neutrophils (within hours after injury), followed by a second wave of monocytes/macrophages and T-cells within days of the TBI. These peripheral immune cells release various signalling factors, which serve to recruit more peripheral immune cells, perpetuate activation of microglia and astrocytes, and damage neurons. The resident microglia and astrocytes become activated (hypertrophy) and increase in number in the injured area in the days following TBI, through migration and/or proliferation. Reactive gliosis results in a glial scar surrounding the damaged area, which is enriched in chondroitin sulphate proteoglycans (CSPGs). This glial scar provides a barrier between damaged and viable nervous tissue, preventing further spread of damage to uninjured parts of the nervous system, as well as restricting plasticity and thus preventing neuronal/axonal regeneration (76,

78, 81). The main neurite growth-inhibitory molecules upregulated in the glial scar are the CSPGs. The inhibitory role of CSPGs has mainly been attributed to the negatively charged side chains, which create a repellent barrier.

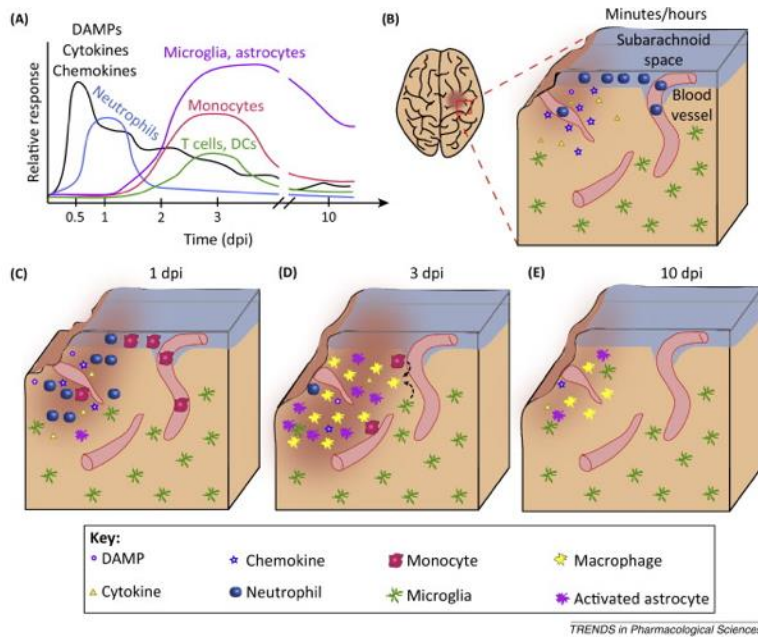


Fig.2-5. The inflammatory response to traumatic brain injury. dpi = days post-injury. (Gyoneva and Ransohoff, 2015)

Inflammation plays a big part in the secondary injury processes and is likely to affect long-term outcome following TBI. Studies in experimental TBI models have for instance shown that inhibition of microglial activation and suppression of the release of proinflammatory cytokines and chemokines can improve cognitive outcome (82-84). While neuroinflammation is meant as a protective response to brain injury, uncontrolled and enduring inflammation is likely to have detrimental effects. As such, inflammation may have both beneficial and deleterious effects on neurons, depending on

the timing and the cell types involved as well as the molecular context in which they act (85, 86).

18 kDa translocator protein (TSPO), previously known as the peripheral benzodiazepine receptor (PBR), is an outer mitochondrial membrane protein, which is upregulated in several cells during brain inflammation, particularly in microglia. Many radioligands that target TSPO have been developed, allowing PET imaging of brain inflammation.

While the glial scar acts as a barrier to prevent neuronal innervation into the damaged area through expression of CSPGs, there are also many ECM components and proteases that can promote plasticity upon brain injury, expressed by both brain parenchymal cells and peripheral immune cells. Remodelling of the ECM following TBI can create a more permissive environment to allow structural plasticity and regeneration, which can be either beneficial or detrimental (as for instance during epileptogenesis). Moreover, bioavailability of neurotrophic factors may increase following ECM modulation.

2.3. Need for more specific prognostic biomarkers

Two large studies were performed to create prognostic models for the outcome after TBI (both published in 2008).

The International Mission for Prognosis and Analysis of Clinical Trials in TBI (IMPACT) study contained 8,509 patients with moderate to severe TBI (Glasgow Coma Scale score of 12 or less). Three models were constructed with increasing complexity. The core model consists of age, motor and pupillary response. This core model can be expanded with computed tomography (CT) characteristics (i.e. diffuse injury, evacuated or non-

evacuated mass lesion) and secondary problems (i.e. hypoxia and hypotension). Finally, addition of laboratory measurements of glucose and haemoglobin renders the most complex model (87). Based on these characteristics, the 6-month outcome in TBI patients can be predicted. The models have value in the classification and characterisation of large cohorts of patients. However, extreme caution is advised when applying the estimated prognosis to individual patients (<http://www.tbi-impact.org/?p=impact/calc>).

The Medical Research Council (MRC) Corticosteroid Randomisation After Significant Head Injury (CRASH) Trial contained data from 10,008 patients with Glasgow Coma Scale of 14 or less. Two models were constructed. The basic model included four predictors: age, Glasgow Coma Scale score, pupillary reactivity, and the presence of major extracranial injury. The CT model also included CT characteristics (i.e. presence of petechial haemorrhages, obliteration of the third ventricle or basal cisterns, subarachnoid bleeding, midline shift or non-evacuated haematoma). These models can be used to predict the mortality at 14 days and the outcome at 6 months following TBI (88) (<http://www.crash2.lshtm.ac.uk/Riskcalculator/>).

A major limitation in the construction of these models was that they only used mortality and unfavourable (dead, vegetative state: unresponsive, and severe disability: able to follow commands, but unable to live independently) versus favourable outcome (moderate disability and good recovery) as possible outcomes, instead of focusing on the prediction of the different sequelae that can develop following TBI. This dichotomisation evidently led to a loss of information and a reduced sensitivity (89).

There is a need for more specific prognostic biomarkers, that 1) are a better reflection of the ongoing neurobiological processes following TBI and 2) provide prognosis for the various different possible TBI-related sequelae, i.e. cognitive, psychiatric and self-regulatory behavioural impairments, as well as posttraumatic epilepsy.

In this PhD thesis subacute brain inflammation (more specifically, TSPO) and changes in brain microstructure were investigated as potential prognostic biomarkers of long-term TBI outcome.

3. Schizophrenia

3.1. Definition, epidemiology and course of the disorder

The word schizophrenia is derived from the ancient Greek *σχίζος* and *φρενη*, respectively meaning “split” and “mind”, referring to the splitting of the psychic functions (90). Schizophrenia is a highly disabling chronic mental disorder, characterised by positive or psychotic symptoms (i.e. functions that are not usually present in healthy people such as delusions, hallucinations), negative symptoms (i.e. lack of functions that are usually present in healthy people: blunted emotion, social withdrawal, inability to experience pleasure or anhedonia), and cognitive symptoms (e.g. impairments in attention, working memory, executive functions).

The prevalence of schizophrenia is approx. 0.3-0.7%. The psychotic symptoms typically emerge between the late teens and mid-30s. The peak age at first psychotic episode is in the early to mid-20s for men and in the late 20s for women. However, impaired cognition is already present during development and precedes the emergence of positive symptoms, taking the form of stable cognitive deficits during adulthood. Most patients remain

chronically ill, with exacerbations and remissions of active symptoms, while others exhibit a course of progressive deterioration. Cognitive symptoms often persist while other symptoms are in remission. The course appears to be favourable in ca. 20% of the patients with a small number of patients showing complete recovery. Negative and cognitive symptoms are more closely related to prognosis than positive symptoms and tend to be more persistent (91).

3.2. Aetiology

Schizophrenia is nowadays thought of as a neurodevelopmental disorder, with several possible genetic and environmental risk factors, which interfere with neurodevelopmental processes during so-called windows of vulnerability.

3.2.1. Genetic risk factors

The concordance rate of schizophrenia for monozygotic twins is approx. 45-60%, while it is only 10-15% for dizygotic twins, indicating a strong genetic component in the aetiology of schizophrenia (92). A spectrum of risk alleles has been associated with an increased risk for schizophrenia, each one contributing only a small fraction to the total population variance (91). Many of the putative susceptibility genes (including disrupted-in-schizophrenia 1 (DISC1), NRG1 and dysbindin) play a role in synaptic plasticity, the development and stabilisation of brain microcircuitry, (NMDAR-mediated) glutamatergic function, dopaminergic function and GABAergic function (93).

3.2.2. Environmental risk factors

A study of concordance rates in monozygotic and dizygotic twins showed that concordance rate of schizophrenia in monozygotic twins who shared a placenta is much higher (60%) than in monozygotic twins that did not share a placenta (11%) (94). This observation is a strong indication that prenatal environment is a strong determinant of the development of schizophrenia. Indeed, many prenatal risk factors have been identified: prenatal infection (reviewed in (95)), malnutrition, exposure to lead, Rhesus incompatibility, and maternal stress. Various prenatal infections have been associated with an increased risk of schizophrenia, i.e. rubella, influenza, *Toxoplasma gondii*, herpes simplex virus type 2, periconceptual genital/reproductive infections, maternal respiratory infections, bacterial infection, pyelonephritis, measles, varicella zoster, and polio. Since many different infections (viral, bacterial, and parasitic) were associated with increased risk of schizophrenia, it was postulated that a common mechanism, i.e. maternal immune activation and induction of cytokines underlies altered foetal brain development and increased vulnerability to schizophrenia (the “cytokine hypothesis”) (96). Given the important roles cytokines fulfil during neurodevelopment (reviewed in (97) and (98)), it is not surprising that a pathological induction of cytokines disturbs brain development. Other prenatal and perinatal risk factors have been associated with a higher risk of schizophrenia, including season of birth (birth during winter/early spring), advanced paternal age and obstetric complications. Finally, there are also several environmental risk factors later in life that increase the risk of developing schizophrenia, including growing up in an urban environment, being part of an ethnic minority, childhood trauma,

cannabis use, severe infections and autoimmune disorders. Environmental risk factors are reviewed in (92). The effect sizes of several prenatal environmental risk factors for schizophrenia are much higher than the effect sizes of susceptibility genes.

3.2.3. Interplay of genetic and environmental risk factors

Finally, there is likely an important interplay between genetic susceptibility and environmental exposures (92). Some environmental exposures may have a greater impact in the presence of susceptibility genes. Some susceptibility genes may only confer increased risk of schizophrenia in the presence of a certain environmental exposure. Some genes may increase the likelihood of becoming exposed to a certain environmental risk factor. Finally, some environmental risk factors may have epigenetic effects and thus influence gene expression. None of the aforementioned risk factors (genetic or environmental) are in themselves sufficient to cause schizophrenia. A combination of multiple risk factors is probably required for the development of schizophrenia.

Several models have been put forward to reconcile the potentially early neurodevelopmental aetiopathogenesis of schizophrenia and its relatively late onset (at least of the positive symptoms). A first model proposes that a fixed brain insult during early life interacts with normal brain maturational events that occur much later in life (99). Appearance of symptoms is linked to normal maturation of brain areas affected by early developmental pathology. A second model considers a deviation of normal neurodevelopmental processes during adolescence (e.g. synaptic pruning), due to abnormal programming or an exogenous factor (e.g. cannabis use), by itself or through interactions with early life events, as the basis for the

development of overt schizophrenia (100). A third model proposes that a combination of genetic and environmental factors disturbs the normal developmental course early in life, which becomes more exacerbated during critical periods, resulting in an altered developmental trajectory that ultimately leads to the expression of schizophrenia (101). Finally, the “two-hit hypothesis”, as it was originally described, postulates that a susceptibility gene (first hit) leads to an abnormal neuronal network, and interacts with second hits (environmental factors), which modulate the gene’s function, to result in schizophrenia (102). An adapted version of this “two-hit hypothesis” interprets the first hit as any risk factor (genetic or environmental) that disrupts early brain development and produces long-term vulnerability to a second hit (so-called priming), which ultimately leads to the expression of schizophrenia symptoms (103).

3.3. Pathophysiology of schizophrenia

3.3.1. Abnormalities in neurotransmission

Several neurotransmitter systems are known to be altered in schizophrenia, including the dopaminergic, glutamatergic, serotonergic, GABAergic and cholinergic systems. For the purpose of this PhD thesis I will focus on the dopamine and glutamate hypotheses of schizophrenia, which are the two major neurotransmitter-based hypotheses that have been postulated to explain the pathophysiology of schizophrenia.

The dopamine hypothesis of schizophrenia postulates that there is 1) hyperdopaminergic function in the mesolimbic pathway (originating in the midbrain and projecting to limbic structures), which explains the positive symptoms, and 2) hypodopaminergic function in the mesocortical pathway

(originating in the midbrain and projecting to frontal cortex), which explains the negative and cognitive symptoms (104). There is evidence that several genetic and environmental risk factors of schizophrenia interact to cause dopaminergic dysfunction (105).

The glutamate or NMDA receptor (NMDAR) hypofunction hypothesis of schizophrenia postulates that deficiency in glutamatergic signalling, especially due to reduced NMDAR functioning on GABAergic interneurons, underlies the positive, negative, and cognitive symptoms of schizophrenia. NMDAR malfunctioning can indirectly cause hyperdopaminergic function in the mesolimbic pathway and hypodopaminergic function in the mesocortical pathway through involvement of the cortical brainstem glutamate projection (projecting from prefrontal cortex to brainstem neurotransmitter centres) (106, 107) (Fig.2-6). Hence, the glutamate and dopamine hypotheses are not mutually exclusive. There is evidence that numerous genetic and environmental risk factors affect the glutamatergic system (108).

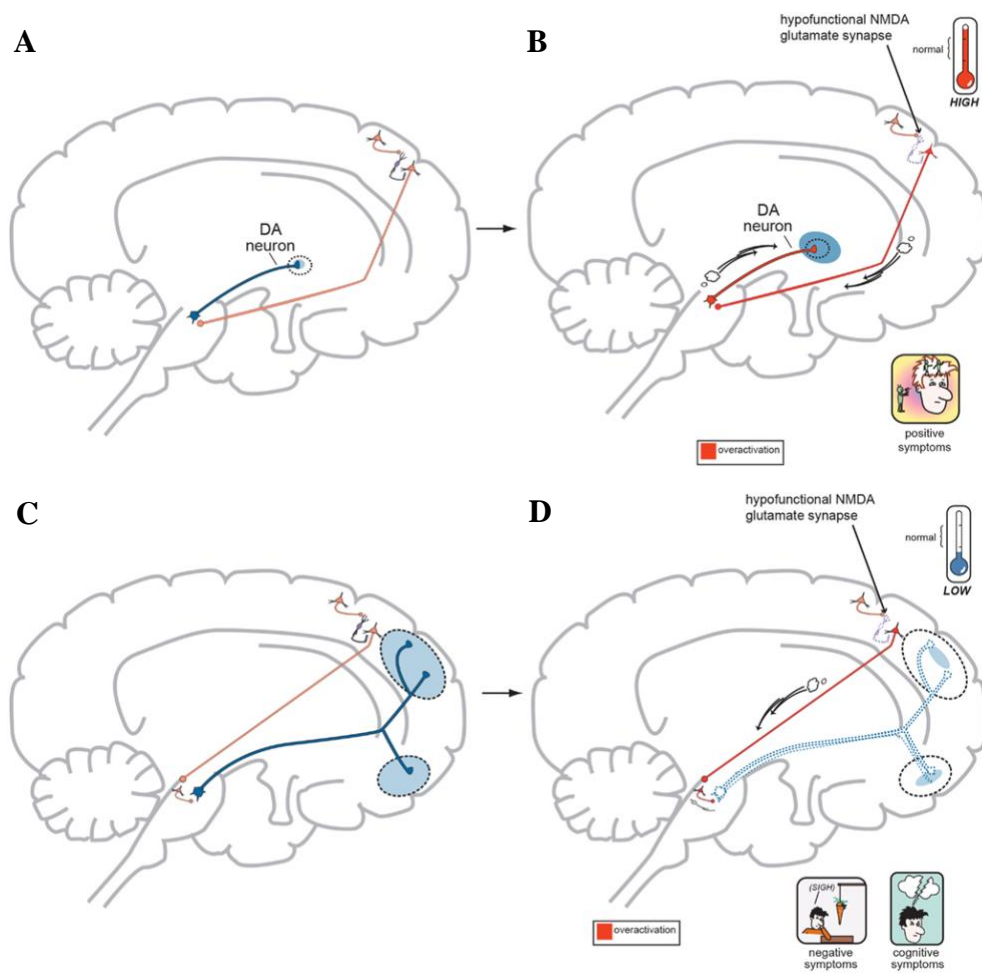


Fig.2-6. The NMDA receptor hypofunction hypothesis can explain positive, negative and cognitive symptoms in schizophrenia patients. A. Normal Glu-GABA-Glu-DA neuronal circuitry. B. Due to hypofunction of the NMDA receptor on the GABAergic interneuron, the glutamatergic projection from cortex to brainstem is overactive (dark red) and leads to hyperdopaminergic function in the mesolimbic pathway, explaining the positive symptoms. C. Normal Glu-GABA-Glu-GABA-DA neuronal circuitry. D. Due to hypofunction of the NMDA receptor on the cortical GABAergic interneuron, the glutamatergic projection from cortex to brainstem is overactive (dark red) and leads to overactivation of the brainstem GABAergic interneuron (dark red), resulting in inhibition of mesocortical dopaminergic neurons and hypofrontality, explaining negative and cognitive symptoms. Glu = glutamatergic neuron, GABA = GABAergic neuron, DA = dopaminergic neuron. (Schwartz et al., 2012)

3.3.2. Neuroanatomical abnormalities

Several neuroanatomical abnormalities have been reported in schizophrenic patients (reviewed in (109)). Enlargement of the lateral ventricles and third ventricle has been observed. Volume decreases were observed in superior temporal gyrus and medial temporal lobe (hippocampus, amygdala, and parahippocampal gyrus). Reductions in frontal lobe volume have also been reported. Most studies of cortical grey matter found that volume reductions were not diffuse, but more pronounced in certain areas. Studies of several subcortical structures (thalamus, corpus callosum, basal ganglia, and cavum septi pellucidi) have also reported abnormalities in their volume. These observations indicate that schizophrenia is not only related to abnormalities in neurotransmitter systems, but also to abnormalities in gross brain structure.

3.3.3. Dysconnectivity

The dysconnection hypothesis of schizophrenia suggests that some schizophrenia symptoms can be best explained by abnormal connectivity between brain regions (110, 111). A large amount of studies has shown abnormal connectivity in schizophrenia patients, both at the structural and functional level (reviewed in (112) and (113)). In general, most studies show a decreased connectivity in schizophrenic patients, which is particularly evident in connections involving the frontal lobe. A possible explanation of decreased connectivity is a deficit in NMDAR-dependent synaptic plasticity, which provides a link between the dysconnection hypothesis and the NMDAR hypofunction hypothesis of schizophrenia.

Many studies of the default mode network (DMN), a brain network that is active during rest and mainly involved in processing information about the self and others, showed an increased functional connectivity within the DMN in schizophrenic patients, as well as abnormal deactivation of the DMN during different tasks, both of which correlated with symptom severity (reviewed in (114) and (115)) (Fig.2-7). On the contrary, structural connectivity was mostly found to be decreased within the DMN in schizophrenia patients (115). DMN hypersynchronicity and hyperactivity could be related to GABAergic and/or dopaminergic dysfunction. Evidence for GABAergic and dopaminergic modulation of the DMN, together with evidence of GABAergic and dopaminergic abnormalities in schizophrenia, suggest a possible role of these two neurotransmitter systems in altered DMN function in schizophrenia. A few studies have shown that the DMN in schizophrenic patients is responsive to antipsychotic drugs, making it a promising predictive biomarker (116-119). Moreover, if these abnormalities in DMN are also present in relevant animal models of schizophrenia, and are found to be responsive to antipsychotics, then they might also be used as a read-out of novel therapeutics in preclinical drug research, which might be more robust than behavioural read-outs in rodents. DMN abnormalities have also been observed in schizophrenia patients with first episode psychosis, suggesting that these abnormalities may already be present in early stages of the disorder. It would be interesting to determine whether DMN hyperconnectivity and hyperactivity are already present early in life before the emergence of symptoms and thus whether it might be a potential prognostic biomarker. This could be tested in a relevant animal model of schizophrenia.

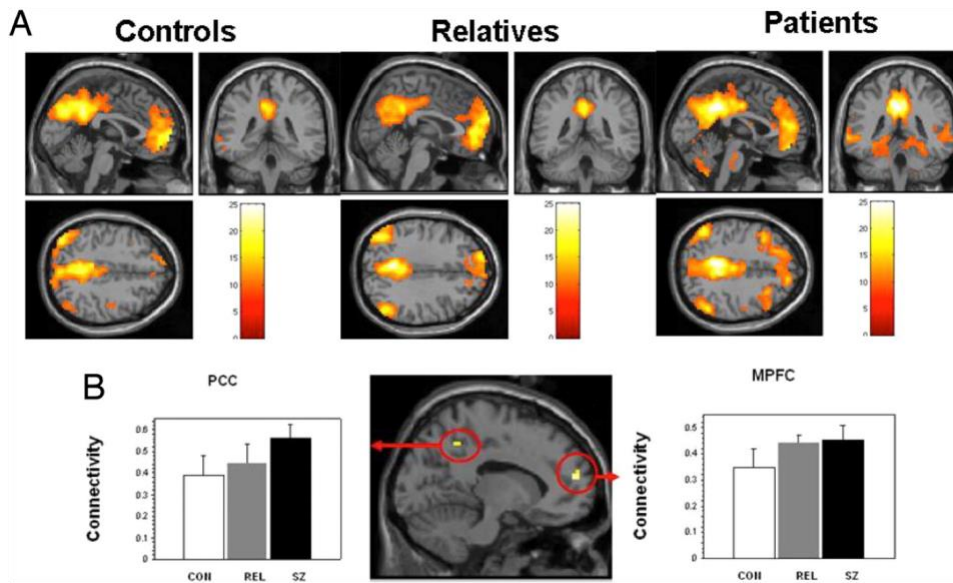


Fig.2-7. Increased functional connectivity during rest in schizophrenia patients and to a lesser degree in first-degree relatives. **A.** Areas showing positive connectivity with default mode network areas (averaged across 4 region of interest seeds, i.e. medial prefrontal cortex (MPFC), posterior cingulate cortex (PCC)/precuneus and bilateral parietal cortices) in controls, first-degree relatives and patients. **B.** Connectivity with default mode network in PCC/precuneus and MPFC. There was significantly more connectivity with PCC/precuneus for patients than for controls and with MPFC for both relatives and patients compared to controls. MPFC and PCC/precuneus seed regions are shown in the middle. (Whitfield-Gabrieli et al., 2009)

3.3.4. Immune system abnormalities

Several immunological/inflammatory disturbances have been reported in schizophrenia (reviewed in (120)). High levels of pro-inflammatory cytokines have been observed in blood and cerebrospinal fluid of schizophrenic patients. Several genetic and environmental risk factors for schizophrenia are related to inflammation and immune functions. Immune alterations influence dopaminergic, serotonergic, and glutamatergic neurotransmission. Altered immune responses in schizophrenia affect the kynurenine pathway, resulting in increased production of kynurenic acid.

Kynurenic acid is an endogenous glutamate receptor antagonist, especially of the NMDAR, thus linking the inflammation hypothesis to the NMDAR hypofunction hypothesis. While some TSPO PET neuroimaging studies have shown increased TSPO expression in schizophrenia patients, other studies have shown no difference or even decreased TSPO expression in schizophrenia patients (reviewed in (121)). Additional support for a role of inflammation in the pathophysiology of schizophrenia comes from the therapeutic benefit of anti-inflammatory medication such as COX-2 inhibitors, and the intrinsic anti-inflammatory and immunomodulatory effects of antipsychotics.

3.4. Need for prognostic and predictive biomarkers

Since the aetiopathogenesis of schizophrenia in many cases is probably to be found in pre- and perinatal life, and the positive and negative symptoms only emerge much later in life, there is a broad window for prevention of these symptoms. The identification of prognostic biomarkers that could be measured early in life (e.g. childhood) and that would identify those at risk for developing schizophrenia would be very useful. Identifying predictive biomarkers that could identify the patients that would benefit from a certain therapy or children that would benefit from novel preventive strategies would also be of extreme value. Moreover, such biomarkers could also be used in relevant animal models of schizophrenia to investigate novel therapies.

In this PhD thesis brain inflammation (more specifically, microglial activation), functional connectivity, brain microstructure and NMDAR function were investigated as potential biomarkers for schizophrenia.

4. References

1. Fisher RS (2015): Redefining epilepsy. *Curr Opin Neurol.* 28:130-135.
2. Fisher RS, van Emde Boas W, Blume W, Elger C, Genton P, Lee P, et al. (2005): Epileptic seizures and epilepsy: definitions proposed by the International League Against Epilepsy (ILAE) and the International Bureau for Epilepsy (IBE). *Epilepsia.* 46:470-472.
3. Banerjee PN, Filippi D, Allen Hauser W (2009): The descriptive epidemiology of epilepsy-a review. *Epilepsy Res.* 85:31-45.
4. Berg AT, Berkovic SF, Brodie MJ, Buchhalter J, Cross JH, van Emde Boas W, et al. (2010): Revised terminology and concepts for organization of seizures and epilepsies: report of the ILAE Commission on Classification and Terminology, 2005-2009. *Epilepsia.* 51:676-685.
5. Scheffer IE, Berkovic S, Capovilla G, Connolly MB, French J, Guilhoto L, et al. (2017): ILAE classification of the epilepsies: Position paper of the ILAE Commission for Classification and Terminology. *Epilepsia.* 58:512-521.
6. Soleman S, Filippov MA, Dityatev A, Fawcett JW (2013): Targeting the neural extracellular matrix in neurological disorders. *Neuroscience.* 253:194-213.
7. Dityatev A (2010): Remodeling of extracellular matrix and epileptogenesis. *Epilepsia.* 51 Suppl 3:61-65.
8. McRae PA, Porter BE (2012): The perineuronal net component of the extracellular matrix in plasticity and epilepsy. *Neurochem Int.* 61:963-972.
9. Rankin-Gee EK, McRae PA, Baranov E, Rogers S, Wandrey L, Porter BE (2015): Perineuronal net degradation in epilepsy. *Epilepsia.* 56:1124-1133.
10. Lukasiuk K, Kontula L, Pitkanen A (2003): cDNA profiling of epileptogenesis in the rat brain. *Eur J Neurosci.* 17:271-279.
11. Kawata M, Morikawa S, Shiosaka S, Tamura H (2017): Ablation of neuropsin-neuregulin 1 signaling imbalances ErbB4 inhibitory networks and disrupts hippocampal gamma oscillation. *Transl Psychiatry.* 7:e1052.
12. Wilczynski GM, Konopacki FA, Wilczek E, Lasiecka Z, Gorlewicz A, Michaluk P, et al. (2008): Important role of matrix metalloproteinase 9 in epileptogenesis. *J Cell Biol.* 180:1021-1035.
13. Smith HW, Marshall CJ (2010): Regulation of cell signalling by uPAR. *Nat Rev Mol Cell Biol.* 11:23-36.
14. Archinti M, Britto M, Eden G, Furlan F, Murphy R, Degryse B (2011): The urokinase receptor in the central nervous system. *CNS Neurol Disord Drug Targets.* 10:271-294.

15. Blasi F, Carmeliet P (2002): uPAR: a versatile signalling orchestrator. *Nat Rev Mol Cell Biol.* 3:932-943.
16. Dent MA, Sumi Y, Morris RJ, Seeley PJ (1993): Urokinase-type plasminogen activator expression by neurons and oligodendrocytes during process outgrowth in developing rat brain. *Eur J Neurosci.* 5:633-647.
17. Krystosek A, Seeds NW (1981): Plasminogen activator release at the neuronal growth cone. *Science.* 213:1532-1534.
18. Menoud PA, Debrot S, Schowing J (1989): Mouse neural crest cells secrete both urokinase-type and tissue-type plasminogen activators in vitro. *Development.* 106:685-690.
19. Pittman RN, Ivins JK, Buettner HM (1989): Neuronal plasminogen activators: cell surface binding sites and involvement in neurite outgrowth. *J Neurosci.* 9:4269-4286.
20. Sumi Y, Dent MA, Owen DE, Seeley PJ, Morris RJ (1992): The expression of tissue and urokinase-type plasminogen activators in neural development suggests different modes of proteolytic involvement in neuronal growth. *Development.* 116:625-637.
21. Lukasiuk K, Wilczynski GM, Kaczmarek L (2011): Extracellular proteases in epilepsy. *Epilepsy Res.* 96:191-206.
22. Montuori N, Ragno P (2014): Role of uPA/uPAR in the modulation of angiogenesis. *Chem Immunol Allergy.* 99:105-122.
23. Shiosaka S, Ishikawa Y (2011): Neuropsin--a possible modulator of synaptic plasticity. *J Chem Neuroanat.* 42:24-29.
24. Attwood BK, Bourgognon JM, Patel S, Mucha M, Schiavon E, Skrzypiec AE, et al. (2011): Neuropsin cleaves EphB2 in the amygdala to control anxiety. *Nature.* 473:372-375.
25. Chen ZL, Yoshida S, Kato K, Momota Y, Suzuki J, Tanaka T, et al. (1995): Expression and activity-dependent changes of a novel limbic-serine protease gene in the hippocampus. *The Journal of neuroscience : the official journal of the Society for Neuroscience.* 15:5088-5097.
26. Ishikawa Y, Tamura H, Shiosaka S (2011): Diversity of neuropsin (KLK8)-dependent synaptic associativity in the hippocampal pyramidal neuron. *J Physiol.* 589:3559-3573.
27. Komai S, Matsuyama T, Matsumoto K, Kato K, Kobayashi M, Imamura K, et al. (2000): Neuropsin regulates an early phase of schaffer-collateral long-term potentiation in the murine hippocampus. *Eur J Neurosci.* 12:1479-1486.
28. Matsumoto-Miyai K, Ninomiya A, Yamasaki H, Tamura H, Nakamura Y, Shiosaka S (2003): NMDA-dependent proteolysis of presynaptic adhesion molecule L1 in the hippocampus by neuropsin. *J Neurosci.* 23:7727-7736.

29. Nakamura Y, Tamura H, Horinouchi K, Shiosaka S (2006): Role of neuropsin in formation and maturation of Schaffer-collateral L1cam-immunoreactive synaptic boutons. *J Cell Sci.* 119:1341-1349.
30. Oka T, Akisada M, Okabe A, Sakurai K, Shiosaka S, Kato K (2002): Extracellular serine protease neuropsin (KLK8) modulates neurite outgrowth and fasciculation of mouse hippocampal neurons in culture. *Neurosci Lett.* 321:141-144.
31. Tamura H, Ishikawa Y, Hino N, Maeda M, Yoshida S, Kaku S, et al. (2006): Neuropsin is essential for early processes of memory acquisition and Schaffer collateral long-term potentiation in adult mouse hippocampus in vivo. *J Physiol.* 570:541-551.
32. Tamura H, Kawata M, Hamaguchi S, Ishikawa Y, Shiosaka S (2012): Processing of neuregulin-1 by neuropsin regulates GABAergic neuron to control neural plasticity of the mouse hippocampus. *J Neurosci.* 32:12657-12672.
33. Ethell IM, Ethell DW (2007): Matrix metalloproteinases in brain development and remodeling: synaptic functions and targets. *J Neurosci Res.* 85:2813-2823.
34. Mizoguchi H, Nakade J, Tachibana M, Ibi D, Someya E, Koike H, et al. (2011): Matrix metalloproteinase-9 contributes to kindled seizure development in pentylenetetrazole-treated mice by converting pro-BDNF to mature BDNF in the hippocampus. *J Neurosci.* 31:12963-12971.
35. Reinhard SM, Razak K, Ethell IM (2015): A delicate balance: role of MMP-9 in brain development and pathophysiology of neurodevelopmental disorders. *Front Cell Neurosci.* 9:280.
36. Keck T, Balcom JHt, Fernandez-del Castillo C, Antoniu BA, Warshaw AL (2002): Matrix metalloproteinase-9 promotes neutrophil migration and alveolar capillary leakage in pancreatitis-associated lung injury in the rat. *Gastroenterology.* 122:188-201.
37. Nagy V, Bozdagi O, Matynia A, Balcerzyk M, Okulski P, Dzwonek J, et al. (2006): Matrix metalloproteinase-9 is required for hippocampal late-phase long-term potentiation and memory. *J Neurosci.* 26:1923-1934.
38. Sang QX (1998): Complex role of matrix metalloproteinases in angiogenesis. *Cell Res.* 8:171-177.
39. Rosell A, Cuadrado E, Ortega-Aznar A, Hernandez-Guillamon M, Lo EH, Montaner J (2008): MMP-9-positive neutrophil infiltration is associated to blood-brain barrier breakdown and basal lamina type IV collagen degradation during hemorrhagic transformation after human ischemic stroke. *Stroke.* 39:1121-1126.

40. Shigemori Y, Katayama Y, Mori T, Maeda T, Kawamata T (2006): Matrix metalloproteinase-9 is associated with blood-brain barrier opening and brain edema formation after cortical contusion in rats. *Acta Neurochir Suppl.* 96:130-133.
41. Justicia C, Panes J, Sole S, Cervera A, Deulofeu R, Chamorro A, et al. (2003): Neutrophil infiltration increases matrix metalloproteinase-9 in the ischemic brain after occlusion/reperfusion of the middle cerebral artery in rats. *J Cereb Blood Flow Metab.* 23:1430-1440.
42. McRae PA, Baranov E, Rogers SL, Porter BE (2012): Persistent decrease in multiple components of the perineuronal net following status epilepticus. *Eur J Neurosci.* 36:3471-3482.
43. Gorter JA, Van Vliet EA, Rauwerda H, Breit T, Stad R, van Schaik L, et al. (2007): Dynamic changes of proteases and protease inhibitors revealed by microarray analysis in CA3 and entorhinal cortex during epileptogenesis in the rat. *Epilepsia.* 48 Suppl 5:53-64.
44. Lahtinen L, Lukasiuk K, Pitkanen A (2006): Increased expression and activity of urokinase-type plasminogen activator during epileptogenesis. *The European journal of neuroscience.* 24:1935-1945.
45. Masos T, Miskin R (1997): mRNAs encoding urokinase-type plasminogen activator and plasminogen activator inhibitor-1 are elevated in the mouse brain following kainate-mediated excitation. *Brain Res Mol Brain Res.* 47:157-169.
46. Cho E, Lee KJ, Seo JW, Byun CJ, Chung SJ, Suh DC, et al. (2012): Neuroprotection by urokinase plasminogen activator in the hippocampus. *Neurobiology of disease.* 46:215-224.
47. Iyer AM, Zurolo E, Boer K, Baayen JC, Giangaspero F, Arcella A, et al. (2010): Tissue plasminogen activator and urokinase plasminogen activator in human epileptogenic pathologies. *Neuroscience.* 167:929-945.
48. Adhami F, Yu D, Yin W, Schloemer A, Burns KA, Liao G, et al. (2008): Deleterious effects of plasminogen activators in neonatal cerebral hypoxia-ischemia. *The American journal of pathology.* 172:1704-1716.
49. Patel TH, Sprague S, Lai Q, Jimenez DF, Barone CM, Ding Y (2008): Blood brain barrier (BBB) dysfunction associated with increased expression of tissue and urokinase plasminogen activators following peripheral thermal injury. *Neuroscience letters.* 444:222-226.
50. Wu F, Catano M, Echeverry R, Torre E, Haile WB, An J, et al. (2014): Urokinase-type plasminogen activator promotes dendritic spine recovery and improves neurological outcome following ischemic stroke. *The Journal of neuroscience : the official journal of the Society for Neuroscience.* 34:14219-14232.

51. Minor KH, Seeds NW (2008): Plasminogen activator induction facilitates recovery of respiratory function following spinal cord injury. *Molecular and cellular neurosciences*. 37:143-152.
52. Adair JC, Baldwin N, Kornfeld M, Rosenberg GA (1999): Radiation-induced blood-brain barrier damage in astrocytoma: relation to elevated gelatinase B and urokinase. *Journal of neuro-oncology*. 44:283-289.
53. Rosenberg GA, Dencoff JE, McGuire PG, Liotta LA, Stetler-Stevenson WG (1994): Injury-induced 92-kilodalton gelatinase and urokinase expression in rat brain. *Laboratory investigation; a journal of technical methods and pathology*. 71:417-422.
54. Lahtinen L, Nnode-Ekane XE, Barinka F, Akamine Y, Esmaeili MH, Rantala J, et al. (2010): Urokinase-type plasminogen activator regulates neurodegeneration and neurogenesis but not vascular changes in the mouse hippocampus after status epilepticus. *Neurobiol Dis*. 37:692-703.
55. Morales D, McIntosh T, Conte V, Fujimoto S, Graham D, Grady MS, et al. (2006): Impaired fibrinolysis and traumatic brain injury in mice. *J Neurotrauma*. 23:976-984.
56. Rantala J, Kempainen S, Nnode-Ekane XE, Lahtinen L, Bolkvadze T, Gurevicius K, et al. (2015): Urokinase-type plasminogen activator deficiency has little effect on seizure susceptibility and acquired epilepsy phenotype but reduces spontaneous exploration in mice. *Epilepsy Behav*. 42:117-128.
57. Seeds N, Mikesell S, Vest R, Bugge T, Schaller K, Minor K (2011): Plasminogen activator promotes recovery following spinal cord injury. *Cellular and molecular neurobiology*. 31:961-967.
58. Karagyaur M, Dyikanov D, Makarevich P, Semina E, Stambolsky D, Plekhanova O, et al. (2015): Non-viral transfer of BDNF and uPA stimulates peripheral nerve regeneration. *Biomedicine & pharmacotherapy = Biomedecine & pharmacotherapie*. 74:63-70.
59. Bolkvadze T, Rantala J, Puhakka N, Andrade P, Pitkanen A (2015): Epileptogenesis after traumatic brain injury in Plau-deficient mice. *Epilepsy Behav*. 51:19-27.
60. Bae MH, Bissonette GB, Mars WM, Michalopoulos GK, Achim CL, Depireux DA, et al. (2010): Hepatocyte growth factor (HGF) modulates GABAergic inhibition and seizure susceptibility. *Exp Neurol*. 221:129-135.
61. Nnode-Ekane XE, Pitkanen A (2013): Urokinase-type plasminogen activator receptor modulates epileptogenesis in mouse model of temporal lobe epilepsy. *Mol Neurobiol*. 47:914-937.
62. Bolkvadze T, Puhakka N, Pitkanen A (2016): Epileptogenesis after traumatic brain injury in Plaur-deficient mice. *Epilepsy Behav*. 60:187-196.

63. He XP, Shiosaka S, Yoshida S (2001): Expression of neuropsin in oligodendrocytes after injury to the CNS. *Neuroscience research*. 39:455-462.
64. Okabe A, Momota Y, Yoshida S, Hirata A, Ito J, Nishino H, et al. (1996): Kindling induces neuropsin mRNA in the mouse brain. *Brain research*. 728:116-120.
65. Tomizawa K, He X, Yamanaka H, Shiosaka S, Yoshida S (1999): Injury induces neuropsin mRNA in the central nervous system. *Brain research*. 824:308-311.
66. Momota Y, Yoshida S, Ito J, Shibata M, Kato K, Sakurai K, et al. (1998): Blockade of neuropsin, a serine protease, ameliorates kindling epilepsy. *The European journal of neuroscience*. 10:760-764.
67. Terayama R, Bando Y, Murakami K, Kato K, Kishibe M, Yoshida S (2007): Neuropsin promotes oligodendrocyte death, demyelination and axonal degeneration after spinal cord injury. *Neuroscience*. 148:175-187.
68. Davies B, Kearns IR, Ure J, Davies CH, Lathe R (2001): Loss of hippocampal serine protease BSP1/neuropsin predisposes to global seizure activity. *J Neurosci*. 21:6993-7000.
69. Engel J, Jr., Pitkanen A, Loeb JA, Dudek FE, Bertram EH, 3rd, Cole AJ, et al. (2013): Epilepsy biomarkers. *Epilepsia*. 54 Suppl 4:61-69.
70. Langlois JA, Sattin RW (2005): Traumatic brain injury in the United States: research and programs of the Centers for Disease Control and Prevention (CDC). *J Head Trauma Rehabil*. 20:187-188.
71. Tagliaferri F, Compagnone C, Korsic M, Servadei F, Kraus J (2006): A systematic review of brain injury epidemiology in Europe. *Acta Neurochir (Wien)*. 148:255-268; discussion 268.
72. Roozenbeek B, Maas AI, Menon DK (2013): Changing patterns in the epidemiology of traumatic brain injury. *Nat Rev Neurol*. 9:231-236.
73. Annegers JF, Hauser WA, Coan SP, Rocca WA (1998): A population-based study of seizures after traumatic brain injuries. *N Engl J Med*. 338:20-24.
74. Tomkins O, Shelef I, Kaizerman I, Eliushin A, Afawi Z, Misk A, et al. (2008): Blood-brain barrier disruption in post-traumatic epilepsy. *J Neurol Neurosurg Psychiatry*. 79:774-777.
75. Pitkanen A, Bolkvadze T (2012): Head Trauma and Epilepsy. In: th, Noebels JL, Avoli M, Rogawski MA, Olsen RW, Delgado-Escueta AV, editors. *Jasper's Basic Mechanisms of the Epilepsies*. Bethesda (MD).
76. Werner C, Engelhard K (2007): Pathophysiology of traumatic brain injury. *Br J Anaesth*. 99:4-9.

77. Prins M, Greco T, Alexander D, Giza CC (2013): The pathophysiology of traumatic brain injury at a glance. *Dis Model Mech.* 6:1307-1315.
78. Chodobski A, Zink BJ, Szmydynger-Chodobska J (2011): Blood-brain barrier pathophysiology in traumatic brain injury. *Transl Stroke Res.* 2:492-516.
79. Price L, Wilson C, Grant G (2016): Blood-Brain Barrier Pathophysiology following Traumatic Brain Injury. In: Laskowitz D, Grant G, editors. *Translational Research in Traumatic Brain Injury.* Boca Raton (FL).
80. Unterberg AW, Stover J, Kress B, Kiening KL (2004): Edema and brain trauma. *Neuroscience.* 129:1021-1029.
81. Gyoneva S, Ransohoff RM (2015): Inflammatory reaction after traumatic brain injury: therapeutic potential of targeting cell-cell communication by chemokines. *Trends Pharmacol Sci.* 36:471-480.
82. James ML, Wang H, Cantillana V, Lei B, Kernagis DN, Dawson HN, et al. (2012): TT-301 inhibits microglial activation and improves outcome after central nervous system injury in adult mice. *Anesthesiology.* 116:1299-1311.
83. Clausen F, Hanell A, Bjork M, Hillered L, Mir AK, Gram H, et al. (2009): Neutralization of interleukin-1beta modifies the inflammatory response and improves histological and cognitive outcome following traumatic brain injury in mice. *Eur J Neurosci.* 30:385-396.
84. Lloyd E, Somera-Molina K, Van Eldik LJ, Watterson DM, Wainwright MS (2008): Suppression of acute proinflammatory cytokine and chemokine upregulation by post-injury administration of a novel small molecule improves long-term neurologic outcome in a mouse model of traumatic brain injury. *J Neuroinflammation.* 5:28.
85. Webster KM, Sun M, Crack P, O'Brien TJ, Shultz SR, Semple BD (2017): Inflammation in epileptogenesis after traumatic brain injury. *J Neuroinflammation.* 14:10.
86. Russo MV, McGavern DB (2016): Inflammatory neuroprotection following traumatic brain injury. *Science.* 353:783-785.
87. Steyerberg EW, Mushkudiani N, Perel P, Butcher I, Lu J, McHugh GS, et al. (2008): Predicting outcome after traumatic brain injury: development and international validation of prognostic scores based on admission characteristics. *PLoS Med.* 5:e165; discussion e165.
88. Collaborators MCT, Perel P, Arango M, Clayton T, Edwards P, Komolafe E, et al. (2008): Predicting outcome after traumatic brain injury: practical prognostic models based on large cohort of international patients. *BMJ.* 336:425-429.

89. Maas AI, Marmarou A, Murray GD, Teasdale SG, Steyerberg EW (2007): Prognosis and clinical trial design in traumatic brain injury: the IMPACT study. *J Neurotrauma*. 24:232-238.
90. Moskowitz A, Heim G (2011): Eugen Bleuler's Dementia praecox or the group of schizophrenias (1911): a centenary appreciation and reconsideration. *Schizophr Bull*. 37:471-479.
91. American Psychiatric Association (2013): *Diagnostic and Statistical Manual of Mental Disorders, Fifth Edition*. Washington, DC.
92. Brown AS (2011): The environment and susceptibility to schizophrenia. *Prog Neurobiol*. 93:23-58.
93. Harrison PJ, Weinberger DR (2005): Schizophrenia genes, gene expression, and neuropathology: on the matter of their convergence. *Mol Psychiatry*. 10:40-68; image 45.
94. Davis JO, Phelps JA, Bracha HS (1995): Prenatal development of monozygotic twins and concordance for schizophrenia. *Schizophr Bull*. 21:357-366.
95. Brown AS, Derkits EJ (2010): Prenatal infection and schizophrenia: a review of epidemiologic and translational studies. *Am J Psychiatry*. 167:261-280.
96. Gilmore JH, Jarskog LF (1997): Exposure to infection and brain development: cytokines in the pathogenesis of schizophrenia. *Schizophr Res*. 24:365-367.
97. Deverman BE, Patterson PH (2009): Cytokines and CNS development. *Neuron*. 64:61-78.
98. Stolp HB (2013): Neuropoietic cytokines in normal brain development and neurodevelopmental disorders. *Mol Cell Neurosci*. 53:63-68.
99. Weinberger DR (1987): Implications of normal brain development for the pathogenesis of schizophrenia. *Arch Gen Psychiatry*. 44:660-669.
100. Feinberg I (1982): Schizophrenia: caused by a fault in programmed synaptic elimination during adolescence? *J Psychiatr Res*. 17:319-334.
101. Lewis DA, Levitt P (2002): Schizophrenia as a disorder of neurodevelopment. *Annu Rev Neurosci*. 25:409-432.
102. Bayer TA, Falkai P, Maier W (1999): Genetic and non-genetic vulnerability factors in schizophrenia: the basis of the "two hit hypothesis". *J Psychiatr Res*. 33:543-548.
103. Maynard TM, Sikich L, Lieberman JA, LaMantia AS (2001): Neural development, cell-cell signaling, and the "two-hit" hypothesis of schizophrenia. *Schizophr Bull*. 27:457-476.

104. Davis KL, Kahn RS, Ko G, Davidson M (1991): Dopamine in schizophrenia: a review and reconceptualization. *Am J Psychiatry*. 148:1474-1486.
105. Howes OD, Kapur S (2009): The dopamine hypothesis of schizophrenia: version III--the final common pathway. *Schizophr Bull*. 35:549-562.
106. Javitt DC (2010): Glutamatergic theories of schizophrenia. *Isr J Psychiatry Relat Sci*. 47:4-16.
107. Schwartz TL, Sachdeva S, Stahl SM (2012): Glutamate neurocircuitry: theoretical underpinnings in schizophrenia. *Front Pharmacol*. 3:195.
108. Snyder MA, Gao WJ (2013): NMDA hypofunction as a convergence point for progression and symptoms of schizophrenia. *Front Cell Neurosci*. 7:31.
109. McCarley RW, Wible CG, Frumin M, Hirayasu Y, Levitt JJ, Fischer IA, et al. (1999): MRI anatomy of schizophrenia. *Biol Psychiatry*. 45:1099-1119.
110. Friston KJ, Frith CD (1995): Schizophrenia: a disconnection syndrome? *Clin Neurosci*. 3:89-97.
111. Stephan KE, Baldeweg T, Friston KJ (2006): Synaptic plasticity and dysconnection in schizophrenia. *Biol Psychiatry*. 59:929-939.
112. Pettersson-Yeo W, Allen P, Benetti S, McGuire P, Mechelli A (2011): Dysconnectivity in schizophrenia: where are we now? *Neurosci Biobehav Rev*. 35:1110-1124.
113. Fornito A, Zalesky A, Pantelis C, Bullmore ET (2012): Schizophrenia, neuroimaging and connectomics. *Neuroimage*. 62:2296-2314.
114. Tregellas JR (2014): Neuroimaging biomarkers for early drug development in schizophrenia. *Biol Psychiatry*. 76:111-119.
115. Hu ML, Zong XF, Mann JJ, Zheng JJ, Liao YH, Li ZC, et al. (2017): A Review of the Functional and Anatomical Default Mode Network in Schizophrenia. *Neurosci Bull*. 33:73-84.
116. Sambataro F, Blasi G, Fazio L, Caforio G, Taurisano P, Romano R, et al. (2010): Treatment with olanzapine is associated with modulation of the default mode network in patients with Schizophrenia. *Neuropsychopharmacology*. 35:904-912.
117. Surguladze SA, Chu EM, Marshall N, Evans A, Anilkumar AP, Timehin C, et al. (2011): Emotion processing in schizophrenia: fMRI study of patients treated with risperidone long-acting injections or conventional depot medication. *J Psychopharmacol*. 25:722-733.
118. Tregellas JR, Tanabe J, Rojas DC, Shatti S, Olincy A, Johnson L, et al. (2011): Effects of an alpha 7-nicotinic agonist on default network activity in schizophrenia. *Biol Psychiatry*. 69:7-11.

119. Wang Y, Tang W, Fan X, Zhang J, Geng D, Jiang K, et al. (2017): Resting-state functional connectivity changes within the default mode network and the salience network after antipsychotic treatment in early-phase schizophrenia. *Neuropsychiatr Dis Treat.* 13:397-406.
120. Muller N, Weidinger E, Leitner B, Schwarz MJ (2015): The role of inflammation in schizophrenia. *Front Neurosci.* 9:372.
121. De Picker LJ, Morrens M, Chance SA, Boche D (2017): Microglia and Brain Plasticity in Acute Psychosis and Schizophrenia Illness Course: A Meta-Review. *Front Psychiatry.* 8:238.

3

Animal models

A good disease model needs to fulfil three main criteria (1, 2). It should have 1) good construct validity, i.e. have a similar aetiology and pathophysiology as the human disease; 2) good face validity, i.e. present with a similar phenotype/phenomenology; and 3) good predictive validity, i.e. have a similar treatment response as patients.

For the purpose of this PhD thesis I will focus on rodent models. While larger animals that are evolutionarily more closely related to humans might have better construct, face and predictive validity than rodents, rodent models are also very good disease models as described below and are more often used due to their low economic cost. While smaller (nonmammalian) animal models also exist (e.g. zebrafish) they have less construct, face and predictive validity than rodent models.

1. Epilepsy

There are several animal models of epilepsy (reviewed in (3)). For the purpose of this thesis we will focus solely on acquired epilepsy.

An initial brain insult (with or without acute seizures) is used to trigger epileptogenesis. After a latent period without any seizures, spontaneous recurrent seizures can occur, i.e. epilepsy. Brain insults that have been used to model different forms of epilepsy are hyperthermic/febrile seizures, neonatal hypoxia, traumatic brain injury, chemoconvulsants, and electrical stimulation.

Traumatic brain injury and posttraumatic epilepsy will be discussed in more detail below.

Electrical stimulation and chemoconvulsants can be used for kindling, i.e. a seizure-induced plasticity phenomenon that occurs when repeated induction of afterdischarges (i.e. neuronal discharges that continue while the stimulus has been stopped) in a specific brain region evokes a progressive enhancement of seizure susceptibility.

Chemoconvulsants and electrical stimulation can also be used to induce a *status epilepticus* to model temporal lobe epilepsy. For these purposes, limbic structures in the temporal lobe are usually targeted, in particular the hippocampus and amygdala. The two most commonly used chemoconvulsants are kainic acid and pilocarpine. Kainic acid activates kainate receptors, one of the three subtypes of ionic glutamate receptors in the brain. Pilocarpine is a muscarinic acetylcholine receptor agonist. They can be administered systemically or intracerebrally and can cause seizures that can build up into a limbic *status epilepticus* (depending on the dosage). Systemically administered kainic acid preferentially destroys hippocampal pyramidal cells.

The kainic acid-induced *status epilepticus* (KASE) model is a good model of temporal lobe epilepsy and has good construct and face validity. KASE rodents develop spontaneous recurrent seizures after a latent period following KASE-induced brain injury and reproduce most of the neuropathological findings (including hippocampal sclerosis), EEG features and behavioural symptoms of temporal lobe epilepsy (4). Not many studies have investigated the effect of antiepileptic drugs during the chronic phase of this model, though several studies have shown good responsiveness to antiepileptic drugs during the acute phase (to abort or attenuate the *status epilepticus*) and some antiepileptogenic effects of different treatments

during the latent period (5). Hence, this model might also have rather good predictive validity.

2. Traumatic brain injury

Various animal models of TBI have been developed (reviewed in (6-9)). Experimental TBI models can be categorised based on the type of injury that they cause: either primarily focal injury (contusion) (including the Controlled Cortical Impact injury model), diffuse injury (including the impact-acceleration weight-drop model of Marmarou) or a combination of both (including the lateral fluid percussion injury model). Furthermore, specialised TBI models have been developed to model specific forms of TBI, including repetitive, mild (concussive) TBI models to model repetitive sports- or military experience-related injuries, penetrating ballistic-like brain injury models to model firearm-related injuries, and blast-induced TBI models.

We will limit ourselves in this section to the three most commonly used models of TBI: weight-drop injury, lateral fluid percussion injury, and Controlled Cortical Impact injury. These three models have been used to study posttraumatic epilepsy (reviewed in (10-12)).

2.1. Weight-drop injury

Weight-drop models make use of weights that are dropped through a guiding apparatus to elicit impact onto the closed skull (closed head injury, with or without a metal plate fixed to the skull), or the exposed dura through a cranial window. The head can either be immobilised or not (the latter is the case in Marmarou's impact-acceleration model of diffuse axonal injury). Depending on the method, a concussion or contusion is created. The severity of brain injury can be easily controlled by adjusting the mass of the

weight and the height from which it is dropped. It is a very simple and inexpensive method of TBI induction and in its most commonly used approach, i.e. impact to the intact skull, a very fast and easy technique with high throughput. Since no craniotomy is then required, preparation of the animal takes very little time, minimising also the exposure to anaesthetics. The weight-drop models replicate many of the neuropathological findings of human TBI, as well as behavioural deficits in the (sub)acute period including neuromotor and cognitive deficits. However, not many studies have been performed in the chronic period of these models. Disadvantages of these models are the relatively high variability in injury severity, the risk of a secondary rebound injury and a risk of skull fractures. Moreover, while increased posttraumatic seizure susceptibility has been reported after weight-drop injury, no posttraumatic epilepsy has been observed. Therefore, this animal model is not suited for studying posttraumatic epilepsy.

2.2. Fluid percussion injury

In the fluid percussion injury models, a craniotomy is performed to expose the dura mater. A plastic syringe adapter is secured into place. The next day, TBI is induced by releasing a pendulum that strikes the piston at one end of a cylindrical reservoir filled with sterile isotonic fluid (saline). A pressure wave is generated and propagated through the medium to the other side of the tube, where the fluid percussion device connects to the previously implanted adapter. Hence, the fluid pressure pulse is transmitted to the surface of the dura, causing deformation of the underlying brain. Injury severity depends on the strength of the fluid pressure pulse, which can be adjusted by releasing the pendulum from a different height. Lateral fluid

percussion injury (over left or right parietal cortex) is the most commonly used TBI model. It produces mixed focal and diffuse brain injury and replicates many of the neuropathological observations of human TBI, as well as many of the behavioural deficits (especially neuromotor and cognitive disturbances), which can persist for up to one year after fluid percussion injury (13). Lateral fluid percussion injury has also been successfully used to model posttraumatic epilepsy in rats and mice. Disadvantages of these models are the limited biomechanical control of the insult (with only pendulum height as an adjustable mechanical parameter), rather high inter-trial variability, long two-stage procedure, and high mortality, probably due to brainstem compression and apnea (respiratory arrest). To improve reproducibility, Kabadi et al. developed a microprocessor-controlled, pneumatically driven instrument, with which the impact pressure and dwell time applied to the piston can be precisely controlled, thus reducing inter-trial variability (14). A rapid lateral fluid percussion injury method was developed to avoid the necessity of implantation of an adapter, resulting in a one-stage procedure that reduces operating time, increases throughput and reduces exposure to anaesthetics (15).

2.3. Controlled Cortical Impact injury

The Controlled Cortical Impact (CCI) injury models, also known as rigid indentation or rigid percussion models also usually require trephination (i.e. opening of the skull by making a burr hole) before TBI induction. Immediately following craniotomy, TBI is induced by impacting the exposed dura with a computer-controlled pneumatically or electromagnetically driven metal rigid impactor at a prespecified velocity, depth and dwell time (i.e. using mechanical energy), resulting in deformation of the underlying

cortex. More recently, several groups have also used CCI directly onto the closed skull to produce milder, more diffuse forms of TBI. In its usual approach (impacting the exposed dura), CCI produces primarily a focal injury, though diffuse axonal injury has also been reported. The great advantage of these models are the precise biomechanical control over injury severity, which can be easily adjusted by changing the different mechanical deformation parameters, and superior reproducibility of lesions. It is a one-stage procedure, hence limiting the exposure to anaesthetics, compared to the traditional fluid percussion injury. There is also no risk of a rebound injury as compared to the gravity-driven devices. An additional advantage is the lack of mortality. These models have good construct and face validity, replicating many of the neuropathological (including neuronal injury, inflammation, altered perfusion, BBB injury, oedema...) and behavioural abnormalities (including neuromotor, cognitive and emotional deficits) seen in human TBI, which can persist up to one year after CCI injury (16). CCI injury has also successfully been used to model posttraumatic epilepsy in mice and rats (17, 18). It is also a valuable tool for the development of novel therapies for TBI.

3. Schizophrenia

Many different animal models with relevance to schizophrenia have been developed (reviewed in (19, 20)). Most of these were designed to test specific mechanistic or etiologic hypotheses. These animal models can be categorised into different groups of models (pharmacological, adult and neonatal lesion, genetic, neurodevelopmental and two-hit models). For the purpose of this dissertation we will focus on neurodevelopmental models.

3.1. Neurodevelopmental models

Several neurodevelopmental animal models have been used to model schizophrenia. These models make either use of drug administration during the perinatal period or manipulations of the environment, based on known environmental risk factors, to alter neurodevelopment. These models replicate several of the core symptoms of schizophrenia and usually show a delayed, postpubertal onset of the symptoms, as is seen in schizophrenia patients.

3.1.1. Gestational MAM

Treatment of pregnant dams with methylazoxymethanol acetate (MAM), an anti-mitotic agent that specifically targets neuroblast proliferation, affects brain development in the foetuses. The most obvious effect is a reduced neuronal cell number in the offspring, which highly depends on the exact timing of gestational MAM treatment. Exposure to MAM on gestational day (GD)15, when cortical neurogenesis is at its peak in rats, results in gross morphological changes, including microcephaly, and decreased volumes of whole brain, cerebrum and hippocampus (21-23). Administration of MAM on GD17, when cortical neurogenesis is much lower, causes a more restricted preferential size reduction in neocortical and limbic structures (including prefrontal cortex, hippocampus and limbic thalamus) and increased neuronal density in several cortical regions (23). MAM on GD17 also results in several schizophrenia-like behavioural abnormalities (including prepulse inhibition deficits, negative and cognitive symptoms), as well as dopaminergic and glutamatergic dysfunction (23-25). The GD17 MAM model has good construct and face validity. However, it remains unknown whether it also has predictive validity.

3.1.2. Social isolation rearing

Post-weaning social isolation rearing (from postnatal day (PND)21 onwards) has been shown to cause altered brain development, as well as several schizophrenia-like behavioural deficits (including hyperactivity, prepulse inhibition deficits, negative and cognitive symptoms) and neurochemical (especially dopaminergic and serotonergic) abnormalities in adulthood (reviewed in (26)). Changes in the glutamatergic system in this model are inconsistent. This model also replicates several of the neurobiological changes seen in schizophrenia patients, and behavioural symptoms could often be reversed with antipsychotics, indicating that this model has good face, construct and predictive validity (reviewed in (19)). A major limitation of this model is the relative fragility of behavioural symptoms, which are very much dependent on housing conditions and handling (26). 24 hour-maternal separation in neonates has also been shown to cause long-lasting abnormalities relevant to schizophrenia.

3.1.3. Maternal or prenatal immune activation models

Many different animal models of prenatal immune activation have been employed to study this risk factor of schizophrenia. The first of these models was established by Fatemi and colleagues in 1998, who used human influenza virus to cause infection in pregnant mice (27). Several studies of this group demonstrated that the offspring had many neuropathological signs, which are implicated in the pathophysiology of schizophrenia. This model also exhibits several behavioural and pharmacological changes in adulthood, which are present in schizophrenia patients. Moreover, behavioural changes could be reversed by antipsychotics (28). However, some aspects of schizophrenia pathology have not been investigated in this

model, including the sensitivity to dopamine agonists. This research group reported in 2003 that maternal immune activation (MIA) by administration of the synthetic double-stranded RNA (and thus viral mimetic) polyinosinic-polycytidylic acid (Poly I:C) also causes a prepulse inhibition deficit in mice offspring, as they observed in offspring from virus-infected mice (28). Similarly, Borrell and colleagues reported in 2002 that MIA with the bacterial endotoxin lipopolysaccharide (LPS) in pregnant rats caused prepulse inhibition impairment in adult offspring, which could be reversed with antipsychotics (29). Zuckerman and colleagues reported in 2003 that MIA with Poly I:C in pregnant rats led to postpubertal emergence of latent inhibition impairment, which could be reinstated with antipsychotics, mesolimbic dopaminergic hyperfunction, and morphological alterations in hippocampus and entorhinal cortex (30). These observations underline that not only maternal infection with a pathogen, but also MIA in the absence of a pathogen can cause long-lasting brain and behavioural abnormalities in offspring, reminiscent of schizophrenia. Moreover, the nature of the immune activating agent seems not to be important, since both viral- and bacterial-like immune activating agents can cause similar deficits. The two best established MIA models make use of Poly I:C and LPS, which bind respectively to Toll-like receptors (TLR) 3 and 4, stimulating the production and release of many pro-inflammatory cytokines. A large body of studies in rats and mice, making use of both Poly I:C and LPS, have provided robust evidence for the emergence of many neuroanatomical, neurochemical (dopaminergic, glutamatergic and GABAergic), pharmacological, behavioural and cognitive deficits in MIA offspring, which are core features of the pathophysiology of schizophrenia. There is also some evidence for altered immune function and inflammation in these models (29). The

specific phenotype is dependent on the precise timing of MIA during the pregnancy. In several studies, behavioural and cognitive symptoms could be reversed by treatment with antipsychotics. Most of the observed behavioural, cognitive and pharmacological deficits only emerged in adulthood and thus seem to rely on peripubertal maturational processes. Taken together, there is a large amount of evidence that shows that MIA models have high construct, face and predictive validity. Finally, some studies have shown that maternal exposure to a single pro-inflammatory cytokine, i.e. IL-6, is sufficient to cause long-lasting structural and functional schizophrenia-like abnormalities in MIA offspring (31, 32).

3.1.4. Miscellaneous neurodevelopmental models

Several other early-life interventions in animals have been shown to cause abnormal brain development and schizophrenia-like abnormalities later in life, including maternal stress, maternal/prenatal protein or vitamin D deprivation, obstetric complications, and perinatal, especially prenatal immune activation (reviewed in (33)).

3.2. Two-hit models

Finally, in recent years, more and more research groups have employed two-hit models to study schizophrenia. This is based on the observation that no single risk factor, either genetic or environmental, can induce schizophrenia. There is probably an extensive interplay needed between risk genes and environmental exposures to induce the full spectrum of schizophrenia pathology. Two-hit models have typically combined a genetic mutation (such as in the genes encoding for DISC1, NRG1, reelin), perinatal or childhood insult (such as perinatal immune activation, neonatal NMDAR

antagonist administration, maternal separation, post-weaning social isolation rearing) and/or a peripubertal insult (peripubertal stress, treatment during adolescence with NMDAR antagonists, cannabinoids or the stress hormone corticosterone).

4. References

1. Willner P (1986): Validation criteria for animal models of human mental disorders: learned helplessness as a paradigm case. *Prog Neuropsychopharmacol Biol Psychiatry*. 10:677-690.
2. O'Connor WT, Smyth A, Gilchrist MD (2011): Animal models of traumatic brain injury: a critical evaluation. *Pharmacol Ther*. 130:106-113.
3. Kandravicius L, Balista PA, Lopes-Aguiar C, Ruggiero RN, Umeoka EH, Garcia-Cairasco N, et al. (2014): Animal models of epilepsy: use and limitations. *Neuropsychiatr Dis Treat*. 10:1693-1705.
4. Levesque M, Avoli M (2013): The kainic acid model of temporal lobe epilepsy. *Neurosci Biobehav Rev*. 37:2887-2899.
5. Leite JP, Garcia-Cairasco N, Cavalheiro EA (2002): New insights from the use of pilocarpine and kainate models. *Epilepsy Res*. 50:93-103.
6. Johnson VE, Meaney DF, Cullen DK, Smith DH (2015): Animal models of traumatic brain injury. *Handb Clin Neurol*. 127:115-128.
7. Morales DM, Marklund N, Lebold D, Thompson HJ, Pitkanen A, Maxwell WL, et al. (2005): Experimental models of traumatic brain injury: do we really need to build a better mousetrap? *Neuroscience*. 136:971-989.
8. Xiong Y, Mahmood A, Chopp M (2013): Animal models of traumatic brain injury. *Nat Rev Neurosci*. 14:128-142.
9. Cernak I (2005): Animal models of head trauma. *NeuroRx*. 2:410-422.
10. Ostergard T, Sweet J, Kusyk D, Herring E, Miller J (2016): Animal models of post-traumatic epilepsy. *J Neurosci Methods*. 272:50-55.
11. Hunt RF, Boychuk JA, Smith BN (2013): Neural circuit mechanisms of post-traumatic epilepsy. *Front Cell Neurosci*. 7:89.
12. Pitkanen A, Bolkvadze T (2012): Head Trauma and Epilepsy. In: th, Noebels JL, Avoli M, Rogawski MA, Olsen RW, Delgado-Escueta AV, editors. *Jasper's Basic Mechanisms of the Epilepsies*. Bethesda (MD).
13. Pierce JE, Smith DH, Trojanowski JQ, McIntosh TK (1998): Enduring cognitive, neurobehavioral and histopathological changes persist for up to one year following severe experimental brain injury in rats. *Neuroscience*. 87:359-369.
14. Kabadi SV, Hilton GD, Stoica BA, Zapple DN, Faden AI (2010): Fluid-percussion-induced traumatic brain injury model in rats. *Nat Protoc*. 5:1552-1563.
15. Hameed MQ, Goodrich GS, Dhamne SC, Amandusson A, Hsieh TH, Mou D, et al. (2014): A rapid lateral fluid percussion injury rodent model of traumatic brain injury and post-traumatic epilepsy. *Neuroreport*. 25:532-536.

16. Dixon CE, Kochanek PM, Yan HQ, Schiding JK, Griffith RG, Baum E, et al. (1999): One-year study of spatial memory performance, brain morphology, and cholinergic markers after moderate controlled cortical impact in rats. *J Neurotrauma*. 16:109-122.
17. Bolkvadze T, Pitkanen A (2012): Development of post-traumatic epilepsy after controlled cortical impact and lateral fluid-percussion-induced brain injury in the mouse. *J Neurotrauma*. 29:789-812.
18. Kelly KM, Miller ER, Lepsveridze E, Kharlamov EA, McHedlishvili Z (2015): Posttraumatic seizures and epilepsy in adult rats after controlled cortical impact. *Epilepsy Res*. 117:104-116.
19. Jones CA, Watson DJ, Fone KC (2011): Animal models of schizophrenia. *Br J Pharmacol*. 164:1162-1194.
20. Marcotte ER, Pearson DM, Srivastava LK (2001): Animal models of schizophrenia: a critical review. *J Psychiatry Neurosci*. 26:395-410.
21. Cattabeni F, Abbracchio MP, Cimino M, Cocchi D, Di Luca M, Mennuni L, et al. (1989): Methylazoxymethanol-induced microencephaly: persistent increase of cortical somatostatin-like immunoreactivity. *Brain Res Dev Brain Res*. 47:156-159.
22. Johnson K, Ryan L, Davis J, Elmore A, Guenther B, Marcus J, et al. (2006): Application of magnetic resonance imaging in developmental neurotoxicity testing: a pilot study. *Neurotoxicology*. 27:846-851.
23. Moore H, Jentsch JD, Ghajarnia M, Geyer MA, Grace AA (2006): A neurobehavioral systems analysis of adult rats exposed to methylazoxymethanol acetate on E17: implications for the neuropathology of schizophrenia. *Biol Psychiatry*. 60:253-264.
24. Flagstad P, Mork A, Glenthøj BY, van Beek J, Michael-Titus AT, Didriksen M (2004): Disruption of neurogenesis on gestational day 17 in the rat causes behavioral changes relevant to positive and negative schizophrenia symptoms and alters amphetamine-induced dopamine release in nucleus accumbens. *Neuropsychopharmacology*. 29:2052-2064.
25. Le Pen G, Gourevitch R, Hazane F, Hoareau C, Jay TM, Krebs MO (2006): Peri-pubertal maturation after developmental disturbance: a model for psychosis onset in the rat. *Neuroscience*. 143:395-405.
26. Fone KC, Porkess MV (2008): Behavioural and neurochemical effects of post-weaning social isolation in rodents-relevance to developmental neuropsychiatric disorders. *Neurosci Biobehav Rev*. 32:1087-1102.
27. Fatemi SH, Sidwell R, Akhter P, Sedgewick J, Thuras P, Bailey K, et al. (1998): Human influenza viral infection in utero increases nNOS expression in hippocampi of neonatal mice. *Synapse*. 29:84-88.

28. Shi L, Fatemi SH, Sidwell RW, Patterson PH (2003): Maternal influenza infection causes marked behavioral and pharmacological changes in the offspring. *J Neurosci.* 23:297-302.
29. Borrell J, Vela JM, Arevalo-Martin A, Molina-Holgado E, Guaza C (2002): Prenatal immune challenge disrupts sensorimotor gating in adult rats. Implications for the etiopathogenesis of schizophrenia. *Neuropsychopharmacology.* 26:204-215.
30. Zuckerman L, Rehavi M, Nachman R, Weiner I (2003): Immune activation during pregnancy in rats leads to a postpubertal emergence of disrupted latent inhibition, dopaminergic hyperfunction, and altered limbic morphology in the offspring: a novel neurodevelopmental model of schizophrenia. *Neuropsychopharmacology.* 28:1778-1789.
31. Samuelsson AM, Jennische E, Hansson HA, Holmang A (2006): Prenatal exposure to interleukin-6 results in inflammatory neurodegeneration in hippocampus with NMDA/GABA(A) dysregulation and impaired spatial learning. *Am J Physiol Regul Integr Comp Physiol.* 290:R1345-1356.
32. Smith SE, Li J, Garbett K, Mirnics K, Patterson PH (2007): Maternal immune activation alters fetal brain development through interleukin-6. *J Neurosci.* 27:10695-10702.
33. Meyer U, Feldon J (2010): Epidemiology-driven neurodevelopmental animal models of schizophrenia. *Prog Neurobiol.* 90:285-326.

4

In vivo imaging and related techniques

In vivo imaging techniques such as PET, SPECT and MRI offer the great advantage of allowing non-invasive investigation of the entire brain. In addition, these techniques enable longitudinal assessment of changes in the brain following e.g. a brain insult. This greatly reduces the number of laboratory animals needed, which is a major advantage from an ethical point of view. Longitudinal follow-up of the same animals also provides more accurate results regarding the evolution of changes in the brain (as compared to a cross-sectional study), which improves the statistical power of a study. Furthermore, early changes in the brain assessed by *in vivo* imaging techniques can be correlated with chronic deficits, making these techniques ideally suited for the exploration of potential prognostic biomarkers.

1. PET and SPECT imaging

1.1. General principle and relative (dis)advantages

Positron emission tomography (PET) and single-photon emission computed tomography (SPECT) are both nuclear medicine imaging techniques, i.e. they make use of radiolabelled (radioisotope-containing) tracers that target a molecule of interest (e.g. a receptor or an enzyme). PET and SPECT imaging both have high sensitivity (pM range, SPECT less sensitive than PET), but moderate spatial resolution (μ PET: 1-2 mm, μ SPECT: 0.25-2 mm). A limitation of PET imaging is the need for a cyclotron (for production of radioisotopes) in close proximity to the imaging facility, due to the short half-lives of most positron emitting radioisotopes. A major advantage of SPECT is that multiple radioprobes can be imaged simultaneously, provided that they emit photons with different gamma-energy. An additional advantage of SPECT is the availability of relatively long-lived radionuclides, which can be

useful to study molecules with relatively slow kinetics. A disadvantage of both techniques is the administration of a radiation dose to the animal.

In both μ PET and μ SPECT imaging the radiotracer is usually administered intravenously (most commonly through the tail vein). For dynamic scanning protocols, the tracer is administered at the start of the scan and data are acquired in multiple short time frames, allowing study of tracer kinetics. In other cases, the tracer can be administered prior to scanning, followed by an optimal uptake period, and static scanning.

1.2. PET

PET radiotracers contain a positron emitting radioisotope, which decays through positron (β^+ , the antiparticle of the electron) emission, such as the commonly used ^{18}F (half-life: 109.8 minutes). After emission of the positron, its energy will dissipate and annihilation with an electron will occur. The mass of the electron and positron (each 511 keV) are converted into electromagnetic energy. Annihilation results in the emission of two photons (γ) with equal energy of 511 keV, which travel in approx. opposite directions. Detection of both photons in coincidence by γ -detectors on the PET ring allow estimation of the location of the radiotracer (Fig.4-1).

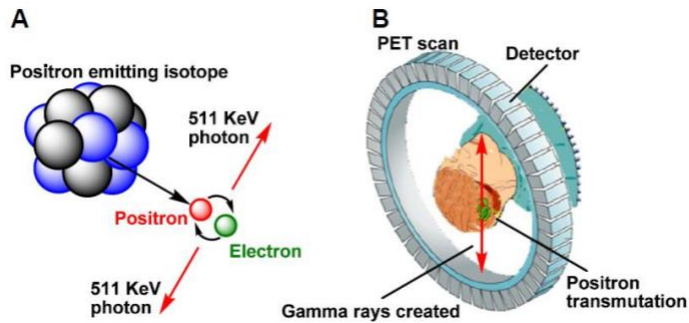


Fig.4-1. Principle of PET. A positron emitting isotope emits a positron, which annihilates with an electron, giving rise to two 511 keV photons, which travel in opposite directions and are detected in coincidence by γ -detectors on the PET ring. (Li and Conti, 2010)

1.3. SPECT

SPECT radiotracers contain a radioisotope that mainly decays through gamma emission, such as the commonly used ^{99m}Tc (half-life: 6 hours), and ^{111}In (half-life: 2.8 days). The single photons emitted by the radioisotope are detected by a gamma detector. Photons only reach the detector if they pass through the holes of a collimator. In this way information is gathered about the origin of the photon and thus the location of the radiotracer. The use of multipinhole collimators in small animal SPECT scanners is necessary to obtain adequate spatial resolution (Fig.4-2). Due to pinhole magnification, the reconstructed spatial resolution exceeds the detector's intrinsic spatial resolution. It is because of this multipinhole collimator that the spatial resolution of μSPECT scanners is better than that of μPET scanners (while the opposite is true for clinical scanners). However, the use of pinholes reduces the sensitivity of this technique due to the small aperture size. A high spatial resolution and detection efficiency are achieved by placing the subject close to the pinholes, which automatically implies a limited field-of-view and thus limits dynamic SPECT scanning.

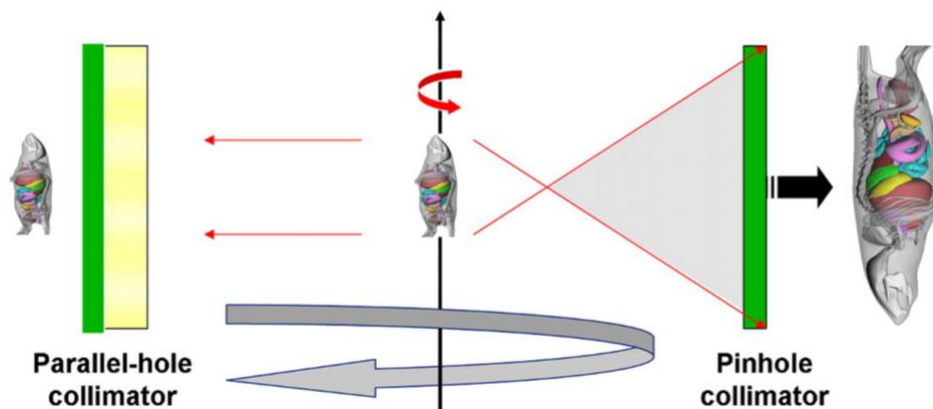


Fig.4-2. Difference between clinical SPECT with a conventional parallel-hole collimator (left) and small animal SPECT with a pinhole collimator (right). Due to pinhole magnification, a greater spatial resolution can be obtained in small animal SPECT scanners than in clinical SPECT scanners. (de Kemp et al., 2010)

2. *In vitro* and *ex vivo* autoradiography

In vitro and *ex vivo* autoradiography are important techniques in the study of radiotracers, especially in the initial evaluation of novel radiotracers.

2.1. *In vitro* autoradiography

In vitro autoradiography assays make use of tissue sections, which are incubated with radiotracer. After incubation, sections are washed to remove unbound radiotracer, dried and exposed to either phosphor imaging plates or films. The radioactive decay of the bound radiotracer causes an image on the phosphor imaging plate or film, which can be made visible by respectively scanning (reading) the phosphor imaging plate in a phosphorimager or developing the film in a dark room. Sections are incubated with radiotracer (“hot ligand”) to determine the total radioligand binding (specific + non-specific binding). Consecutive sections are incubated with radiotracer and an excess amount ($>1,000$ -fold the IC_{50}/K_i) of non-

radiolabelled ligand (“cold ligand”, which can be the same compound without radioisotope or a different probe with the same target) to determine the non-specific binding of the radioligand. The difference between total and non-specific binding gives the specific binding of the radiotracer. Sections are exposed to phosphor imaging plates or films alongside calibrated standards, which can either be commercially available (e.g. a ^{14}C standard) or self-made (e.g. a ^{18}F standard). These standards are used to plot standard curves, which can then be employed to translate grey values in regions of interest to concentrations of radioactivity through interpolation. Phosphor imaging plates need less exposure time to radioisotopes than films in order to obtain an adequate image, but their spatial resolution is lower compared to films. The choice between phosphor imaging plate and film depends on the experimental conditions and needs. Before performing *in vitro* autoradiography experiments on tissue from disease models, it is advisable to perform a saturation binding assay first on control tissue to determine the concentration of radiotracer that is needed to obtain full occupancy of the desired target in the tissue. In such an experiment, consecutive tissue sections are incubated with increasing concentrations of radioligand. While non-specific binding increases linearly with increasing concentration of radiotracer, the specific binding reaches a plateau. In further *in vitro* autoradiography experiments, a concentration of radioligand can be used at which there is 100% occupancy of the target. Hence, differences between control samples and disease model samples can be explained by a difference in target expression and not due to different binding affinity. *In vitro* autoradiography is also particularly useful for the corroboration of *in vivo* neuroimaging results in disease models with altered perfusion and/or blood-brain barrier (BBB) integrity (such as in TBI models),

which influence *in vivo* radiotracer uptake in the brain. If similar results are obtained in *in vitro* autoradiography and *in vivo* imaging assays, then one can reasonably exclude the bias of altered perfusion or BBB integrity in the *in vivo* imaging assay.

2.2. *Ex vivo* autoradiography

In *ex vivo* autoradiography assays, the radiotracer is administered to the live animal through the normal route of administration (usually the lateral tail vein). After some time, the animal is sacrificed, the tissue of interest extracted and sectioned. The obtained tissue sections are then exposed to phosphor imaging plates or films alongside a standard, as in *in vitro* autoradiography assays. *Ex vivo* autoradiography can also be performed following *in vivo* PET or SPECT scanning of the animal. The advantage of *ex vivo* autoradiography compared to PET and SPECT imaging is the superior sensitivity and resolution (especially when using film). Hence, *ex vivo* autoradiography may reveal differences that cannot be picked up by *in vivo* imaging.

3. Radiotracers employed in this PhD thesis

In this PhD thesis, a total of four radiotracers were used.

3.1. [^{111}In]MICA-401

A SPECT probe with high affinity for active uPA and KLK8 (neuropsin), i.e. [^{111}In]MICA-401 (1) (Fig.4-3), was used to explore differences in uPA/KLK8 activity following epileptogenic insults and is described into more detail in chapter 5. The radiotracer contains a diphenyl phosphonate group, which binds covalently to the alcohol group of the serine in the catalytic centre of serine proteases, resulting in the phosphorylation and inhibition of these enzymes. The radiotracer also contains a benzylguanidine group, which provides high selectivity and potency towards uPA, KLK8 and KLK4 compared to other serine proteases (Table 4-1). A polyethylene glycol (PEG) linker connects the tetraazacyclododecane-1,4,7,10-tetraacetic acid (DOTA) chelator, which is used as a complexing agent for the radioisotope ^{111}In .

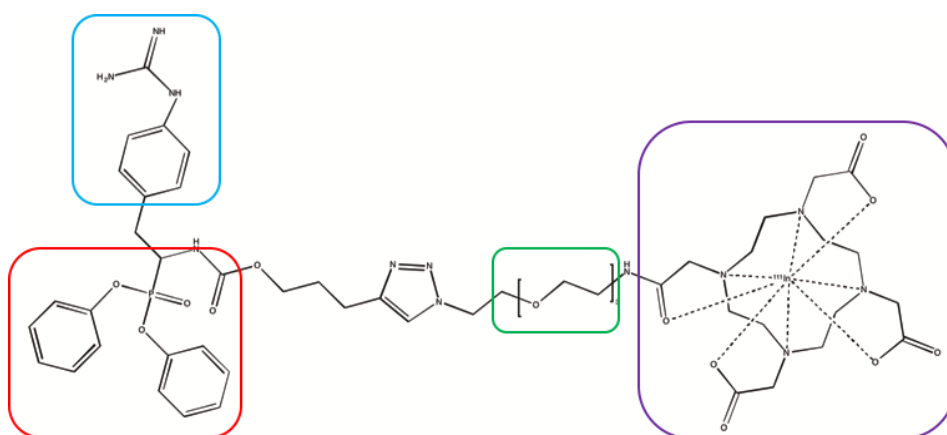


Fig.4-3. Chemical structure of [^{111}In]MICA-401. The diphenyl phosphonate group, which derivatises the catalytic site serine alcohol of serine proteases, is indicated in red. The benzyl guanidine moiety, which provides specificity for uPA and KLK8 is indicated in blue. The polyethylene glycol (PEG) linker is indicated in green. The DOTA chelator, which chelates ^{111}In , is indicated in purple.

3.2. [¹⁸F]BR351 and [¹⁸F]BR420

Two PET probes with high affinity for the zinc-dependent MMPs, i.e. [¹⁸F]BR351 (2) and [¹⁸F]BR420 (3) (Fig.4-4), were investigated to explore MMP-9 expression following traumatic brain injury. [¹⁸F]BR351 contains a hydroxamic acid zinc-binding group, which binds the catalytic Zn²⁺ ion in the catalytic centre of MMPs (thus displacing the Zn²⁺-bound water molecule needed for substrate cleavage through hydrolysis) and inhibits the enzymes. [¹⁸F]BR420 contains a pyrimidine-2,4,6-trione (barbituric acid) zinc-binding group, which also binds to Zn²⁺ in the catalytic centre, resulting in MMP inhibition (4). While [¹⁸F]BR351 has high affinity for all investigated MMPs (though somewhat lower for MMP-9), [¹⁸F]BR420 shows more selectivity towards the gelatinases (i.e. MMP-9 and MMP-2), especially MMP-9 (Table 4-1). A low IC₅₀, i.e. the concentration of the inhibitor at which 50% of the target is inhibited, indicates a potent ligand. These tracers were first evaluated in a colorectal cancer model, i.e. Colo205-bearing nude mice, which was published as “Vazquez N, Missault S, et al.: Evaluation of [¹⁸F]BR420 and [¹⁸F]BR351 as radiotracers for MMP-9 imaging in colorectal cancer.” (5). The tracers were further evaluated for neuroimaging purposes (unpublished data). While no individual chapter will be dedicated to these radiotracers, some of the results will be briefly discussed in chapter 9.

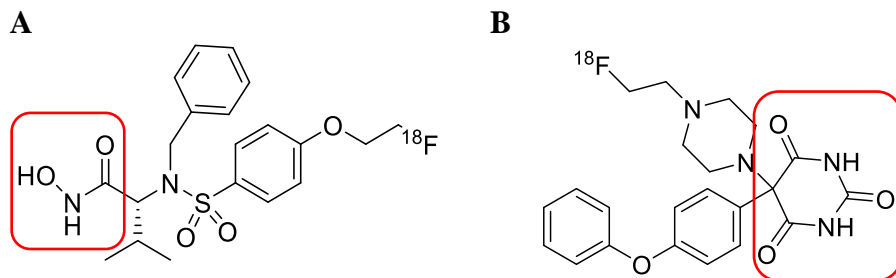


Fig.4-4. Chemical structures of $[^{18}\text{F}]$ BR351 (A) and $[^{18}\text{F}]$ BR420 (B). The zinc-binding groups are indicated in red, respectively hydroxamic acid (A) and barbituric acid (B).

3.3. $[^{18}\text{F}]$ PBR111

Certain limitations of the aforementioned SPECT and PET probes hindered their implementation in a longitudinal *in vivo* imaging study for the investigation of uPA/CLK8 and MMP-9 as potential prognostic biomarkers for long-term outcome following TBI. Hence, we used $[^{18}\text{F}]$ PBR111 (6) (Fig.4-5), a well-characterised second-generation radioligand of TSPO, in a longitudinal imaging study to explore the potential of brain inflammation as a prognostic biomarker of long-term TBI outcome. $[^{18}\text{F}]$ PBR111 has been shown to have high affinity for TSPO (peripheral benzodiazepine receptor - PBR) and low affinity for GABA_A receptors (central benzodiazepine receptor - CBR) (Table 4-1). $[^{18}\text{F}]$ PBR111 is a metabolically stable radiotracer with high specific *in vitro* and *in vivo* binding to TSPO (6, 7).

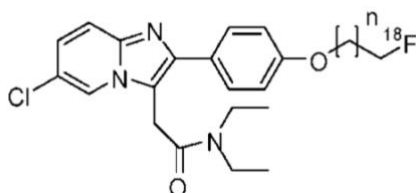


Fig.4-5. Chemical structure of $[^{18}\text{F}]$ PBR111 (n=2).

Table 4-1. Affinity of the different radiotracers used in this thesis for their respective targets and related enzymes/receptors, as well as their logD values (an index of lipophilicity). IC_{50} is the concentration needed to inhibit 50% of the target. K_i is the inhibition constant, reflecting the binding affinity of the ligand. A low IC_{50} and K_i (in nM range) indicate a potent ligand. A radiotracer with moderate lipophilicity, indicated by a $logD_{7.4}$ value between 2.0–3.5, shows optimal passive brain entry in vivo (8).

	IC_{50} (nM)							$logD_{7.4}$
	uPA	tPA	plasmin	KLK8	KLK4	KLK 1	Plasma KLK	
[^{111}In]MICA-401	22 ± 2	>10,000	>10,000	33 ± 4	36 ± 3	>10,000	>10,000	-2.73 ± 0.01
	IC_{50} (nM)				$logD_{7.4}$			
	MMP-9	MMP-2	MMP-8	MMP-13				
[^{18}F]BR420	7 ± 2	23 ± 9	138 ± 12	645 ± 17	2.15 ± 0.02			
[^{18}F]BR351	50 ± 27	4 ± 3	2 ± 1	11 ± 0.3	2.02 ± 0.03			
	K_i (nM)			$logD_{7.5}$				
	PBR ([3H]PK11195)	PBR ([3H]Ro 5-4864)	CBR ([3H]flumazenil)					
[^{18}F]PBR111	3.7 ± 0.4	4.2 ± 0.4	800 ± 120	3.2 ± 0.1				

4. MRI

Magnetic resonance imaging (MRI) has a much higher spatial resolution ($\leq 100 \mu\text{m}$) than PET and SPECT imaging. The sensitivity, however, is much lower (μM - mM range). A major advantage of this technique is that it can provide both anatomical (structural) and functional information about organs. An additional advantage of the technique is that no radioactive compounds are needed for imaging. A disadvantage is the high instrumentation cost. We will discuss two MRI techniques relevant for this thesis, i.e. diffusion MRI and blood-oxygen level dependent (BOLD) contrast-based functional MRI (fMRI).

4.1. Diffusion MRI: Diffusion tensor imaging

4.1.1. Diffusion MRI

Diffusion MRI techniques can be used to probe the tissue microstructure in the brain. Diffusion-weighted MRI assesses the random displacement of water molecules due to molecular diffusion or Brownian motion in each voxel, which can be described by a displacement distribution or displacement probability density function. Diffusion MRI techniques make use of a pulsed gradient spin-echo (SE) sequence, which sensitises the MR signal to diffusion of spins (i.e. hydrogen protons of water molecules). Compared with a classic SE sequence, this sequence includes two additional magnetic field diffusion gradient pulses (Fig.4-6). The application of a magnetic field gradient causes a phase shift to the spins, which varies with their position along the gradient axis. The first gradient pulse causes an initial phase shift, which is dependent on the strength and duration of the

gradient. After application of the 180° RF (radiofrequency) pulse that flips the spins, the second diffusion gradient pulse is applied, which has exactly the same amplitude and duration as the first one. Hence, stationary spins will experience a similar phase shift and return to their initial state and not undergo a net phase shift. However, spins that moved due to diffusion will be subjected to a different field strength during the second pulse and thus experience a net phase shift. Because of the random nature of diffusion, diffusing spins will experience different phase shifts. This spin dephasing results in a decrease of the MR signal intensity. The longer the diffusion distance is, the higher the spin dephasing and thus the greater the decrease in signal intensity. The diffusion-weighted image has low signal in regions with high diffusion along the applied diffusion gradient (9).

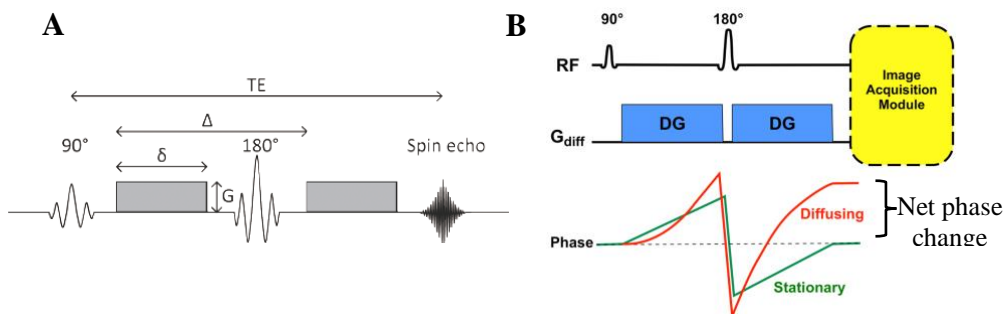


Fig.4-6. Pulsed gradient spin-echo sequence used in diffusion MRI. A. Two identical diffusion gradients are applied, one before and one after the 180° refocusing pulse. The degree of diffusion weighting (b value) depends on the amplitude of the gradients (G), the duration of the gradients δ and the time between the two gradients Δ . **B.** The diffusion gradients introduce a phase shift in the spins. Ultimately, stationary spins will have no phase change, but diffusing spins will, which leads to signal loss in the diffusion-weighted image. (Winston, 2012)

4.1.2. Diffusion-weighted imaging

Diffusion-weighted imaging is the simplest diffusion MRI technique (9). Here it is assumed that diffusion has no restrictions and that the displacement distribution can be described by a Gaussian distribution. Only two images need to be acquired: one with a diffusion weighting gradient along a certain direction (as described above) and a reference image (b_0 image) without diffusion weighting. The physical diffusion coefficient D (mm^2/s) is in this case replaced by the apparent diffusion coefficient (ADC), which can be calculated from the following equation:

$$S = S_0 e^{-bD}$$

with S being the signal intensity in the diffusion-weighted image for a specific b value (Fig.4-7) and diffusion gradient direction, S_0 the signal intensity in the reference image and b the degree of diffusion weighting:

$$b = \gamma^2 G^2 \delta^2 (\Delta - \delta/3)$$

which depends on the amplitude G of the applied gradient pulses, the duration of the gradients δ and the time between the two gradient pulses Δ . γ is the gyromagnetic ratio, which for protons equals 42.58 MHz/T. More frequently, diffusion gradients are applied in three orthogonal directions to get an estimate of the average diffusion.

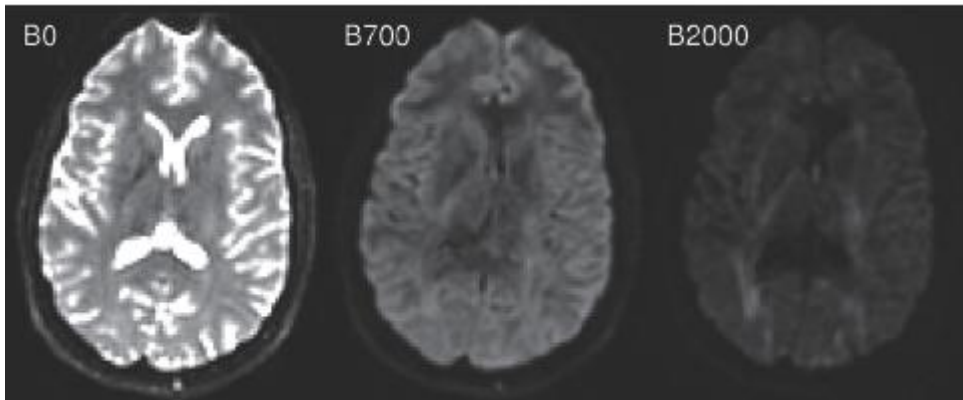


Fig.4-7. Diffusion-weighted images with different degrees of diffusion weighting. The image on the left is a T_2 -weighted echo planar imaging (EPI) image without diffusion-weighting ($b=0$ s/mm²), the middle image has a modest degree of diffusion-weighting ($b=700$ s/mm²) and the image on the right has a high degree of diffusion-weighting ($b=2,000$ s/mm²). Note the high signal loss in the ventricles, which have a high diffusion coefficient. (Winston, 2012)

4.1.3. Diffusion tensor imaging

The model above, however, is often too simplistic. In most cases in the brain, diffusion is anisotropic, i.e. not the same in all directions. The ADC, described above, is dependent on the direction of the diffusion weighting gradients. Anisotropic Gaussian distributions have six degrees of freedom instead of one and are fully characterised by a diffusion tensor. Hence, at least six diffusion-weighted images must be acquired in addition to a non-diffusion-weighted image. Usually, a b value of 800-1,000 s/mm² is used. A set of six equations like the one above must be solved, resulting in a The diffusion tensor can be represented by an ellipsoid (Fig.4-8) or an orientation distribution function. The tensor has three orthogonal eigenvectors and three corresponding positive eigenvalues, which describe the properties of the tensor. Eigenvalues are ordered as $\lambda_1 \geq \lambda_2 \geq \lambda_3$. The eigenvector that corresponds to the largest eigenvalue is the principal diffusion direction. If the eigenvalues are significantly different from each other, diffusion is

anisotropic. From the eigenvalues, several useful scalars (DTI metrics) can be derived, which fall into two categories: those pertaining diffusion magnitude and those pertaining anisotropy. The mean of the three eigenvalues gives the mean diffusivity (MD), which is similar to the average of ADCs in three orthogonal directions (average diffusion) in diffusion-weighted imaging. λ_1 equals the axial diffusivity (AD), i.e. the diffusion along the main axis of the tensor. The mean of λ_2 and λ_3 is the radial diffusivity (RD). The most commonly used metric of anisotropy is the fractional anisotropy (FA), given by the following formula:

$$FA = \sqrt{\frac{3}{2}} \sqrt{\frac{(\lambda_1 - \lambda)^2 + (\lambda_2 - \lambda)^2 + (\lambda_3 - \lambda)^2}{\lambda_1^2 + \lambda_2^2 + \lambda_3^2}}$$

with λ being the mean of the three eigenvalues. FA has a value between 0 and 1. A high FA indicates a pronounced preference of diffusion direction (high anisotropy), which is for example the case in white matter tracts. Here, the diffusion is high along the axis of the fibers (high AD) and low perpendicular to the axis of the fibers (low RD). When there is no preferred direction of diffusion ($\lambda_1 = \lambda_2 = \lambda_3$), FA is zero and diffusion is isotropic (9, 10).

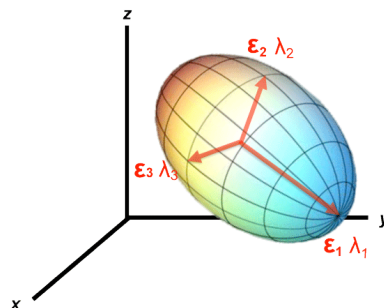


Fig.4-8. The diffusion tensor has three eigenvectors ϵ_1 , ϵ_2 and ϵ_3 with corresponding eigenvalues λ_1 , λ_2 and λ_3 . In this case, diffusion is anisotropic, since λ_1 is significantly different from λ_2 and λ_3 .

DTI has many advantages compared to diffusion-weighted imaging: it is a rotationally invariant description of diffusion and allows to measure anisotropic diffusion. It is therefore especially useful for the study of white matter tracts and has been used in many neuroimaging studies of various disorders including traumatic brain injury (TBI) and schizophrenia (10).

However, DTI also has some disadvantages. There is a low specificity of the DTI metrics to identify particular cellular features. Alterations in MD, AD, RD and FA following TBI for example can be explained by several different underlying physiological and cellular/molecular changes pertaining to neurodegenerative, regenerative and inflammatory processes (reviewed in (11)). The diffusion tensor is also a simplified representation of water diffusion in tissue. First of all, diffusion in biological tissue is not completely Gaussian. Non-Gaussian behaviour of water diffusion can be modelled using diffusion kurtosis imaging. Second of all, while DTI gives a good depiction of fiber orientation in regions where there is only one fiber population (i.e. fibers aligned along a single axis), it fails to describe crossing fiber tracts. To resolve crossing fibers, diffusion MRI techniques with higher angular resolution are needed, such as diffusion spectrum imaging and q-ball imaging. These techniques generally make use of many diffusion gradient directions, a higher b value than the standard 800-1,000 s/mm² for DTI and/or multiple b values (rendering multiple 'shells' of data in q-space) (9-11).

4.2. BOLD contrast-based fMRI: pharmacological MRI and resting-state fMRI

4.2.1. BOLD contrast-based fMRI

Blood-oxygen level dependent (BOLD) contrast-based functional MRI (fMRI) is based on the observation that neuronal activity is tightly linked to localised blood supply (Fig.4-9). The brain needs a constant supply of glucose and oxygen to maintain proper functioning. When a certain brain region becomes activated (e.g. in response to a sensory stimulus or a cognitive task), the regional metabolic demand for oxygen and glucose increases, causing an increase in local blood flow (i.e. the haemodynamic response). This results in an increased ratio of oxygenated (oxyHb) and deoxygenated haemoglobin (deoxyHb), which have different magnetic properties. In deoxyHb, the iron ions (Fe^{2+}) are in a paramagnetic state, since four of the six outer electrons of each Fe^{2+} are unpaired. Magnetic susceptibility differences between deoxyHb-containing compartments and the surrounding area induce local magnetic field gradients, which results in magnetic field inhomogeneities. Pulse sequences that are highly sensitive to such inhomogeneities (T_2^* -weighted sequences) will generate an MR signal that changes with the concentration of deoxyHb. Activated brain regions actually receive more oxygen than they need, resulting in an increase of oxyHb/deoxyHb ratio compared to basal levels and thus a higher BOLD signal than in a non-activated state. As such, BOLD contrast does not solely depend on the oxygen consumption, but also on cerebral blood flow and volume (12).

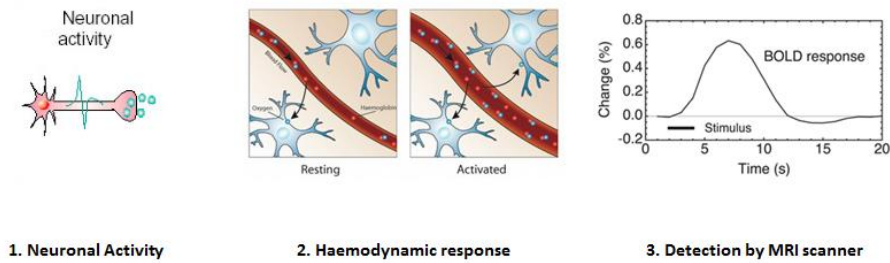


Fig.4-9. Mechanism of the blood-oxygen level dependent (BOLD) contrast. An increase in neuronal activity (in response to a stimulus) leads to increased supply of oxygenated haemoglobin (haemodynamic response) and thus an increased ratio of oxygenated (diamagnetic) vs. deoxygenated haemoglobin (paramagnetic). Hence, there is an increase in MR signal intensity in T_2^* -weighted images.

4.2.2. Pharmacological MRI

In pharmacological MRI the effect of a pharmacological compound on neuronal activity can be assessed using BOLD contrast imaging as described above. A pharmacological drug may activate neurons and thus increase signal intensity in T_2^* -weighted images (Fig.4-10) or inhibit neuronal activity and result in signal intensity reduction. A series of T_2^* -weighted images is acquired before, during and after injection of e.g. a bolus of the pharmacological drug. The signal intensity in the images before and after administration of the drug (after detrending etc.) is compared and thus information about the influence of the drug on regional neural activity changes is obtained.

4.2.3. Resting-state fMRI

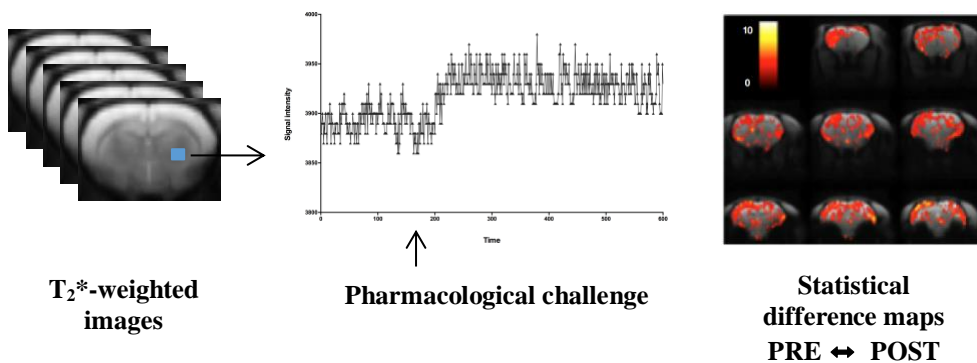


Fig.4-10. Principle of pharmacological MRI. A pharmacological challenge is given during acquisition of T_2^* -weighted images. A change in neuronal activity will induce a change in the BOLD signal intensity.

The brain consists of several networks, i.e. brain regions that are anatomically and/or functionally connected. While anatomical (structural) connectivity between brain regions can be investigated with diffusion MRI techniques, functional connectivity is commonly explored using BOLD contrast imaging. Functionally connected brain regions are defined as anatomically distinct brain regions that display similar patterns of neuronal activity.

Several brain networks are active during rest. One of the best-described resting-state networks is the default mode network, which is involved in information processing about the self and others (including self-referential information, autobiographical information, theory of mind, etc.), as well as in remembering the past and thinking about the future. Acquisition of a time-series of BOLD contrast fMRI images during rest (i.e. resting-state fMRI) reveals spontaneous low-frequency (0.01-0.1 Hz) fluctuations in the BOLD signal in brain regions, reflecting spontaneous neuronal activity patterns. A high correlation between the BOLD signal fluctuations of two anatomically separate brain regions suggests a high functional connectivity between

these regions (Fig.4-11). While many studies support the neuronal basis of the resting-state fMRI signal, non-neuronal oscillations may also contribute to the observed BOLD signal fluctuations (13).

Many neuroimaging studies have made use of resting-state fMRI to explore resting-state functional connectomics in a myriad of neurological and psychiatric disorders, including schizophrenia.

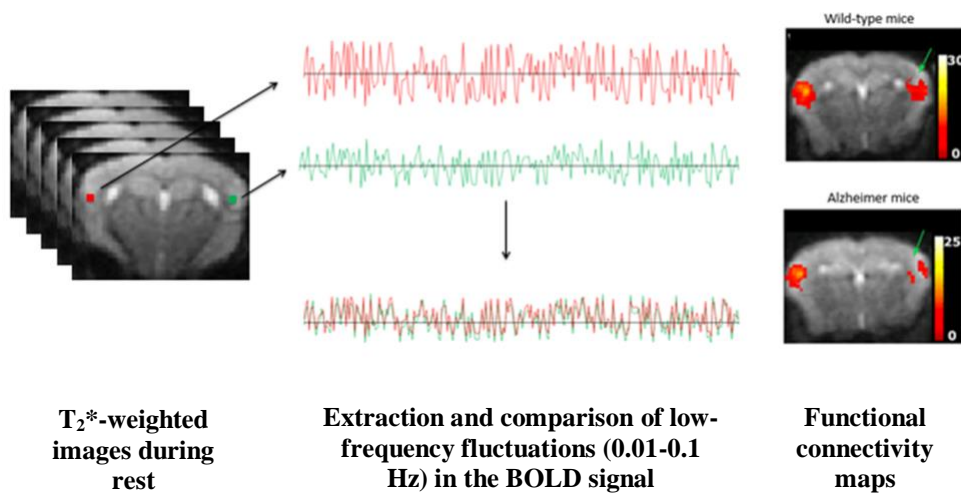


Fig.4-11. Principle of resting-state functional MRI. T_2^* -weighted images are acquired during rest. Correlation analysis is performed on spontaneous low-frequency fluctuations in the BOLD signal time-courses of anatomically distinct brain regions. In case of a high correlation, these brain regions are said to be functionally connected. Functional connectivity maps are obtained by extracting the BOLD signal time-course of a seed region of interest (yellow blob in the figure on the right) and investigating which other voxels in the brain show a similar (i.e. highly correlated) BOLD signal time-course. In the figure on the right there is a breakdown of a bilateral connection in a mouse model of Alzheimer's disease.

5. References

1. Vangestel C, Thomae D, Van Soom J, Ides J, Wyffels L, Pauwels P, et al. (2016): Preclinical evaluation of [^{111}In]MICA-401, an activity-based probe for SPECT imaging of in vivo uPA activity. *Contrast Media Mol Imaging*.
2. Wagner S, Breyholz HJ, Law MP, Faust A, Holtke C, Schroer S, et al. (2007): Novel fluorinated derivatives of the broad-spectrum MMP inhibitors N-hydroxy-2(R)-[[4-methoxyphenyl)sulfonyl](benzyl)- and (3-picolyl)-amino]-3-methyl-butanamide as potential tools for the molecular imaging of activated MMPs with PET. *J Med Chem*. 50:5752-5764.
3. Breyholz HJ, Wagner S, Faust A, Riemann B, Holtke C, Hermann S, et al. (2010): Radiofluorinated pyrimidine-2,4,6-triones as molecular probes for noninvasive MMP-targeted imaging. *ChemMedChem*. 5:777-789.
4. Jacobsen JA, Major Jourden JL, Miller MT, Cohen SM (2010): To bind zinc or not to bind zinc: an examination of innovative approaches to improved metalloproteinase inhibition. *Biochim Biophys Acta*. 1803:72-94.
5. Vazquez N, Missault S, Vangestel C, Deleye S, Thomae D, Van der Veken P, et al. (2017): Evaluation of [(18) F]BR420 and [(18) F]BR351 as radiotracers for MMP-9 imaging in colorectal cancer. *J Labelled Comp Radiopharm*. 60:69-79.
6. Fookes CJ, Pham TQ, Mattner F, Greguric I, Loc'h C, Liu X, et al. (2008): Synthesis and biological evaluation of substituted [18F]imidazo[1,2-a]pyridines and [18F]pyrazolo[1,5-a]pyrimidines for the study of the peripheral benzodiazepine receptor using positron emission tomography. *J Med Chem*. 51:3700-3712.
7. Van Camp N, Boisgard R, Kuhnast B, Theze B, Viel T, Gregoire MC, et al. (2010): In vivo imaging of neuroinflammation: a comparative study between [(18)F]PBR111, [(11)C]CLINME and [(11)C]PK11195 in an acute rodent model. *Eur J Nucl Med Mol Imaging*. 37:962-972.
8. Pike VW (2009): PET radiotracers: crossing the blood-brain barrier and surviving metabolism. *Trends Pharmacol Sci*. 30:431-440.
9. Haggmann P, Jonasson L, Maeder P, Thiran JP, Wedeen VJ, Meuli R (2006): Understanding diffusion MR imaging techniques: from scalar diffusion-weighted imaging to diffusion tensor imaging and beyond. *Radiographics*. 26 Suppl 1:S205-223.
10. O'Donnell LJ, Westin CF (2011): An introduction to diffusion tensor image analysis. *Neurosurg Clin N Am*. 22:185-196, viii.
11. Hutchinson EB, Schwerin SC, Avram AV, Juliano SL, Pierpaoli C (2017): Diffusion MRI and the detection of alterations following traumatic brain injury. *J Neurosci Res*.

12. Logothetis NK (2002): The neural basis of the blood-oxygen-level-dependent functional magnetic resonance imaging signal. *Philos Trans R Soc Lond B Biol Sci.* 357:1003-1037.
13. van den Heuvel MP, Hulshoff Pol HE (2010): Exploring the brain network: a review on resting-state fMRI functional connectivity. *Eur Neuropsychopharmacol.* 20:519-534.

PART 1

Brain insults during young adulthood

5

*Decreased levels of active uPA and KLK8
assessed by [¹¹¹In]MICA-401 binding correlate
with the seizure burden in an animal model of
temporal lobe epilepsy*

Published in Epilepsia (2017)

1. Abstract

Objective: Urokinase-type plasminogen activator (uPA) and kallikrein-related peptidase 8 (KLK8) are serine proteases that contribute to extracellular matrix (ECM) remodelling after brain injury. They can be labelled with the novel radiotracer [^{111}In]MICA-401. As the first step to explore the applicability of [^{111}In]MICA-401 in tracing the mechanisms of post-injury ECM reorganisation *in vivo*, we performed *in vitro* and *ex vivo* studies assessing [^{111}In]MICA-401 distribution in the brain in two animal models: kainic acid-induced *status epilepticus* (KASE) and controlled cortical impact (CCI)–induced traumatic brain injury (TBI). **Methods:** In KASE model, *in vitro* autoradiography with [^{111}In]MICA-401 was performed at 7d and 12w post-*SE*. To assess seizure burden, rats were video-EEG monitored for 1 month prior to the 12w time point. In CCI model, *in vitro* autoradiography was performed at 4d and *ex vivo* autoradiography at 7d post-TBI. **Results:** At 7d post-*SE*, *in vitro* autoradiography revealed significantly decreased [^{111}In]MICA-401 binding in hippocampal CA3 subfield and extrahippocampal temporal lobe (ETL). In the chronic phase, when animals had developed spontaneous seizures, specific binding was decreased in CA3 and CA1/CA2 subfields of hippocampus, dentate gyrus, ETL, and parietal cortex. Interestingly, KASE rats with the highest frequency of seizures had the lowest hippocampal [^{111}In]MICA-401 binding ($r=-0.76$, $p\leq 0.05$). Similarly at 4d post-TBI, *in vitro* [^{111}In]MICA-401 binding was significantly decreased in medial and lateral perilesional cortex and ipsilateral dentate gyrus. *Ex vivo* autoradiography at 7d post-TBI, however, revealed increased tracer uptake in perilesional cortex and hippocampus, which was likely related to tracer leakage due to blood-brain barrier (BBB) disruption. **Significance:** Strong

association of reduced [^{111}In]MICA-401 binding with seizure burden in the KASE model suggests that analysis of reduced levels of active uPA/KLK8 represents a novel biomarker candidate to be explored as biomarker for epilepsy severity. However, limited BBB permeability of [^{111}In]MICA-401 currently limits its *in vivo* applications.

Key words: extracellular matrix, urokinase-type plasminogen activator, kallikrein-related peptidase 8, epilepsy, traumatic brain injury, SPECT

2. Introduction

Epilepsy affects approximately 69 million people worldwide (1). Despite of >20 antiepileptic drugs on the market, 30% of patients remain in unsatisfactory seizure control (2). Therefore, identification of epileptogenic mechanisms remains a major unmet need in neurology.

Studies over the past 10 years have revealed involvement of extracellular proteases in the pathogenesis of epilepsy (reviewed in (3, 4)). These proteases degrade various components of the extracellular matrix, facilitating plasticity in both physiological and pathological conditions. One family of extracellular proteases are serine proteases, which include urokinase-type plasminogen activator (uPA) and kallikrein-related peptidase 8 (KLK8), also known as neuropsin or brain serine protease 1 (BSP1) (5). Since these enzymes are located extracellularly, assessment of their activity *in vivo* would provide an attractive tool to monitor the progression of extracellular plasticity.

Our research group has recently reported the synthesis of a novel activity-based single-photon emission computed tomography (SPECT) probe, [^{111}In]MICA-401 (6). The probe was designed based on a diphenyl

phosphonate scaffold, which binds covalently to the alcohol group of the active site serine of serine proteases. It also bears a benzylguanidine moiety, which provides a high selectivity towards uPA (7), KLK8 and KLK4, and a PEG linker to connect the DOTA-chelator, which is used as a complexing agent for radioisotope indium-111 (^{111}In). *In vitro* evaluation of the binding kinetics of [^{111}In]MICA-401 revealed that the probe was highly selective towards uPA, KLK8 and KLK4 as compared to other related trypsin-like serine proteases (tPA, thrombin, plasmin, FXa, plasma KLK, KLK1, HNE and AChE). Recently, [^{111}In]MICA-401 was evaluated for its capacity to image uPA activity *in vivo* by SPECT in two different cancer models (6). Interestingly, the best SPECT images were acquired at 4 d post-injection due to a slow blood clearance of the tracer.

Since the tracer can only bind to active enzyme, i.e. enzyme in which the catalytic site serine is available for binding, tracer binding reflects levels of active uPA and KLK8 (6). Because little is known about the role of KLK4 in the brain, we limit the interpretation of the results to uPA and KLK8.

The present study was designed to evaluate the capacity of [^{111}In]MICA-401 to image the spatiotemporal dynamics of active uPA and KLK8 in the brain in two rodent models of acquired epilepsy: the KASE model of mesial temporal lobe epilepsy (TLE) and the CCI model of posttraumatic epilepsy. Our *in vitro* data show a reduction in [^{111}In]MICA-401 binding in several injured brain areas during the first post-injury week in both models, which is even more pronounced and widespread in the chronic phase in the KASE model, when spontaneous seizures have developed. Moreover, the reduced hippocampal binding of [^{111}In]MICA-401 correlated with the seizure burden.

3. Methods

3.1. Study design

Study design is shown in Fig.5-1.

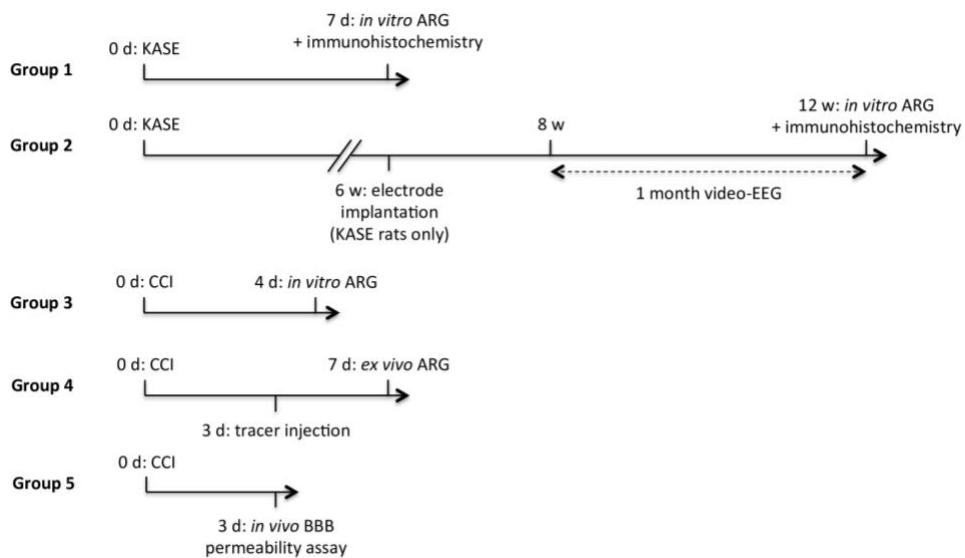


Fig.5-1. Study design. *In vitro* autoradiography (ARG) with [^{111}In]MICA-401 was performed in rats with kainic acid-induced status epilepticus (KASE) and in rats with controlled cortical impact (CCI)-induced traumatic brain injury, and their respective controls. KASE and healthy control rats were sacrificed either at 7 d (Group 1) or 12 w post-SE (Group 2). Neuronal loss was assessed at both time points in KASE and healthy control rats with immunohistochemistry. In the 12 w KASE group, electrodes were implanted at 6 w post-SE and a one-month continuous video-EEG monitoring was performed between the 8th and 12th w post-SE to assess the seizure burden. In CCI- and sham-injured rats, *in vitro* autoradiography was done at 4 d post-injury (Group 3). Another cohort of CCI rats was injected with [^{111}In]MICA-401 at 3 d post-injury and sacrificed 4 d later for *ex vivo* autoradiography (Group 4). To assess the contribution of blood-brain-barrier (BBB) disruption to *in vivo* tracer uptake, we performed an *in vivo* BBB permeability assay at 3 d post-CCI injury (i.e. at the time of tracer injection) (Group 5).

3.2. Animals

Fifty-four male Sprague-Dawley rats were purchased from Harlan Laboratories, the Netherlands. Upon arrival, animals were single housed in

a temperature- and humidity-controlled environment on a 12 hour light-dark cycle with standard food and water available *ad libitum*. Animals were treated in accordance with the guidelines approved by the European Ethics Committee (decree 2010/63/EU) and the Animal Welfare Act (7 USC 2131). Animal experiments were approved by the ethical committee of the University of Antwerp, Belgium (ECD 2012-62).

3.3. Kainic acid-induced *status epilepticus* (KASE)

Animals were about 8 weeks old at the time of *status epilepticus* (SE) induction (mean weight: 250.9 ± 5.2 g). The KASE model was induced as previously described (8) with a few modifications. Briefly, animals received multiple low-dose subcutaneous injections of kainic acid (A.G. Scientific, USA) until they reached SE (average total dose: 16.2 ± 5.4 mg/kg). Animals were sacrificed at 7 days post-SE while undergoing epileptogenesis (11 KASE, 6 healthy controls) or at 12 weeks post-SE when they had already developed spontaneous recurrent seizures (SRS) (9 KASE, 6 healthy controls). Occurrence of SRS was confirmed with continuous video-EEG monitoring (see below).

3.4. Controlled Cortical Impact (CCI)-induced traumatic brain injury (TBI)

Rats of about 8 weeks old (mean weight: 225.5 ± 2.5 g) were anaesthetised using isoflurane in oxygen (induction: 5%, maintenance: 2.5%; Abbott, Belgium). A craniotomy of 5 mm diameter was performed with a hand-held trephine over the left parietal cortex (midway between bregma and lambda, bordering the lateral ridge). Great care was taken to avoid damage of the underlying dura. CCI-injury was performed with the Leica Impact One

apparatus (Leica Biosystems, USA) using the following parameters: flat tip of 3 mm diameter, impact angle 18°, impact velocity 4 m/s, depth of penetration 2.5 mm, dwell-time 500 ms. Following impact, the craniotomy was sealed with a piece of plastic, and skin sutured. Sham-operated animals received the same surgery, but were not exposed to impact. Rats were sacrificed at 3 days (3 CCI, 3 shams), 4 days (5 CCI, 5 shams) or 7 days post-injury (3 CCI, 3 shams).

3.5. Video-EEG

Electrode implantation. Implantation of EEG electrodes was performed at 6 w post-SE in KASE rats as previously described (8). Briefly, animals were anaesthetised and six epidural electrodes were implanted bilaterally: four recording electrodes (two frontal, two parietal), one reference and one ground electrode (both occipital). The electrodes were fixed into a plastic plug (Bilaney Consultants, Plastics One, UK) and secured to the skull using dental cement (Simplex Rapid, Kemdent, UK; Durelon, 3M ESPE, USA).

Recording. KASE rats were subjected to continuous video-EEG monitoring for 29 ± 1 d between the second and third month post-SE. One animal was monitored only for 5 days due to loss of the electrode assembly, and was excluded from the seizure analysis. Animals were connected to a digital EEG acquisition system (Ponemah P3 Plus, Data Sciences International, USA) through a cable system as previously described (8).

Analysis. Video-EEG data were analysed manually using NeuroScore 3.0 (Data Sciences International, USA). SRS were identified as previously described (8, 9). Briefly, an electrographic seizure was defined as an aberrant EEG signal with an amplitude of at least three times the baseline signal and

a duration of at least 5 s (10). The severity of the seizures was determined by analysing the corresponding video recording and scored according to a modified scale of Racine (9). To assess the seizure burden for each animal, we calculated the total number of SRS per day.

3.6. Radiochemistry

Radiosynthesis of [^{111}In]MICA-401 was performed as recently described(6). The radiolabelling precursor, an uPA/KLK8 inhibitor linked to a DOTA-chelator, was incubated with [^{111}In]- InCl_3 (PerkinElmer, Belgium) for 45 min at 60°C to achieve complexation of indium (^{111}In). [^{111}In]MICA-401 was synthesised with a 59% yield and a chemical and radiochemical purity of >98%. The specific activity was 15.44 GBq/ μmol .

3.7. Inhibitory potential of the radiolabelling precursor for serine proteases in rat

The inhibitory potential of the radiolabelling precursor for human uPA, KLK8 and a set of related trypsin-like serine proteases as well as mouse uPA has recently been described (6). Since there was a large difference in IC_{50} values for human and mouse uPA, we decided to assess the IC_{50} values for human and rat uPA and KLK8 of UAMC-01162, the compound from which the radiolabelling precursor was derived, according to previously described protocols (7). Briefly, recombinant rat uPA or KLK8 was incubated with an enzyme-specific chromogenic substrate and different concentrations of UAMC-01162. Inhibition of the enzymatic reaction was evaluated through spectrophotometry.

3.8. Autoradiography

Tissue collection and preparation. Animals were sacrificed by decapitation. Brains were immediately resected and snap-frozen in 2-methylbutane on dry ice (-35°C, 3 min). Brains were stored at -80°C. In KASE model, only the right hemisphere was snap-frozen for the present analysis (kainate-induced lesion is symmetric). Serial coronal cryosections (20 µm) were collected in triplicate at two coronal levels: at -2.92 mm from bregma (sections containing lesion core and dorsal hippocampus: CCI and shams) and -4.80 mm from bregma (sections containing ventral hippocampus: KASE and healthy controls).

In vitro autoradiography. Coronal brain sections were dried at room temperature and incubated with 50 nM [¹¹¹In]MICA-401 in 50 mM Tris-HCl buffer for one hour at room temperature to assess total receptor-ligand binding. In order to assess non-specific binding of the radiotracer, consecutive brain sections were incubated under the same conditions with an excess amount (1 mM) of UAMC-01162, the compound from which the radiolabelling precursor is derived, in addition to 50 nM [¹¹¹In]MICA-401. Sections were washed with ice-cold Tris-HCl buffer and distilled water to remove unbound tracer. After drying, sections were exposed on hyperfilm (Amersham Hyperfilm MP; GE Healthcare, Belgium) for three days, alongside a ¹⁴C standard (American Radiolabeled Chemicals Inc., USA). The hyperfilms were developed manually and digitalised using an Epson V700 photo scanner (Seiko Epson Corporation, Japan).

In KASE model (20 KASE, 12 healthy controls), specific binding of [¹¹¹In]MICA-401 was assessed in CA1/CA2 and CA3 subregions of hippocampus, dentate gyrus (DG), extrahippocampal temporal lobe and parietal cortex. In CCI

model (5 CCI, 5 shams), we analysed perilesional cortex (both medial and lateral to the lesion), contralateral cortex (regions symmetric to the medial and lateral perilesional cortex), ipsilateral and contralateral CA1, CA3 and DG. All ROIs were outlined manually in triplicate samples (sections with total binding and non-specific binding separately).

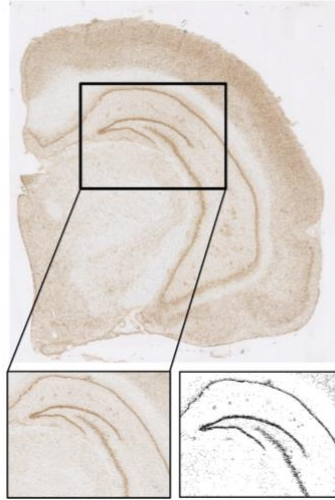
Grey values were measured using ImageJ software (National Institute of Health, USA). The mean grey values were converted to doses of radioactivity (kBq/g ^{14}C) by interpolation from a standard curve that was derived from the ^{14}C standard grey values. The specific binding of [^{111}In]MICA-401 was obtained by subtracting the non-specific binding from the total binding. The average specific binding for the hippocampus proper was calculated by taking the mean of the specific binding values for CA1/2 and CA3.

Ex vivo autoradiography. Three CCI-injured and three sham-operated rats were injected intravenously with [^{111}In]MICA-401 (39.1 ± 2.2 MBq) at 3 d post-injury. At 4 d post-injection, animals were sacrificed by decapitation and brains were resected, snap-frozen and sectioned as above. This time point was chosen based on our previous observations showing very slow blood clearance of the radiotracer(6). At 4 d post-injection, most of the signal in the blood has been cleared and tracer binding in various organs can be more readily distinguished (6). Sections were dried at room temperature and exposed on hyperfilm for two weeks along with a ^{14}C standard. The film was developed manually and analysed in the same way as the *in vitro* autoradiography films. ROIs included perilesional cortex and ipsilateral hippocampus.

3.9. Immunohistochemistry

To provide a potential explanation for the observed decrease in levels of active uPA/KLK8, a NeuN staining was performed to evaluate the extent of neuronal loss in the KASE model. Coronal brain sections adjacent to the brain sections used for *in vitro* autoradiography were acclimatised to room temperature, fixated with 4% paraformaldehyde and rinsed with PBS. Sections were treated with 3% H₂O₂ and 5% Normal Donkey Serum (NDS) containing 0.5% Triton X-100. Sections were incubated overnight with mouse anti-rat NeuN antibody (1:2000; clone A60; Merck Millipore, Belgium) in 1% NDS. The following morning, sections were rinsed and incubated for one hour with horse radish peroxidase-conjugated donkey anti-mouse IgG antibody (1:500; Jackson ImmunoResearch Laboratories, Inc., UK) in 1% NDS. Sections were rinsed again and incubated with 3,3'-diaminobenzidine for 10 min. The reaction was stopped with dH₂O and sections were gradually dehydrated and coverslipped.

Images were obtained with a NanoZoomer-XR slide scanner (Hamamatsu, Japan) equipped with a 20x objective and analysed with ImageJ software. Images were transformed to 8-bit images and a threshold was set to select specifically stained neuronal nuclei from background staining (Suppl.Fig.5-1). The area fraction, i.e. the % area of the ROI that consists of NeuN-stained nuclei (as set by the threshold), was calculated for the following ROIs: CA1/CA2 and CA3 subregions of hippocampus, granule cell layer of the dentate gyrus (DG), extrahippocampal temporal lobe and parietal cortex. A higher area fraction reflects a higher neuronal density in this ROI. Furthermore, the area (in mm²) of each ROI was measured in ImageJ. All ROIs were outlined manually in triplicate samples.



Suppl. Fig. 5-1. Example of a NeuN-stained brain section and setting of the threshold. In the lower panels, an inset is shown of the hippocampus, before (left) and after (right) setting of the threshold as described in the Methods section. The percentage of the area of the ROI that contains black pixels (i.e. above the threshold) is calculated to give the area fraction.

3.10. Assessment of blood-brain barrier (BBB) permeability

One group of CCI-injured (n=3) and sham-operated rats (n=3) was injected intravenously with 2% Evans blue (in 0.9% saline, 4 ml/kg) at 3 d post-injury. Evans blue was allowed to circulate for one hour, after which the animal was perfused transcardially with 100 ml of ice-cold PBS under deep anaesthesia (60 mg/kg Nembutal, Ceva Santé Animale, Belgium; intraperitoneally) to remove the blood from the blood vessels. Following perfusion, brains were resected and snap-frozen as above. During sectioning photographs were taken for visual inspection of Evans blue extravasation. Evans blue has a very high affinity for serum albumin, which cannot cross the intact BBB. In case of increased BBB permeability, Evans blue (bound to albumin) can extravasate into the brain parenchyma.

3.11. Statistics

All data were analysed using non-parametric tests in GraphPad Prism 5. The Mann-Whitney U test was used to compare specific binding and tracer uptake between either KASE and controls or CCI and sham rats or between KASE and controls of two different time points. The Wilcoxon matched-pairs signed rank test was used to investigate possible differences between ipsilateral and contralateral hemispheres of CCI-injured rats. Spearman's rank correlation was used to investigate the relationship between specific binding of [^{111}In]MICA-401 and i) neuronal loss in KASE rats, and ii) number of SRS per day in chronic KASE rats. Statistical significance was set at $p \leq 0.05$.

4. Results

4.1. High affinity of UAMC-01162 for rat uPA and KLK8

UAMC-01162, the compound from which the radiolabelling precursor is derived, has a high affinity for both rat uPA and KLK8. The IC_{50} values were 21 ± 1 nM for rat uPA and 15 ± 2 nM for rat KLK8 (Table 5-1).

4.2. Decreased specific binding of [^{111}In]MICA-401 in the KASE model

In vitro [^{111}In]MICA-401 autoradiography of normal rat brain revealed a prominent binding in several brain regions, including cerebral cortex, hippocampus, amygdala and caudate putamen whereas binding in the thalamus was low. At 7 d post-SE, while KASE rats were undergoing epileptogenesis, specific binding of [^{111}In]MICA-401 was reduced in extrahippocampal temporal lobe (ETL, defined as amygdala, piriform cortex and entorhinal cortex) ($p \leq 0.01$) and CA3 subregion of hippocampus ($p \leq 0.05$) as compared to healthy controls (Fig.5-2A,C). At 12 w post-SE, when all KASE

rats had SRS, [^{111}In]MICA-401 specific binding was reduced in the ETL and parietal cortex ($p \leq 0.001$), CA1/CA2 subregion of hippocampus and dentate gyrus ($p \leq 0.05$). We also found a trend towards decreased binding in CA3 ($p \leq 0.1$) (Fig.5-2B,D). Moreover, at 12 w post-*SE* specific binding of [^{111}In]MICA-401 in CA1/CA2 and parietal cortex was lower than at 7 d post-*SE* ($p \leq 0.01$) (Fig.5-2I). There were no significant differences between healthy controls of 7 d and 12 w.

4.3. Specific binding of [^{111}In]MICA-401 is not correlated with neuronal loss

We investigated whether the decrease in [^{111}In]MICA-401 binding was related to neuronal loss in the KASE model. KASE rats exhibited a significantly lower area fraction of NeuN staining in CA1/2 and CA3 subfields of hippocampus, parietal cortex ($p \leq 0.01$) and ETL ($p \leq 0.05$) at 7 d post-*SE* compared to healthy controls, indicating extensive neuronal cell loss (Fig.5-2E,G). At 12 w post-*SE* KASE rats had a significantly lower area fraction of NeuN staining in CA3 subfield ($p \leq 0.05$) as well as a trend for a lower area fraction in the granule cell layer of the dentate gyrus ($p \leq 0.1$) (Fig.5-2F,H). At the same time point, a trend for an increased area was observed for the granule cell layer of the dentate gyrus ($p \leq 0.1$) (data not shown). At 7 d post-*SE* KASE rats had a significantly lower area fraction of NeuN staining in parietal cortex compared to 12 w post-*SE* ($p \leq 0.01$) as well as a trend for a lower area fraction of NeuN staining in CA1/2 ($p \leq 0.1$) (Fig.5-2J). There were no significant differences between healthy controls of 7 d and 12 w. There was no correlation between neuronal cell loss and [^{111}In]MICA-401 binding in any of the studies brain regions at any time point (data not shown).

Table 5-1. Inhibitory potential of UAMC-01162 and the radiolabelling precursor MICA-401 for several serine proteases (*Vangestel C et al., 2016).

	IC ₅₀ (μM)	
	UAMC-01162 (1)	MICA-401 (2)
Human uPA	0.007	0.022*
Rat uPA	0.021	
Human tPA	38.05	>10*
Human thrombin	30	>10*
Human plasmin	27	>10*
Human Factor Xa	35.2	>10*
Human plasma KLK	10.16	>10*
Human KLK1	>10	>10*
Human KLK4	0.012	0.036*
Rat KLK4	0.044	0.082
Human KLK8	0.050	0.033*
Rat KLK8	0.015	0.034
Human HNE	>10	>2.5*
Human AChE	>20	>20*

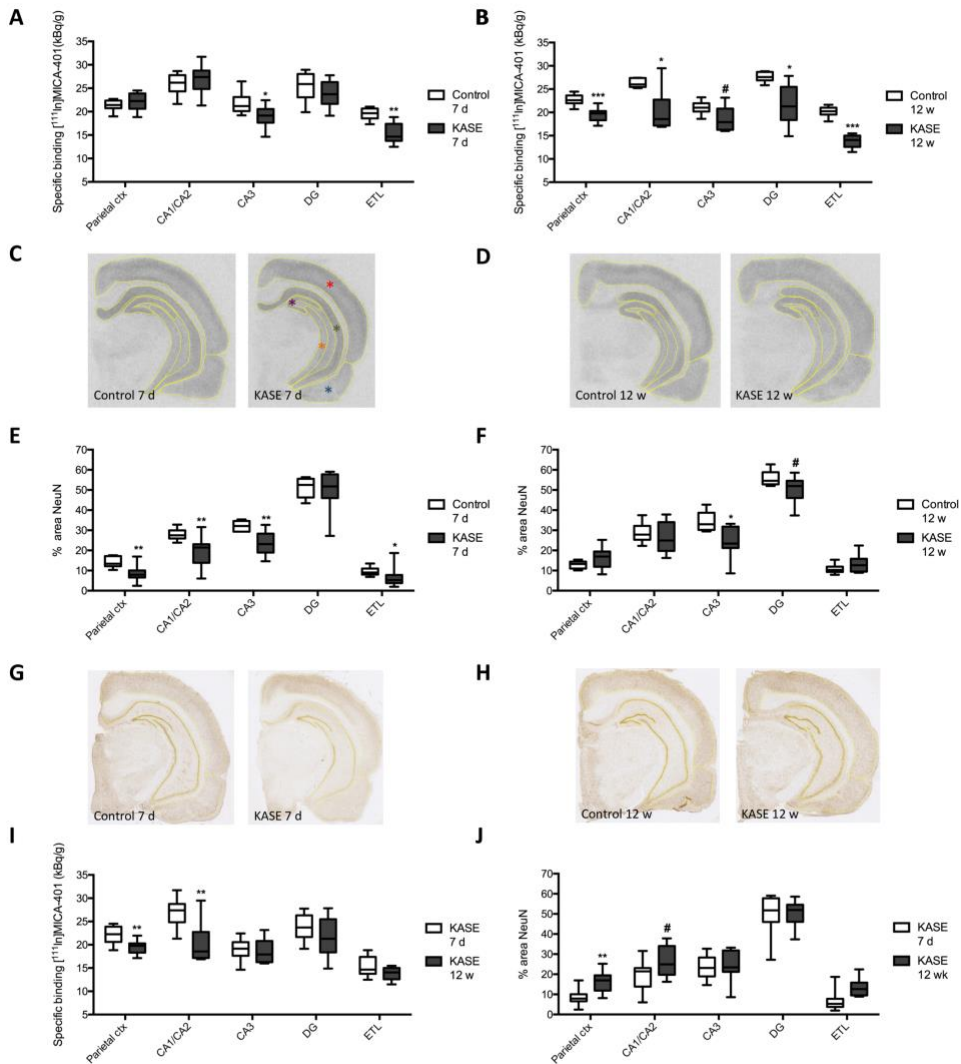


Fig.5-2. Decreased in vitro binding of [^{111}In]MICA-401 and neuronal cell loss in kainic acid-induced status epilepticus (KASE) model. (A) At 7 d post-SE, when rats were undergoing epileptogenesis, specific binding of [^{111}In]MICA-401 was decreased in the extrahippocampal temporal lobe (ETL) and hippocampal CA3 subfield of KASE rats ($n=11$) compared to healthy controls ($n=6$). **(B)** At 12 w post-SE, when KASE rats had spontaneous recurrent seizures, specific binding of [^{111}In]MICA-401 was decreased in most brain areas, including ETL, hippocampal CA1/CA2 subfield, dentate gyrus and parietal cortex. **(C-D)** Representative in vitro autoradiographs of total [^{111}In]MICA-401 binding in healthy control and KASE rats at 7 d (C) and 12 w post-SE (D). The regions of interest (ROIs) are drawn in yellow. Red asterisk: parietal cortex; green asterisk: CA1/CA2; orange asterisk: CA3; purple asterisk: dentate gyrus; blue asterisk: ETL. **(E)** Neuronal cell loss was observed in hippocampal CA1/CA2 and

CA3 subfields, parietal cortex and ETL of KASE rats at 7 d post-SE. **(F)** Neuronal loss was observed in CA3 of KASE rats at 12 w post-SE. **(G-H)** Representative images of NeuN staining in KASE and healthy control rats at 7 d (G) and 12 w post-SE (H). The ROIs are drawn in yellow. **(I)** Specific binding of [^{111}In]MICA-401 was significantly lower in KASE rats at 12 w post-SE compared to 7 d post-SE in parietal cortex and CA1/2. **(J)** The area fraction of NeuN staining was significantly higher in KASE rats at 12 w post-SE compared to 7 d post-SE in parietal cortex. Statistical significances: * $p \leq 0.05$, ** $p \leq 0.01$, *** $p \leq 0.001$ (compared to age-matched control group). Data are represented as boxplots.

4.4. Specific binding of [^{111}In]MICA-401 correlated with epilepsy phenotype in KASE rats at 12 w post-SE

All KASE rats experienced SRS in the chronic stage. They had on average 10.8 ± 2.9 SRS per day (range: 0.6-19.9 SRS per day). A negative correlation was found between the specific binding of [^{111}In]MICA-401 in hippocampus proper and a daily seizure frequency in KASE rats at 12 w post-SE (Fig.5-3).

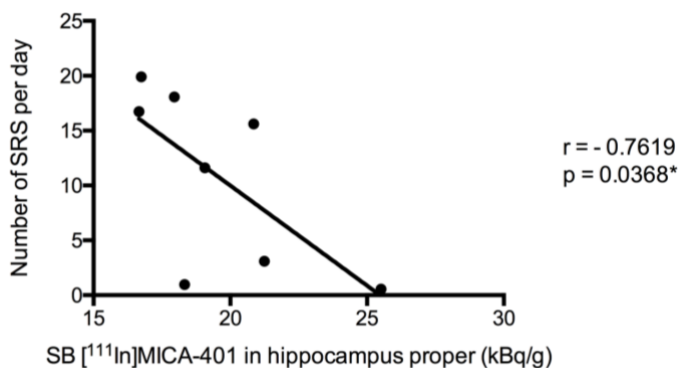


Fig.5-3. *In vitro* [^{111}In]MICA-401 binding is correlated with the seizure burden in chronic kainic acid-induced status epilepticus (KASE) rats. The KASE rats with the highest daily number of seizures had the largest decrease in [^{111}In]MICA-401 binding in the hippocampus proper. Statistical significance: * $p \leq 0.05$.

4.5. Decreased specific binding of [¹¹¹In]MICA-401 in the CCI-injury model

In vitro autoradiographic evaluation of [¹¹¹In]MICA-401 binding in CCI-injured rats revealed reduced specific binding in medial and lateral perilesional cortex and ipsilateral dentate gyrus as compared to the corresponding regions in sham-operated rats at 4 d post-injury ($p \leq 0.01$) (Fig.5-4A,B). Specific binding of [¹¹¹In]MICA-401 was significantly decreased in both medial and lateral perilesional cortex of CCI-injured rats compared to the corresponding contralateral cortical regions ($p \leq 0.01$). Moreover, a trend towards a decreased binding was observed in the ipsilateral CA1 subfield and dentate gyrus of CCI-injured rats as compared to the contralateral CA1 subfield and dentate gyrus, respectively ($p \leq 0.1$).

4.6. *In vivo* uptake of [¹¹¹In]MICA-401 after CCI-injury

Ex vivo autoradiography of [¹¹¹In]MICA-401 showed an increased uptake of the radiotracer in perilesional cortex and hippocampus in CCI rats as compared to shams at 7 d post-injury (Fig.5-4C,D). In addition, tracer accumulation was observed in the ventricles of both sham and CCI rats. Similarly, extravasation of Evans blue was observed in the perilesional area in another cohort of CCI rats at 3 d post-injury (i.e. the time point of tracer injection) (Fig.5-4E). Evans blue was also perceived in the ventricles of both sham and CCI rats.

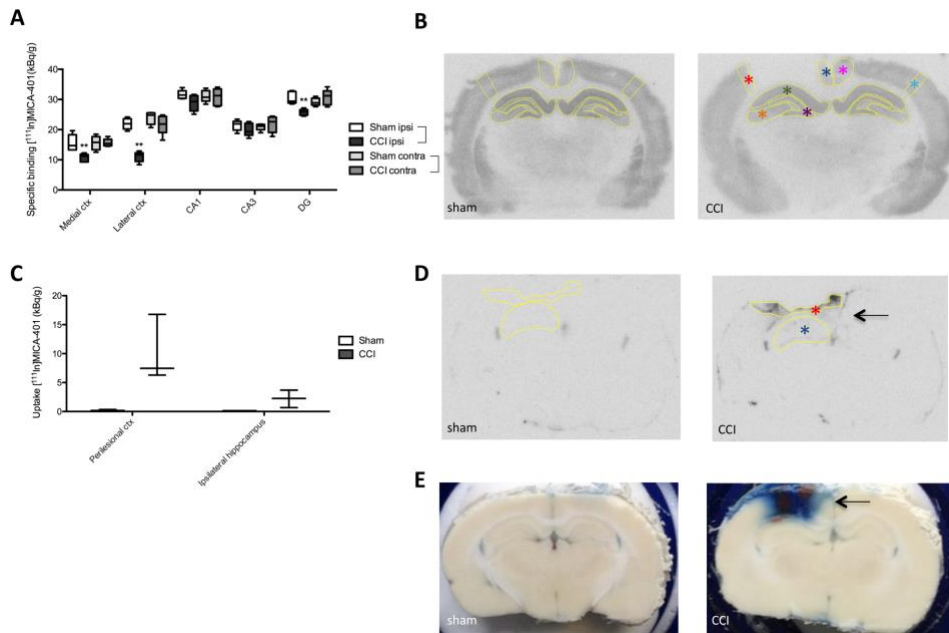


Fig.5-4. Decreased in vitro binding of $[^{111}\text{In}]\text{MICA-401}$ and increased in vivo uptake of $[^{111}\text{In}]\text{MICA-401}$ and Evans blue extravasation in Controlled Cortical Impact (CCI)-injured rats. (A) Specific binding of $[^{111}\text{In}]\text{MICA-401}$ was decreased in medial and lateral perilesional cortex and ipsilaterally in the dentate gyrus of CCI rats ($n=5$) compared to shams ($n=5$) at 4 d post-injury. (B) Representative in vitro autoradiographs of total $[^{111}\text{In}]\text{MICA-401}$ binding in sham-operated and CCI-injured rats at 4 d post-injury. The regions of interest (ROIs) are drawn in yellow. Dark blue asterisk: medial perilesional cortex; red asterisk: lateral perilesional cortex; pink asterisk: medial contralateral cortex; light blue asterisk: lateral contralateral cortex; green asterisk: CA1; orange asterisk: CA3; purple asterisk: dentate gyrus. (C) Increased radiotracer uptake was observed with ex vivo autoradiography in perilesional cortex and ipsilateral hippocampus of CCI-injured but not sham-operated rats injected with radiotracer 4 days earlier. (D) Representative ex vivo autoradiographs of $[^{111}\text{In}]\text{MICA-401}$ accumulation in sham-operated and CCI-injured rats. Tracer uptake can be observed in perilesional cortex and ipsilateral hippocampus of CCI-injured rats (arrow), but not in shams. ROIs are drawn in yellow. Red asterisk: perilesional cortex, blue asterisk: ipsilateral hippocampus. (E) Extravasation of Evans blue is visible in the perilesional area of CCI rats (arrow), but not in shams. Statistical significance: ** $p \leq 0.01$. Data are represented as boxplots.

5. Discussion

The objective of this study was to investigate the capacity of the novel activity-based SPECT probe [^{111}In]MICA-401 to image brain alterations in active uPA and KLK8 in two rodent models of acquired epilepsy. In this study we observed a (sub)acute decrease of [^{111}In]MICA-401 binding in the temporal lobe in a TLE model and in the perilesional cortex and dentate gyrus in a TBI model. This decrease in [^{111}In]MICA-401 binding was even more pronounced and widespread when animals had developed SRS in the TLE model. Moreover, the hippocampal decrease in [^{111}In]MICA-401 binding was correlated with the severity of the epilepsy phenotype.

Since [^{111}In]MICA-401 can only bind to active uPA/KLK8, [^{111}In]MICA-401 binding is an indirect measure of uPA/KLK8 activity.

5.1. Decreased [^{111}In]MICA-401 binding after epileptogenic insults

In the *in vitro* autoradiography assays we observed a decrease in [^{111}In]MICA-401 binding and thus levels of active uPA and KLK8 in several relevant brain regions after *SE* and CCI-injury. While several studies have reported an increase in uPA and KLK8 expression and activity following epileptogenic insults, most of these used electrical stimulation of the amygdala or hippocampus to trigger epileptogenesis (11-16). On the contrary, most studies that used KASE to evoke epileptogenesis showed primarily that the basal neuronal expression of these proteases was lost due to neuronal degeneration in some brain regions, in addition to an overexpression of uPA and KLK8 by respectively astrocytes and oligodendrocytes (17-19). Masos and Miskin did not report a decreased neuronal expression of uPA following KASE, but they used a rather low dose

of KA (i.e. 12 mg/kg, in mice), resulting in relatively mild seizures during *SE* and possibly less pronounced neurodegeneration compared to the other studies (14). Moreover, they mainly focused on the expression of uPA mRNA (not protein), which was increased during the first 72 hours post-*SE* but had already declined at 100 hours post-*SE* (14). Our study focused on the expression of active proteases at later time points post-*SE*. Based on these studies we hypothesised that the decreased [¹¹¹In]MICA-401 binding might be explained by neuronal loss. Consequently, we assessed the extent of neuronal loss in the KASE model. Indeed, neuronal loss was observed in several brain regions that exhibited a decreased [¹¹¹In]MICA-401 binding. However, while the decrease in levels of active uPA/KLK8 clearly progressed in KASE rats, with only few regions affected at 7 days post-*SE* and many more regions at the chronic time point, no such spatiotemporal profile was observed for the neuronal loss in these animals. Extensive neuronal loss was already overt in all investigated brain regions except the granule cell layer of the dentate gyrus at 7 days post-*SE* and was not more pronounced or widespread at the chronic time point. At the chronic time point, a trend for a decreased area fraction of NeuN staining was seen in the granule cell layer of dentate gyrus, but at the same time, a trend for an increased area of the granule cell layer of the dentate gyrus was observed. The decreased area fraction in the dentate gyrus may not necessarily reflect true cell loss, but might point to granule cell dispersion, which would indeed result in a less compact and broader granule cell layer of the dentate gyrus. No correlation could be established between the level of [¹¹¹In]MICA-401 binding and neuronal loss in all investigated brain regions at any given time point. We must therefore conclude that neuronal degeneration does not fully explain the observed decrease in levels of active uPA and KLK8.

Another possible explanation for the decreased levels of active uPA and KLK8 is a decreased neuronal activity due to hypometabolism, which is known to occur following *SE* (20-26) and CCI-injury (27) and which affects more brain regions than just those that are marked by severe neuronal loss. A decreased neuronal activity can result in a decreased expression and activity of uPA and KLK8 as well as of upstream activators of these proteases, which all contribute to a lower binding of [¹¹¹In]MICA-401. However, while cerebral glucose hypometabolism is widespread in the acute phase after *SE*, persistent hypometabolism in the chronic phase is less pronounced and less widespread than in the acute phase (20-23, 25, 26). On the contrary, we observed a distinct progression of uPA/KLK8 decrease in the KASE model. Hypometabolism can therefore not completely explain the observed progressive decrease in levels of active uPA and KLK8.

5.2. Hippocampal decrease in [¹¹¹In]MICA-401 binding is correlated with seizure outcome in a TLE model

Interestingly, the hippocampal decrease in [¹¹¹In]MICA-401 binding was correlated with the number of seizures in the chronic phase of the KASE model. Our results also show that this decrease in levels of active uPA and KLK8 is already present in the temporal lobe in the early phase of the model. It would therefore be very interesting to have a radiotracer that can be used for *in vivo* assessment of uPA/KLK8, in order to investigate whether the early decrease in levels of active uPA and KLK8 correlates with chronic seizure burden. This would allow us to investigate whether uPA/KLK8 can serve as a prognostic biomarker for the disease outcome following *SE*. Whether the widespread decrease in levels of active uPA and KLK8 is the cause or the consequence of the seizures or simply an epiphenomenon cannot be

inferred from this study. More research is warranted to investigate the precise relationship of the uPA/KLK8 decrease and the SRS. Regardless of the exact sequence of events, a decrease of active uPA and KLK8 will affect the extracellular matrix and contribute to the pathophysiology of the disease. It has been suggested that uPA plays a neuroprotective role following epileptogenic insults. Indeed, lack of uPA in mice resulted in more neurodegeneration and less neurogenesis after KASE (17, 28), as well as in a bigger lesion and a worse behavioural outcome following CCI-injury (29, 30). However, in this study no correlation was observed between uPA/KLK8 expression and neuronal loss. Other studies have shown that uPA is necessary for synaptic remodelling, repair and recovery following different kinds of injury (31-34). A pronounced decrease in uPA expression following KASE might result in the failure to initiate the appropriate repair mechanisms, leading to a worse behavioural phenotype. However, uPA deficiency did not have an effect on epilepsy phenotype following KASE nor epileptogenesis following CCI injury in mice (28, 35). On the other hand, deficiency of KLK8 did result in increased seizure susceptibility to kainic acid (36, 37). It has been shown that KLK8 regulates the balance between excitation and inhibition in hippocampus and inhibits pyramidal neuron hyperexcitability through its regulation of parvalbumin-expressing interneuron activity via NRG1-ErbB4 signaling (37, 38). Thus, a decrease in KLK8 expression following an insult may lead to decreased activity of GABAergic interneurons and increased pyramidal neuron activity, resulting in increased seizure activity. We hypothesise that a more pronounced decreased expression of KLK8, rather than uPA, may be responsible for the increased seizure frequency in KASE rats observed in this study.

5.3. [¹¹¹In]MICA-401 does not penetrate the intact blood-brain barrier

Our *ex vivo* autoradiography assay revealed an opposite trend compared to the *in vitro* autoradiography assay. An increased tracer uptake was observed in perilesional cortex and ipsilateral hippocampus of CCI rats in the *ex vivo* autoradiography assay, while a decreased binding of the radiotracer had been established in perilesional cortex and ipsilateral dentate gyrus in the *in vitro* autoradiography assay. We confirmed that these brain regions exhibit a disrupted BBB with the Evans blue BBB permeability assay and could therefore infer that we were most likely merely observing local BBB leakage, which allowed regional accumulation of the otherwise non-permeable radiotracer in these brain regions. Indeed, the radiotracer has an unfavourable $\log D_{7.4}$ (-2.73 ± 0.01) for BBB penetration (6), which limits its *in vivo* application. The radiotracer may be useful to implement in animal models with a consistent BBB injury where an altered activity of uPA/KLK8 is to be expected. However, one cannot compare results with healthy controls. One can only compare the difference of active uPA/KLK8 levels between subjects of the disease model, preferably after correcting for possible interanimal variability in BBB disruption. Another possibility to implement the radiotracer in *in vivo* assays of active uPA/KLK8 levels is to disrupt the BBB using e.g. mannitol or focused ultrasound in order to enhance the delivery of the radiotracer into the brain. Tracer accumulation, as well as Evans blue, was observed in the ventricles of both sham and CCI rats, which is due to the higher permeability of the blood-cerebrospinal fluid barrier at the choroid plexus as compared to the BBB (39).

Finally, this study underlines the importance of performing *in vitro* autoradiography experiments in combination with *in vivo* or *ex vivo* assays,

which might otherwise lead to incorrect interpretations of the *in vivo/ex vivo* assays.

5.4. Limitations of the study

In the current study we used healthy male age-matched Sprague-Dawley rats as controls for the KASE rats at the chronic time point, rather than controls that underwent electrode implantation and vEEG monitoring like the KASE rats. Although we only used epidural electrodes and no depth electrodes, some damage to the dura and possibly the superficial parietal cortex might have occurred in the KASE rats with concomitant alterations in the extracellular matrix, which might have contributed to the observed decreases in levels of active uPA/KLK8. However, in this study we clearly showed that decreases in uPA/KLK8 were already present in the early phase post-*SE* when neither KASE nor control rats underwent electrode implantation. Moreover, in the chronic phase post-*SE*, decreased levels of active uPA/KLK8 were observed in all investigated brain regions, which is unlikely solely due to the presence of epidural electrodes. Additionally, we observed that the chronic KASE rats had no neuronal loss in parietal cortex at the investigated level, indicating that the electrodes did not induce pronounced damage.

6. Conclusions

Our study showed a (sub)acute decrease in levels of active uPA/KLK8 in the temporal lobe in a TLE model and in perilesional cortex and dentate gyrus in a TBI model. In the TLE model this decrease in active uPA/KLK8 was even more pronounced and widespread in the chronic phase of the model, when SRS had developed. Moreover, the hippocampal decrease in [¹¹¹In]MICA-401

binding correlated with the severity of the epilepsy phenotype in this disease model, which suggests that analysis of reduced levels of active uPA/KLK8 might represent a novel biomarker candidate for epilepsy severity. *In vivo* applications of the radiotracer are currently limited due to its incapacity to cross the intact BBB. Different strategies to improve the delivery of the radiotracer into the brain are under consideration. This will allow us to determine whether the (sub)acute decrease in active uPA/KLK8 can predict the epilepsy phenotype in animal models of acquired epilepsy.

Acknowledgements

We thank Krystyna Szewczyk, Philippe Joye and Ingmar Stuyver for their excellent technical support and Dr. Tamuna Bolkvadze for her help in setting up the CCI model. Human and rat KLK8 and KLK4 were kindly donated by Prof. Viktor Magdolen, Klinische Forschergruppe der Frauenklinik der TU München Klinikum rechts der Isar. We are grateful to UCB Biopharma and in particular Georges Mairet-Coello, Mathieu Schmitt and Tania Deprez for the use of the slide scanner. This study was supported by ERA-NET NEURON/Research Foundation Flanders GA00913N, the Special Fund for Research of the University of Antwerp (BOF-UA), the Industrial Research Fund of the University of Antwerp (IOF-UA), the Agency for Innovation by Science and Technology (IWT) with a Strategic Basic Research (SBO) grant (ChemProTools) and the Hercules Foundation Flanders with medium-scale research infrastructure. The Laboratory of Medicinal Chemistry belongs to the Department of Pharmaceutical Sciences and is a partner of the Antwerp Drug Discovery Network (www.ADDN.be). Stephan Missault has a PhD fellowship of the Research Foundation Flanders (11K3714N/11K3716N).

Key Point Box

- The radiotracer [^{111}In]MICA-401 has a high affinity for active urokinase-type plasminogen activator (uPA) and kallikrein-related peptidases 4 and 8 (KLK4/8).
- *Post-mortem* [^{111}In]MICA-401 binding reveals decreased levels of active uPA/KLK8 in brain following *status epilepticus* and traumatic brain injury.
- *Post-mortem* [^{111}In]MICA-401 binding correlates with seizure burden in a model of temporal lobe epilepsy.
- *In vivo* application of [^{111}In]MICA-401 is currently limited due to its incapacity to cross the intact blood-brain barrier.

7. References

1. Ngugi AK, Bottomley C, Kleinschmidt I, Sander JW, Newton CR (2010): Estimation of the burden of active and life-time epilepsy: a meta-analytic approach. *Epilepsia*. 51:883-890.
2. Eadie MJ (2012): Shortcomings in the current treatment of epilepsy. *Expert review of neurotherapeutics*. 12:1419-1427.
3. Lukasiuk K, Wilczynski GM, Kaczmarek L (2011): Extracellular proteases in epilepsy. *Epilepsy Res*. 96:191-206.
4. Pitkanen A, Nodde-Ekane XE, Lukasiuk K, Wilczynski GM, Dityatev A, Walker MC, et al. (2014): Neural ECM and epilepsy. *Progress in brain research*. 214:229-262.
5. Shiosaka S (2004): Serine proteases regulating synaptic plasticity. *Anat Sci Int*. 79:137-144.
6. Vangestel C, Thomae D, Van Soom J, Ides J, Wyffels L, Pauwels P, et al. (2016): Preclinical evaluation of [¹¹¹In]MICA-401, an activity-based probe for SPECT imaging of in vivo uPA activity. *Contrast Media Mol Imaging*.
7. Joossens J, Ali OM, El-Sayed I, Surpateanu G, Van der Veken P, Lambeir AM, et al. (2007): Small, potent, and selective diaryl phosphonate inhibitors for urokinase-type plasminogen activator with in vivo antimetastatic properties. *Journal of medicinal chemistry*. 50:6638-6646.
8. Amhaoul H, Hamaide J, Bertoglio D, Reichel SN, Verhaeghe J, Geerts E, et al. (2015): Brain inflammation in a chronic epilepsy model: Evolving pattern of the translocator protein during epileptogenesis. *Neurobiol Dis*. 82:526-539.
9. Amhaoul H, Ali I, Mola M, Van Eetveldt A, Szewczyk K, Missault S, et al. (2016): P2X7 receptor antagonism reduces severity of spontaneous seizures in a chronic model of temporal lobe epilepsy. *Neuropharmacology*.
10. Dedeurwaerdere S, van Raay L, Morris MJ, Reed RC, Hogan RE, O'Brien TJ (2011): Fluctuating and constant valproate administration gives equivalent seizure control in rats with genetic and acquired epilepsy. *Seizure*. 20:72-79.
11. Gorter JA, Van Vliet EA, Rauwerda H, Breit T, Stad R, van Schaik L, et al. (2007): Dynamic changes of proteases and protease inhibitors revealed by microarray analysis in CA3 and entorhinal cortex during epileptogenesis in the rat. *Epilepsia*. 48 Suppl 5:53-64.
12. Lahtinen L, Lukasiuk K, Pitkanen A (2006): Increased expression and activity of urokinase-type plasminogen activator during epileptogenesis. *The European journal of neuroscience*. 24:1935-1945.

13. Lukasiuk K, Kontula L, Pitkanen A (2003): cDNA profiling of epileptogenesis in the rat brain. *Eur J Neurosci.* 17:271-279.
14. Masos T, Miskin R (1997): mRNAs encoding urokinase-type plasminogen activator and plasminogen activator inhibitor-1 are elevated in the mouse brain following kainate-mediated excitation. *Brain Res Mol Brain Res.* 47:157-169.
15. Okabe A, Momota Y, Yoshida S, Hirata A, Ito J, Nishino H, et al. (1996): Kindling induces neuropsin mRNA in the mouse brain. *Brain research.* 728:116-120.
16. Momota Y, Yoshida S, Ito J, Shibata M, Kato K, Sakurai K, et al. (1998): Blockade of neuropsin, a serine protease, ameliorates kindling epilepsy. *The European journal of neuroscience.* 10:760-764.
17. Cho E, Lee KJ, Seo JW, Byun CJ, Chung SJ, Suh DC, et al. (2012): Neuroprotection by urokinase plasminogen activator in the hippocampus. *Neurobiology of disease.* 46:215-224.
18. He XP, Shiosaka S, Yoshida S (2001): Expression of neuropsin in oligodendrocytes after injury to the CNS. *Neuroscience research.* 39:455-462.
19. Tomizawa K, He X, Yamanaka H, Shiosaka S, Yoshida S (1999): Injury induces neuropsin mRNA in the central nervous system. *Brain research.* 824:308-311.
20. Goffin K, Van Paesschen W, Dupont P, Van Laere K (2009): Longitudinal microPET imaging of brain glucose metabolism in rat lithium-pilocarpine model of epilepsy. *Experimental neurology.* 217:205-209.
21. Guo Y, Gao F, Wang S, Ding Y, Zhang H, Wang J, et al. (2009): In vivo mapping of temporospatial changes in glucose utilization in rat brain during epileptogenesis: an 18F-fluorodeoxyglucose-small animal positron emission tomography study. *Neuroscience.* 162:972-979.
22. Jupp B, Williams J, Binns D, Hicks RJ, Cardamone L, Jones N, et al. (2012): Hypometabolism precedes limbic atrophy and spontaneous recurrent seizures in a rat model of TLE. *Epilepsia.* 53:1233-1244.
23. Lee EM, Park GY, Im KC, Kim ST, Woo CW, Chung JH, et al. (2012): Changes in glucose metabolism and metabolites during the epileptogenic process in the lithium-pilocarpine model of epilepsy. *Epilepsia.* 53:860-869.
24. Park GY, Lee EM, Seo MS, Seo YJ, Oh JS, Son WC, et al. (2015): Preserved Hippocampal Glucose Metabolism on 18F-FDG PET after Transplantation of Human Umbilical Cord Blood-derived Mesenchymal Stem Cells in Chronic Epileptic Rats. *Journal of Korean medical science.* 30:1232-1240.

25. Shiha AA, de Cristobal J, Delgado M, Fernandez de la Rosa R, Bascunana P, Pozo MA, et al. (2015): Subacute administration of fluoxetine prevents short-term brain hypometabolism and reduces brain damage markers induced by the lithium-pilocarpine model of epilepsy in rats. *Brain research bulletin*. 111:36-47.
26. Zhang L, Guo Y, Hu H, Wang J, Liu Z, Gao F (2015): FDG-PET and NeuN-GFAP immunohistochemistry of hippocampus at different phases of the pilocarpine model of temporal lobe epilepsy. *International journal of medical sciences*. 12:288-294.
27. Park BN, Yoon JK, An YS (2013): Bone marrow mesenchymal stem cell transplantation in acute brain trauma. Improvement of brain glucose metabolism in a rat model. *Nuklearmedizin Nuclear medicine*. 52:192-197.
28. Lahtinen L, Nnode-Ekane XE, Barinka F, Akamine Y, Esmaeili MH, Rantala J, et al. (2010): Urokinase-type plasminogen activator regulates neurodegeneration and neurogenesis but not vascular changes in the mouse hippocampus after status epilepticus. *Neurobiol Dis*. 37:692-703.
29. Morales D, McIntosh T, Conte V, Fujimoto S, Graham D, Grady MS, et al. (2006): Impaired fibrinolysis and traumatic brain injury in mice. *J Neurotrauma*. 23:976-984.
30. Rantala J, Kemppainen S, Nnode-Ekane XE, Lahtinen L, Bolkvadze T, Gurevicius K, et al. (2015): Urokinase-type plasminogen activator deficiency has little effect on seizure susceptibility and acquired epilepsy phenotype but reduces spontaneous exploration in mice. *Epilepsy Behav*. 42:117-128.
31. Wu F, Catano M, Echeverry R, Torre E, Haile WB, An J, et al. (2014): Urokinase-type plasminogen activator promotes dendritic spine recovery and improves neurological outcome following ischemic stroke. *The Journal of neuroscience : the official journal of the Society for Neuroscience*. 34:14219-14232.
32. Minor KH, Seeds NW (2008): Plasminogen activator induction facilitates recovery of respiratory function following spinal cord injury. *Molecular and cellular neurosciences*. 37:143-152.
33. Seeds N, Mikesell S, Vest R, Bugge T, Schaller K, Minor K (2011): Plasminogen activator promotes recovery following spinal cord injury. *Cellular and molecular neurobiology*. 31:961-967.
34. Karagyaur M, Dyikanov D, Makarevich P, Semina E, Stambolsky D, Plekhanova O, et al. (2015): Non-viral transfer of BDNF and uPA stimulates peripheral nerve regeneration. *Biomedicine & pharmacotherapy = Biomedecine & pharmacotherapie*. 74:63-70.

35. Bolkvadze T, Rantala J, Puhakka N, Andrade P, Pitkanen A (2015): Epileptogenesis after traumatic brain injury in Plau-deficient mice. *Epilepsy & behavior : E&B*. 51:19-27.
36. Davies B, Kearns IR, Ure J, Davies CH, Lathe R (2001): Loss of hippocampal serine protease BSP1/neuropsin predisposes to global seizure activity. *The Journal of neuroscience : the official journal of the Society for Neuroscience*. 21:6993-7000.
37. Kawata M, Morikawa S, Shiosaka S, Tamura H (2017): Ablation of neuropsin-neuregulin 1 signaling imbalances ErbB4 inhibitory networks and disrupts hippocampal gamma oscillation. *Translational psychiatry*. 7:e1052.
38. Tamura H, Kawata M, Hamaguchi S, Ishikawa Y, Shiosaka S (2012): Processing of neuregulin-1 by neuropsin regulates GABAergic neuron to control neural plasticity of the mouse hippocampus. *J Neurosci*. 32:12657-12672.
39. Cipolla MJ (2009): *The Cerebral Circulation*. San Rafael (CA).

6

*Neuroimaging of subacute brain inflammation
and microstructural changes predicts long-term
functional outcome after experimental traumatic
brain injury*

Submitted to Journal of Neurotrauma

1. Abstract

There is currently a lack of prognostic biomarkers to predict the different sequelae following traumatic brain injury (TBI). The present study investigated the hypothesis that subacute neuroinflammation and microstructural changes correlate with chronic TBI deficits. Rats were subjected to Controlled Cortical Impact (CCI) injury, sham surgery or skin incision (naïve). CCI-injured (n=18) and sham-operated rats (n=6) underwent positron emission tomography (PET) imaging with the translocator protein (TSPO) radioligand [¹⁸F]PBR111 and diffusion tensor imaging (DTI) in the subacute phase (<3 weeks post-injury) to quantify inflammation and microstructural alterations. CCI-injured, sham-operated and naïve rats (n=8) underwent behavioural testing in the chronic phase (5.5-10 months post-injury): open field and sucrose preference tests, two one-week video-EEG monitoring periods, pentylenetetrazole seizure susceptibility tests, and a Morris water maze test. *In vivo* imaging revealed pronounced neuroinflammation, decreased fractional anisotropy and increased diffusivity in perilesional cortex and ipsilesional hippocampus of CCI-injured rats. Behavioural analysis revealed disinhibition, anhedonia, increased seizure susceptibility and impaired learning in CCI-injured rats. Subacute TSPO expression and changes in DTI metrics significantly correlated with several chronic deficits (Pearson's $|r| = 0.50-0.90$). Specific PET and DTI parameters had good sensitivity and specificity (area under the ROC curve = 0.83-0.89) to distinguish between TBI animals with and without particular behavioural deficits. Depending on the investigated behavioural deficit, PET or DTI data alone, or the combination, could satisfactorily predict the variability in functional outcome data (adjusted $R^2 = 0.50-1.00$). Taken

together, both TSPO PET and DTI seem promising prognostic biomarkers to predict different chronic TBI sequelae.

Key words: positron emission tomography, diffusion tensor imaging, posttraumatic epilepsy, TSPO PET, MRI

2. Introduction

Traumatic brain injury (TBI) is a major public health and socioeconomic problem, which affects all ages and populations throughout the world. TBI is defined as any kind of brain injury due to external force and is a leading cause of mortality and morbidity worldwide. It is commonly referred to as a silent epidemic, partly due to the public unawareness of the major long-lasting consequences that can occur following TBI including posttraumatic epilepsy, cognitive problems and psychiatric deficits (1, 2). Prognostic models have been developed to predict the outcome following TBI, but a major limitation in the construction of these models was that they only used mortality and unfavourable outcome (dead, vegetative state and severe disability) as possible outcomes, while the prediction of the different sequelae that can develop following TBI remains unaddressed (3, 4). This dichotomisation evidently leads to a loss of information and a reduced sensitivity of the prognostic models (5). Moreover, these models use rather unspecific predictors such as age, motor score, and pupillary reactivity (3, 4). A more comprehensive approach to identify specific predictors may be to investigate the link between a potential prognostic biomarker that is linked to the underlying neurobiological response to TBI and the development of chronic deficits. Moreover, while the existing prognostic models have been shown to be of value for the classification of patients, great caution is required when applying them to determine the individual risk of a single

patient (6). The identification of specific prognostic biomarkers would be of major value to identify patients that will develop a certain chronic consequence. Additionally, they might provide insight into the underlying neurobiological mechanisms that give rise to the TBI-related sequelae and open new avenues towards treatment and possibly prevention of these secondary consequences.

Inflammation is a very important secondary injury mechanism in TBI. Upon initial injury, a neuroinflammatory response is elicited, which involves both resident and peripheral immune cells. This response is complex and can have both beneficial and detrimental consequences for the neurons, depending on the timing and the cell types involved, as well as the molecular context in which they act (7, 8). Several inflammatory mediators have been demonstrated to exhibit epileptogenic and ictogenic properties and might be involved in the development of posttraumatic epilepsy (7). Neuroinflammation has also been demonstrated to play an important role in cognitive dysfunction and psychiatric deficits following TBI. Inhibition of (sub)acute microglial activation and suppression of (sub)acute release of proinflammatory cytokines and chemokines has been shown to improve the cognitive outcome following experimental TBI (9-11). Acute inflammatory biomarker profiles in cerebrospinal fluid of TBI patients have been shown to predict the risk for developing depression (12). Evidence suggests that TBI induces microglial priming, which renders microglia more susceptible to a secondary inflammatory stimulus. An exaggerated inflammatory response to a secondary insult has been shown to concur with cognitive impairment and depressive behaviour (13, 14).

Positron emission tomography (PET) radioligands that bind to the translocator protein 18 kDa (TSPO), which is highly upregulated on the outer mitochondrial membrane of activated microglia (amongst other cell types), are ideally suited to assess brain inflammation *in vivo* and to investigate whether early inflammation following brain insults can act as a prognostic biomarker for the long-term functional outcome. We have recently shown that *in vivo* assessment of TSPO expression in the early phase following *status epilepticus* could predict the frequency of chronic spontaneous recurrent seizures and behavioural comorbidities in a rat model of temporal lobe epilepsy (15). Few *in vivo* imaging studies with TSPO radioligands have been performed in TBI models. Wang et al. reported a peak in TSPO ligand binding at 6 days after controlled cortical impact (CCI) injury, which decreased gradually to near normal levels at 28 days post-injury (16). Yu et al. also observed a peak in TSPO ligand binding at 1 week after fluid percussion injury, which decreased during the next eight weeks of observation (17).

Diffusion imaging has emerged as a very powerful tool to characterise microstructural changes in both grey and white matter following TBI. Both diffusion-weighted imaging (DWI) and diffusion tensor imaging (DTI) have been proven to be highly sensitive techniques to assess alterations in tissue microstructure and diffuse axonal injury after TBI (18-21). The average diffusion (average of three diffusion coefficients in three orthogonal directions) has been investigated as a potential prognostic biomarker of the long-term functional outcome following experimental TBI. Kharatishvili et al. showed that average diffusion in the ipsilesional hippocampus at both early and chronic time-points following lateral fluid percussion injury (FPI)

correlated with pentylenetetrazole (PTZ)-evoked seizure susceptibility at 12 months post-injury (22). In an extended reanalysis of these data, Immonen et al. observed that average diffusion in the perilesional cortex and thalamus at 2 months post-injury showed the highest predictive value for increased seizure susceptibility at 12 months post-injury (23). In another study from Immonen and colleagues it was demonstrated that average diffusion in the ipsilateral hippocampus at 23 days following FPI correlated with Morris water maze performance at 7 months post-TBI (24). Frey et al. showed that the (sub)acute apparent diffusion coefficient (DWI in one direction) in injured cortex after FPI correlated with chronic kainate-evoked seizure susceptibility (25). Several clinical studies also indicate that DTI can be useful for the prognosis of TBI (reviewed in (18)).

In this study we have first of all investigated whether i) subacute brain inflammation, assessed by *in vivo* PET imaging with the TSPO ligand [¹⁸F]PBR111, and ii) subacute microstructural changes, assessed by *in vivo* DTI, correlated with the different chronic sequelae that may occur following TBI, including psychiatric deficits, spontaneous recurrent seizures, increased seizure susceptibility and visuospatial learning and memory deficits. Next, we have evaluated the sensitivity and specificity of these parameters in distinguishing between TBI animals with and without particular deficits. Finally, we have investigated whether PET or DTI data alone, or the combination of these two imaging modalities, could best predict the variability in the different behavioural outcome parameters.

3. Materials and methods

3.1. Animals

Sixty-three male Sprague-Dawley rats were purchased from Envigo (previously Harlan Laboratories), the Netherlands. Animals were group-housed in a temperature- and humidity-controlled room on a 12 hour light-dark cycle with standard food and water available ad libitum until the moment of electrode implantation. From this point onward, animals were single-housed. Animals were treated in accordance with the EU directive 2010/63/EU. Animal experiments were approved by the animal ethics committee of the University of Antwerp, Belgium (ECD 2012-62).

3.2. Study design

The study design of the longitudinal *in vivo* imaging and behavioural study is shown in Fig.6-1. A total of 8 naïve, 7 sham-operated and 19 CCI-injured rats were included in this study. Six sham-operated and 18 CCI-injured rats were subjected to *in vivo* imaging (PET/CT and MRI) in the subacute phase following TBI. PET imaging was performed at 7 and 21 days post-injury and MRI at 4 and 18 days post-injury. One sham-operated rat and one CCI-injured rat were scanned at the first time-point, but died before the second time-point. Eight naïve, six sham-operated and 18 CCI-injured rats (including all rats that had undergone *in vivo* imaging in the subacute phase) underwent behavioural testing in the chronic period (5.5-10 months post-injury). In total, 17 CCI-injured rats were used to investigate a possible relationship between early brain inflammation and microstructural changes and chronic behavioural deficits.

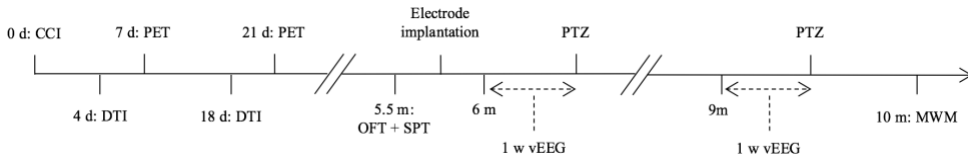


Fig.6-1. Study design. Young adult male Sprague-Dawley rats were subjected to Controlled Cortical Impact (CCI) injury, sham surgery or skin incision. CCI-injured ($n=18$) and sham-operated rats ($n=6$) underwent positron emission tomography (PET) imaging with the TSPO radioligand [^{18}F]PBR111 at 7 days and 21 days post-injury, as well as diffusion tensor imaging (DTI) at 4 days and 18 days post-injury. CCI-injured ($n=18$), sham-operated ($n=6$) and naïve rats ($n=8$) were subjected to chronic behavioural testing: an open field test (OFT) and sucrose preference test (SPT) at 5.5 months post-injury, one-week continuous video-EEG (vEEG) monitoring periods at 6 and 9 months post-injury, followed by pentylenetetrazole (PTZ) seizure susceptibility assays, and a Morris water maze (MWM) test at 10 months post-injury.

Additionally, a separate cohort consisting of 9 naïve, 10 sham-operated and 10 CCI-injured rats was subjected to an open field test at 2 months and a PTZ seizure susceptibility assay at 6 months post-injury to corroborate observations from the other cohort.

3.3. Controlled Cortical Impact-induced Traumatic Brain Injury

CCI-injury was performed as previously described (26). Eight-week old rats (mean \pm SEM: 281 ± 3 g) were anaesthetised with isoflurane in oxygen (5% induction, 2.5% maintenance; Forene; Abbott, Belgium). During the surgery, the animal was kept warm by means of a temperature-controlled heating pad. A craniectomy of 5 mm diameter was performed with a trephine over the left parietal cortex (midway between bregma and lambda, bordering the lateral edge) without damaging the dura. CCI was done with the Leica Impact One device (Leica Biosystems, USA) using the following parameters: flat tip of 3 mm diameter, impact angle 18° , impact velocity 4 m/s, depth of penetration 2.5 mm, dwell-time 500 ms ($n = 19$). After impact, the cranial

window was sealed with a piece of plastic, and skin sutured. Sham-operated animals were subjected to the same surgery, but were not exposed to impact ($n = 7$). Since previous work has shown that craniotomised animals can display behavioural deficits compared to naïve animals, naïve rats were included in this study as well (27). Naïve animals received anaesthesia and a skin incision, but no craniectomy ($n = 8$). Naïve rats were treated in exactly the same way as sham-operated and CCI-injured rats, but did not undergo *in vivo* imaging.

3.4. PET imaging with [^{18}F]PBR111

Radiosynthesis of the TSPO radioligand [^{18}F]PBR111 was performed on a FluorSynton I automated synthesis module (Comecer, the Netherlands) according to Bourdier et al. (28). PET scans were performed on an Inveon PET/CT scanner (Siemens Preclinical Solution, USA) as previously described with a few minor modifications (15). Rats were anaesthetised with isoflurane in oxygen (5% induction, 2-2.5% maintenance; Abbott, Belgium), after which 8.6 ± 0.4 MBq radiotracer (molar activity: 149.8 ± 11.0 GBq/ μmol) was administered by tail vein injection in a volume of 0.5 ml. During the uptake period of 45 min, the animal remained anaesthetised and was kept warm by means of a temperature-controlled heating pad. Next, animals were subjected to a static PET scan of 15 min, followed by a 7 min CT scan. At 50 min post-injection, an arterial blood sample was collected from the tail artery for radiometabolite analysis according to Katsifis et al. (29). During the scanning session, breathing rate and temperature were constantly monitored (Minerve, France) and maintained within normal physiological ranges. The temperature of the animal was maintained by supplying heated air through the imaging cell. PET images were

reconstructed using a 2D ordered subset expectation maximization algorithm (4 iterations, 16 subsets) after Fourier rebinning (30, 31). Normalisation, dead time, random, CT-based attenuation, and scatter corrections were applied.

Image processing was done using PMOD v3.3 (PMOD Technologies, Switzerland). The CT images were co-registered to three-dimensional (3D) T₂-weighted MR images that were acquired earlier that week (see below) by manually guided automatic rigid matching. This CT to MR transformation was used to co-register the PET images to the MR images. The following volumes of interest (VOIs) were manually drawn on each individual 3D MR scan: lesion (hyperintense on the T₂-weighted MR image), perilesional cortex, contralateral cortex, ipsilesional hippocampus and contralesional hippocampus. VOI statistics in kBq/cc were generated and used to calculate the standardised uptake values (SUV: average tissue radioactivity concentration [kBq/cc] / injected dose [kBq] / body weight [g]). For correlation analyses, we also calculated the relative change in SUV over time in CCI-injured rats according to the following formula:

$$\% \text{ change} = \left(\frac{SUV \text{ at } 21 \text{ days} - SUV \text{ at } 7 \text{ days}}{SUV \text{ at } 7 \text{ days}} \right) * 100$$

One CCI-injured rat died during the CT scan at the first time-point. One sham-operated rat got an infection of the tail following the first scanning time-point and was subsequently sacrificed. These rats were not scanned at the second time-point (neither PET/CT or MRI).

3.5. *In vivo* MRI: DTI and 3D T₂-weighted anatomical MRI

Rats were anaesthetised with isoflurane in a mixture of O₂ (30%) and N₂ (70%) (5% induction, 2-2.5% maintenance; Abbott, Belgium). Breathing rate and blood oxygenation were monitored constantly using a pressure sensitive pad and a pulse oximeter (MR-compatible Small Animal Monitoring and Gating System, SA Instruments, Inc., USA), and maintained between normal physiological ranges. The temperature of the animals was monitored by means of a rectal probe and maintained at (37 ± 0.5) °C through a feedback-controlled warm air system (MR-compatible Small Animal Heating System, SA Instruments, Inc., USA).

Data were acquired on a 7T PharmaScan with Paravision 5.1 software using a standard Bruker crosscoil set-up with a quadrature volume coil and a quadrature surface coil designed for rats (Bruker, Germany). The rats' head was immobilised in an MR-compatible stereotaxic device using blunt earplugs and a tooth bar. Three orthogonal multi-slice Turbo Rapid Acquisition with Relaxation Enhancement (RARE) T₂-weighted images were acquired to ensure consistent slice positioning between DTI data of different animals. A field map was acquired to measure field homogeneity, followed by local shimming, which corrects for the measured inhomogeneity in a rectangular volume within the brain. Coronal diffusion-weighted (DW) images were acquired with a 2-shot spin-echo echo planar imaging (SE-EPI) sequence with 60 optimally spread diffusion gradient directions. Fifteen non-DW b₀ images (b-value 0 s/mm²; 5 b₀ per 20 DW images) were acquired. The imaging parameters were: repetition time (TR) 7500 ms, echo time (TE) 26 ms, diffusion gradient pulse duration δ 4 ms, diffusion gradient separation Δ 12 ms, b-value 800 s/mm², 20 slices of 0.7 mm (limited to

cerebrum), 0.1 mm slice gap, scan duration approx. 20 min. The FOV was (30 x 30) mm² and the matrix size [128 x 128], resulting in pixel dimensions of (0.234 x 0.234) mm². Following DTI, a 3D RARE T₂-weighted scan was acquired with the following parameters: TR 3185 ms, TE 11 ms (TE_{eff} 44 ms), RARE factor 8, 2 averages, FOV (29.0 x 16.0 x 10.2) mm³, acquisition matrix [256 x 64 x 50], spatial resolution (0.113 x 0.250 x 0.204) mm³, scan duration approx. 45 min.

Image processing was performed with SPM12 in MATLAB 2014a (MathWorks, USA). First, images were realigned to correct for subject motion using the diffusion toolbox in SPM12. A rigid registration was performed between the b₀ images, which was followed by an extended registration taking also all DW images into account. Next, the diffusion tensor was estimated and the DTI parameter maps were computed (i.e., fractional anisotropy (FA), mean diffusivity (MD), axial diffusivity (AD) and radial diffusivity (RD)). Finally, the DTI parameter maps were smoothed in plane using a Gaussian kernel with full width at half maximum (FWHM) of twice the voxel size (FWHM (0.468 x 0.468 x 0.800) mm³). Regions of interest (ROIs) (lesion, perilesional cortex, contralateral cortex, ipsilesional hippocampus and contralesional hippocampus) were manually drawn in Amira 5.4.0 on the average b₀ (T₂-weighted) image of each animal and then adjusted on the individual FA and MD maps to ensure exclusion of white matter and ventricles. For each ROI, the mean value of the different DTI parameters was extracted in Amira 5.4.0. For correlation analyses, the relative change in DTI metrics over time in CCI-injured rats was calculated analogous to the % change in [¹⁸F]PBR111 SUVs above.

One sham-operated rat exhibited very large ventricles at the first scanning time-point as compared to other sham-operated rats and CCI-injured rats, and showed a worse performance in several behavioural assays than the other sham-operated rats. This rat was excluded from the entire analysis. Spontaneous congenital hydrocephalus has been reported in this and other rat strains (32).

3.6. Long-term outcome

3.6.1. Open field test

An open field test was performed to explore the presence of anxiety or disinhibition in CCI-injured rats. Animals were placed in the periphery of a well-lit square arena ((48 x 48) cm²) and allowed to explore the novel environment for 10 min. During this trial, animals were video-tracked with EthoVision XT software (version 10.0, Noldus, the Netherlands). For analysis, the arena was divided in a central zone (inner square, (24 x 24) cm²) and a peripheral zone. The following parameters were calculated: latency to first entry in central zone, number of transitions from periphery to centre, % time spent in centre, % distance moved in centre, total distance moved and mean velocity.

3.6.2. Sucrose preference test

A sucrose preference test was done to assess the presence of anhedonia in the CCI-injured rats. The test was performed as previously described (33). Briefly, animals received two drinking bottles, one filled with water and one with 2% sucrose solution. After 48 h of habituation, the % sucrose preference and total fluid intake were calculated over a test period of 24 h.

3.6.3. Video-EEG: spontaneous recurrent seizures and seizure susceptibility

Electrode implantation. All animals were implanted with six epidural screw electrodes as described before (34), however, with a different positioning. One electrode was implanted rostral to the lesion over the left cortex (between bregma and lesion), two electrodes were implanted over the right cortex: one contralateral to the first electrode and the other opposite to the core of the lesion near the sagittal midline, one electrode was positioned over the left frontal lobe, and two more over the occipital lobe. Electrodes were fixed into a plastic plug (Bilaney Consultants, Plastics One, UK) and secured to the skull using dental cement (Simplex Rapid, Kemdent, UK; Durelon, 3M ESPE, USA) and additional anchor screws. Animals were allowed to recover for at least one week before recording started.

Recording. Animals were subjected to continuous video-EEG (vEEG) recording for two periods of one week, once at 6 months post-injury and once at 9 months post-injury. The week of recording spontaneous epileptiform activity and seizures was each time followed by a PTZ seizure susceptibility test (see below). Animals were connected to a digital EEG acquisition system (Ponemah P3 Plus, Data Sciences International, USA) through a cable system as previously described (34). EEG was recorded from the electrode rostral to the lesion and the contralateral electrode. The occipital electrodes were used as reference and ground electrodes. Due to limited capacity of the recording system, only four out of the eight naïve animals were subjected to continuous vEEG recording at the 6-month time-point. For the same reason, the CCI-injured rat and sham-operated rat that were not subjected to *in vivo* imaging did not undergo vEEG recording at this

time-point. Between the 6-month and 9-month time-points, several animals lost their electrode assembly (4/8 naïve, 1/6 sham, 11/18 CCI). Hence, fewer rats underwent vEEG recording at the 9-month time-point.

Analysis. Video-EEG data were analysed manually using NeuroScore 3.0 (Data Sciences International, USA) as described before (34). For the analysis of the spontaneous epileptiform activity and seizures, we quantified the number and duration of epileptiform discharges (EDs) and seizures per day, as well as the duration of all epileptiform activity (EDs + seizures) per day. An ED was defined as a high-amplitude (equalling at least two times the baseline amplitude) rhythmic discharge containing spikes and/or uniform sharp waves, lasting ≥ 1 s but < 5 s. Most of the observed events were either spike-wave discharges or high-voltage rhythmic spike discharges. A similar event that lasted > 5 s was defined as a seizure. Video-analysis allowed us to classify seizures as purely electrographic events or behavioural seizures, which were scored according to a modified Racine scale as described before (35). In this study, rats were considered epileptic if they experienced two or more unprovoked convulsive seizures (S3-5) (36).

PTZ-evoked seizure susceptibility test. Animals were injected subcutaneously (s.c.) with a single subconvulsive dose (25-30 mg/kg) of PTZ, after which they underwent one hour of vEEG recording, a protocol adapted from (22). For this test, we also quantified the number of spikes, in addition to EDs and seizures. We calculated the latency to first spike, first ED, first seizure (purely electrographic or behavioural) and first convulsive seizure, as well as the number of spikes, EDs, seizures (purely electrographic and behavioural) and convulsive seizures, and finally also the total duration of EDs, all seizures and convulsive seizures. At 6 months post-injury, rats received 25 mg/kg PTZ

(s.c.). Due to the low occurrence of convulsive seizures following this dose and previous reports in the literature that observed a more pronounced difference in the occurrence of convulsive seizures between TBI and control rats with a 30 mg/kg dose (22, 37), we decided to administer 30 mg/kg PTZ (s.c.) at 9 months post-injury. Three rats lost their electrode assembly during the PTZ tests (one CCI rat and one naïve rat at 6 months, one CCI rat at 9 months). They were excluded from the analysis of number of spikes, EDs and seizures, but included in the analysis of latency to first spike, ED and seizure (if recorded). For uniformity/standardisation, all animals received PTZ injections at both 6 and 9 months, even if the animals had previously lost their electrode assembly and no EEG recording could be obtained. However, these were not included in the analysis.

3.6.4. Morris water maze test

Rats were subjected to a Morris water maze (MWM) test to investigate the extent of visuospatial learning and memory deficits in the CCI-injured rats. The test was performed as previously described (38). The experimental set-up consisted of a circular pool (150 cm diameter) filled with white opaque water (kept between 20 and 24°C), containing a submerged round platform (15 cm diameter) and surrounded by visual cues. Prior to the test, rats were dyed black with a non-toxic hair dye to provide contrast with the white pool for video-tracking purposes (EthoVision XT 10.0, Noldus, the Netherlands). The test consisted of a training period (acquisition) of eight days with the platform fixed in one place, and a probe trial (retention) during which the platform was removed from the swimming pool. Every training day consisted of four trials of maximally 120 s each, with the rat starting from a different position for each trial (15 min intertrial interval, semi-random

order for each training day). If the rat could not locate the platform, it was placed on the platform for approximately 10 s before being returned to its home cage. A learning curve was plotted for escape latency and path length to platform (sum of the four daily trials). In addition, we calculated the mean velocity. Four days after finishing the eight-day training period, the platform was removed and a probe trial of 100 s was performed. We calculated the % time spent in the target quadrant (i.e., the quadrant that previously contained the platform), as well as the number of crossings through the previous platform position.

3.7. Statistics

Normal distribution of the data was tested using the D'Agostino-Pearson omnibus normality test. Outlier analyses were performed with the ROUT test. For the analysis of the open field test, sucrose preference test, spontaneous epileptiform activity and seizures at each time-point, seizure susceptibility tests and probe trial of the MWM test, we used Kruskal-Wallis tests to compare the three study groups (naïve, sham, CCI) and Dunn's multiple comparisons test as post-hoc test. When pooling all controls (naïve + sham), we used Mann-Whitney U tests to compare the two groups (control, CCI). For correlation analyses, we used the Pearson correlation test. Chi-square tests for trend were performed to investigate whether the occurrence of convulsive seizures in the PTZ tests was associated with injury (naïve, sham, CCI). For receiver operating characteristic (ROC) curve analysis, CCI-injured animals were divided into two groups for each behavioural outcome parameter: CCI-injured rats with and without a deficit. Depending on the nature of the response, CCI-injured rats with a value higher than the mean + one standard deviation of the naïve rats or a value lower than the

mean - one standard deviation of the naïve rats were considered to have a deficit. These analyses were performed using GraphPad Prism 6. For the analysis of longitudinal data (PET, DTI, spontaneous epileptiform activity and seizures over time, MWM learning curves) we made use of linear mixed models in JMP Pro 13, which allowed us to take animals into account for which a data point was missing. Additionally, linear mixed models are more robust against non-normality of data than repeated-measures ANOVAs. For each data set, we fitted linear mixed models with Group (naïve/sham/CCI), Time (two time-points) and the interaction between Group and Time as fixed effects and either Subject alone (random intercept model, smaller model) or both Subject and Subject*Time as random effects (random slope model, larger model). We tested the necessity for the random slope (Subject*Time) with the likelihood ratio test. If the interaction between Group and Time proved to be significant, we performed the appropriate post-hoc tests. We did Student's t pairwise comparisons and corrected the p-values for the number of comparisons (Bonferroni correction). Finally, we also performed forward stepwise regression analysis in JMP Pro 13 with p-value threshold as stopping rule (prob to enter: 0.25, prob to leave: 0.1). Statistical significance was set at $p \leq 0.05$.

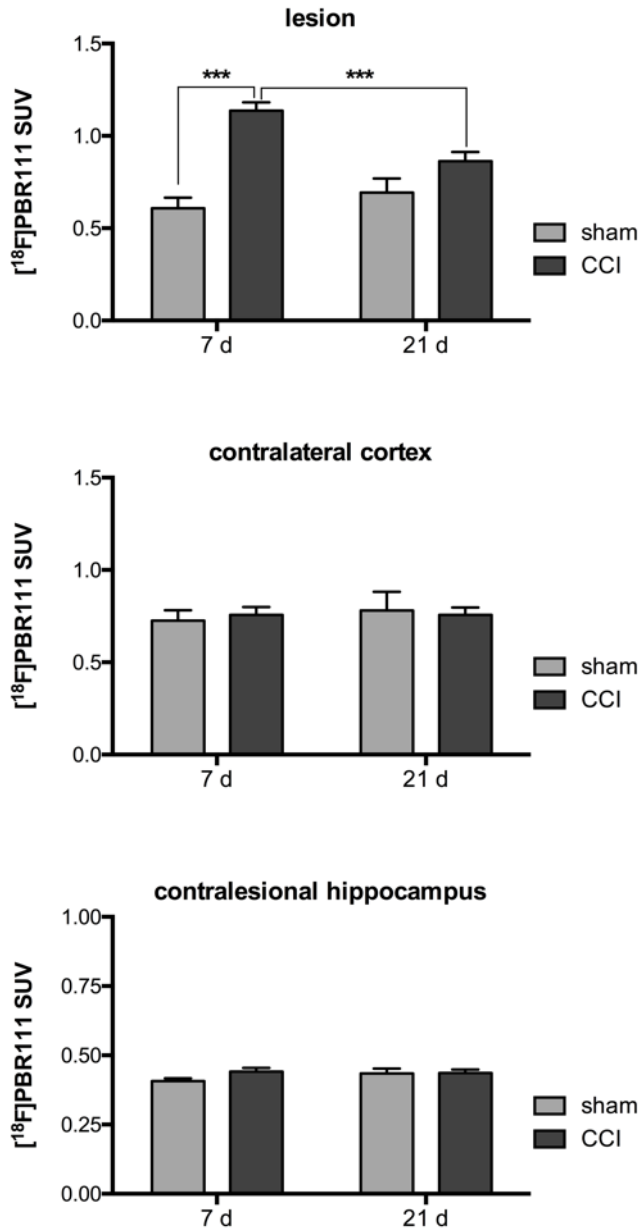
4. Results

4.1. Subacute brain inflammation after CCI-injury

Analysis of the PET scans revealed significantly higher SUVs of TSPO ligand [¹⁸F]PBR111 in the lesion (left parietal cortex, mean \pm SEM volume: 16.43 ± 1.78 mm³), perilesional cortex and ipsilesional hippocampus of CCI-injured rats compared to sham-operated rats, which decreased over time (Fig.6-2A,B; Suppl.Fig.6-1). For each of these brain regions, a significant interaction

between Group and Time ($p \leq 0.01$) was noted. Post-hoc testing revealed a significantly higher SUV for each of these brain regions in CCI-injured rats compared to shams at 7 days post-injury (lesion and ipsilesional hippocampus: $p \leq 0.0001$, perilesional cortex: $p \leq 0.001$). At 21 days post-injury, there was still a significantly higher SUV in the ipsilesional hippocampus of CCI-injured rats vs. shams ($p \leq 0.05$), but the difference was smaller than at 7 days post-injury. In the other brain regions, no significant difference was present anymore at 21 days post-injury. There was a significant decrease in SUVs between 7 days and 21 days post-injury in the lesion, perilesional cortex and ipsilesional hippocampus of CCI-injured rats ($p \leq 0.001$), while in sham-operated rats there was no change in SUV over time. No significant difference in SUVs between CCI-injured and sham-operated rats was observed at any time-point in contralateral brain regions.

Radiometabolite analysis revealed no significant difference in metabolisation of the radiotracer between sham-operated and CCI-injured rats (respectively, $(14.4 \pm 0.9)\%$ and $(15.8 \pm 1.0)\%$ intact tracer in plasma at 50 min post-injection).



Suppl.Fig.6-1. PET imaging with [¹⁸F]PBR111 in CCI-injured rats. [¹⁸F]PBR111 standardised uptake values (SUVs) in the lesion, contralateral cortex and contralesional hippocampus of sham-operated (n=5) and CCI-injured rats (n=18). The [¹⁸F]PBR111 SUV was significantly higher in the lesion of CCI-injured rats compared to shams at 7 days post-injury. The SUV decreased in the lesion over time in CCI-injured rats. There was no significant difference in SUVs in contralateral cortex and contralesional hippocampus between sham-operated and CCI-injured rats at any given time-point. Mean ± SEM is given. ***p≤0.001

4.2. Subacute microstructural alterations after CCI-injury

After CCI-injury, fractional anisotropy (FA) was decreased in the lesion, perilesional cortex and ipsilesional hippocampus at 4 days post-injury compared to shams. At 18 days post-injury, FA was significantly decreased in the lesion, but not in any other brain region (Fig.6-3A,B; Suppl.Fig.6-2A). Linear mixed model analysis showed a significant effect of Group on FA in the lesion ($p \leq 0.0001$), while in the perilesional cortex and ipsilesional hippocampus, a significant interaction between Group and Time (respectively $p \leq 0.0001$ and $p \leq 0.05$) was present. Post-hoc analysis showed a significant difference between sham-operated and CCI-injured rats at 4 days post-injury in perilesional cortex ($p \leq 0.001$) and a trend for ipsilesional hippocampus ($p = 0.06$). In addition, there was a significant difference between 4 and 18 days in CCI-injured rats in the perilesional cortex ($p \leq 0.0001$) and ipsilesional hippocampus ($p \leq 0.05$). Finally, there was also an effect of time on FA in contralateral cortex ($p \leq 0.05$) (Suppl.Fig.6-2A). No significant effect of Group or Time on FA was noted in the contralesional hippocampus (Suppl.Fig.6-2A).

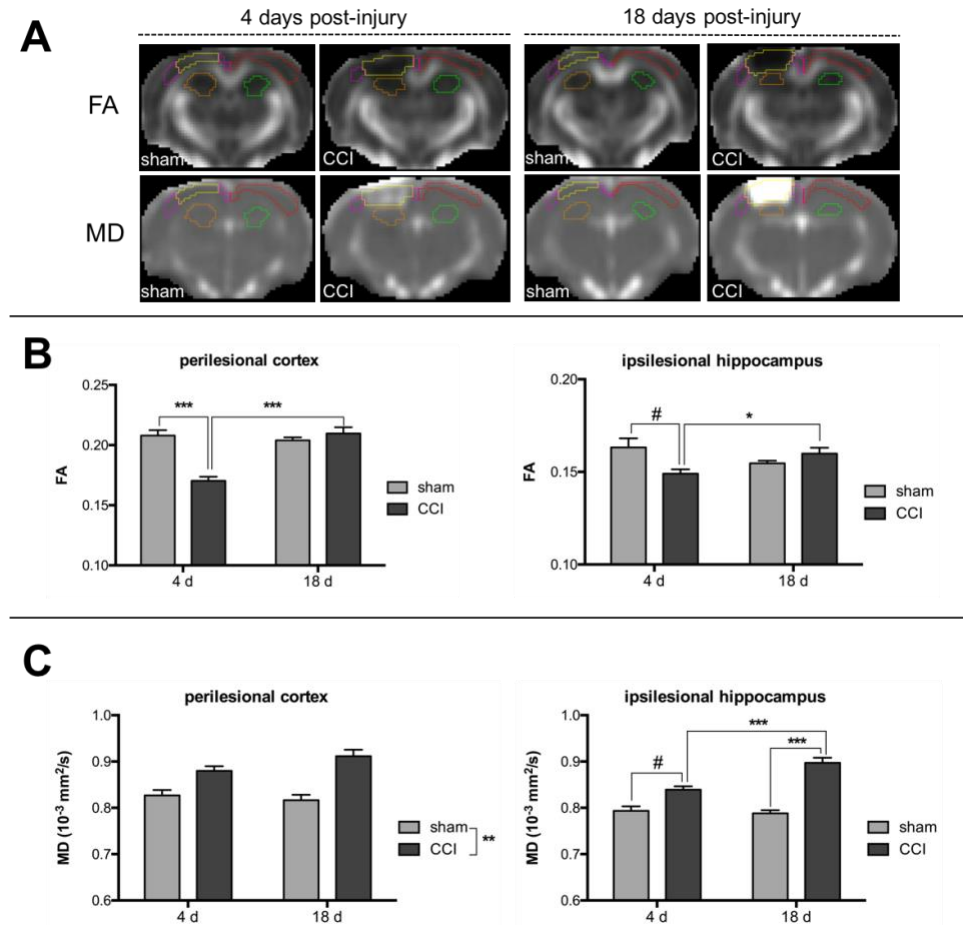
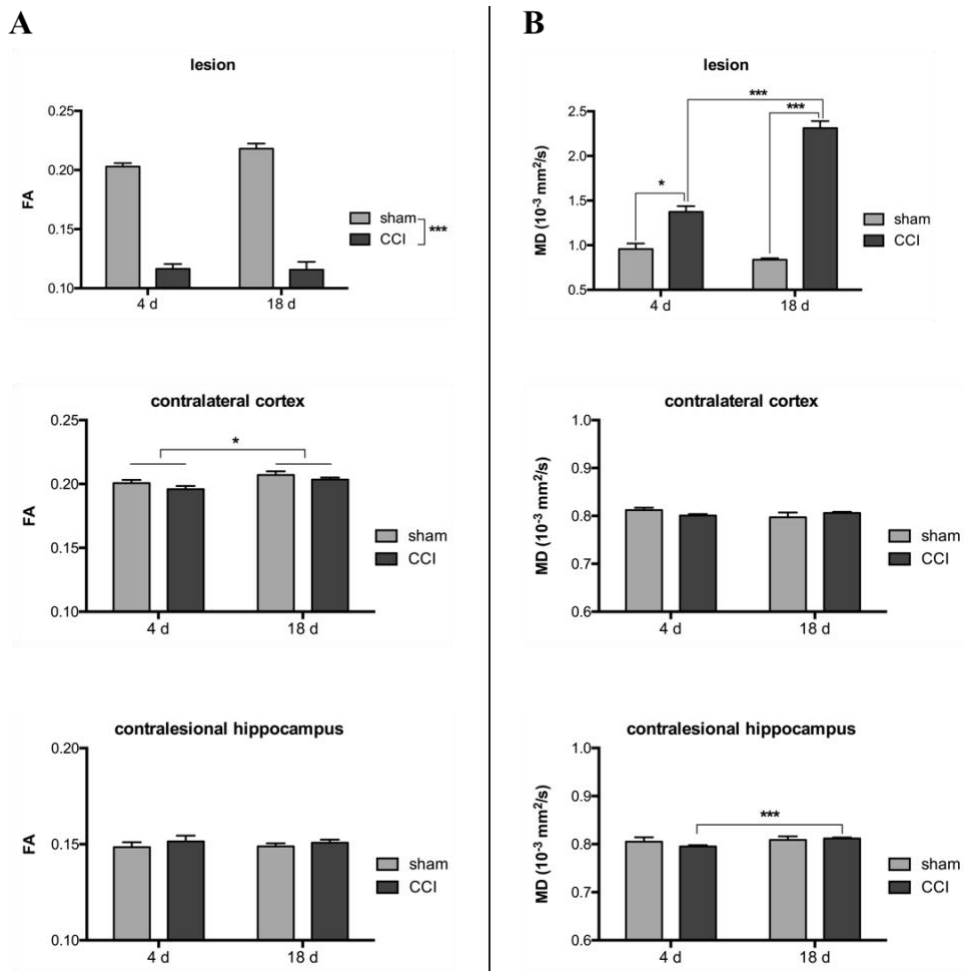


Fig. 6-3. Diffusion tensor imaging in CCI-injured rats. **A.** Representative fractional anisotropy (FA) and mean diffusivity (MD) maps of sham-operated and CCI-injured rats at 4 and 18 days post-injury. Yellow: lesion, pink: perilesional cortex, red: contralateral cortex, orange: ipsilesional hippocampus, green: contralesional hippocampus. **B.** FA in perilesional cortex and ipsilesional hippocampus of sham-operated ($n=5$) and CCI-injured rats ($n=18$). FA was significantly lower in the perilesional cortex of CCI-injured rats compared to shams at 4 days post-injury. A trend towards significance for a lower FA was observed in the ipsilesional hippocampus of CCI-injured rats vs. shams at 4 days post-injury. FA increased significantly over time in both perilesional cortex and ipsilesional hippocampus of CCI-injured rats. **C.** MD in perilesional cortex and ipsilesional hippocampus of sham-operated ($n=6$) and CCI-injured rats ($n=18$). MD was significantly higher in the perilesional cortex of CCI-injured rats compared to shams. A trend towards significance for a higher MD was observed in the ipsilesional hippocampus of CCI-injured rats vs. shams at 4 days post-injury. MD was significantly higher in the ipsilesional hippocampus of CCI-injured rats vs. shams at 18 days post-injury. MD increased significantly over time

*in ipsilesional hippocampus of CCI-injured rats. Mean \pm SEM is given. # $p \leq 0.1$, * $p \leq 0.05$, ** $p \leq 0.01$, *** $p \leq 0.001$*

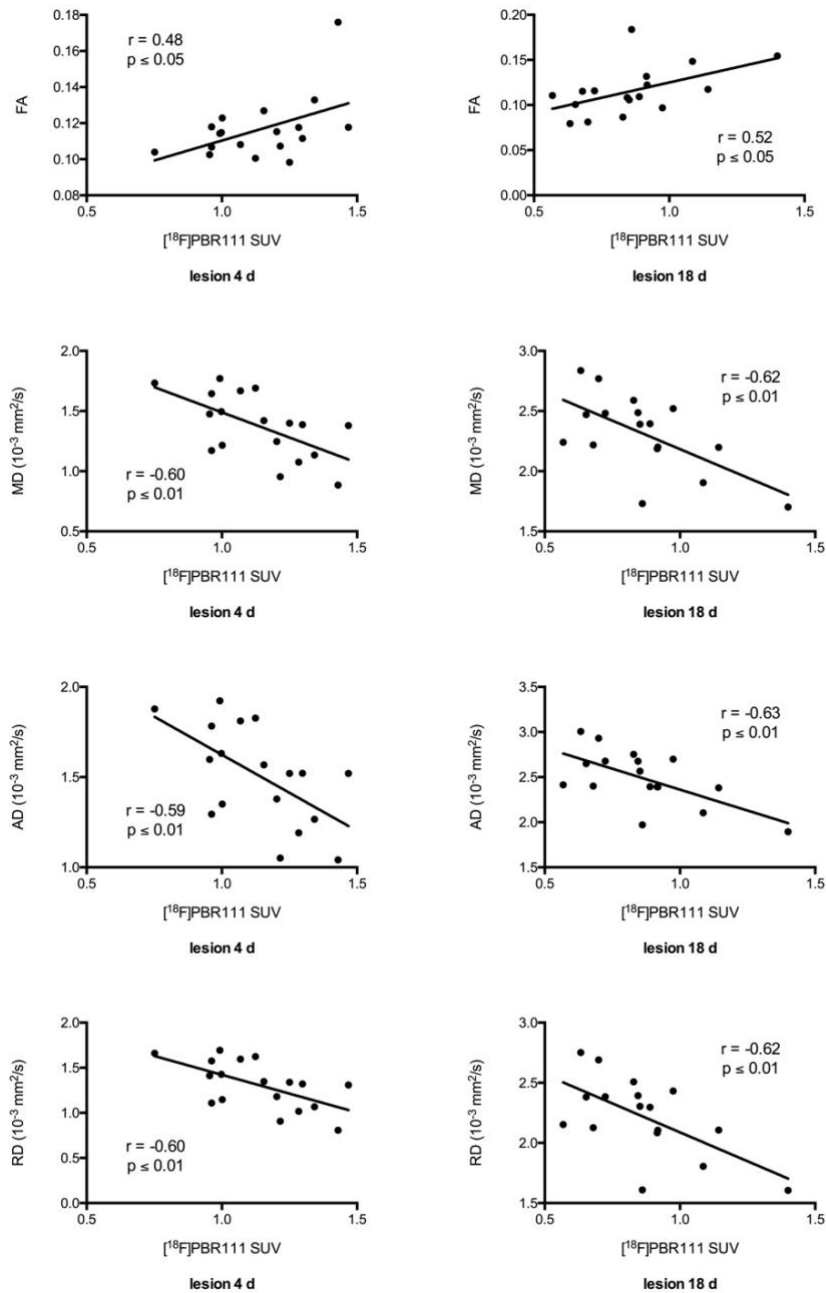
After CCI-injury mean diffusivity (MD), axial diffusivity (AD) and radial diffusivity (RD) were increased in the lesion, perilesional cortex and ipsilesional hippocampus vs. shams, which was more pronounced at the later time-point (Fig.6-3A,C; Suppl.Fig.6-2B). Analysis with linear mixed models revealed a significant effect of Group on MD, AD and RD in the perilesional cortex (MD: $p \leq 0.01$, AD: $p \leq 0.05$, RD: $p \leq 0.001$). For all of these parameters, there was a significant interaction between Group and Time for lesion ($p \leq 0.0001$) and ipsilesional hippocampus ($p \leq 0.01$). Post-hoc analysis showed a significant increase in MD, AD and RD in the lesion of CCI-injured rats at 4 days ($p \leq 0.05$) and 18 days post-injury ($p \leq 0.0001$) vs. shams, as well as a significant effect of time in CCI-injured rats ($p \leq 0.0001$). There was a significant increase in RD in ipsilesional hippocampus between sham-operated and CCI-injured rats at 4 days post-injury ($p \leq 0.05$) and a trend for an increased MD ($p = 0.07$). At 18 days post-injury MD, AD, RD were all significantly increased in CCI-injury rats vs. shams (MD, RD: $p \leq 0.0001$, AD: $p \leq 0.001$). All of these parameters significantly differed between 4 and 18 days in CCI-injured rats ($p \leq 0.0001$). There was also a significant interaction between Group and Time effects on MD in the contralesional hippocampus ($p \leq 0.05$). Post-hoc analysis showed that there was a significant difference between 4 and 18 days post-injury in CCI-injured rats ($p \leq 0.001$) (Suppl.Fig.6-2B). There was also a significant effect of Time on RD in the contralesional hippocampus (increase over time, $p \leq 0.05$). Finally, there was no significant effect of Group or Time on MD, AD or RD in the contralateral cortex (Suppl.Fig.6-2B).



Suppl. Fig. 6-2. Diffusion tensor imaging in CCI-injured rats. A. FA in lesion, contralateral cortex and contralesional hippocampus of sham-operated ($n=5$) and CCI-injured rats ($n=18$). FA was significantly lower in the lesion of CCI-injured rats compared to shams. FA was significantly higher in contralateral cortex of all rats at 18 days vs. 4 days post-injury. There was no difference in FA in contralesional hippocampus between sham-operated and CCI-injured rats at any given time-point. **B.** MD in lesion, contralateral cortex and contralesional hippocampus of sham-operated ($n=6$) and CCI-injured rats ($n=18$). MD was significantly higher in the lesion of CCI-injured rats compared to shams at 4 and 18 days post-injury. MD increased significantly over time in the lesion of CCI-injured rats. There was no difference in MD in contralateral cortex between sham-operated and CCI-injured rats at any given time-point. MD was significantly higher in contralesional hippocampus of CCI-injured rats at 18 days vs. 4 days post-injury. Mean \pm SEM is given. * $p \leq 0.05$, *** $p \leq 0.001$

4.3. TSPO binding correlates with DTI parameters in the lesion of CCI-injured rats

We investigated whether there was a relationship between [¹⁸F]PBR111 SUVs and DTI parameters (FA, MD, AD and RD) in the different ROIs in CCI-injured rats. A positive correlation was observed between [¹⁸F]PBR111 SUV and FA in the lesion at 4 days ($p \leq 0.05$, $r = 0.48$) and 18 days post-injury ($p \leq 0.05$, $r = 0.52$), as well as negative correlations between [¹⁸F]PBR111 SUV and MD, AD and RD at 4 days (MD: $p \leq 0.01$, $r = -0.60$; AD: $p \leq 0.01$, $r = -0.59$; RD: $p \leq 0.01$, $r = -0.60$) and 18 days post-injury (MD: $p \leq 0.01$, $r = -0.62$; AD: $p \leq 0.01$, $r = -0.63$; RD: $p \leq 0.01$, $r = -0.62$) (Suppl.Fig.6-3). No significant correlations were observed for the other investigated brain regions.



Suppl. Fig. 6-3. Significant correlation between $[^{18}\text{F}]\text{PBR111 SUV}$ and FA, MD, AD and RD in the lesion of CCI-injured rats. Positive correlations were observed between the $[^{18}\text{F}]\text{PBR111 SUV}$ and FA in the lesion of CCI rats at 4 days (A) and 18 days post-injury (B). Negative correlations were observed between the $[^{18}\text{F}]\text{PBR111 SUV}$ and MD, AD and RD in the lesion of CCI-injured rats at 4 days (C,E,G) and 18 days post-injury (D,F,H).

4.4. Chronic deficits after CCI-injury

4.4.1. Disinhibition

The % distance moved in the centre of the open field arena was significantly higher in CCI-injured rats than in naïve rats ($p \leq 0.05$) (Fig.6-4A). There was no significant difference between the three groups in any of the other investigated parameters. To corroborate this observation, we performed the same test in a separate cohort of animals at approx. 2 months post-injury (naïve: $n=9$, sham: $n=10$, CCI: $n=10$) and we observed a significantly increased % distance moved in the centre ($p \leq 0.05$), a significantly increased number of entries into the centre ($p \leq 0.05$) and a trend for an increased % time spent in centre ($p=0.06$) in CCI-injured rats compared to naïve animals (data not shown).

4.4.2. Anhedonia

CCI-injured rats had a significantly lower % sucrose preference compared to sham-operated rats and all controls (sham-operated + naïve rats) ($p \leq 0.05$) (Fig.6-4B).

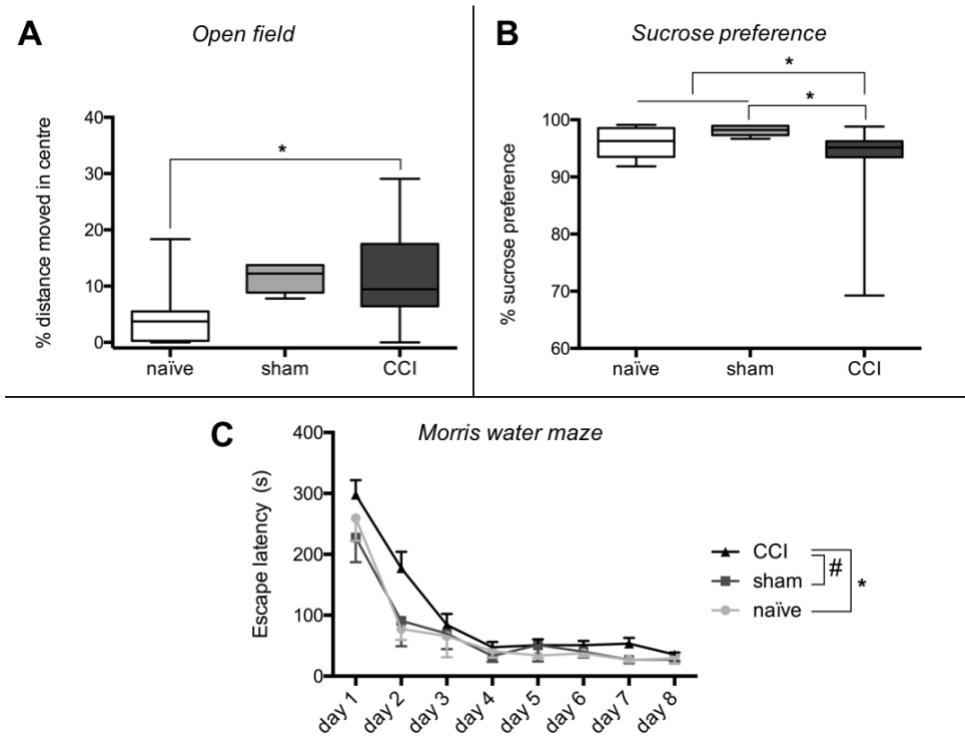


Fig.6-4. Chronic behavioural deficits in CCI-injured rats. **A. Open field test.** CCI rats showed a significantly higher % distance moved in the centre of the open field arena compared to naïve rats (naïve: $n=8$, sham: $n=5$, CCI: $n=18$). **B. Sucrose preference test.** CCI rats had a significantly lower % sucrose preference compared to shams and all controls (naïve: $n=8$, sham: $n=5$, CCI: $n=18$). **C. Morris water maze (MWM) test.** CCI rats had a significantly longer escape latency than naïve rats as well as a trend for a longer latency compared to shams during acquisition of the MWM test (naïve: $n=8$, sham: $n=5$, CCI: $n=16$). Data are presented as boxplots (A,B) or mean \pm SEM is given (C). # $p<0.1$, * $p<0.05$

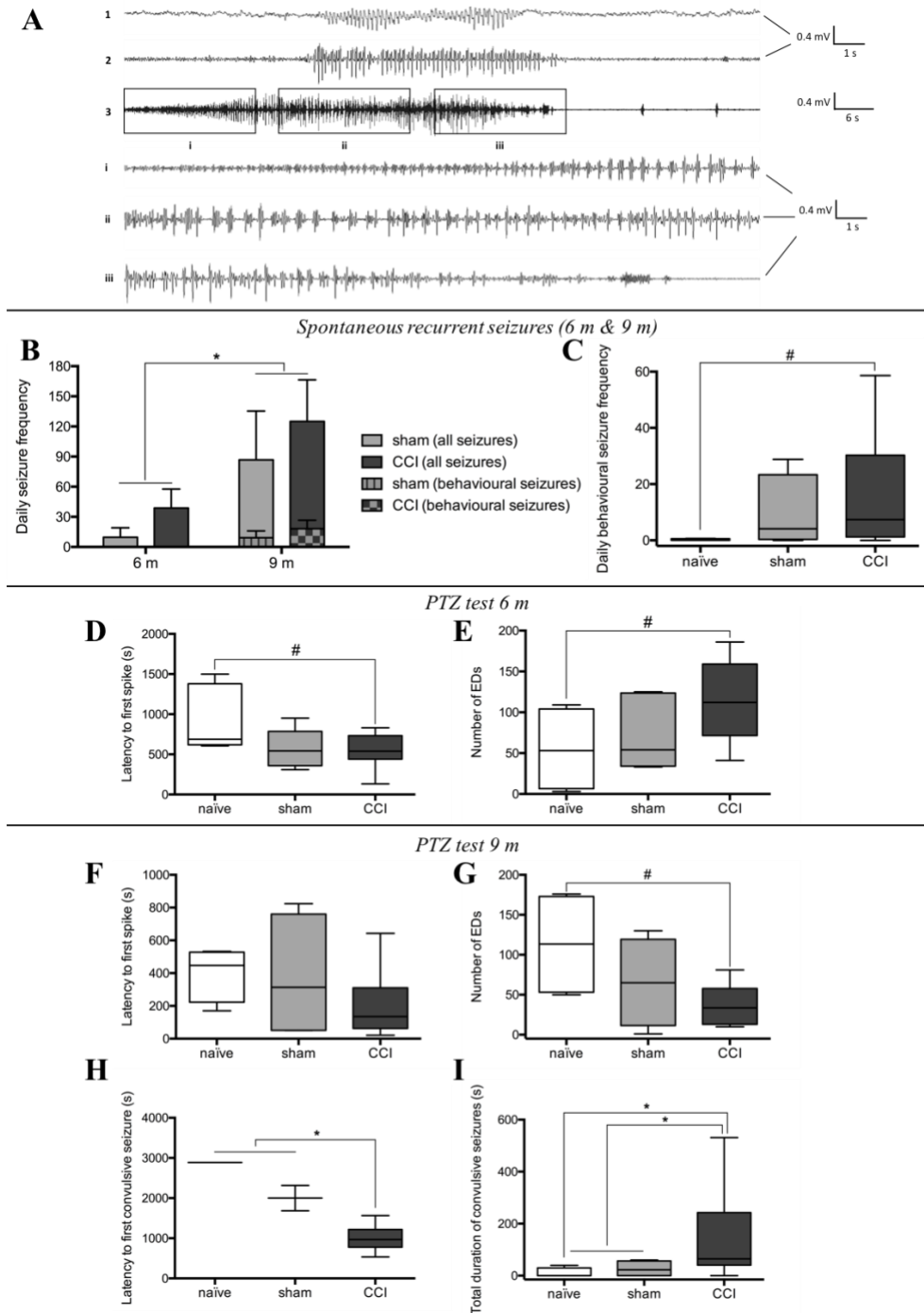


Fig.6-5. Spontaneous recurrent seizures (SRS) and seizure susceptibility in CCI-injured rats. A-C. SRS.
A. Representative examples of SRS that were observed during vEEG monitoring. 1: spike-wave discharge (SWD), 2: high-voltage rhythmic spike (HVRS) discharge, 3: convulsive S3 seizure. i:

beginning, ii: middle and iii: end of the convulsive seizure. **B.** Both sham-operated and CCI-injured rats had a significantly higher spontaneous seizure frequency at 9 months vs. 6 months post-injury (6 months: $n=4$ sham, $n=17$ CCI; 9 months: $n=4$ sham, $n=7$ CCI) **C.** There was a trend for a higher daily frequency of behavioural SRS in CCI-injured rats compared to naïve rats (naïve: $n=4$, sham: $n=4$, CCI: $n=7$). **D-E. Pentylentetrazole (PTZ) seizure susceptibility test at 6 months post-injury.** **D.** CCI-injured rats showed a trend for a shorter latency to first spike following 25 mg/kg PTZ injection compared to naïve rats (naïve: $n=5$, sham: $n=5$, CCI: $n=13$). **E.** CCI-injured rats showed a trend for a higher number of epileptiform discharges (EDs) (naïve: $n=4$, sham: $n=5$, CCI: $n=13$). **F-I. PTZ test at 9 months post-injury.** **F.** There was no difference in latency to first spike following 30 mg/kg PTZ injection between any of the groups (naïve: $n=4$, sham: $n=4$, CCI: $n=7$). **G.** CCI-injured rats showed a trend for a lower number of epileptiform discharges (EDs) (naïve: $n=4$, sham: $n=4$, CCI: $n=6$). **H.** CCI rats had a significantly shorter latency to first convulsive seizure vs. all controls (naïve: $n=1$, sham: $n=2$, CCI: $n=6$). **I.** CCI rats had a significantly higher total duration of convulsive seizures than naïve rats and all controls following 30 mg/kg PTZ injection (naïve: $n=4$, sham: $n=4$, CCI: $n=6$). Data are presented as boxplots (C-I) or mean \pm SEM is given (B). # $p \leq 0.1$, * $p \leq 0.05$

4.4.3. Spontaneous epileptiform activity and seizures

At 6 months post-injury no difference was observed between naïve, sham-operated and CCI-injured animals regarding number of epileptiform discharges (EDs) per day, number of seizures per day (all electrographic) or duration of all epileptiform activity per day (data not shown). At this time-point no behavioural seizures were observed.

At 9 months post-injury behavioural seizures were observed. CCI-injured rats showed a trend for an increased frequency of behavioural seizures compared to naïve animals ($p=0.06$) (Fig.6-5C). No difference was observed between the three groups for any other investigated parameter. Most behavioural seizures that were recorded were S1 seizures, typically displaying a spike-wave pattern (Fig.6-5A-1) or high-voltage rhythmic spike pattern (Fig.6-5A-2), and manifested by a behavioural arrest (absence-like seizures). A few other types of behavioural seizures were recorded. One CCI-

injured rat experienced two S3 seizures (Fig.6-5A-3) and one S2 seizure during the one-week monitoring period at 9 months post-injury. Another CCI-injured rat experienced one S2 seizure. A sham-operated rat experienced one S4 seizure during the one-week monitoring period.

In addition, we investigated the evolution of spontaneous epileptiform activity and seizures over time. There were significantly more EDs and seizures per day at 9 months post-injury than at 6 months post-injury ($p \leq 0.05$) (Fig.6-5B). Finally, the duration of all epileptiform activity per day was significantly higher at 9 months vs. 6 months post-injury ($p \leq 0.01$). However, there was no difference between sham-operated and CCI-injured rats. No naïve rats were longitudinally subjected to vEEG monitoring.

4.4.4. Seizure susceptibility

At 6 months post-injury, CCI-injured rats showed a non-significant trend for a shorter latency to the first spike compared to naïve animals ($p=0.08$) (Fig.6-5D). A very weak trend was observed for an increased number of EDs in TBI rats compared to naïve rats ($p=0.10$) (Fig.6-5E). There was no difference between the three groups for latency to first ED and seizure, and number of spikes and seizures. At this time-point only 23% (5/22) of all rats experienced a convulsive seizure (usually S5) after injection with 25 mg/kg PTZ with no difference between the three groups (χ^2 , $p > 0.05$) (data not shown).

At 9 months post-injury 60% (9/15) of all rats developed a convulsive seizure (usually S5) after administration of 30 mg/kg PTZ: 25% (1/4) naïve rats, 50% (2/4) sham-operated rats and 86% (6/7) CCI-injured rats (χ^2 , $p \leq 0.05$). When comparing the three groups, we observed a trend for an increased number of convulsive seizures ($p=0.08$) and a significantly increased total duration of

convulsive seizures in CCI-injured rats compared to naïve animals ($p \leq 0.05$) (Fig.6-5I). We pooled the two control groups (naïve and sham-operated animals) to be able to perform statistics regarding the latency to the first convulsive seizure and observed a significantly shorter latency to first convulsive seizure in CCI-injured rats vs. controls ($p \leq 0.05$) (Fig.6-5H). In addition, we observed a trend for a decreased number of EDs in CCI-injured rats compared to naïve rats ($p = 0.07$) (Fig.6-5G). Upon further investigation, we observed a strong relationship between number of EDs and latency to first convulsive seizure in the rats ($r = 0.88$, $p \leq 0.1$) (data not shown). Hence, a decreased latency to the first convulsive seizure coincides with a decreased number of EDs. We observed no difference between the three groups for any other investigated parameter (latency to first spike and ED, number of spikes and EDs) (Fig.6-5F). Additionally, we performed a PTZ test in a separate cohort of animals at approx. 6 months post-injury, but without EEG monitoring. Behavioural monitoring of animals indicated that 11% (1/9) naïve rats, 40% (4/10) sham-operated rats and 78% (7/9) CCI-injured rats developed a generalised tonic-clonic (S5) seizure following administration of 30 mg/kg PTZ (χ^2 , $p \leq 0.01$).

One CCI-injured animal went into *status epilepticus* (six convulsive seizures in one hour) after administration of 30 mg/kg PTZ. The rat died shortly after the test, before diazepam could be administered to stop the *status epilepticus*. This was also the only CCI-injured rat that experienced multiple spontaneous convulsive seizures during the one-week monitoring period at 9 months post-injury.

4.4.5. Impaired visuospatial learning

Analysis with linear mixed models showed a significant effect of both Group ($p \leq 0.05$) and Time (= trial block) ($p \leq 0.0001$) on both escape latency and path length to the platform. There was no significant interaction between Group and Time. Post-hoc analysis revealed that CCI-injured animals had a significantly longer escape latency than naïve animals ($p \leq 0.05$) and a weak trend for a longer latency compared to sham-operated rats ($p = 0.09$) (Fig.6-4C). The difference was seen to be greatest at the second day of training. CCI-injured animals also showed a trend for an increased path length compared to naïve rats ($p = 0.07$) (data not shown). There was no difference in the swimming speed between the three groups.

Though a numerically lower % time spent in the target quadrant during the probe trial was observed in CCI-injured animals versus the controls, no significant difference between the three groups was noted. There was a trend for a lower frequency of platform crossings in CCI-injured rats compared to sham-operated rats ($p = 0.08$) (data not shown).

4.5. Correlation between subacute TSPO binding and microstructural changes and chronic deficits in CCI-injured rats

First of all, we investigated if there was a correlation between i) subacute TSPO expression ($[^{18}\text{F}]\text{PBR111}$ SUV) and ii) DTI metrics in perilesional cortex and ipsilesional hippocampus of CCI-injured rats and chronic behavioural deficits. In addition, we investigated whether the evolution in TSPO expression and DTI metrics (i.e., the % change in SUV, FA, MD, AD and RD over time) correlated with the chronic functional outcome.

Several correlations were observed between individual TSPO PET and DTI parameters on the one hand and chronic deficits on the other hand (Fig.6-6 and Fig.6-7). Correlations that were significant are summarised in Table 6-1 (TSPO PET) and Table 6-2 (DTI). Most importantly, both TSPO PET and DTI parameters correlated with disinhibition in the open field, increased seizure susceptibility and MWM performance.

A

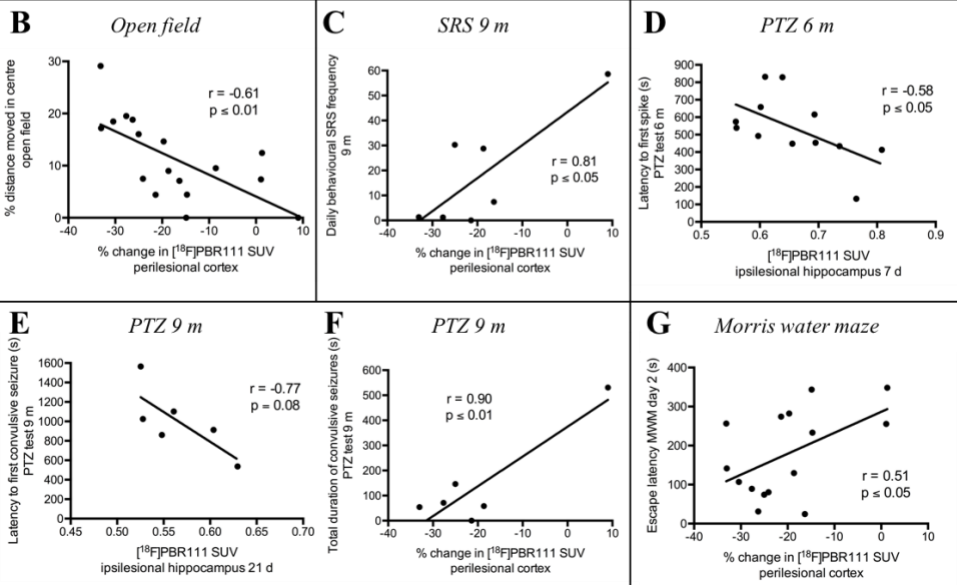
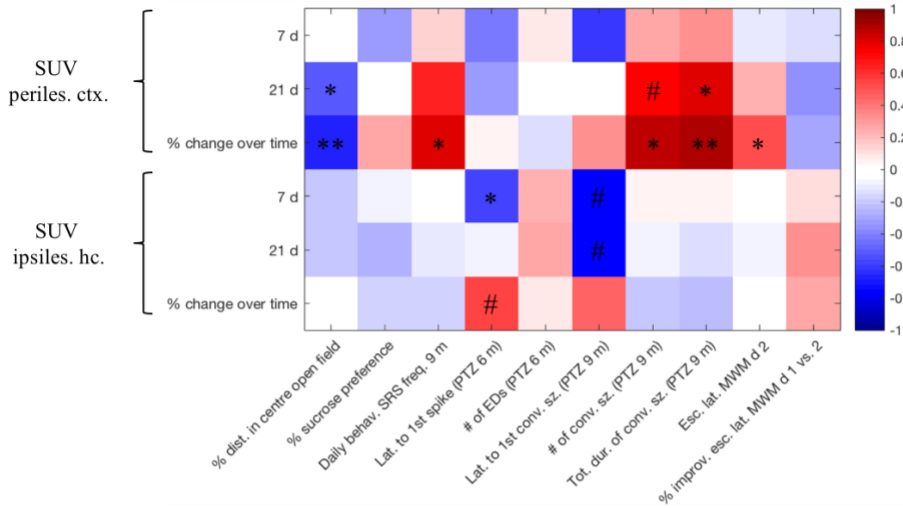


Fig. 6-6. Correlation between subacute brain inflammation and long-term functional outcome in CCI-injured rats. A. Colour-coded correlation matrix between TSPO PET measurements and functional deficits (red=positive Pearson's r , blue=negative Pearson's r). Periles. ctx. = perilesional cortex, ipsiles. hc. = ipsilesional hippocampus, dist. = distance, behav. = behavioural, freq. = frequency, lat. = latency, # = number, conv. = convulsive, sz. = seizure(s), tot. = total, dur. = duration, esc. = escape, improv. = improvement. B. There was a negative correlation between the % change in $[^{18}\text{F}]\text{PBR111}$ SUV in perilesional cortex over time and the % distance moved in the centre of the open field. C. A positive correlation was observed between the % change in SUV in perilesional cortex over time and the daily

behavioural seizure frequency at 9 months post-injury. **D.** A negative correlation was observed between the SUV in ipsilesional hippocampus at 7 days post-injury and the latency to the first spike following PTZ administration at 6 months post-injury. **E.** There was a trend for a negative correlation between the SUV in ipsilesional hippocampus at 21 days post-injury and the latency to the first convulsive seizure following PTZ administration at 9 months post-injury. **F.** There was a positive correlation between the % change in [^{18}F]PBR111 SUV in perilesional cortex over time and the total duration of convulsive seizures during the PTZ seizure susceptibility assay at 9 months post-injury. **G.** A positive correlation was seen between the % change in SUV in perilesional cortex over time and the escape latency on day 2 of the Morris water maze (MWM) test. # $p \leq 0.1$, * $p \leq 0.05$, ** $p \leq 0.01$

Table 6-1. Significant correlations between subacute TSPO PET measurements and chronic functional deficits.

Chronic deficit	TSPO PET parameter	Pearson's r	p-value
% distance moved in centre open field	SUV 21 d perilesional cortex	-0.52	$p \leq 0.05$
	% change SUV over time perilesional cortex	-0.66	$p \leq 0.01$
Daily behavioural seizure frequency 9 m	% change SUV over time perilesional cortex	0.81	$p \leq 0.05$
Latency to first spike (PTZ test 6 m)	SUV 7 d ipsilesional hippocampus	-0.58	$p \leq 0.05$
Number of convulsive seizures (PTZ test 9 m)	% change SUV over time perilesional cortex	0.85	$p \leq 0.05$
Total duration of convulsive seizures (PTZ test 9 m)	SUV 21 d perilesional cortex	0.81	$p \leq 0.05$
	% change SUV over time perilesional cortex	0.90	$p \leq 0.01$
Escape latency MWM day 2	% change SUV over time perilesional cortex	0.51	$p \leq 0.05$

Table 6-2. Significant correlations between subacute DTI measurements and chronic functional deficits.

Chronic deficit	DTI parameter	Pearson's r	p-value
% distance moved in centre open field	% change FA over time ipsilesional hippocampus	-0.50	$p \leq 0.05$
Latency to first spike (PTZ test 6 m)	FA 4 d perilesional cortex	0.61	$p \leq 0.05$
	MD 4 d perilesional cortex	-0.71	$p \leq 0.01$
	AD 4 d perilesional cortex	-0.65	$p \leq 0.05$
	RD 4 d perilesional cortex	-0.72	$p \leq 0.01$
Number of EDs (PTZ test 6 m)	% change FA over time ipsilesional hippocampus	-0.58	$p \leq 0.05$
Latency to first convulsive seizure (PTZ test 9 m)	% change FA over time perilesional cortex	-0.83	$p \leq 0.05$
% improvement escape latency MWM day 1 vs. 2	MD 18 d ipsilesional hippocampus	-0.52	$p \leq 0.05$
	RD 18 d ipsilesional hippocampus	-0.54	$p \leq 0.05$

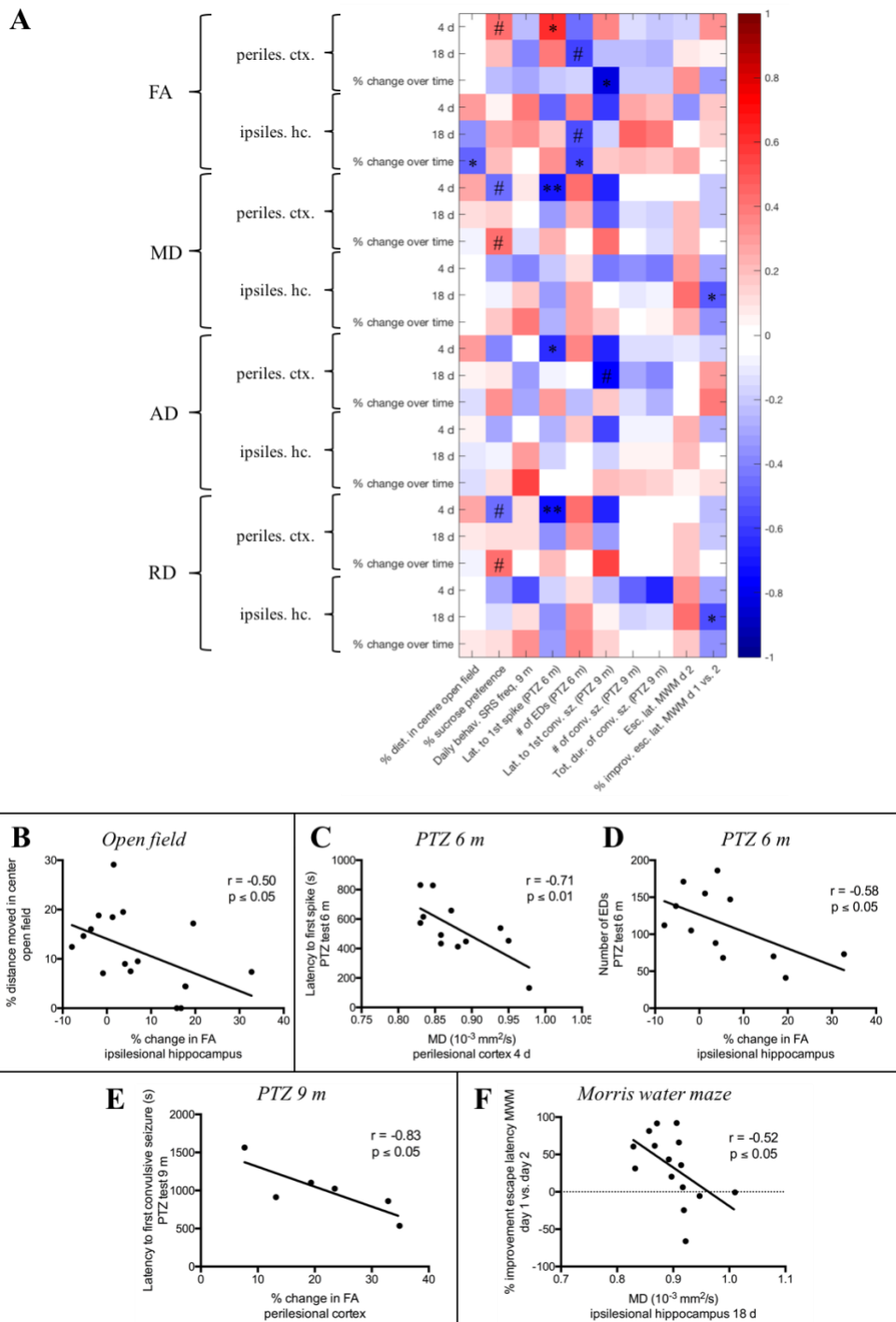


Fig.6-7. Correlation between subacute microstructural changes and long-term functional outcome in CCI-injured rats. A. Colour-coded correlation matrix between DTI measurements and functional

deficits (red=positive Pearson's r , blue=negative Pearson's r). Periles. ctx. = perilesional cortex, ipsiles. hc. = ipsilesional hippocampus, dist. = distance, behav. = behavioural, freq. = frequency, lat. = latency, # = number, conv. = convulsive, sz. = seizure(s), tot. = total, dur. = duration, esc. = escape, improv. = improvement. **B.** There was a negative correlation between the % change in FA in ipsilesional hippocampus over time and the % distance moved in the centre of the open field. **C.** A negative correlation was seen between MD in perilesional cortex at 4 days post-injury and the latency to the first spike following PTZ administration at 6 months post-injury. **D.** A negative correlation was found between the % change in FA in ipsilesional hippocampus over time and the total number of epileptiform discharges (EDs) during the PTZ seizure susceptibility assay at 6 months post-injury. **E.** There was a negative correlation between the relative change in FA in perilesional cortex and the latency to first convulsive seizure following PTZ administration at 9 months post-injury. **F.** A negative correlation was observed between MD in ipsilesional hippocampus at 18 days post-injury and the % improvement in escape latency between day 1 and day 2 of the Morris water maze (MWM) test. # $p \leq 0.1$, * $p \leq 0.05$

4.6. ROC curve analysis

ROC curves were plotted for those *in vivo* imaging parameters that significantly correlate with chronic deficits based on the Pearson correlation analysis. ROC curves were only plotted if there was a sufficient number of animals ($n \geq 6$) in each group (i.e., CCI-injured animals with deficit and CCI-injured animals without deficit). This excluded ROC curves with behavioural seizure frequency and seizure susceptibility at 9 months post-injury as outcome.

The relative change over time in [^{18}F]PBR111 SUV in perilesional cortex and FA in ipsilesional hippocampus showed good sensitivity and specificity in distinguishing between CCI-injured rats with and without disinhibition in the open field (respectively, $\text{AUC} = 0.86$, $p \leq 0.01$ and $\text{AUC} = 0.85$, $p \leq 0.05$) (Fig. 6-8A,C).

[^{18}F]PBR111 SUV in the ipsilesional hippocampus at 7 days, as well as MD and RD in the perilesional cortex at 4 days post-injury had good sensitivity

and specificity in distinguishing between CCI-injured rats with decreased and normal latency to first spike during the PTZ test at 6 months post-injury (respectively AUC = 0.86, $p \leq 0.05$; AUC = 0.83, $p \leq 0.05$ and AUC = 0.83, $p \leq 0.05$) (Fig.6-8B,D). The relative change in FA in ipsilesional hippocampus exhibited good sensitivity and specificity in distinguishing between CCI-injured rats with increased and normal number of EDs following PTZ administration at 6 months post-injury (AUC = 0.83, $p \leq 0.05$) (Fig.6-8E).

MD and RD in ipsilesional hippocampus at 18 days post-injury showed good sensitivity and specificity in distinguishing between CCI-injured rats with and without a learning deficit in the MWM test (respectively AUC = 0.86, $p \leq 0.05$ and AUC = 0.84, $p \leq 0.05$) (Fig.6-8F).

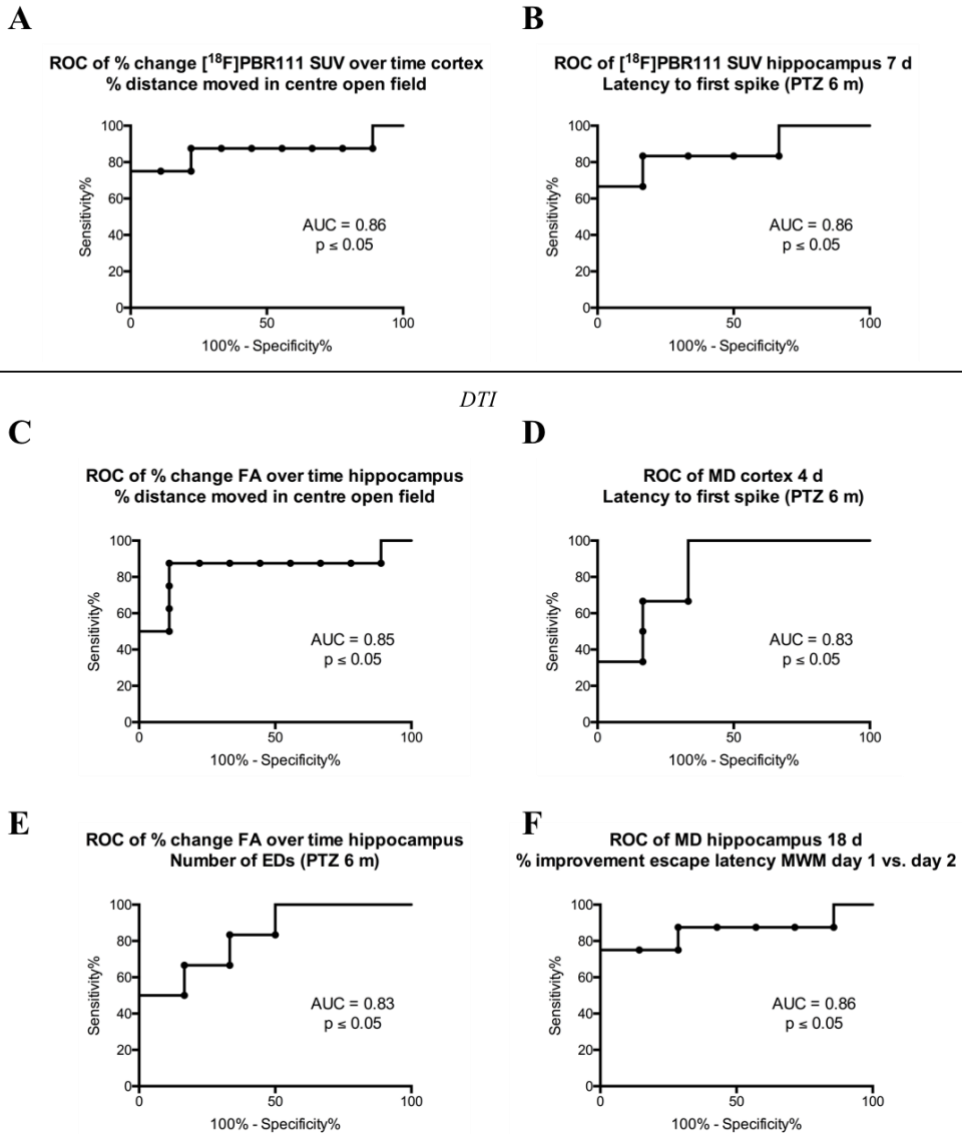
PET with [^{18}F]PBR111

Fig.6-8. ROC curve analysis. Several in vivo imaging parameters showed good sensitivity and specificity to distinguish between CCI-injured rats with and without a particular deficit. A. The % change in [^{18}F]PBR111 SUV in perilesional cortex over time could distinguish between TBI rats with ($n=8$) and without disinhibition ($n=9$). **B.** The [^{18}F]PBR111 SUV in ipsilesional hippocampus at 7 days post-injury was able to distinguish between TBI rats with decreased ($n=6$) and normal ($n=6$) latency to first spike following PTZ at 6 months post-injury. **C.** The % change in FA in ipsilesional hippocampus could distinguish between TBI rats with ($n=8$) and without disinhibition ($n=9$). **D.** The MD in perilesional cortex at 4 days post-injury was able to distinguish between TBI rats with decreased ($n=6$) and normal

(n=6) latency to first spike following PTZ at 6 months post-injury. **E.** The % change in FA in ipsilesional hippocampus could distinguish between TBI rats with increased (n=6) and normal (n=6) number of epileptiform discharges (EDs) during the PTZ test at 6 months post-injury. **F.** MD in ipsilesional hippocampus at 18 days post-injury was able to distinguish between TBI rats with (n=8) and without (n=7) learning impairment in the Morris water maze (MWM) test. AUC = area under the curve.

4.7. Stepwise regression analysis

Finally, we performed stepwise regression analysis to investigate whether TSPO PET or DTI alone are sufficient to predict the long-term functional deficits or whether combining TSPO PET and DTI has an added value. To this end, automated forward stepwise regression analysis was done with three different sets of possible predictors, i.e., only TSPO PET parameters, only DTI metrics and both TSPO PET and DTI parameters to build different regression models. The models were then compared to see which of the three models was best at explaining the variability in the data (i.e., the chronic functional deficits). The obtained data are summarised in Table 6-3.

TSPO PET parameters alone could explain some of the variability in the % distance moved in centre open field of CCI-injured rats (R^2 adj. = 0.42, $p=0.0082$). Combining TSPO PET and DTI parameters resulted in a better model (R^2 adj. = 0.51, $p=0.0027$).

DTI parameters alone can predict the variability in behavioural SRS frequency at 9 months post-injury (R^2 adj. = 1, $p=0.0034$), as well as the increased seizure susceptibility at 6 months post-injury (latency to first spike: R^2 adj. = 0.91, $p=0.0081$; number of EDs: R^2 adj. = 0.92, $p=0.0070$). Combining DTI and TSPO PET parameters slightly improves the models (behavioural SRS frequency at 9 m: R^2 adj. = 1, $p=0.0008$; latency to first spike at 6 m: R^2 adj. = 1, $p=0.0026$; number of EDs at 6 m: R^2 adj. = 0.98, $p=0.0026$).

Both TSPO PET and DTI parameters alone can predict the latency to the first convulsive seizure after PTZ injection at 9 months post-injury (TSPO PET: R^2 adj. = 1, $p=0.0388$; DTI: R^2 adj. = 1, $p=0.0077$). TSPO PET parameters can reasonably well explain the variability in the number and total duration of convulsive seizures during the 9 month PTZ assay (number of convulsive seizures: R^2 adj. = 0.66, $p=0.0159$; total duration of convulsive seizures: R^2 adj. = 0.76, $p=0.0146$). Adding DTI parameters further improves the models (number of convulsive seizures: R^2 adj. = 1, $p=0.0055$; total duration of convulsive seizures: R^2 adj. = 1, $p=0.0005$).

Variability in MWM performance can mainly be explained by DTI metrics (escape latency MWM training day 2: R^2 adj. = 0.78, $p=0.0013$; % improvement escape latency MWM training day 1 vs. day 2: R^2 adj. = 0.55, $p=0.0081$), but TSPO PET parameters can have some added value (TSPO PET + DTI: escape latency MWM training day 2: R^2 adj. = 0.94, $p=0.0003$; % improvement escape latency MWM training day 1 vs. day 2: R^2 adj. = 0.55, $p=0.0081$).

Table 6-3 (PART 1). Stepwise regression models of chronic functional deficits with TSPO PET measurements alone, DTI measurements alone and the combination of TSPO PET and DTI measurements as predictors. The best models for each functional outcome parameter are indicated in bold, italic and red.

Functional outcome	Imaging modality	R ²	Adjusted R ²	p-value
Open field % distance moved in centre	TSPO PET	0.50	0.42	0.0082
	DTI	0.25	0.20	0.0419
	<i>TSPO PET + DTI</i>	<i>0.57</i>	<i>0.51</i>	<i>0.0027</i>
Sucrose preference % sucrose preference	TSPO PET	0.23	0.12	0.1609
	DTI	0.31	0.22	0.0688
	TSPO PET + DTI	0.32	0.22	0.0688
PTZ 6 m Latency to first spike	TSPO PET	0.44	0.32	0.0710
	<i>DTI</i>	<i>0.97</i>	<i>0.91</i>	<i>0.0081</i>
	<i>TSPO PET + DTI</i>	<i>1.00</i>	<i>1.00</i>	<i>0.0026</i>
Number of EDs	TSPO PET	/	/	/
	<i>DTI</i>	<i>0.97</i>	<i>0.92</i>	<i>0.0070</i>
	<i>TSPO PET + DTI</i>	<i>0.99</i>	<i>0.98</i>	<i>0.0026</i>

Table 6-3 (PART 2). Stepwise regression models of chronic functional deficits with TSPO PET measurements alone, DTI measurements alone and the combination of TSPO PET and DTI measurements as predictors. The best models for each functional outcome parameter are indicated in bold, italic and red.

Functional outcome	Imaging modality	R ²	Adjusted R ²	p-value
SRS 9 m	TSPO PET	0.66	0.60	0.0256
	<i>DTI</i>	<i>1.00</i>	<i>1.00</i>	<i>0.0034</i>
	<i>TSPO PET + DTI</i>	<i>1.00</i>	<i>1.00</i>	<i>0.0008</i>
Latency to first convulsive seizure	<i>TSPO PET</i>	<i>1.00</i>	<i>1.00</i>	<i>0.0388</i>
	<i>DTI</i>	<i>1.00</i>	<i>1.00</i>	<i>0.0077</i>
	<i>TSPO PET + DTI</i>	<i>1.00</i>	<i>1.00</i>	<i>0.0347</i>
PTZ 9 m	TSPO PET	0.72	0.66	0.0159
	DTI	/	/	/
	<i>TSPO PET + DTI</i>	<i>1.00</i>	<i>1.00</i>	<i>0.0055</i>
Total duration of convulsive seizures	TSPO PET	0.81	0.76	0.0146
	DTI	0.70	0.51	0.1606
	<i>TSPO PET + DTI</i>	<i>1.00</i>	<i>1.00</i>	<i>0.0005</i>

Table 6-3 (PART 3). Stepwise regression models of chronic functional deficits with TSPO PET measurements alone, DTI measurements alone and the combination of TSPO PET and DTI measurements as predictors. The best models for each functional outcome parameter are indicated in bold, italic and red.

Functional outcome	Imaging modality	R ²	Adjusted R ²	p-value
MWM	TSPO PET	0.26	0.20	0.0527
	<i>DTI</i>	<i>0.86</i>	<i>0.78</i>	<i>0.0013</i>
	<i>TSPO PET + DTI</i>	<i>0.98</i>	<i>0.94</i>	<i>0.0003</i>
% improvement escape latency day 1 vs. day 2	TSPO PET	0.25	0.13	0.1777
	<i>DTI</i>	<i>0.64</i>	<i>0.55</i>	<i>0.0081</i>
	TSPO PET + DTI	0.64	0.55	0.0081

5. Discussion

The main finding of our study was that both subacute TSPO expression and changes in DTI metrics following CCI injury correlated with several chronic sequelae. Importantly, not only the absolute SUV and DTI values at distinct time-points were good correlates of the functional outcome, but also the relative change in TSPO expression and FA over time. Some of the TSPO PET and DTI measurements showed good sensitivity and specificity in distinguishing TBI rats with and without a particular chronic deficit, making them promising prognostic biomarkers. Depending on the behavioural deficit that is investigated, TSPO PET data or DTI metrics alone, or the combination of the two imaging modalities, can predict the long-term deficit.

5.1. Subacute brain inflammation and microstructural changes after TBI

High TSPO binding of [¹⁸F]PBR111 was observed at 7 days post-contusion, which decreased over time. This temporal profile was similar to previously reported binding of other TSPO radioligands in rat contusion models (16, 17, 39).

Decreased anisotropy and increased diffusivity have previously been observed after experimental TBI (reviewed in (40)) in line with our findings at 4 days post-TBI. Neuronal cell loss, resulting in a decreased neurite density, axon damage, demyelination and disorganised gliosis can underlie the decreased anisotropy. The subsequent increase in anisotropy at 18 days post-TBI may be due to neuronal regeneration/reorganisation (e.g., axon sprouting), remyelination and organised gliosis (e.g., glial scarring). The

increased diffusivity may be explained by vasogenic edema, neuronal cell death and gliosis (e.g., amoeboid microglia).(40) A worsening of the diffusivity over time may reflect secondary injury (41). Furthermore, we observed a correlation between TSPO binding in the lesion on the one hand and decreased anisotropy (FA) and increased diffusivity (MD, AD and RD) on the other hand, supporting the hypothesis that gliosis contributed to the observed changes in DTI parameters.

5.2. Chronic sequelae of TBI

CCI-injured rats exhibited several chronic deficits compared to naïve and/or sham-operated animals. In several instances, CCI-injured animals only differed significantly from naïve animals, but not from sham-operated rats (the latter often showing an intermediate response compared to naïve and CCI-injured rats). This is not that surprising, since it has been shown that craniotomised animals can display behavioural deficits compared to naïve animals (27).

CCI-injured rats exhibited an increased tendency to enter the centre of the open field compared to controls, which may be due to disinhibition and impulsivity (common symptoms in TBI patients (42) and observed in rats following CCI-injury (43)) or decreased anxiety, which has been observed in CCI-injured mice (44). Several studies have observed increased thigmotaxis in an open field following experimental TBI in rodents, while some failed to observe a difference between TBI and sham-operated animals. Differences in observation might be explained by differences in injury type, location and severity, species and strain differences, and a different timing of the open field test (44-48). Reduced anxiety-like behaviour and increased disinhibition/impulsivity has been observed in other behavioural tests

following CCI-injury, including elevated zero maze and light-dark box tests and the delay discounting task (43, 44).

CCI-injured rats exhibited anhedonia in the chronic period, which is an indication of depression-like behaviour. Some studies have failed to observe anhedonia following experimental TBI in rodents, which could be due to differences in injury type, location and severity, species and strain differences, and a different timing of the sucrose preference test (44, 45).

Most of the EDs and seizures that we observed during this study were either spike-wave discharges (SWDs) or high-voltage rhythmic spike (HVRS) discharges and were bilateral in onset. If there was a behavioural manifestation, then it was usually a behavioural arrest. These SWDs and HVRS discharges have been shown to occur spontaneously in this and other rat strains (both inbred and outbred) and their occurrence progresses with age, which complicates the use of rodents to study acquired epilepsy (49-51). While some have argued that there is no difference in the occurrence of SWDs between sham-operated and fluid percussion-injured (FPI) animals (52), others have described a higher frequency of SWDs in FPI animals compared to shams (53). In our study we did not observe a significant difference between naïve, sham-operated and CCI-injured rats regarding the occurrence of EDs. Because of the controversy regarding SWDs, HVRS discharges and non-convulsive (especially absence-like) seizures in models of posttraumatic epilepsy, we limit ourselves to the occurrence of convulsive (i.e., S3-5) seizures to make conclusions regarding the development of posttraumatic epilepsy (PTE) in our CCI rat model. At 6 months post-injury none of the rats had any convulsive seizures. At the 9-month time-point, one CCI-injured animal experienced two spontaneous convulsive seizures during

the one-week monitoring period. This rat was considered epileptic and was also the only animal that went into *status epilepticus* during the subsequent PTZ test. It is important to note that this rat also had the highest frequency of spontaneous non-convulsive behavioural seizures during the one-week monitoring period at 9 months post-injury. Hence, 14% (1/7 vEEG-monitored) rats developed posttraumatic epilepsy by the end of our study, which is comparable to the study of Kelly and colleagues, who perceived spontaneous convulsive seizures in 15% of all CCI-injured rats (5% (2/40) in vEEG-monitored and 19% (17/88) in video-monitored rats) (54). The development of posttraumatic epilepsy has also been studied after CCI-injury in mice. Bolkvadze and Pitkänen observed spontaneous convulsive seizures in 9% of the CCI-injured mice (55), while Hunt and colleagues reported that 13-18% of severely injured CCI mice had spontaneous convulsive seizures (56, 57). In our study one sham-operated rat experienced one convulsive seizure during the monitoring period, which is uncommon, but has been reported previously by others as well (58). None of the naïve animals had convulsive seizures.

We observed a clear increase in seizure susceptibility during the second PTZ assay at 9 months post-injury when we used 30 mg/kg PTZ (86% CCI rats developed convulsive seizures vs. 38% controls), but not at 6 months post-injury with the 25 mg/kg PTZ dose. However, in a separate cohort, we also observed a clear increase in seizure susceptibility at 6 months post-injury when using the 30 mg/kg dose (78% CCI rats vs. 26% controls) (similar to previous observations in CCI mice at this time-point(55)), suggesting that the dose of PTZ is important to distinguish between TBI animals and controls. Similar observations have been made by the group of Pitkänen, who also

employed 25 mg/kg and 30 mg/kg PTZ doses in Sprague-Dawley rats to assess seizure susceptibility after TBI (FPI) (22, 37).

The CCI rats exhibited a clear deficit in the acquisition of the MWM task, which was most pronounced on day 2 of the training phase. In addition, they also displayed a slight non-significant deficit in the retention trial. Deficits in hippocampus-dependent spatial learning and memory have consistently been shown after experimental TBI in rodents using the MWM test (59-61). Cognitive impairment following experimental TBI has been shown using several different paradigms, showing both retrograde and anterograde amnesia, as well as working memory deficits (reviewed in (62)).

5.3. Correlation between subacute brain inflammation and microstructural alterations and chronic TBI sequelae

Several correlations were observed between subacute TSPO expression and DTI metrics in the perilesional cortex and ipsilesional hippocampus and long-term functional deficits. Importantly, not only the absolute [^{18}F]PBR111 SUVs and DTI values at the two subacute time-points correlated with chronic outcome, but also the relative change in TSPO expression and DTI parameters over time, i.e., the dynamics of the neuroinflammatory response and degeneration/regeneration processes.

Surprisingly, a pronounced decrease in TSPO expression in the perilesional cortex over time correlated with a higher disinhibition level in CCI rats as suggested by the open field test. Interestingly, TSPO itself is involved in the synthesis of neurosteroids, some of which have anxiolytic effects (e.g., allopregnanolone). Overexpression of TSPO in mice has been shown to produce anxiolytic behaviour (63). While no positive correlation could be

established between the subacute increase in TSPO and the long-term increase in disinhibition, it cannot be excluded that TSPO played some role in the subsequent disinhibited behaviour. CCI animals with an increase in FA in ipsilesional hippocampus over time showed less disinhibition than animals where the initial FA deficit did not resolve or even worsened over time. An increase in FA might indicate neuronal regeneration and repair, which may explain the better functional outcome (40, 64).

High levels of subacute TSPO in the ipsilesional hippocampus and perilesional cortex correlated with high spontaneous behavioural seizure frequency and increased seizure susceptibility at 6 and 9 months post-TBI. Animals that had a minimal decrease in TSPO binding over time, i.e., persistent inflammation, were shown to have a high frequency of behavioural seizures and increased seizure susceptibility at 9 months post-TBI. Interestingly, the only rat that developed spontaneous recurrent convulsive seizures in this study and that went into *status epilepticus* following PTZ administration at the final time-point was also the only animal that had a prominent increase in subacute TSPO expression over time in the perilesional cortex. Several inflammatory mediators have been implicated in epileptogenesis, seizure initiation and TBI-induced pathogenesis and might play a role in the development of posttraumatic epilepsy (PTE) (reviewed in (7)). A pronounced and enduring inflammatory response following TBI might lead to the development of PTE, as supported by our study. Changes in FA, MD, AD and RD also correlated with increased seizure susceptibility. A more pronounced deficit in FA, MD, AD and RD in perilesional cortex correlated with a shorter latency to the first spike during the 6-month PTZ assay. Our observations are in line with studies performed by Kharatishvili and

Immonen and colleagues, who showed that increased average diffusion in ipsilesional hippocampus and perilesional cortex correlated with increased chronic seizure susceptibility after FPI (latency to first spike, number of spikes and number of EDs) and with the severity of mossy fiber sprouting post-FPI, a form of hippocampal circuitry reorganisation that is thought to be related to epileptogenesis (22, 23). This indicates that these diffusion measurements can be good predictors of seizure susceptibility in different TBI models. CCI rats with a limited increase or even a decrease in FA over time in ipsilesional hippocampus had a higher number of EDs during the PTZ assay at 6 months post-injury, while a more pronounced increase in FA in perilesional cortex over time correlated with a shorter latency to the first convulsive seizure during the 9-month PTZ assay. An increase in FA can be due to increased plasticity (beneficial or aberrant) or increased organised gliosis (e.g., glial scarring).

A pronounced subacute neuroinflammatory response in the perilesional cortex correlated with a more severe learning deficit in our CCI rats. Part of the lesioned and perilesional cortex is the parietal association cortex, which is implicated in spatial processing. Lesions of this area have been shown to cause deficits in the acquisition of the MWM task (65). Neuroinflammation has been shown to affect cognition; inhibition of subacute inflammation has been demonstrated to improve the cognitive outcome following experimental TBI (9-11). CCI rats with a more pronounced increase in MD and RD in ipsilesional hippocampus at 18 days post-injury displayed a greater deficit in the acquisition of the MWM task. Similarly, Immonen et al. showed that FPI rats with a higher increase in average diffusion in ipsilesional hippocampus at 23 days post-injury exhibited a greater impairment in the

MWM test at 7 months post-injury (24). This research group also observed a correlation between average diffusion in hippocampus at several acute and chronic time-points post-FPI and mossy fiber sprouting at a chronic time-point (22). Interestingly, inhibition of mossy fiber sprouting has been shown to coincide with an amelioration of MWM performance in pilocarpine-treated mice (66).

The interpretation of diffusion metrics remains challenging, since various cellular alterations can cause a similar DTI abnormality. In addition, several cellular processes (increased plasticity, gliosis) can have both beneficial and detrimental effects, possibly affecting different behavioural processes in a different manner.

5.4. Prognostic biomarkers and models

ROC curve analysis showed that several TSPO PET and DTI parameters had good sensitivity and specificity (area under the ROC curve = 0.83-0.89) to distinguish between traumatised rats with and without a particular chronic deficit and hence are very promising prognostic biomarkers for the long-term outcome following TBI.

Stepwise regression analysis showed that both TSPO PET and DTI data alone, as well as the combination of TSPO PET and DTI parameters provided good regression models (adjusted $R^2 = 0.50-1.00$) to explain the variability in the chronic outcome parameters, depending on which behavioural parameter was investigated. These data indicate that both TSPO PET and DTI parameters could be useful characteristics to be implemented into novel, improved prognostic models for the outcome of TBI. Moreover, these models may give a more precise prognosis than the current prognostic

models. More research is warranted to conclude whether such prognostic models would be of value to predict the outcome of individual subjects.

6. Conclusion

Our study shows that subacute neuroinflammation, measured by PET imaging with a TSPO radioligand, and microstructural changes, measured by DTI, correlate with several chronic deficits after CCI injury in rats, including disinhibition, spontaneous behavioural seizure frequency, seizure susceptibility and impaired visuospatial learning. Importantly, not only the absolute PET/DTI values at the two subacute time-points correlated with chronic outcome, but also the subacute evolution of brain inflammation and microstructural changes proved to be good correlates of long-term behavioural deficits. Moreover, our study suggests that TSPO PET/DTI parameters could be useful prognostic biomarkers and be implemented in novel, improved prognostic models for prediction of the development of different TBI sequelae.

Acknowledgments

We thank Krystyna Szewczyk, Annemie Van Eetveldt, Philippe Joye and Caroline Berghmans for their excellent technical assistance. This research was supported by ERA-NET NEURON/Research Foundation Flanders GA00913N. Stephan Missault has a PhD fellowship of the Research Foundation Flanders (11K3714N/11K3716N). The 7T PharmaScan MR system was purchased through Hercules foundation funding (Belgium) under the promotership of Prof. Annemie Van der Linden. We also acknowledge the Interuniversity Poles of Attraction of the Belgian Federal Science Policy Office (IAP7/16), Belgian Alzheimer Research Foundation

(SAO-FRA), agreement between Institute Born-Bunge and University of Antwerp, the Medical Research Foundation Antwerp, the Thomas Riellaerts research fund, the Alzheimer Research Center Groningen (UMCG) and Neurosearch Antwerp.

7. References

1. Roozenbeek B, Maas AI, Menon DK (2013): Changing patterns in the epidemiology of traumatic brain injury. *Nat Rev Neurol*. 9:231-236.
2. Bramlett HM, Dietrich WD (2015): Long-Term Consequences of Traumatic Brain Injury: Current Status of Potential Mechanisms of Injury and Neurological Outcomes. *J Neurotrauma*. 32:1834-1848.
3. Collaborators MCT, Perel P, Arango M, Clayton T, Edwards P, Komolafe E, et al. (2008): Predicting outcome after traumatic brain injury: practical prognostic models based on large cohort of international patients. *BMJ*. 336:425-429.
4. Steyerberg EW, Mushkudiani N, Perel P, Butcher I, Lu J, McHugh GS, et al. (2008): Predicting outcome after traumatic brain injury: development and international validation of prognostic scores based on admission characteristics. *PLoS Med*. 5:e165; discussion e165.
5. Maas AI, Marmarou A, Murray GD, Teasdale SG, Steyerberg EW (2007): Prognosis and clinical trial design in traumatic brain injury: the IMPACT study. *J Neurotrauma*. 24:232-238.
6. Young NH, Andrews PJ (2008): Developing a prognostic model for traumatic brain injury--a missed opportunity? *PLoS Med*. 5:e168.
7. Webster KM, Sun M, Crack P, O'Brien TJ, Shultz SR, Semple BD (2017): Inflammation in epileptogenesis after traumatic brain injury. *J Neuroinflammation*. 14:10.
8. Russo MV, McGavern DB (2016): Inflammatory neuroprotection following traumatic brain injury. *Science*. 353:783-785.
9. James ML, Wang H, Cantillana V, Lei B, Kernagis DN, Dawson HN, et al. (2012): TT-301 inhibits microglial activation and improves outcome after central nervous system injury in adult mice. *Anesthesiology*. 116:1299-1311.
10. Clausen F, Hanell A, Bjork M, Hillered L, Mir AK, Gram H, et al. (2009): Neutralization of interleukin-1beta modifies the inflammatory response and improves histological and cognitive outcome following traumatic brain injury in mice. *Eur J Neurosci*. 30:385-396.
11. Lloyd E, Somera-Molina K, Van Eldik LJ, Watterson DM, Wainwright MS (2008): Suppression of acute proinflammatory cytokine and chemokine upregulation by post-injury administration of a novel small molecule improves long-term neurologic outcome in a mouse model of traumatic brain injury. *J Neuroinflammation*. 5:28.
12. Juengst SB, Kumar RG, Failla MD, Goyal A, Wagner AK (2015): Acute inflammatory biomarker profiles predict depression risk following moderate to severe traumatic brain injury. *J Head Trauma Rehabil*. 30:207-218.

13. Witcher KG, Eiferman DS, Godbout JP (2015): Priming the inflammatory pump of the CNS after traumatic brain injury. *Trends Neurosci.* 38:609-620.
14. Fenn AM, Gensel JC, Huang Y, Popovich PG, Lifshitz J, Godbout JP (2014): Immune activation promotes depression 1 month after diffuse brain injury: a role for primed microglia. *Biol Psychiatry.* 76:575-584.
15. Bertoglio D, Verhaeghe J, Santermans E, Amhaoul H, Jonckers E, Wyffels L, et al. (2017): Non-invasive PET imaging of brain inflammation at disease onset predicts spontaneous recurrent seizures and reflects comorbidities. *Brain Behav Immun.* 61:69-79.
16. Wang Y, Yue X, Kiesewetter DO, Niu G, Teng G, Chen X (2014): PET imaging of neuroinflammation in a rat traumatic brain injury model with radiolabeled TSPO ligand DPA-714. *Eur J Nucl Med Mol Imaging.* 41:1440-1449.
17. Yu I, Inaji M, Maeda J, Okauchi T, Nariai T, Ohno K, et al. (2010): Glial cell-mediated deterioration and repair of the nervous system after traumatic brain injury in a rat model as assessed by positron emission tomography. *J Neurotrauma.* 27:1463-1475.
18. Irimia A, Wang B, Aylward SR, Prastawa MW, Pace DF, Gerig G, et al. (2012): Neuroimaging of structural pathology and connectomics in traumatic brain injury: Toward personalized outcome prediction. *Neuroimage Clin.* 1:1-17.
19. Koerte IK, Hufschmidt J, Muehlmann M, Lin AP, Shenton ME (2016): Advanced Neuroimaging of Mild Traumatic Brain Injury. In: Laskowitz D, Grant G, editors. *Translational Research in Traumatic Brain Injury.* Boca Raton (FL).
20. Wright DK, Johnston LA, Kershaw J, Ordidge R, O'Brien TJ, Shultz SR (2017): Changes in Apparent Fiber Density and Track-Weighted Imaging Metrics in White Matter following Experimental Traumatic Brain Injury. *J Neurotrauma.* 34:2109-2118.
21. Wright DK, Trezise J, Kamnaksh A, Bekdash R, Johnston LA, Ordidge R, et al. (2016): Behavioral, blood, and magnetic resonance imaging biomarkers of experimental mild traumatic brain injury. *Sci Rep.* 6:28713.
22. Kharatishvili I, Immonen R, Grohn O, Pitkanen A (2007): Quantitative diffusion MRI of hippocampus as a surrogate marker for post-traumatic epileptogenesis. *Brain.* 130:3155-3168.
23. Immonen R, Kharatishvili I, Grohn O, Pitkanen A (2013): MRI biomarkers for post-traumatic epileptogenesis. *J Neurotrauma.* 30:1305-1309.

24. Immonen RJ, Kharatishvili I, Grohn H, Pitkanen A, Grohn OH (2009): Quantitative MRI predicts long-term structural and functional outcome after experimental traumatic brain injury. *Neuroimage*. 45:1-9.
25. Frey L, Lepkin A, Schickedanz A, Huber K, Brown MS, Serkova N (2014): ADC mapping and T1-weighted signal changes on post-injury MRI predict seizure susceptibility after experimental traumatic brain injury. *Neurol Res*. 36:26-37.
26. Missault S, Peeters L, Amhaoul H, Thomae D, Van Eetveldt A, Favier B, et al. (2017): Decreased levels of active uPA and KLK8 assessed by [111 In]MICA-401 binding correlate with the seizure burden in an animal model of temporal lobe epilepsy. *Epilepsia*.
27. Cole JT, Yarnell A, Kean WS, Gold E, Lewis B, Ren M, et al. (2011): Craniotomy: true sham for traumatic brain injury, or a sham of a sham? *J Neurotrauma*. 28:359-369.
28. Bourdier T, Pham TQ, Henderson D, Jackson T, Lam P, Izard M, et al. (2012): Automated radiosynthesis of [18F]PBR111 and [18F]PBR102 using the Tracerlab FXFN and Tracerlab MXFDG module for imaging the peripheral benzodiazepine receptor with PET. *Appl Radiat Isot*. 70:176-183.
29. Katsifis A, Loc'h C, Henderson D, Bourdier T, Pham T, Greguric I, et al. (2011): A rapid solid-phase extraction method for measurement of non-metabolised peripheral benzodiazepine receptor ligands, [(18)F]PBR102 and [(18)F]PBR111, in rat and primate plasma. *Nucl Med Biol*. 38:137-148.
30. Hudson HM, Larkin RS (1994): Accelerated image reconstruction using ordered subsets of projection data. *IEEE Trans Med Imaging*. 13:601-609.
31. Defrise M, Kinahan PE, Townsend DW, Michel C, Sibomana M, Newport DF (1997): Exact and approximate rebinning algorithms for 3-D PET data. *IEEE Trans Med Imaging*. 16:145-158.
32. Tu TW, Turtzo LC, Williams RA, Lescher JD, Dean DD, Frank JA (2014): Imaging of spontaneous ventriculomegaly and vascular malformations in Wistar rats: implications for preclinical research. *J Neuropathol Exp Neurol*. 73:1152-1165.
33. Missault S, Van den Eynde K, Vanden Berghe W, Franssen E, Weeren A, Timmermans JP, et al. (2014): The risk for behavioural deficits is determined by the maternal immune response to prenatal immune challenge in a neurodevelopmental model. *Brain Behav Immun*. 42:138-146.
34. Amhaoul H, Hamaide J, Bertoglio D, Reichel SN, Verhaeghe J, Geerts E, et al. (2015): Brain inflammation in a chronic epilepsy model: Evolving pattern of the translocator protein during epileptogenesis. *Neurobiol Dis*. 82:526-539.

35. Amhaoul H, Ali I, Mola M, Van Eetveldt A, Szewczyk K, Missault S, et al. (2016): P2X7 receptor antagonism reduces the severity of spontaneous seizures in a chronic model of temporal lobe epilepsy. *Neuropharmacology*. 105:175-185.
36. Fisher RS (2015): Redefining epilepsy. *Curr Opin Neurol*. 28:130-135.
37. Huusko N, Romer C, Ndode-Ekane XE, Lukasiuk K, Pitkanen A (2015): Loss of hippocampal interneurons and epileptogenesis: a comparison of two animal models of acquired epilepsy. *Brain Struct Funct*. 220:153-191.
38. van der Werf IM, Van Dam D, Missault S, Yalcin B, De Deyn PP, Vandeweyer G, et al. (2017): Behavioural characterization of AnkyrinG deficient mice, a model for ANK3 related disorders. *Behav Brain Res*. 328:218-226.
39. Donat CK, Gaber K, Meixensberger J, Brust P, Pinborg LH, Hansen HH, et al. (2016): Changes in Binding of [(123)I]CLINDE, a High-Affinity Translocator Protein 18 kDa (TSPO) Selective Radioligand in a Rat Model of Traumatic Brain Injury. *Neuromolecular Med*. 18:158-169.
40. Hutchinson EB, Schwerin SC, Avram AV, Juliano SL, Pierpaoli C (2017): Diffusion MRI and the detection of alterations following traumatic brain injury. *J Neurosci Res*.
41. Immonen RJ, Kharatishvili I, Niskanen JP, Grohn H, Pitkanen A, Grohn OH (2009): Distinct MRI pattern in lesional and perilesional area after traumatic brain injury in rat--11 months follow-up. *Exp Neurol*. 215:29-40.
42. Kocka A, Gagnon J (2014): Definition of Impulsivity and Related Terms Following Traumatic Brain Injury: A Review of the Different Concepts and Measures Used to Assess Impulsivity, Disinhibition and other Related Concepts. *Behav Sci (Basel)*. 4:352-370.
43. Vonder Haar C, Martens KM, Riparip LK, Rosi S, Wellington CL, Winstanley CA (2017): Frontal Traumatic Brain Injury Increases Impulsive Decision Making in Rats: A Potential Role for the Inflammatory Cytokine Interleukin-12. *J Neurotrauma*.
44. Tucker LB, Burke JF, Fu AH, McCabe JT (2017): Neuropsychiatric Symptom Modeling in Male and Female C57BL/6J Mice after Experimental Traumatic Brain Injury. *J Neurotrauma*. 34:890-905.
45. Jones NC, Cardamone L, Williams JP, Salzberg MR, Myers D, O'Brien TJ (2008): Experimental traumatic brain injury induces a pervasive hyperanxious phenotype in rats. *J Neurotrauma*. 25:1367-1374.
46. Kim H, Yu T, Cam-Etoz B, van Groen T, Hubbard WJ, Chaudry IH (2017): Treatment of traumatic brain injury with 17alpha-ethinylestradiol-3-sulfate in a rat model. *J Neurosurg*. 127:23-31.

47. McNamara KC, Lisembee AM, Lifshitz J (2010): The whisker nuisance task identifies a late-onset, persistent sensory sensitivity in diffuse brain-injured rats. *J Neurotrauma*. 27:695-706.
48. Rowe RK, Ziebell JM, Harrison JL, Law LM, Adelson PD, Lifshitz J (2016): Aging with Traumatic Brain Injury: Effects of Age at Injury on Behavioral Outcome following Diffuse Brain Injury in Rats. *Dev Neurosci*. 38:195-205.
49. Kelly KM (2004): Spike-wave discharges: absence or not, a common finding in common laboratory rats. *Epilepsy Curr*. 4:176-177.
50. Pearce PS, Friedman D, Lafrancois JJ, Iyengar SS, Fenton AA, Maclusky NJ, et al. (2014): Spike-wave discharges in adult Sprague-Dawley rats and their implications for animal models of temporal lobe epilepsy. *Epilepsy Behav*. 32:121-131.
51. Shaw FZ (2004): Is spontaneous high-voltage rhythmic spike discharge in Long Evans rats an absence-like seizure activity? *J Neurophysiol*. 91:63-77.
52. Rodgers KM, Dudek FE, Barth DS (2015): Progressive, Seizure-Like, Spike-Wave Discharges Are Common in Both Injured and Uninjured Sprague-Dawley Rats: Implications for the Fluid Percussion Injury Model of Post-Traumatic Epilepsy. *J Neurosci*. 35:9194-9204.
53. Sick T, Wasserman J, Bregy A, Sick J, Dietrich WD, Bramlett HM (2017): Increased Expression of Epileptiform Spike/Wave Discharges One Year after Mild, Moderate, or Severe Fluid Percussion Brain Injury in Rats. *J Neurotrauma*. 34:2467-2474.
54. Kelly KM, Miller ER, Lepsveridze E, Kharlamov EA, McHedlishvili Z (2015): Posttraumatic seizures and epilepsy in adult rats after controlled cortical impact. *Epilepsy Res*. 117:104-116.
55. Bolkvadze T, Pitkanen A (2012): Development of post-traumatic epilepsy after controlled cortical impact and lateral fluid-percussion-induced brain injury in the mouse. *J Neurotrauma*. 29:789-812.
56. Hunt RF, Scheff SW, Smith BN (2009): Posttraumatic epilepsy after controlled cortical impact injury in mice. *Exp Neurol*. 215:243-252.
57. Hunt RF, Scheff SW, Smith BN (2010): Regionally localized recurrent excitation in the dentate gyrus of a cortical contusion model of posttraumatic epilepsy. *J Neurophysiol*. 103:1490-1500.
58. Nissinen J, Andrade P, Natunen T, Hiltunen M, Malm T, Kanninen K, et al. (2017): Disease-modifying effect of atipamezole in a model of post-traumatic epilepsy. *Epilepsy Res*. 136:18-34.

59. Hamm RJ, Dixon CE, Gbadebo DM, Singha AK, Jenkins LW, Lyeth BG, et al. (1992): Cognitive deficits following traumatic brain injury produced by controlled cortical impact. *J Neurotrauma*. 9:11-20.
60. Scheff SW, Baldwin SA, Brown RW, Kraemer PJ (1997): Morris water maze deficits in rats following traumatic brain injury: lateral controlled cortical impact. *J Neurotrauma*. 14:615-627.
61. Smith DH, Okiyama K, Thomas MJ, Claussen B, McIntosh TK (1991): Evaluation of memory dysfunction following experimental brain injury using the Morris water maze. *J Neurotrauma*. 8:259-269.
62. Whiting MD, Baranova AI, Hamm RJ (2006): Cognitive Impairment following Traumatic Brain Injury. In: Levin ED, Buccafusco JJ, editors. *Animal Models of Cognitive Impairment*. Boca Raton (FL).
63. Li L, Wang W, Zhang LM, Jiang XY, Sun SZ, Sun LJ, et al. (2017): Overexpression of the 18 kDa translocator protein (TSPO) in the hippocampal dentate gyrus produced anxiolytic and antidepressant-like behavioural effects. *Neuropharmacology*. 125:117-128.
64. Wang S, Chopp M, Nazem-Zadeh MR, Ding G, Nejad-Davarani SP, Qu C, et al. (2013): Comparison of neurite density measured by MRI and histology after TBI. *PLoS One*. 8:e63511.
65. Save E, Moghaddam M (1996): Effects of lesions of the associative parietal cortex on the acquisition and use of spatial memory in egocentric and allocentric navigation tasks in the rat. *Behav Neurosci*. 110:74-85.
66. Ikegaya Y, Nishiyama N, Matsuki N (2000): L-type Ca(2+) channel blocker inhibits mossy fiber sprouting and cognitive deficits following pilocarpine seizures in immature mice. *Neuroscience*. 98:647-659.

PART 2

Brain insult during foetal development



*The risk for behavioural deficits is determined
by the maternal immune response to prenatal
immune challenge in a neurodevelopmental
model*

Published in Brain, Behavior, and Immunity (2014)

1. Abstract

Background: Schizophrenia is a highly disabling psychiatric disorder with a proposed neurodevelopmental basis. One mechanism through which genetic and environmental risk factors might act is by triggering persistent brain inflammation, as evidenced by long-lasting neuro-immunological disturbances in patients. Our goal was to investigate whether microglia activation is a neurobiological correlate to the altered behaviour in the maternal immune activation (MIA) model, a well-validated animal model with relevance to schizophrenia. A recent observation in the MIA model is the differential maternal body weight response to the immune stimulus, correlated with a different behavioural outcome in the offspring. Although it is generally assumed that the differences in maternal weight response reflect differences in cytokine response, this has not been investigated so far. Our aim was to investigate whether i) the maternal weight response to MIA reflects differences in the maternal cytokine response, ii) the differential behavioural phenotype of the offspring extends to depressive symptoms such as anhedonia and iii) there are changes in chronic microglia activation dependent on the behavioural phenotype. **Methods:** Based on a dose-response study, MIA was induced in pregnant rats by injecting 4mg/kg Poly I:C at gestational day 15. Serum samples were collected to assess the amount of TNF- α in the maternal blood following MIA. MIA offspring were divided into weight loss (WL; n=14) and weight gain (WG; n=10) groups, depending on the maternal body weight response to Poly I:C. Adult offspring were behaviourally phenotyped for prepulse inhibition, locomotor activity with and without amphetamine and MK-801 challenge, and sucrose preference. Finally, microglia activation was scored on CD11b- and Iba1-

immunohistochemically stained sections. Results: Pregnant dams that lost weight following MIA showed increased levels of TNF- α compared to controls, unlike dams that gained weight following MIA. Poly I:C WL offspring showed the most severe behavioural outcome. Poly I:C WG offspring, on the other hand, did not show clear behavioural deficits. Most interestingly a reduced sucrose preference indicative of anhedonia was found in Poly I:C WL but not Poly I:C WG offspring compared to controls. Finally, there were no significant differences in microglia activation scores between any of the investigated groups. Conclusions: The individual maternal immune response to MIA is an important determinant of the behavioural outcome in offspring, including negative symptoms such as anhedonia. We failed to find any significant difference in the level of microglia activation between Poly I:C WL, Poly I:C WG and control offspring.

Key words: Poly I:C; Maternal Immune Activation; Neuroinflammation; Schizophrenia; Autism; Locomotion

2. Introduction

Around young adulthood, schizophrenia patients start experiencing various symptoms that have a major impact on their quality of life, including positive (e.g. hallucinations), negative (e.g. anhedonia) and cognitive symptoms (e.g. attention deficits) (1). Although there is a clear genetic component, a large variety of perinatal environmental factors are known to increase the risk of developing schizophrenia, including prenatal infection and malnutrition, obstetric complications and maternal stress (2-4). These environmental insults have been suggested to act through common mediators of inflammation such as oxidative stress and apoptosis, interfering with neurodevelopmental processes like neurogenesis and synaptogenesis (2).

Since the current treatments with antipsychotics are unsatisfactory, there is need for a better understanding of the disease aetiology and pathology. One way to achieve this goal is by testing new hypotheses and treatment strategies in relevant animal models. In the past decade, a maternal immune activation (MIA) animal model with relevance to schizophrenia has been developed, although behavioural readouts have not always been reproducible or consistent. This model is based on the induction of immune effectors in the pregnant mother that cross the placenta and interfere with normal foetal brain development (5, 6). Given their substantial roles during gestation, it is hypothesised that an imbalance in pro- and anti-inflammatory cytokines in the foetal brain may lead to neurodevelopmental abnormalities (5).

Recent reports have described a significant variability in the maternal body weight response to Poly I:C and more importantly, a differential behavioural outcome of the offspring dependent on the individual maternal body weight response. Body weight change serves as an indicator of the pregnant dam's individual responsiveness to the MIA challenge, but it has not been investigated whether this correlates with differences in circulating cytokine levels. Differences in behavioural outcome between offspring of dams that lost weight and offspring of dams that gained weight have been observed in different behavioural paradigms including prepulse inhibition and psychotomimetic-induced locomotor activity. Hyperactivity responses to amphetamine (AMPH), an indirect dopamine agonist, and MK-801, a direct NMDA-receptor antagonist, are interesting behavioural assessments, since they can reflect underlying dopaminergic and glutamatergic (NMDA-receptor-associated) network alterations, which are both involved in

schizophrenia pathology. So far, differences in depressive symptoms such as anhedonia have not been investigated in the rat MIA model.

The relevance of the immune system in schizophrenia pathology is further supported by recent reports of persistent immunological disturbances in schizophrenia patients including aberrant levels of pro-inflammatory cytokines in the blood and cerebrospinal fluid (7-11). These pro-inflammatory cytokines are produced primarily by activated immune cells such as cells of the mononuclear phagocyte system (12). Being the mononuclear phagocytes of the brain, microglia play a major role in early brain development while in adulthood they play a key role in the brain's innate immune reaction. However, depending on their phenotype, microglia have been shown to exert detrimental effects in various neurological conditions (13, 14). Recently, three *post-mortem* studies and three *in-vivo* PET studies have demonstrated a significant increase in activated microglia in the frontotemporal brain regions of schizophrenic patients (15-20). However, these retrospective studies cannot provide a direct link between prenatal infection, behavioural deficits and brain inflammation.

The aim of this study was to investigate whether the individual maternal response to MIA determines behavioural outcome including depressive symptoms in offspring and whether microglia activation acts as a neurobiological correlate to the altered phenotype.

3. Materials and Methods

3.1. Animals

Animals were treated in accordance with the guidelines approved by the European Ethics Committee (decree 86/609/CEE) and the Animal Welfare

Act (7 USC 2131). Animal experiments were approved by the ethical committee of the University of Antwerp (Belgium).

Forty-nine male and forty-nine female Wistar-Hannover rats (Charles River Laboratories, France, 10 weeks of age) were used for timed mated breeding. Upon arrival, the rats were housed individually under standard laboratory conditions in a temperature- ($22\pm 2^{\circ}\text{C}$) and humidity- ($55\pm 10\%$) controlled room on a 12h light-dark cycle (lights on at 6:00 am) with standard food and water available *ad libitum*.

3.2. Poly I:C dose-response study

MIA was induced in thirty-six pregnant rats either in early/mid pregnancy (GD9, n=17) or in mid/late pregnancy (GD15, n=19) by subcutaneous (s.c.) injection with vehicle (nuclease-free water) (n=4 for GD9, n=5 for GD15), 2mg/kg (n=4 for GD9, n=5 for GD15), 4mg/kg (n=4 for GD9, n=4 for GD15) or 8mg/kg (n=5 for GD9, n=5 for GD15) Poly I:C (Polyinosinic-polycytidylic acid sodium salt, Sigma-Aldrich, USA). Six hours after injection, the pregnant rats were sacrificed by decapitation. Maternal blood and central nervous system (CNS) samples from two foetuses per litter were collected and preserved in RNA*later* (Ambion, Life Technologies, USA) at -80°C . RNA was extracted from whole blood using the RiboPure™-Blood Kit (Ambion, Life Technologies, USA) and quantified using a NanoDrop spectrophotometer (NanoDrop, USA). RNA was extracted from foetal CNS samples by homogenizing them in QIAzol and mixing the resulting cell lysates with chloroform. The RNA-containing aqueous phase was recovered and 100% ethanol was added. Final RNA purification was achieved using the RNeasy Mini Kit (Qiagen, the Netherlands). After conversion of mRNA to cDNA (Applied Biosystems, Life Technologies, USA), all samples were tested in triplicate by qPCR (ABI 7300,

Applied Biosystems, Life Technologies, USA) for the relative quantification of IL-1 β , TNF- α , IL-6 and IL-10 (primers from Eurogentec, Japan). qPCR data were analyzed using the 2^{-ddCt} method (21). Ct-values of target transcripts in treated samples were normalized to the geometrical mean of the Ct-values of three housekeeping genes (β -actin, 28S rRNA and hypoxanthine-guanine phosphoribosyltransferase) and then compared to the normalized Ct-values in the untreated reference samples for relative quantification.

3.3. Behavioural study in MIA offspring

Based on the dose-response study, 13 pregnant dams were injected with either vehicle (n=6) or 4mg/kg Poly I:C (n=7) on GD15 (Fig.7-1). Six hours after injection a blood sample was collected from the tail vein. Weight change was measured 24h post-injection. On the day of birth, nests were culled to eight pups per litter. At postnatal day 21 (PND21), male offspring were group-housed under reversed 12h light-dark cycle (lights out at 10:00 am). In total, 22 male control and 24 male Poly I:C offspring were included in the study. In order to avoid possible confounding effects of the psychotomimetic challenges on the level of brain inflammation, offspring from each treatment group were divided into “no challenge” and “challenge” groups, with the latter receiving indirect dopamine agonist AMPH or NMDA-receptor antagonist MK-801 during locomotion testing.

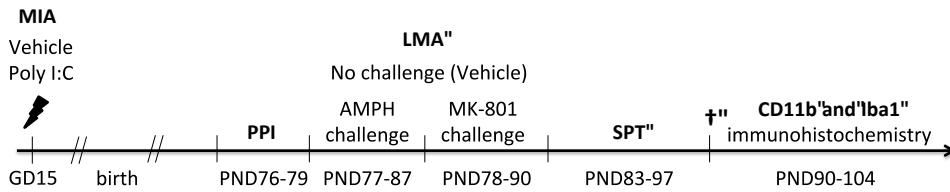


Fig.7-1. Experimental design. Pregnant dams received either a saline or Poly I:C injection at gestational day 15 (GD15). Male adult offspring were behaviourally phenotyped from postnatal day 76 (PND76) onwards, starting with prepulse inhibition (PPI, PND76-79). Locomotor activity was measured, initially spontaneously for 1h, followed by either vehicle (“non-challenge” group) or AMPH (PND77-87) and MK-801 (PND78-90) injection with 2h of subsequent locomotor activity monitoring. In the “challenge” group AMPH and MK-801 were administered on separate days. Sucrose preference test was performed (PND79-96) before sacrificing animals for immunohistochemical analysis of microglial density and activation (PND90-104).

3.4. Follow-up of MIA induction

Six hours after injection with Poly I:C or vehicle a blood sample was collected from the tail vein. Blood samples were allowed to clot for 30min, then centrifuged for 10min at 2000g after which serum was collected. The relative amount of TNF- α was determined using the Rat TNF- α Chemiluminescence ELISA Kit (Novex, Life Technologies, USA). Briefly, serum samples were added to the wells and incubated for 2 hours at room temperature. Wells were washed 5 times and incubated for 1 hour at room temperature with Rat TNF- α Detection Antibody. After washing, wells were incubated with Novobright CSPD-Emerald II Substrate for 30min at room temperature. Finally, samples were semi-quantified by luminescence readings.

3.5. Behavioural analysis

3.5.1. Prepulse inhibition (PPI)

PPI of the acoustic startle response was determined using standard startle boxes (Kinder Scientific, USA) in 46 rats (Vehicle n=22; Poly I:C n=24) at

PND76-79 as described previously (22) with a few modifications. The startle response of the rat was normalised by a train of 5 startle pulses. Next, PPI testing was initialized by subjecting the rat to 8 blocks of 10 trials consisting of the following acoustic stimuli in semi-random order: no stimulus (65dB), startle pulse (120dB; 40ms), prepulse (70dB, 75dB, 80dB; 20ms) and prepulse + startle pulse (interpulse delay of 100ms). The intertrial interval varied randomly between 10 and 20s. PPI was calculated according to the formula: $PPI = [1 - (\text{Prepulse} + \text{pulse} / \text{Pulse})] \times 100$ (23).

3.5.2. Locomotor activity (LMA)

LMA was measured using the home cage - 4x8 photobeam activity system (San Diego Instruments, USA) on the same rats (Vehicle n=22; Poly I:C n=24) at PND82-90 using a protocol adapted from (24). Animals were allowed to acclimatise to the cage for at least 15min. Next, a 60min-test period was initialized in which spontaneous locomotion was recorded in 5min-bins followed by a 120min recording period after s.c. injection of vehicle (control n=14 and Poly I:C n=14 offspring in the “no challenge” groups) or 1mg/kg AMPH (Janssen Pharmaceuticals, Belgium; control n=8 and Poly I:C n=10 in the “challenge” groups). The next day, the experiment was repeated in the “challenge” offspring with injection of a low dose MK-801 (0.2mg/kg, s.c., (+)-MK-801 hydrogen maleate, Sigma-Aldrich, USA).

3.5.3. Sucrose preference test

For the final behavioural test, rats (Vehicle n=22; Poly I:C n=24) were individually housed (PND83-97) to monitor sucrose preference using a protocol adapted from (25). Bottles were weighed and sucrose preference was calculated according to the formula: % sucrose preference = (sucrose solution consumption/total fluid consumption)x100.

3.6. Histological analysis in MIA offspring

Between PND90-104, vehicle (n=22) and Poly I:C (n=24) offspring were sacrificed by decapitation. Brains were fixed overnight in 4% paraformaldehyde, then impregnated overnight with 20% sucrose (containing 0.1% sodium azide) and finally snap-frozen. Serial sagittal cryosections (10 μ m) were collected in triplicate (2.10 mm lateral from bregma (26)).

For visualisation of microglia, immunohistochemical staining against the CD11b-receptor (OX-42) was carried out as described previously (22) with cresyl violet counterstaining. The same procedure was followed for Iba1 (primary antibody rabbit anti-rat; 1:500; Wako Chemicals GmbH, Germany; secondary antibody goat anti-rabbit; 1:500; Jackson Immunoresearch, UK).

Next, CD11b- and Iba1-stained sections were analysed microscopically blinded for treatment. CD11b-stained sections received a visual score representing the level of brain inflammation as described previously (22, 27) in frontotemporal cortex, corpus callosum, hippocampus, thalamus, striatum and pons. Two aspects of the microglia were taken into account when scoring i.e. the density and morphology. Density scores of 1, 2 and 3 were given for low, moderate and high numbers of microglia, respectively, in a given brain region. For the level of activation, a score of 1, 2 or 3 was given for no, a few or several microglia with a thick soma, respectively. Microglia were counted on the Iba1-stained sections in the same regions as above.

3.7. Statistical analysis

Data on cytokine levels (qPCR and ELISA) were analysed using Kruskal-Wallis tests with Dunn's multiple comparison test for post-hoc testing. The

behavioural and histological data were analysed by fitting mixed models with litter as an additional term (random effect) to take possible litter effects into account. PPI data were analysed by fitting a two-way ANOVA model with group and intensity as independent variables. Random intercepts for litter and rat (nested within litter) were added to account for the dependence between the observations within the same litter, and within the same rat, respectively. Data on sucrose preference, total fluid intake and histological data were analysed using a one-way ANOVA model with a random intercept for litter to account for the dependence between the observations within the same litter.

Locomotor activity was analysed by performing linear mixed model analysis to model the number of beam crossings as a function of time and group, accounting for the structure of the data. The same strategy was followed for the AMPH and MK-801 stimuli. To allow for a different slope and intercepts before and after the stimulus at time interval 60, two distinct time-variables were created. The variable inactive time gives the time prior to the stimulus, which was set equal to zero after the stimulus. The variable active time shows the time after the stimulus and was set equal to zero before the stimulus. In addition, we created an indicator variable stimulated that indicated whether the recording took place before or after the stimulus.

The initial fixed-effects model included group membership as a main effect, and an interaction term between group and stimulated. The former term estimates the intercept before the stimulus, while the latter estimates the change in intercept after the stimulus for every group. Main effects for inactive time, and active time, and interaction terms with the group membership. These latter terms test whether the LMA change with time is

different between the groups, before and after the stimulus, respectively. The fixed-effects model was simplified in a stepwise backward way. Significance was tested using an F-test with Kenward-Roger correction for the number of degrees of freedom.

To account for the dependencies between the observations in our dataset, several random effect terms were included in our model. Firstly, possible litter effects needed to be taken into account. Secondly, rats were analysed repeatedly over time. Therefore we included random intercept terms for individual rat, nested within litter, and random slope terms for active time and inactive time, to account for individually varying slopes before and after the stimulus.

Statistical analyses were performed using R 3.1.0, SAS 9.4 and GraphPad Prism 6 (GraphPad Software Inc., USA). Statistical significance was set at $p \leq 0.05$.

4. Results

4.1. Poly I:C dose-response study

Surprisingly, not the highest dose tested but the 4mg/kg dose induced the largest increase in IL-1 β mRNA in maternal blood, which was significant at GD15 ($p \leq 0.05$) (Fig.7-2 panels A, B). The highest increase in TNF- α mRNA expression in the blood of GD15 mothers was also observed at the 4mg/kg dose, while at GD9 the strongest expression was observed using 8mg/kg Poly I:C, an effect which was statistically significant ($p \leq 0.05$) (Fig.7-2 panels E, F). There was no significant increase in IL-6 mRNA expression at either of the gestational time points (Fig.7-2 panels I, J). There was also no indication of increased anti-inflammatory IL-10 at either GD9 or GD15 in maternal blood (Fig.7-2 panels M, N). Interestingly, not all dams responded to Poly I:C with

an induction in cytokine mRNA levels. When comparing the cytokine response of rats in early/mid (GD9) to mid/late (GD15) pregnancy, no statistically significant differences were found for any of the treatments.

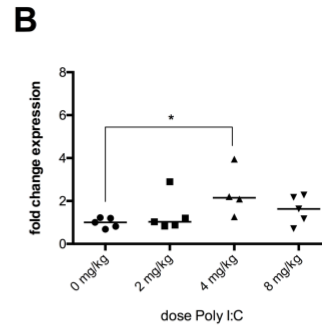
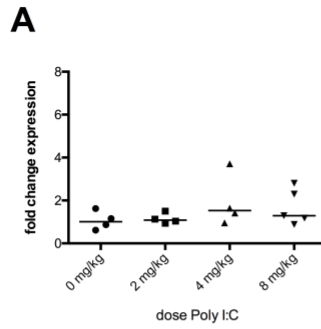
Some foetuses exhibited a moderate to high increase in the mRNA levels of inflammatory cytokines compared to controls, while others showed no increase at all (Fig.7-2 panels C-D; G-H; K-L; O-P). The largest increase in pro-inflammatory cytokines was observed in offspring belonging to the 4mg/kg group (Fig.7-2 panels C;D;G;K;L). While at GD9 this rise in pro-inflammatory cytokines was balanced by a rise in anti-inflammatory IL-10, this was not the case at GD15 (Fig.7-2 panels O, P). It is interesting to note that littermates have similar responses in some nests, but also have quite different responses to the treatment in other nests.

IL-1 β

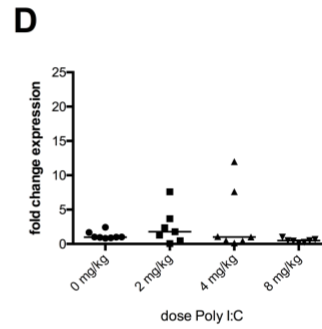
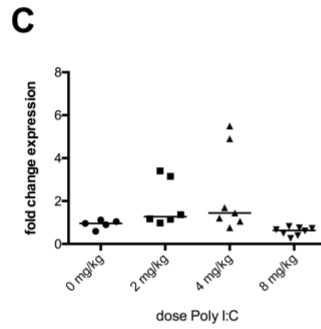
GD9

GD15

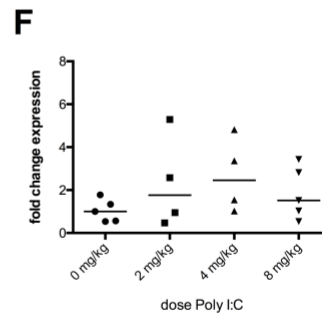
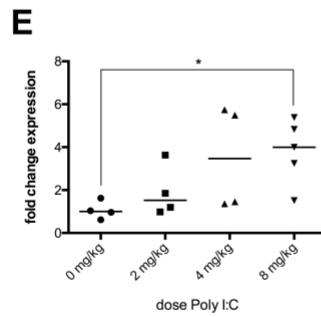
Maternal blood



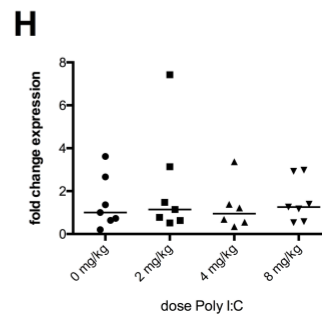
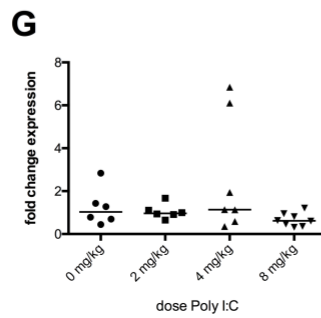
Foetal CNS

TNF- α

Maternal blood



Foetal CNS

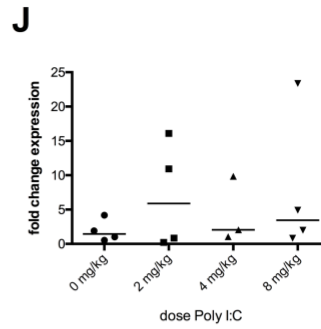
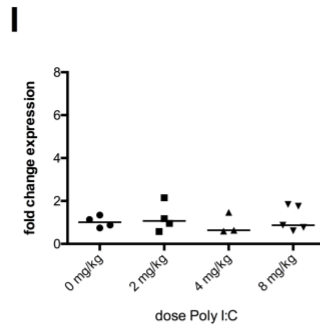


IL-6

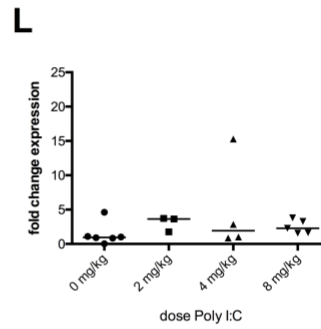
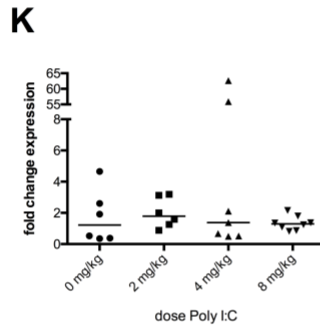
GD9

GD15

Maternal blood

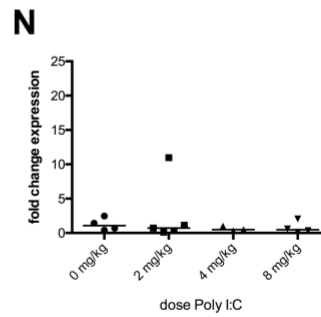
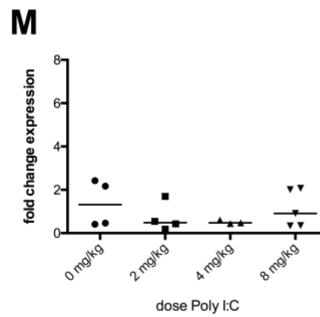


Foetal CNS



IL-10

Maternal blood



Foetal CNS

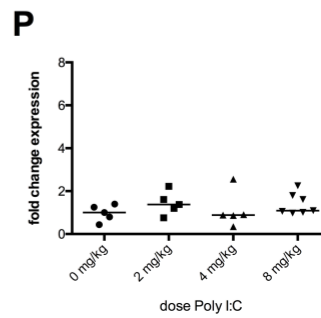
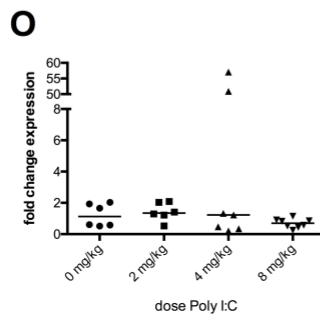


Fig.7-2. Induction of the pro-inflammatory cytokines IL-1 β , TNF- α and IL-6 and of the anti-inflammatory cytokine IL-10 in maternal blood and in foetal central nervous system (CNS) tissue 6h after injection of the dam with either vehicle (nuclease-free water) or one out of three doses of Poly I:C (2mg/kg, 4mg/kg or 8mg/kg, subcutaneously) on gestational days GD9 (left) and GD15 (right) of the pregnancy. All data are represented as separate data points in the plot, with a line representing the median of the group. The highest increases in IL-1 β (A-D) and TNF- α (E-H) mRNA in both maternal blood (A-B and E-F) and foetal CNS (C-D and G-H) were most frequently found in the 4mg/kg dose group, except for the induction of TNF- α in maternal blood at GD9 which was highest in the 8mg/kg dose group. Some fetuses exhibited a very high induction of IL-6 mRNA after the 4mg/kg treatment (K-L). Significance was only reached in maternal blood at GD15 for IL-1 β after 4mg/kg treatment (* $p \leq 0.05$)(B) and at GD9 for TNF- α after 8mg/kg treatment (* $p \leq 0.05$)(E), probably because not all dams and fetuses seemed to respond to maternal immune activation (MIA) by inducing cytokines, at least not at this time point. Interestingly, this rise in pro-inflammatory cytokines seemed to be balanced by a rise in anti-inflammatory IL-10 only at GD9 (O) but not at GD15 (P) after 4mg/kg treatment.

4.2. Behavioural analysis in MIA offspring

4.2.1. Follow-up of MIA induction

There was a clear differentiation within the Poly I:C-treated group regarding weight change 24h post-injection. Three out of seven Poly I:C-treated dams gained weight ($+3.7 \pm 1.2$ g) as did the control group ($n=6$; $+1.7 \pm 0.2$ g), while the others lost weight (-2.5 ± 0.7 g). The Poly I:C-treated dams that lost weight following MIA showed a significant increase in TNF- α 6h post-injection compared to control dams, as determined by ELISA ($p \leq 0.05$). On the other hand, there was no significant increase in TNF- α in the Poly I:C-treated dams that gained weight compared to controls (Fig.7-3).

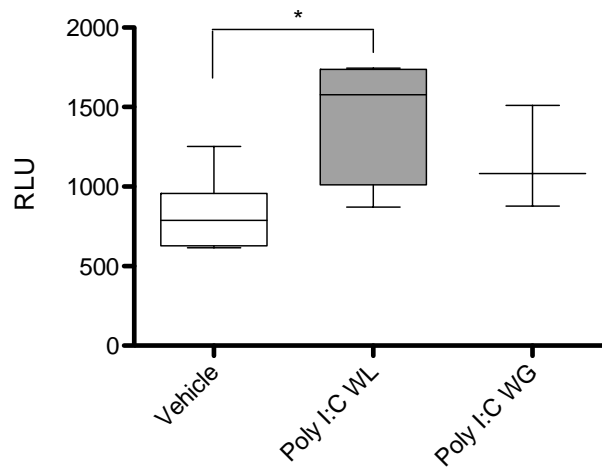


Fig.7-3. Semi-quantification of TNF- α in maternal serum 6h after subcutaneous administration of vehicle (nuclease-free water) or 4mg/kg Poly I:C on GD15. Pregnant dams that received Poly I:C and subsequently lost weight ($n=4$) had a significant increase in circulating TNF- α compared to vehicle-treated dams ($n=6$, $*p\leq 0.05$). On the other hand, pregnant dams that gained weight following Poly I:C injection ($n=3$) had no significant rise in TNF- α levels compared to controls. (RLU = Relative Luminescence Units)

4.2.2. Prepulse inhibition (PPI)

A significant interaction between group and prepulse intensity was observed ($p\leq 0.05$), indicating that the difference in %PPI between the three groups is not uniform across the three different prepulse intensities. However, at none of the three prepulse intensities, the %PPI was significantly different between the three offspring groups (Fig. 7-4). The basal startle response did not differ between treatment groups (data not shown).

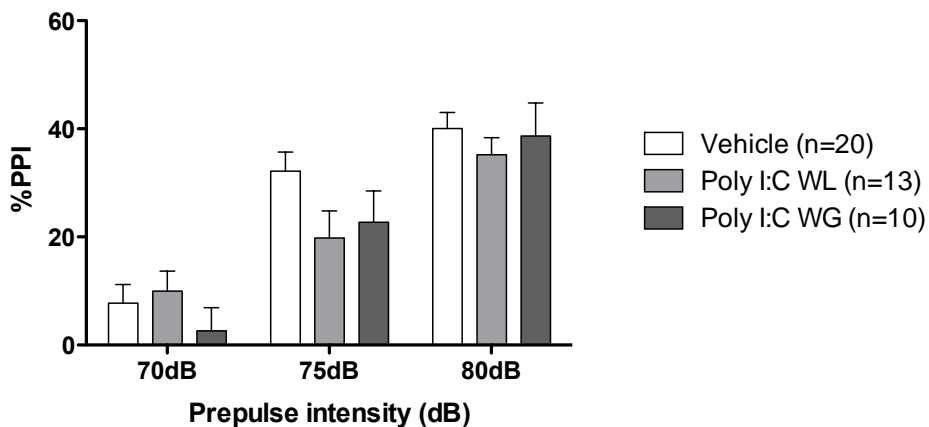


Fig.7-4. Mean (\pm SEM) representation of the effects of MIA on prepulse inhibition of the acoustic startle response. A significant interaction between group and prepulse intensity was observed ($p \leq 0.05$), indicating that the difference in %PPI between the vehicle ($n=20$), Poly I:C WL ($n=13$) and Poly I:C WG ($n=10$) offspring groups is not uniform across the three prepulse intensities (70, 75 and 80dB). There was however no significant difference in %PPI between the three offspring groups at any of the investigated prepulse intensities.

4.2.3. Locomotor activity (LMA)

Overall, no significant differences in spontaneous LMA were observed between offspring groups. The mean LMA did not change significantly with time before the AMPH or MK-801 stimulus, and there was no significant difference in slope between the three offspring groups. Both the AMPH and MK-801 stimuli caused a highly significant increase in LMA across all three offspring groups ($p \leq 0.001$) (Fig.7-5). The immediate response to the stimulus in the Poly I:C WL offspring group was consistently lower compared to the Poly I:C WG and vehicle groups, although in the AMPH-experiment pairwise differences between groups did not reach significance (Fig.7-5 panel A). In the MK-801-experiment, the pairwise difference between the Poly I:C WL group and Poly I:C WG group showed a trend towards significance ($p=0.08$), although neither of these groups was significantly

different from the control group (Fig.7-5 panel B). This observation underlines that Poly I:C WL offspring and Poly I:C WG offspring exhibited opposite responses to the MK-801 challenge.

On average, the LMA kept increasing in the first hour after the stimulus (that is, beyond the immediate response to the stimulus). In the MK-801-experiment, this increase was highly significant ($p \leq 0.001$), whereas in the AMPH-experiment there was only a trend towards significance ($p = 0.06$). In neither of the two experiments, the increase in LMA in the later time intervals differed significantly between the three offspring groups. However, the graph shows that in the MK-801-experiment Poly I:C WL offspring generally had a lower mean LMA compared to vehicle offspring in the later time intervals, while Poly I:C WG offspring generally had a higher mean LMA compared to controls (Fig.7-5 panel B).

4.2.4. Sucrose preference

Poly I:C WL rats demonstrated a significantly reduced sucrose preference compared to controls ($p \leq 0.05$) and Poly I:C WG offspring ($p \leq 0.01$) (Fig.7-6). There was no significant difference in total fluid consumption between any of the offspring groups, indicating that the decreased sucrose preference reflects true anhedonia. Poly I:C WL offspring had a mean \pm SEM total liquid consumption of 2.3 ± 0.2 ml per hour, Poly I:C WG offspring 2.2 ± 0.2 ml per hour and vehicle offspring 3.9 ± 0.5 ml per hour.

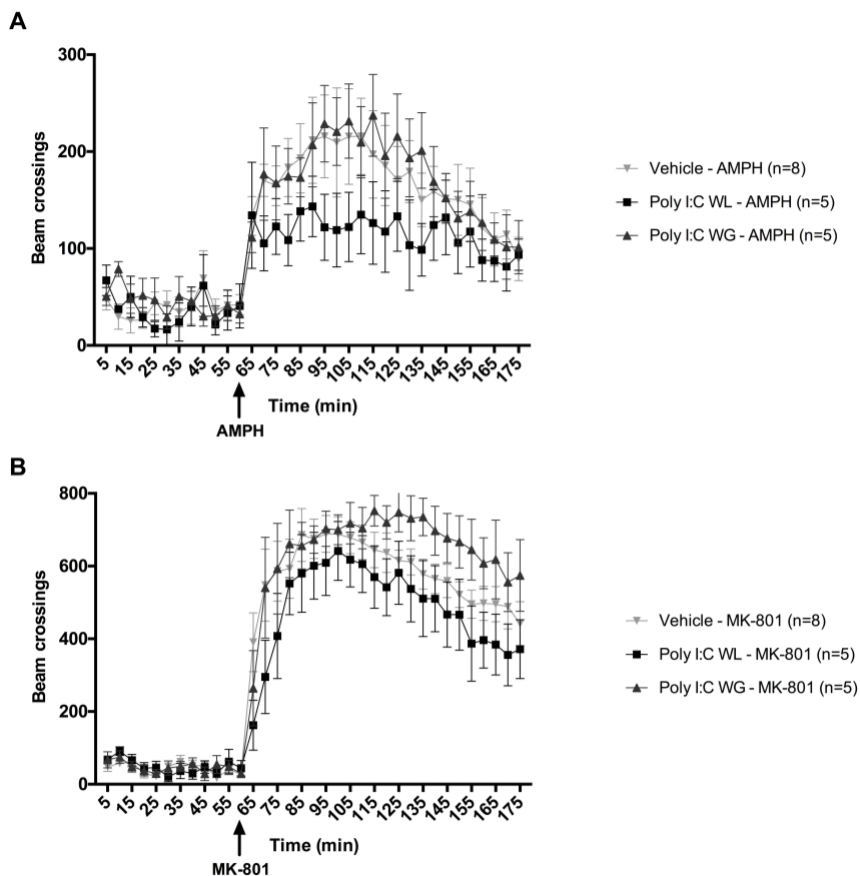


Fig. 7-5. Effects of MIA on psychotomimetic-induced locomotor activity (LMA). Mean (\pm SEM) number of beam crossings per 5min of vehicle (n=8), Poly I:C WL (n=5) and Poly I:C WG (n=5) offspring before (60min) and after (120min) injection (arrow) of AMPH (1mg/kg) (A) and MK-801 (0.2mg/kg) (B). Poly I:C WL offspring showed consistently lower responses to AMPH and MK-801 compared to the Poly I:C WG and vehicle offspring groups, although in the AMPH-experiment pairwise differences between groups did not reach significance (A). In the MK-801-experiment, the pairwise difference between the Poly I:C WL and Poly I:C WG groups showed a trend toward significance ($p=0.08$), whereas neither of these offspring groups differed significantly from the control offspring (B). This indicates that Poly I:C WL and Poly I:C WG offspring showed opposite responses to the MK-801 challenge. In the MK-801-experiment Poly I:C WL offspring generally had a lower mean LMA compared to vehicle offspring in the later time intervals, while Poly I:C WG offspring generally had a higher mean LMA compared to controls (B).

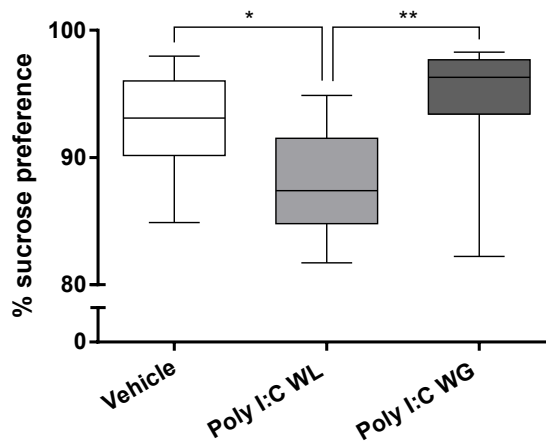


Fig.7-6. Effects of MIA on sucrose preference. Boxplot representation of the percentage sucrose preference of vehicle ($n=18$), Poly I:C WL ($n=9$) and Poly I:C WG ($n=7$) offspring. Poly I:C WL offspring showed a significantly lower sucrose preference compared to control offspring ($*p\leq 0.05$) and Poly I:C WG offspring ($**p\leq 0.01$).

4.2.5. Histological analysis in MIA offspring

There were no significant differences in CD11b-scores or density of Iba1-positive microglia between the three offspring groups in any of the investigated brain regions (data not shown).

5. Discussion

The present study provides important evidence that the individual maternal immune response plays an important role in the development of MIA-induced behavioural deficits. More specifically, we report a differential behavioural outcome in offspring exposed to MIA during mid/late gestation, depending on whether the dam lost or gained weight, an indication of sickness following MIA. Although it is conceivable that the differential maternal weight response following Poly I:C administration is correlated with differences in immune response, this had not been investigated so far. We report here for the first time that pregnant dams that lost weight

following Poly I:C injection exhibited a significant increase in serum TNF- α compared to vehicle-treated dams, while Poly I:C-treated dams that gained weight showed no difference compared to controls. We showed that offspring of dams that experienced weight loss after MIA exhibited a worse outcome in the tested behavioural experiments than the offspring of dams that gained weight. These observations are in line with recent reports of variability in the body weight response to Poly I:C in pregnant rats, which is associated with a significantly different behavioural outcome in offspring (28, 29). We report here for the first time that Poly I:C WL and Poly I:C WG offspring had significant differences in a depressive symptom i.e. anhedonia.

A variety of parameters are used in the literature to induce the MIA model in rodents. In rats, MIA is predominantly induced at GD15 while in mice different gestational time points are used including GD9, GD12.5 and GD17, corresponding to GD10, GD14 and GD20 in rat in terms of neurodevelopment (24, 30-33). A dose-response study based on the working hypothesis of the model was performed in order to obtain more information on the optimal dose (2-8 mg/kg) and time point during pregnancy (GD9 and GD15) of the Poly I:C challenge. More specifically, vehicle injection was compared to Poly I:C for the induction of the most relevant pro- and anti-inflammatory cytokines (IL-1 β , TNF- α , IL-6 and IL-10) involved in the toll-like receptor 3 mediated response using RT-qPCR. Although a differential maternal immune response could be expected at different stages during gestation due to febrile hyporesponsiveness in late pregnancy (34), we did not observe a significant difference in cytokine response between GD9 and GD15. As expected, exposure to Poly I:C in pregnant dams resulted in the induction of mRNA expression of pro-inflammatory cytokines. Most clearly was the significant rise in IL-1 β which was observed in maternal blood 6h

after 4mg/kg Poly I:C administration at GD15. Peripheral pro-inflammatory cytokines, such as IL-1 β , have been suggested to be the prime inducers of sickness behaviour, including decreased food intake and subsequent body weight loss (35). However, clear dose-response effects were not observed for all cytokines including IL-6, an important intermediary of the MIA response (36), or time points probably due to the presence of non-responders in the different dose-groups, both in maternal blood and in foetal CNS tissue. However, it is also possible that these seemingly non-responders had a different time course of mRNA cytokine inductions as the response to an acute immune challenge is strongly time-dependent and different cytokines are known to peak at different time points. Of all the doses tested, the 4mg/kg dose was the most consistent in inducing cytokine mRNA increases in both the maternal and foetal compartments. While the rise in pro-inflammatory cytokines was balanced by an increase in anti-inflammatory IL-10 in GD9 fetuses, this was not the case at GD15. Meyer and colleagues reported that induction of IL-10 could prevent the emergence of behavioural deficits in the Poly I:C mouse model, but that excessive levels of IL-10 alone could also result in behavioural deficits, indicating the importance of a balance in pro- versus anti-inflammatory cytokines (5). Our decision to induce MIA in the behavioural study by injecting 4mg/kg Poly I:C at GD15 is further supported by the fact that these are the most common parameters used to induce MIA in rats (24, 31, 37, 38).

Our study provides supportive evidence for an inherent immune response of the foetus to the MIA challenge, at least in some of the fetuses. While many studies have described increases in inflammatory cytokine protein levels in the foetal brain after MIA challenges (Poly I:C, LPS), they could often

not find any difference in inflammatory cytokine mRNA expression, leading to the assumption that the increased cytokines are not derived from the foetus, but originate in the mother and are transferred to the foetus through the amniotic fluid and placenta (39-41). However, Meyer and colleagues observed some alterations (both decreases and increases) in mRNA expression of inflammatory cytokines in the foetal brain of mice exposed to Poly I:C on GD9 or GD17 (42). Ghiani and colleagues observed elevated mRNA levels of pro-inflammatory cytokines in the foetal brain of rats that were exposed on both GD15 and GD16 to an LPS challenge (43). Our study shows that at least some (apparently responder) foetuses experienced increased mRNA expression of inflammatory cytokines 6h after subcutaneous injection with Poly I:C on GD9 and GD15. Based on the results of our study we can hypothesize that the contradictory findings regarding altered transcription of inflammatory cytokine genes may be ascribed to the presence of responders and non-responders, often resulting in non-significant overall findings. However, limiting factors for a proper comparison of these studies are the use of different species, different immune challenges, different time points during gestation, different administration routes (i.v., i.p., s.c.) and consequently other time courses of cytokine induction responses.

Since we also observed the presence of responders and non-responders in our behavioural experiments, even within the Poly I:C WL and Poly I:C WG groups, it would be interesting to be able to follow-up these foetuses into adulthood and to correlate the data on cytokine mRNA alterations in the foetus with behavioural data in the same adult individual. In this way we could determine whether it is only the maternal immune response that is important for the behavioural outcome in offspring, or the individual foetal

immune response as well. As mentioned above, littermates could have very similar or very different cytokine mRNA inductions. Possible explanations for this observation are 1) a differential distribution of maternal cytokines to the different foetuses, because of the individual maternal-foetal interface (placenta and amniotic sac) of each foetus, and 2) a different genetic predisposition of the foetuses to respond to transient changes in (maternally derived) cytokines with an increase or decrease of cytokine gene transcription, i.e. a different individual foetal immune response.

The pathological outcome of offspring can also be determined by maternal behaviour, possibly through its effects on the offspring's epigenome (44). MIA can alter post-partum maternal behaviour, which may thus pose an additional risk for the development of brain and behavioural pathology in offspring (45). This phenomenon hinders the unequivocal interpretation of results, since the pathology of offspring may result from the prenatal immune challenge but also from abnormal post-partum maternal behaviour, and poses thus an important limitation to many studies. This issue can be addressed by implementing simultaneous cross-fostering designs in which both prenatally immune challenged and control offspring are fostered by control and immune challenged dams (46). While it is known that MIA can influence maternal behaviour, it has not been investigated whether there is a difference in behaviour between dams that lose weight following MIA compared to dams that gain weight. This is a limitation to our study and should be addressed in future experiments.

Offspring were behaviourally phenotyped at young adulthood (PND81) since most behavioural deficits described in the MIA model start to emerge at this stage (24). The most widely described behavioural outcome parameter in

this model is a PPI deficit (31, 37, 47-50), reflecting a sensorimotor gating dysfunction, which is typically observed in both schizophrenia patients and individuals at high-risk of developing schizophrenia (51). However, negative findings have been published as well in the MIA model (22, 30, 52, 53). In the present study, a significant interaction between group and prepulse intensity was observed ($p \leq 0.05$), indicating that the difference in %PPI between the three offspring groups is not uniform across the three different prepulse intensities. However, at none of the tested prepulse intensities, the %PPI was significantly different between the three offspring groups.

Poly I:C WL offspring showed consistently lower responses to AMPH and MK-801 compared to the Poly I:C WG and vehicle groups. A decreased responsiveness to AMPH probably reflects alterations in dopaminergic circuits and is consistent with the observations of Bronson and colleagues who also dichotomized offspring based on the maternal body weight response to MIA (28). Additionally, there is an increasing amount of evidence for glutamatergic and NMDA-receptor abnormalities in schizophrenia (54). The involvement of the glutamatergic system in general and the NMDA-receptor in particular was evaluated by assessing the response to the NMDA-receptor antagonist MK-801, which is known to induce hyperlocomotion in rodents (55). As with AMPH, both hyperresponsiveness (45, 56, 57) and hyporesponsiveness (29, 38) to MK-801 have been described in the MIA model. We observed that Poly I:C WL and Poly I:C WG offspring showed opposite responses to the MK-801 challenge. While neither of the treated offspring groups differed significantly from the control group, the Poly I:C WL and Poly I:C WG groups showed a trend toward significance when compared with each other. Poly I:C WL offspring generally had a lower mean LMA compared with control offspring,

while Poly I:C WG offspring had a higher mean LMA relative to controls. These observations are consistent with those made by Bronson and colleagues who reported a strongly reduced sensitivity to MK-801 in Poly I:C WL offspring and a modestly increased response in Poly I:C WG offspring (28). Vorhees and colleagues reported a decreased response in Poly I:C WL offspring as well (29). A decreased responsiveness to MK-801 is consistent with the NMDA-receptor hypofunction hypothesis of schizophrenia.

An important negative symptom of schizophrenia is anhedonia i.e. the inability to experience pleasure, which is linked to a dysfunction in the brain's reward system. In the present study, Poly I:C WL offspring showed a significantly lower sucrose preference than control and Poly I:C WG offspring. The difference in mean sucrose preference between Poly I:C WL and control offspring was approximately 5%, which is similar to the decrease in sucrose preference previously reported in Poly I:C mice offspring (58). This depressive-like behaviour in Poly I:C WL offspring may be linked to the altered dopaminergic state observed in these animals in the LMA test, since dopamine is one of the most important neurotransmitters involved in reward. We observed no significant difference in total liquid consumption between any of the offspring groups, indicating that the decreased sucrose preference reflects true anhedonia. Depressive-like behaviour such as anhedonia can also be linked to microglia activation. Treatment with minocycline, an inhibitor of microglia activation, has for instance been shown to prevent lipopolysaccharide-induced anhedonia and to improve the recovery from sickness behaviour in mice (59).

One mechanism through which pro-inflammatory cytokines could act prenatally to increase the risk of schizophrenia is by triggering uncontrolled

brain inflammation, which might persist into adulthood (60). Increased microglia activation has been observed in schizophrenia patients in three *post-mortem* and three *in-vivo* PET studies (15-20). Preclinical data on microglial changes in Poly I:C offspring are growing, but are equally contradictory. While some studies have reported an increase in microglial density and activation (22, 61, 62), others have reported no change in density and morphology (63) or even a decrease in reactivity in some brain regions (33, 62). In the present study, we observed no significant differences in CD11b-stained microglial density and activity, nor in Iba1-stained microglial density.

Recently, data are emerging on the importance of chronic alterations in brain cytokines in the MIA model in the absence of overt brain inflammation. Garay et al. described that Poly I:C-induced MIA resulted in complex alterations of many brain cytokines in mice, but no alterations in (Iba1) microglial density or morphology (33). Very recently, Mattei et al. evaluated microglial changes in adult Poly I:C rats. While (Iba1) microglial density was not changed in most brain regions and Iba1 reactivity was actually decreased in hippocampus and cerebellum, the microglial production of TNF- α and IL-1 β was significantly increased in the hippocampus (but not cerebellum) of Poly I:C offspring (62). These observations indicate that alterations in brain cytokines, produced by microglia but possibly also by other immune cells, may have important effects on neural development and behaviour without overt signs of brain inflammation. Future studies should take this into account and focus more on brain cytokines in addition to microglial density/reactivity changes.

Today, a lot of conflicting data exist regarding behavioural changes and neuroinflammation in MIA models. The present study shows that the variability of behavioural outcome in offspring is at least partly determined by the individual maternal immune response to MIA. Most interestingly anhedonia is present in the offspring of mothers with weight loss following MIA compared to the weight gain and vehicle dams.

Acknowledgements

The present study was supported by Research Foundation Flanders (FWO) funding (G.0586.12) and Lanceringsproject BOF of the University of Antwerp. Stephan Missault has a Ph. D. fellowship of the Research Foundation Flanders (FWO). We are extremely grateful to Prof Jean-Michel Rigo, Ajay Palagani, Prof Rudi D'Hooge, Zsuzsanna Vegh, Isabel Pintelon, Annemie Van Eetveldt, Krystyna Szewczyk, Halima Amhaoul and Joery Goossens for their support and practical assistance during this study. We kindly thank Oto Therapeutics and in particular Prof Van de Heyning for the use of the PPI set-up. We are very grateful to Janssen Pharmaceutica and especially Wilhelmus Drinkenburg for providing the photobeam activity system that was used in this study.

6. References

1. Kneeland RE, Fatemi SH (2012): Viral infection, inflammation and schizophrenia. *Progress in neuro-psychopharmacology & biological psychiatry*.
2. Brown AS (2011): The environment and susceptibility to schizophrenia. *Prog Neurobiol*. 93:23-58.
3. Geddes JR, Lawrie SM (1995): Obstetric complications and schizophrenia: a meta-analysis. *The British journal of psychiatry : the journal of mental science*. 167:786-793.
4. Malaspina D, Harlap S, Fennig S, Heiman D, Nahon D, Feldman D, et al. (2001): Advancing paternal age and the risk of schizophrenia. *Archives of general psychiatry*. 58:361-367.
5. Meyer U, Feldon J, Yee BK (2009): A review of the fetal brain cytokine imbalance hypothesis of schizophrenia. *Schizophrenia bulletin*. 35:959-972.
6. Hsiao EY, Patterson PH (2012): Placental regulation of maternal-fetal interactions and brain development. *Developmental neurobiology*. 72:1317-1326.
7. Garver DL, Tamas RL, Holcomb JA (2003): Elevated interleukin-6 in the cerebrospinal fluid of a previously delineated schizophrenia subtype. *Neuropsychopharmacology : official publication of the American College of Neuropsychopharmacology*. 28:1515-1520.
8. Lin A, Kenis G, Bignotti S, Tura GJ, De Jong R, Bosmans E, et al. (1998): The inflammatory response system in treatment-resistant schizophrenia: increased serum interleukin-6. *Schizophrenia research*. 32:9-15.
9. McAllister CG, van Kammen DP, Rehn TJ, Miller AL, Gurklis J, Kelley ME, et al. (1995): Increases in CSF levels of interleukin-2 in schizophrenia: effects of recurrence of psychosis and medication status. *The American journal of psychiatry*. 152:1291-1297.
10. Miller BJ, Buckley P, Seabolt W, Mellor A, Kirkpatrick B (2011): Meta-analysis of cytokine alterations in schizophrenia: clinical status and antipsychotic effects. *Biol Psychiatry*. 70:663-671.
11. Zhang XY, Zhou DF, Cao LY, Zhang PY, Wu GY, Shen YC (2004): Changes in serum interleukin-2, -6, and -8 levels before and during treatment with risperidone and haloperidol: relationship to outcome in schizophrenia. *The Journal of clinical psychiatry*. 65:940-947.
12. Beumer W, Gibney SM, Drexhage RC, Pont-Lezica L, Doorduyn J, Klein HC, et al. (2012): The immune theory of psychiatric diseases: a key role for activated microglia and circulating monocytes. *J Leukoc Biol*. 92:959-975.

13. Cagnin A, Brooks DJ, Kennedy AM, Gunn RN, Myers R, Turkheimer FE, et al. (2001): In-vivo measurement of activated microglia in dementia. *Lancet*. 358:461-467.
14. Imamura K, Hishikawa N, Sawada M, Nagatsu T, Yoshida M, Hashizume Y (2003): Distribution of major histocompatibility complex class II-positive microglia and cytokine profile of Parkinson's disease brains. *Acta neuropathologica*. 106:518-526.
15. Bayer TA, Buslei R, Havas L, Falkai P (1999): Evidence for activation of microglia in patients with psychiatric illnesses. *Neuroscience letters*. 271:126-128.
16. Radewicz K, Garey LJ, Gentleman SM, Reynolds R (2000): Increase in HLA-DR immunoreactive microglia in frontal and temporal cortex of chronic schizophrenics. *Journal of neuropathology and experimental neurology*. 59:137-150.
17. Takano A, Arakawa R, Ito H, Tateno A, Takahashi H, Matsumoto R, et al. (2010): Peripheral benzodiazepine receptors in patients with chronic schizophrenia: a PET study with [11C]DAA1106. *Int J Neuropsychopharmacol*. 13:943-950.
18. Doorduyn J, de Vries EF, Willemsen AT, de Groot JC, Dierckx RA, Klein HC (2009): Neuroinflammation in schizophrenia-related psychosis: a PET study. *Journal of nuclear medicine : official publication, Society of Nuclear Medicine*. 50:1801-1807.
19. Busse S, Busse M, Schiltz K, Biellau H, Gos T, Brisch R, et al. (2012): Different distribution patterns of lymphocytes and microglia in the hippocampus of patients with residual versus paranoid schizophrenia: further evidence for disease course-related immune alterations? *Brain, behavior, and immunity*. 26:1273-1279.
20. van Berckel BN, Bossong MG, Boellaard R, Kloet R, Schuitmaker A, Caspers E, et al. (2008): Microglia activation in recent-onset schizophrenia: a quantitative (R)-[11C]PK11195 positron emission tomography study. *Biological psychiatry*. 64:820-822.
21. Livak KJ, Schmittgen TD (2001): Analysis of relative gene expression data using real-time quantitative PCR and the 2⁻(-Delta Delta C(T)) Method. *Methods*. 25:402-408.
22. Van den Eynde K, Missault S, Fransen E, Raeymaekers L, Willems R, Drinkenburg W, et al. (2013): Hypolocomotive behaviour associated with increased microglia in a prenatal immune activation model with relevance to schizophrenia. *Behavioural brain research*. 258C:179-186.

23. Fortier ME, Luheshi GN, Boksa P (2007): Effects of prenatal infection on prepulse inhibition in the rat depend on the nature of the infectious agent and the stage of pregnancy. *Behav Brain Res.* 181:270-277.
24. Zuckerman L, Rehavi M, Nachman R, Weiner I (2003): Immune activation during pregnancy in rats leads to a postpubertal emergence of disrupted latent inhibition, dopaminergic hyperfunction, and altered limbic morphology in the offspring: a novel neurodevelopmental model of schizophrenia. *Neuropsychopharmacology.* 28:1778-1789.
25. Vloeberghs E, Van Dam D, Franck F, Staufenbiel M, De Deyn PP (2007): Mood and male sexual behaviour in the APP23 model of Alzheimer's disease. *Behavioural brain research.* 180:146-151.
26. Paxinos G, Watson C (1998): *The rat brain in stereotaxic coordinates.* 4th ed. San Diego: Academic Press.
27. Won SJ, Kim JH, Yoo BH, Sohn M, Kauppinen TM, Park MS, et al. (2012): Prevention of hypoglycemia-induced neuronal death by minocycline. *Journal of neuroinflammation.* 9:225.
28. Bronson SL, Ahlbrand R, Horn PS, Kern JR, Richtand NM (2011): Individual differences in maternal response to immune challenge predict offspring behavior: contribution of environmental factors. *Behavioural brain research.* 220:55-64.
29. Vorhees CV, Graham DL, Braun AA, Schaefer TL, Skelton MR, Richtand NM, et al. (2012): Prenatal immune challenge in rats: altered responses to dopaminergic and glutamatergic agents, prepulse inhibition of acoustic startle, and reduced route-based learning as a function of maternal body weight gain after prenatal exposure to poly IC. *Synapse.* 66:725-737.
30. Meyer U, Nyffeler M, Yee BK, Knuesel I, Feldon J (2008): Adult brain and behavioral pathological markers of prenatal immune challenge during early/middle and late fetal development in mice. *Brain Behav Immun.* 22:469-486.
31. Wolff AR, Bilkey DK (2008): Immune activation during mid-gestation disrupts sensorimotor gating in rat offspring. *Behav Brain Res.* 190:156-159.
32. Clancy B, Darlington RB, Finlay BL (2001): Translating developmental time across mammalian species. *Neuroscience.* 105:7-17.
33. Garay PA, Hsiao EY, Patterson PH, McAllister AK (2013): Maternal immune activation causes age- and region-specific changes in brain cytokines in offspring throughout development. *Brain, behavior, and immunity.* 31:54-68.
34. Spencer SJ, Mouihate A, Galic MA, Pittman QJ (2008): Central and peripheral neuroimmune responses: hyporesponsiveness during pregnancy. *J Physiol.* 586:399-406.

35. Kent S, Bret-Dibat JL, Kelley KW, Dantzer R (1996): Mechanisms of sickness-induced decreases in food-motivated behavior. *Neuroscience and biobehavioral reviews*. 20:171-175.
36. Smith SE, Li J, Garbett K, Mirnics K, Patterson PH (2007): Maternal immune activation alters fetal brain development through interleukin-6. *J Neurosci*. 27:10695-10702.
37. Dickerson DD, Wolff AR, Bilkey DK (2010): Abnormal long-range neural synchrony in a maternal immune activation animal model of schizophrenia. *The Journal of neuroscience : the official journal of the Society for Neuroscience*. 30:12424-12431.
38. Howland JG, Cazakoff BN, Zhang Y (2012): Altered object-in-place recognition memory, prepulse inhibition, and locomotor activity in the offspring of rats exposed to a viral mimetic during pregnancy. *Neuroscience*. 201:184-198.
39. Oskvig DB, Elkahloun AG, Johnson KR, Phillips TM, Herkenham M (2012): Maternal immune activation by LPS selectively alters specific gene expression profiles of interneuron migration and oxidative stress in the fetus without triggering a fetal immune response. *Brain, behavior, and immunity*. 26:623-634.
40. Ning H, Wang H, Zhao L, Zhang C, Li XY, Chen YH, et al. (2008): Maternally-administered lipopolysaccharide (LPS) increases tumor necrosis factor alpha in fetal liver and fetal brain: its suppression by low-dose LPS pretreatment. *Toxicology letters*. 176:13-19.
41. Gayle DA, Beloosesky R, Desai M, Amidi F, Nunez SE, Ross MG (2004): Maternal LPS induces cytokines in the amniotic fluid and corticotropin releasing hormone in the fetal rat brain. *American journal of physiology Regulatory, integrative and comparative physiology*. 286:R1024-1029.
42. Meyer U, Nyffeler M, Engler A, Urwyler A, Schedlowski M, Knuesel I, et al. (2006): The time of prenatal immune challenge determines the specificity of inflammation-mediated brain and behavioral pathology. *J Neurosci*. 26:4752-4762.
43. Ghiani CA, Mattan NS, Nobuta H, Malvar JS, Boles J, Ross MG, et al. (2011): Early effects of lipopolysaccharide-induced inflammation on foetal brain development in rat. *ASN neuro*. 3.
44. Weaver IC, Cervoni N, Champagne FA, D'Alessio AC, Sharma S, Seckl JR, et al. (2004): Epigenetic programming by maternal behavior. *Nature neuroscience*. 7:847-854.
45. Meyer U, Nyffeler M, Schwendener S, Knuesel I, Yee BK, Feldon J (2008): Relative prenatal and postnatal maternal contributions to schizophrenia-related neurochemical dysfunction after in utero immune

challenge. *Neuropsychopharmacology : official publication of the American College of Neuropsychopharmacology*. 33:441-456.

46. Meyer U, Feldon J, Fatemi SH (2009): In-vivo rodent models for the experimental investigation of prenatal immune activation effects in neurodevelopmental brain disorders. *Neuroscience and biobehavioral reviews*. 33:1061-1079.

47. Ozawa K, Hashimoto K, Kishimoto T, Shimizu E, Ishikura H, Iyo M (2006): Immune activation during pregnancy in mice leads to dopaminergic hyperfunction and cognitive impairment in the offspring: a neurodevelopmental animal model of schizophrenia. *Biol Psychiatry*. 59:546-554.

48. Meyer U, Spoerri E, Yee BK, Schwarz MJ, Feldon J (2010): Evaluating early preventive antipsychotic and antidepressant drug treatment in an infection-based neurodevelopmental mouse model of schizophrenia. *Schizophrenia bulletin*. 36:607-623.

49. Vuillermot S, Weber L, Feldon J, Meyer U (2010): A longitudinal examination of the neurodevelopmental impact of prenatal immune activation in mice reveals primary defects in dopaminergic development relevant to schizophrenia. *The Journal of neuroscience : the official journal of the Society for Neuroscience*. 30:1270-1287.

50. Wolff AR, Bilkey DK (2010): The maternal immune activation (MIA) model of schizophrenia produces pre-pulse inhibition (PPI) deficits in both juvenile and adult rats but these effects are not associated with maternal weight loss. *Behavioural brain research*. 213:323-327.

51. Ziermans T, Schothorst P, Magnee M, van Engeland H, Kemner C (2011): Reduced prepulse inhibition in adolescents at risk for psychosis: a 2-year follow-up study. *Journal of psychiatry & neuroscience : JPN*. 36:127-134.

52. Giovanoli S, Engler H, Engler A, Richetto J, Voget M, Willi R, et al. (2013): Stress in puberty unmasks latent neuropathological consequences of prenatal immune activation in mice. *Science*. 339:1095-1099.

53. Li Q, Cheung C, Wei R, Hui ES, Feldon J, Meyer U, et al. (2009): Prenatal immune challenge is an environmental risk factor for brain and behavior change relevant to schizophrenia: evidence from MRI in a mouse model. *PloS one*. 4:e6354.

54. Hammer C, Stepniak B, Schneider A, Papiol S, Tantra M, Begemann M, et al. (2013): Neuropsychiatric disease relevance of circulating anti-NMDA receptor autoantibodies depends on blood-brain barrier integrity. *Molecular psychiatry*.

55. Andine P, Widermark N, Axelsson R, Nyberg G, Olofsson U, Martensson E, et al. (1999): Characterization of MK-801-induced behavior

as a putative rat model of psychosis. *The Journal of pharmacology and experimental therapeutics*. 290:1393-1408.

56. Zuckerman L, Weiner I (2005): Maternal immune activation leads to behavioral and pharmacological changes in the adult offspring. *J Psychiatr Res*. 39:311-323.

57. Meyer U, Engler A, Weber L, Schedlowski M, Feldon J (2008): Preliminary evidence for a modulation of fetal dopaminergic development by maternal immune activation during pregnancy. *Neuroscience*. 154:701-709.

58. Bitanhirwe BK, Peleg-Raibstein D, Mouttet F, Feldon J, Meyer U (2010): Late prenatal immune activation in mice leads to behavioral and neurochemical abnormalities relevant to the negative symptoms of schizophrenia. *Neuropsychopharmacology*. 35:2462-2478.

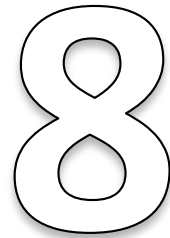
59. Henry CJ, Huang Y, Wynne A, Hanke M, Himler J, Bailey MT, et al. (2008): Minocycline attenuates lipopolysaccharide (LPS)-induced neuroinflammation, sickness behavior, and anhedonia. *Journal of neuroinflammation*. 5:15.

60. Na KS, Jung HY, Kim YK (2012): The role of pro-inflammatory cytokines in the neuroinflammation and neurogenesis of schizophrenia. *Progress in neuro-psychopharmacology & biological psychiatry*.

61. Juckel G, Manitz MP, Brune M, Friebe A, Heneka MT, Wolf RJ (2011): Microglial activation in a neuroinflammatory animal model of schizophrenia--a pilot study. *Schizophr Res*. 131:96-100.

62. Mattei D, Djodari-Irani A, Hadar R, Pelz A, de Cossio LF, Goetz T, et al. (2014): Minocycline rescues decrease in neurogenesis, increase in microglia cytokines and deficits in sensorimotor gating in an animal model of schizophrenia. *Brain Behav Immun*. 38:175-184.

63. Garay PA, Hsiao EY, Patterson PH, McAllister AK (2012): Maternal immune activation causes age- and region-specific changes in brain cytokines in offspring throughout development. *Brain, behavior, and immunity*.



Hypersynchronicity in the default mode-like network is correlated with behavioural outcome in a neurodevelopmental model with relevance for schizophrenia

Submitted to Brain, Behavior, and Immunity

1. Abstract

Background: Immune activation during pregnancy is an important risk factor for schizophrenia. Brain dysconnectivity and NMDA receptor (NMDAR) hypofunction have been postulated to be central to schizophrenia pathophysiology. The aim of this study was to investigate resting-state functional connectivity (resting-state functional MRI - rsfMRI), microstructure (diffusion tensor imaging – DTI) and NMDAR function (pharmacological fMRI – phMRI) using multimodal MRI in adult offspring of pregnant dams exposed to an immune challenge (maternal immune activation – MIA model), and to determine whether these neuroimaging readouts correlate with schizophrenia-related behaviour. **Methods:** Pregnant rats were injected with Poly I:C or saline on gestational day 15. Maternal weight and immune responses were assessed. Based on the maternal weight response, offspring were divided into three groups: controls (saline, n=11), offspring of dams that gained weight (1.43 ± 0.56 % increase, Poly I:C WG, n=12) and offspring of dams that lost weight post-MIA (-1.00 ± 0.60 % decrease, Poly I:C WL, n=16). Male adult offspring were subjected to rsfMRI, DTI, phMRI with NMDAR antagonist MK-801, behavioural testing and histological assessment. **Results:** Poly I:C WL offspring exhibited increased functional connectivity in the default mode-like network (DMN), while Poly I:C WG offspring showed the most pronounced attenuation in NMDAR function versus controls. DTI revealed no differences in MIA offspring versus controls. Behavioural deficits were subtle with the most prominent increased anxiety, especially in Poly I:C WL offspring. **Conclusions:** MIA offspring displayed a differential pathophysiology depending on the maternal response to the immune

challenge. Functional connectivity in DMN correlated with behaviour in MIA offspring.

Key words: resting-state functional MRI, diffusion MRI, pharmacological MRI, NMDA receptor, maternal/prenatal immune activation, autism, biomarker

2. Introduction

Immune activation during pregnancy is an important risk factor for several neuropsychiatric disorders, including schizophrenia, which supports the neurodevelopmental hypothesis of this disorder (1, 2). Several hypotheses regarding the pathophysiology of schizophrenia have been proposed, including the dysconnectivity and NMDA receptor (NMDAR) hypofunction hypotheses (3, 4).

Many neuroimaging studies have reported altered functional and structural connectivity in schizophrenia patients (5). Of particular interest is the default mode network (DMN), a network of brain regions that is active during rest. Several studies investigating DMN reported increased functional connectivity (FC) in this network in schizophrenia patients, as well as unaffected first-degree relatives and individuals at ultra-high risk for psychosis (reviewed in (6, 7)). In addition, schizophrenia patients show abnormal deactivation or activity of the DMN during specific tasks and aberrant DMN connectivity/deactivation correlated with symptom severity (reviewed in (6)). Some studies have shown that DMN connectivity/activation alters with antipsychotic treatment in schizophrenia patients concurrent with symptomatic improvement (8-10). Altogether this suggests that neuroimaging of the DMN may be a promising biomarker of

disease and potentially predictive of treatment response. A decreased structural connectivity has also been described in the DMN of schizophrenia patients, reviewed in (6).

To date, a few diffusion magnetic resonance imaging (MRI) studies have been performed in MIA models, focusing on microstructural changes. Changes in fractional anisotropy or apparent diffusion coefficient in white and grey matter at ages ranging from birth to adulthood have been observed (11-15). However, no FC studies have been performed in MIA models.

A mounting body of evidence supports NMDAR hypofunction as a key factor of schizophrenia pathophysiology (3). NMDAR antagonists can produce the entire range of schizophrenia symptoms in healthy subjects. Abnormal transcript and protein expression of NMDAR subunits have been observed in schizophrenia patients, as well as altered glutamate levels and abnormalities of modulators of the NMDAR glycine modulatory site. Altered NMDAR function (through behavioural testing with NMDAR antagonists) and expression has been demonstrated in MIA models (16-23).

Interestingly, depending on the maternal weight response to immune challenge (weight loss vs. gain), offspring of polyinosinic:polycytidylic acid (Poly I:C)-treated rats have been shown to display different behavioural deficits, including different locomotive responses to NMDAR antagonists (18, 24-26). This indicates that the maternal response to the immune stimulus is an important determinant of the long-term behavioural outcome in offspring, and likely also of the underlying pathophysiology.

Since the behavioural outcome in this model is variable and poorly replicable, novel predictive biomarkers are needed for evaluation of new

treatments for schizophrenia at the preclinical stage. As a first step, we evaluated resting-state functional connectivity, microstructure and NMDAR function using multimodal MRI in rats prenatally exposed to an immune challenge and evaluated whether changes in these *in vivo* imaging read-outs correlated with schizophrenia-like behavioural deficits.

In this study we aimed to elucidate the following research questions:

- i) Is there increased FC in the default mode-like network (DMN) of adult rats exposed to prenatal immune challenge?
- ii) Are FC changes associated with microstructural alterations?
- iii) Do adult MIA offspring display a different hemodynamic response to an NMDAR antagonist?
- iv) Do offspring of dams that lose weight post-MIA show a different pathophysiology (dysconnectivity/NMDAR dysfunction) from offspring of dams that gain weight?
- v) Do FC, microstructural and NMDAR function abnormalities correlate with behavioural deficits in adult MIA offspring?
- vi) Is NMDAR dysfunction (altered response to an NMDAR antagonist) related to abnormal NMDAR levels?

3. Material and methods

3.1. Animals

Thirteen male and 13 female 10-week old Wistar Han rats were purchased from Charles River Laboratories (France). Animals were single-housed in a

temperature- and humidity-controlled room on a 12-hour light-dark cycle with standard food and water available ad libitum. After minimum one week of acclimatization, animals were subjected to timed mating. Male offspring were group-housed under the same conditions. Animals were treated in accordance with EU directive 2010/63/EU. Animal experiments were approved by the animal ethics committee of the University of Antwerp, Belgium (ECD 2015-77).

3.2. Study design

Study design is shown in Fig.1. Pregnant Wistar Han dams received an immune challenge (viral mimetic Poly I:C, N=9) or saline (N=4) on gestational day (GD) 15 as previously described (24). Maternal weight and immune responses were assessed as before (24). Offspring were divided into three groups: controls (n=11), offspring of dams that gained weight post-MIA (Poly I:C Weight Gain offspring, n=12) and offspring of dams that lost weight or showed no weight change (Poly I:C Weight Loss offspring, n=16) (24). On the day of birth, litters were culled to eight pups per litter. Adult male offspring (usually three per litter) were subjected to MRI and behavioural testing during postnatal weeks (PNW) 12 and 13. MRI consisted of resting-state functional MRI (rsfMRI), diffusion tensor imaging (DTI) (scanning session 1), and pharmacological fMRI (phMRI) with the NMDAR antagonist MK-801 (10 min baseline and 30 min post-intravenous MK-801 administration) (scanning session 2). Behavioural tests included prepulse inhibition of the acoustic startle reflex, spontaneous locomotion, open field test, sucrose preference test and MK-801-induced locomotion (24). PhMRI and locomotion with MK-801 were the last tests to be performed, in order to exclude possible effects of the psychotomimetic drug on the other imaging and behavioural read-

outs. Animals were sacrificed in PNW 14 and their brains processed for GluN1 immunohistochemical staining and quantification.

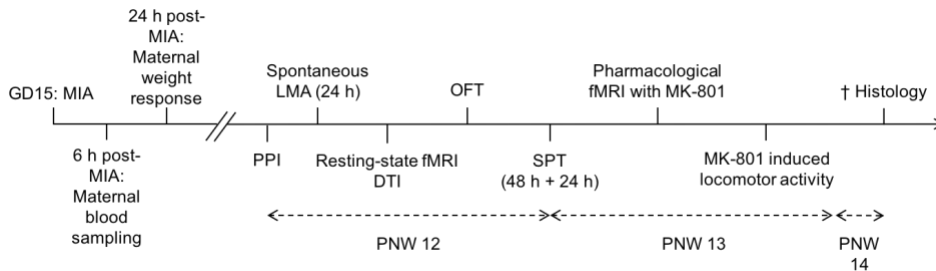


Fig.8-1. Study design. Pregnant dams were administered 4 mg/kg Poly I:C (maternal immune activation: MIA) or saline on gestational day (GD) 15. Six hours post-injection, a venous blood sample was collected and 24 h post-injection, the maternal weight response was recorded. Male offspring were tested during adulthood in postnatal weeks (PNW) 12 and 13. Behavioural testing included assessment of the prepulse inhibition (PPI) of the acoustic startle reflex, spontaneous locomotor activity (LMA), open field (OFT) and sucrose preference tests (SPT), and finally assessment of the locomotor response to the NMDA receptor (NMDAR) antagonist MK-801. Animals underwent resting-state functional MRI (fMRI) and diffusion tensor imaging (DTI) during PNW 12 and pharmacological fMRI with MK-801 during PNW 13. Rats were sacrificed in the beginning of PNW 14 for histological assessments.

3.3. Maternal immune activation (MIA) and response

Pregnant dams were injected subcutaneously (s.c.) with saline or 4 mg/kg Poly I:C (10 ml/kg) on GD 15. Six hours post-injection, a blood sample was collected from the lateral tail vein for assessment of the immune response. Blood samples were allowed to clot for 30 min at room temperature (RT), after which serum was obtained (10 min, 3000 rpm, 4°C). The weight of the dam was recorded before and 24 h after Poly I:C/vehicle injection to calculate the maternal weight response.

The maternal immune response was assessed in serum using a customized Luminex multiplex assay (Procartaplex, eBiosciences) for the following

cytokines and chemokines: TNF- α , IL-1 β , IL-6, IL-10, CCL2 (MCP-1), CCL5 (RANTES), and IP-10 (CXCL10). Luminex analyses were performed according to the instructions from the manufacturer in duplicates. Briefly, serum samples were centrifuged at 10,000 g for 10 min at 4°C for removal of remaining platelets and supernatants were 1:2 diluted in assay buffer. Samples were incubated with magnetic beads for 2 h at 500 rpm at RT followed by detection antibody mixture incubation for 30 min. For visualization, samples were incubated with streptavidin conjugated R-Phycoerythrin for 30 min and samples analysed on Magpix Luminex platform. Data were analysed using Bio-plex Data Pro software.

3.4. Magnetic resonance imaging (MRI)

3.4.1. Acquisition

All data were acquired on a 7T PharmaScan MR system (Bruker, Germany) with Paravision 5.1 software using a standard Bruker crosscoil set-up with a quadrature volume coil and a quadrature surface coil designed for rats (Bruker, Germany). The rats' head was immobilized in an MR-compatible stereotaxic device using blunt earplugs and a tooth bar.

RsfMRI, DTI and three-dimensional (3D) T₂-weighted anatomical MRI scans were all performed during one scanning session in PNW 12. PhMRI with the NMDAR antagonist MK-801 was performed during a second scanning session in PNW 13.

For the first scanning session, rats were anesthetized with isoflurane in a mixture of O₂ (30%) and N₂ (70%) (5% induction; Forene; Abbott, Belgium) after which a s.c. bolus injection of 0.05 mg/kg medetomidine hydrochloride (Domitor, Pfizer, Karlsruhe, Germany) was administered to sedate the

animals. After 15 min, continuous s.c. infusion of 0.1 mg/kg/h medetomidine was started. Following bolus injection, isoflurane was gradually decreased to 0.4% during the rsfMRI scan. After the rsfMRI scan was finished, infusion of medetomidine was discontinued and isoflurane was increased to $\pm 1\%$. At the end of the scanning session, animals received a s.c. injection of 0.25 mg/kg atipamezole (Antisedan, Pfizer, Karlsruhe, Germany) to reverse the effects of medetomidine. For the second scanning session, only isoflurane was used as anesthetic (5% induction, 2% maintenance). Breathing rate and blood oxygenation were monitored constantly using a pressure sensitive pad and a pulse oximeter (MR-compatible Small Animal Monitoring and Gating System, SA Instruments, Inc., USA) and maintained between normal physiological ranges. The temperature of the animals was monitored by means of a rectal probe and maintained at $(37 \pm 0.5)^\circ\text{C}$ through a feedback-controlled warm air system (MR-compatible Small Animal Heating System, SA Instruments, Inc., USA).

Three orthogonal multi-slice Turbo Rapid Acquisition with Relaxation Enhancement (RARE) T_2 -weighted images were acquired to ensure uniform slice positioning for rsfMRI, DTI and pHMRI data of different animals. A field map was acquired in each scanning session to measure field homogeneity, followed by local shimming, which corrects for the measured inhomogeneity in a rectangular volume within the brain.

During the first scanning session, coronal rsfMR images were acquired between 40 and 50 min post-bolus injection using a single-shot T_2^* -weighted gradient-echo echo planar imaging (GE-EPI) sequence with the following parameters: repetition time (TR) 2000 ms, echo time (TE) 29 ms, 20 slices of 0.7 mm (limited to cerebrum), slice gap 0.1 mm, 300 repetitions,

scan duration 10 min. The field of view (FOV) was (30 x 30) mm² and the matrix size [128 x 128], resulting in voxel dimensions of (0.234 x 0.234 x 0.800) mm³.

Coronal diffusion-weighted (DW) images were acquired with a two-shot spin-echo echo planar imaging (SE-EPI) sequence with 60 optimally spread diffusion gradient directions. In addition, 15 non-DW b_0 images (b-value 0 s/mm²; 5 b_0 per 20 DW images) were acquired. The following imaging parameters were used: TR 7500 ms, TE 26 ms, diffusion gradient pulse duration δ 4 ms, diffusion gradient separation Δ 12 ms, b-value 800 s/mm², 20 slices of 0.7 mm (limited to cerebrum, same slices as rsfMRI), 0.1 mm slice gap, scan duration approx. 20 min. The FOV was (30 x 30) mm² and the matrix size [128 x 128], resulting in voxel dimensions of (0.234 x 0.234 x 0.800) mm³.

A 3D RARE T_2 -weighted scan of the entire brain was acquired with the following parameters: TR 2250 ms, TE 11 ms (TE_{eff} 44 ms), RARE factor 8, scan duration 15 min. The FOV was (29 x 20 x 15) mm³ and the acquisition matrix [256 x 64 x 50], resulting in a spatial resolution of (0.113 x 0.313 x 0.300) mm³.

During the second scanning session, coronal phMR images were acquired using a single-shot T_2^* -weighted GE-EPI sequence with the following parameters: TR 4000 ms, TE 25 ms, 13 slices of 1.0 mm (limited to cerebrum), slice gap 0.2 mm, 600 repetitions, scan duration 40 min. The FOV was (25 x 25) mm² and the matrix size [128 x 64], resulting in voxel dimensions of (0.195 x 0.391 x 1.200) mm³. Baseline scans were acquired for 10 min (150 repetitions) after which a single bolus of 0.2 mg/kg MK-801 (0.8 ml/kg) was

administered through an intravenous (i.v.) catheter and the measurements continued until 30 min (450 repetitions) post-injection.

3.4.2. Data preprocessing

All image preprocessing was performed using SPM12 in MATLAB 2014a (MathWorks, USA).

Resting-state fMRI. First, images within each session were realigned to the first image using a least-squares approach and a 6-parameter (rigid body) spatial transformation. Secondly, EPI images were coregistered to the individual 3D RARE scan. The individual 3D RARE scans were normalised to a study-specific 3D T₂-weighted anatomical template using an affine transformation followed by the estimation of the nonlinear deformations. These transformation parameters were used to normalise all EPI datasets to the study-specific 3D template. This template was made in Advanced Normalisation Tools (ANTs) using all individual 3D RARE scans. Next, in plane smoothing was done using a Gaussian kernel with full width at half maximum (FWHM) of twice the voxel size (FWHM (0.468 x 0.468 x 0.800) mm³). Finally, datasets were filtered using the Resting State fMRI Data Analysis toolbox (REST1.8). The band-pass filter was set between 0.01 and 0.1 Hz to retain the low frequency fluctuations of the blood-oxygen level dependent (BOLD) signal time course.

Diffusion tensor imaging. Firstly, images were realigned by performing a rigid registration between the b₀ images, which was followed by an extended registration taking all the DW images into account. Secondly, DW images were coregistered to the individual 3D RARE scan. The individual 3D RARE scans were normalised to the study-specific 3D T₂-weighted

anatomical template using an affine transformation followed by the estimation of the nonlinear deformations. These transformation parameters were used to normalise all DWI datasets to the study-specific 3D template. Next, the diffusion tensor was estimated and the DTI parameter maps were computed (i.e. fractional anisotropy (FA), mean diffusivity (MD), axial diffusivity (AD) and radial diffusivity (RD)). Finally, the DTI parameter maps were smoothed in plane using a Gaussian kernel with FWHM of twice the voxel size (FWHM (0.468 x 0.468 x 0.800) mm³).

Pharmacological fMRI with MK-801. All images within each session were realigned to the mean image using a rigid registration. Secondly, all datasets were normalised to the study-specific EPI template using an affine transformation followed by the estimation of the nonlinear deformations. The study-specific EPI template was made using the EPI data from 8 control rats. Finally, in plane smoothing was performed using a Gaussian kernel with FWHM of twice the voxel size (FWHM (0.390 x 0.782 x 1.200) mm³).

3.4.3. Data analysis

Resting-state fMRI. A region of interest (ROI)-based analysis was performed for all three groups including the following ROIs: left and right anterior cingulate cortex (Cg), retrosplenial cortex (RS), parietal association cortex (PtA), posterior parietal cortex (PtP), temporal association cortex (TeA), primary motor cortex (M1), primary somatosensory cortex (S1), primary auditory cortex (Au1) and primary visual cortex (V1). These ROIs were defined as square regions of four voxels using MRICron software, based on the Paxinos and Watson rat brain atlas. The filtered datasets and a mask for each ROI were used as an input to REST to extract the time courses for each ROI. Correlation coefficients between the time courses of each pair of ROIs

were calculated and z-transformed using an in-house program developed in MATLAB. The average group z-transformed correlation values were presented in a functional connectivity (FC) strength matrix. The FC strength in the default mode-like network was computed by calculating the average correlation value between Cg, RS, PtA, PtP and TeA. The default mode-like network in rat was defined based on previous literature (27). Orbitofrontal and prelimbic cortex could not be included in our analysis due to susceptibility artefacts in the images at the level of these regions. The FC strength in motor and sensory areas was computed by calculating the average correlation value between M1, S1, Au1 and V1.

Seed-based analyses were performed for each of the ROIs within the default mode-like network. BOLD signal time courses for each of these ROIs were extracted from all filtered datasets using the REST toolbox. These were used in SPM12 in a generalized linear model with the motion parameters resulting from the realignment as covariates to obtain individual statistical FC maps for all animals with the right Cg, RS, PtA, PtP and TeA as seed regions. A whole brain mask was implemented in this analysis. The total cluster sizes of these individual FC maps (family wise error (FWE) corrected, $p \leq 0.05$, minimal cluster size $k \geq 10$) were determined. In addition, the mean T-value was extracted from each individual FC map. A mask containing all clusters that were significantly correlated with the seed region at group-level (one-sample t-test per group, FWE corrected, $p \leq 0.05$, $k \geq 10$) was used in this analysis. These masks were the sum of all clusters that were significantly correlated with the seed in each group ("all group masks"). Finally, mean FC maps for each seed region were computed per group (one-sample t-test,

FWE corrected, $p \leq 0.05$, $k \geq 10$). Further statistics to compare between groups are described in 2.7.

Diffusion tensor imaging. Voxel-based analysis was performed for each of the obtained DTI metrics (i.e. FA, MD, AD and RD) in SPM12. First, we used a whole brain approach. Next, we explored differences within a ROI that contained all cortical DMN regions (bilateral Cg, RS, PtA, PtP and TeA), overlaid as a mask. Statistics are described in 2.7.

Pharmacological fMRI with MK-801. For each animal, the first 140 baseline scans (“pre”) were compared with the last 140 scans (i.e. 20-30 min post-injection, “post”) in SPM12. The motion parameters resulting from the realignment were added as covariates to account for movement. A whole brain mask was used in this analysis. Mean T-values were extracted from the individual T-maps (pre > post) in MATLAB 2014a for the following ROIs: anterior cingulate cortex (Cg), primary and secondary motor cortex (M1/2), striatum, hippocampus, thalamus, default mode-like network and entire cortex. Finally, mean difference maps were computed for each group (paired t-test, pre > post, uncorrected, $p \leq 0.01$, $k \geq 10$). Further statistics to compare between groups are described in 2.7.

3.5. Behaviour

3.5.1. Prepulse inhibition of the acoustic startle reflex

Prepulse inhibition of the acoustic startle reflex was assessed for prepulses of three different intensities (70 dB, 75 dB and 80 dB) using standard startle boxes (Kinder Scientific, USA) as previously described (24).

3.5.2. Spontaneous locomotor activity

Spontaneous ambulatory locomotion was measured for a period of 24 h (12 h light-dark) using a home-cage 4 x 8 photobeam activity system (San Diego Instruments, USA). The average number of photobeam crossings per hour was calculated for both the light and the dark phase.

3.5.3. Open field test

Animals were placed in the periphery of a well-lit square arena (48 x 48 cm) and allowed to explore the novel environment for 10 min. During this trial, animals were video-tracked with EthoVision XT software (version 10.0, Noldus, USA). For analysis, the arena was divided in a central zone (inner square, 24 x 24 cm) and a peripheral zone. The following parameters were calculated: latency to first entry in central zone, number of transitions from periphery to centre, % time spent in centre, % distance moved in centre, total distance moved and mean velocity.

3.5.4. Sucrose preference test

Sucrose preference and total liquid consumption were assessed as previously described during a test period of 24 h, following a habituation period of 48 h (24).

3.5.5. MK-801 induced locomotor activity

MK-801 induced hyperlocomotion was measured using the home-cage 4 x 8 photobeam activity system as previously described (24) with one important modification: four hours of locomotor activity (i.e. beam crossings) were recorded following administration of 0.2 mg/kg MK-801 (s.c., 10 ml/kg).

3.6. Histology: GluN1

Animals were sacrificed by decapitation. Brains were resected and snap-frozen in isopentane on dry ice (3 min, -35°C) and stored at -80°C. Sagittal sections of 20 µm were obtained using a CryoStar NX50 cryostat (Thermo Scientific, Belgium) at ca. 1.90 mm lateral to the midline (right hemisphere) and collected in triplicate.

Sections in triplicate were incubated for 1 h with Dako wash buffer (Dako, Belgium) and for 30 min with 10% normal goat serum in PBS to block aspecific binding. Next, sections were incubated for 3 h with anti-GluN1 monoclonal mouse antibody (1:400 in Dako diluent) (Synaptic Systems, Germany). After washing, sections were incubated for 1 h with goat anti-mouse antibody conjugated with horseradish peroxidase (GAM IgG2b-HRP, 1:1000 in PBS), rinsed again, and incubated for 10 min with the colorimetric substrate 3,3'-diaminobenzidine (DAB) for visualization. The reaction was stopped with dH₂O and sections were gradually dehydrated and coverslipped.

Images were obtained with a NanoZoomer-XR slide scanner (Hamamatsu, Japan) equipped with a 20x objective and analysed with ImageJ software. The following ROIs were manually drawn in ImageJ using the curation function of an in-house developed plugin SliceMap (28): frontal cortex, corpus callosum, striatum, hippocampus and thalamus. For each ROI, the % area of positive staining was calculated. Positive staining was defined as signal higher than three standard deviations above the mean intensity in the corpus callosum (reference region) of that section. This effectively normalises the signal intensity in each ROI, in order to reduce inter-slice and inter-subject variability in staining.

3.7. Statistics

Normal distribution of the data was tested using the D'Agostino-Pearson omnibus normality test. Outlier analyses were performed with the ROUT test. Differences between the three groups (control, Poly I:C WG and Poly I:C WL offspring) in average FC strength in default mode-like network and motor/sensory areas, total cluster sizes of FC maps, acoustic startle reflex, prepulse inhibition and spontaneous locomotion were analysed using one-way ANOVA tests and Dunnett's multiple comparisons tests as post-hoc tests. When pooling all MIA offspring, unpaired t-tests were used to compare the two groups (control and Poly I:C offspring). Differences in MK-801 induced hyperlocomotion between the groups were investigated using a repeated measures two-way ANOVA test with either Dunnett's (three groups) or Sidak's (two groups) multiple comparisons test as post-hoc tests. Differences between the three groups (control, Poly I:C WG and Poly I:C WL dams or offspring) in cytokine and chemokine expression, T-values from pHMRI T-maps, open field performance, sucrose preference, total liquid consumption, GluN1 levels were analysed using Kruskal-Wallis tests and Dunn's multiple comparisons tests as post-hoc tests. When pooling all MIA dams/offspring, Mann-Whitney U tests were used to compare the two groups (control and Poly I:C dams/offspring). A chi-square test and chi-square test for trend were used to investigate a difference in the proportion of the group that displayed anhedonia (defined as a sucrose preference of less than 90%) in the different groups. Pearson correlation tests were performed to investigate the relationship between in vivo imaging measurements and behavioural assessments. These analyses were performed using GraphPad Prism 6. Statistical significance was set at $p \leq 0.05$.

Differences in seed-based FC maps and FA, MD, AD and RD maps between the three groups were investigated using one-way ANOVA tests with F-contrasts to compare between the three groups and t-contrasts to compare between two groups. When pooling all MIA offspring, two-sample t-tests were used to investigate the difference in seed-based FC maps and FA, MD, AD and RD maps between the two groups. To investigate the difference in seed-based FC maps between the different groups, a mask was used that contained all clusters that were significantly correlated with the seed at group-level (FWE corrected, $p \leq 0.05$, $k \geq 10$). These masks were the sum of all clusters that were significantly correlated with the seed in each group (“all group masks”). These analyses were performed in SPM12 and MATLAB 2014a. Finally, stepwise regression analyses were performed to investigate whether in vivo imaging measurements could explain the variability in the behavioural assessments. Forward stepwise regression analysis was performed in JMP Pro 13 with p-value threshold as stopping rule (probability to enter: 0.25, probability to leave: 0.1).

4. Results

4.1. Maternal response to MIA

Pregnant dams injected with Poly I:C exhibited a variable weight response as reported before (24), with some animals having a reduction in weight (N=4) or no weight change (N=1) (N=5, mean \pm SEM: -3.2 ± 1.9 g, -1.00 ± 0.60 % decrease in body weight) and others showing weight gain (N=4, mean \pm SEM: 4.7 ± 2.2 g, 1.43 ± 0.56 % increase) (Fig.2A). Pregnant dams injected with saline showed a slight weight increase (N=4, mean \pm SEM: 1.4 ± 0.8 g, 0.47 ± 0.26 % increase).

Pregnant dams that lost weight or showed no weight change post-MIA showed a non-significant trend for an increased concentration of CCL5 in serum at 6 h post-MIA vs. control dams ($p=0.078$), while dams that gained weight did not (Fig.2B). When pooling all Poly I:C-injected dams, there was also a trend for an increase in CCL5 vs. controls ($p=0.073$). There were no differences in the other investigated cytokines (TNF- α , IL-1 β , IL-6, IL-10, CCL2 and IP-10) between the three groups (data not shown).

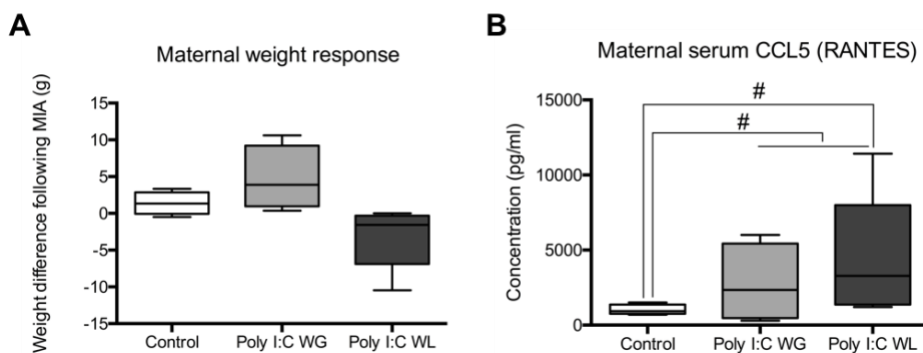


Fig.8-2. Maternal response to the viral mimetic Poly I:C. **A.** Maternal weight response at 24 hours following Poly I:C or vehicle injection. Poly I:C-treated dams exhibited a wide range of weight change responses to the immune challenge in comparison with controls and were divided into dams that lost weight (Poly I:C WL) and gained weight (Poly I:C WG). **B.** Concentration of CCL5 (RANTES) in maternal serum at 6 hours post-injection. A trend towards significance was observed for a higher concentration of CCL5 in Poly I:C WL dams and all Poly I:C-treated dams. Data are presented as boxplots. Control dams: $N=4$, Poly I:C WG dams: $N=4$, Poly I:C WL dams: $N=5$. Kruskal-Wallis test with Dunn's multiple comparisons test (three groups) and Mann-Whitney test (two groups). $\#p<0.1$

4.2. Increased FC in DMN of adult Poly I:C WL offspring

Region-of-interest (ROI)-based analysis of the rsfMRI data revealed significantly increased average FC in the DMN of Poly I:C WL offspring vs. controls, but not in Poly I:C WG offspring ($p\leq 0.05$) (Fig.3). FC within the DMN was also significantly increased when comparing all MIA offspring to controls ($p\leq 0.05$). FC was not significantly altered in motor and sensory cortical areas.

Seed-based analysis revealed i) significantly larger total cluster sizes of functionally connected clusters (FWE corrected, $p \leq 0.05$, $k \geq 10$) with posterior parietal cortex (PtP) ($p \leq 0.05$) (Fig.4A) and temporal association cortex (TeA) ($p \leq 0.01$), and ii) significantly higher mean T-values of the FC maps with parietal association cortex (PtA) ($p \leq 0.05$), PtP ($p \leq 0.05$) (Fig.4A) and TeA ($p \leq 0.001$) as seed regions in Poly I:C WL offspring vs. controls, but not in Poly I:C WG offspring (Fig.4B). No significant group difference was observed for i) total size of clusters significantly correlated with anterior cingulate cortex (Cg), retrosplenial cortex (RS) and PtA, and ii) mean T-values of the FC maps with Cg and RS as seed regions. When pooling all MIA offspring, we observed i) a significantly larger total cluster size of significantly correlated clusters with TeA ($p \leq 0.01$) and ii) significantly higher mean T-values of FC maps with PtP ($p \leq 0.05$) and TeA ($p \leq 0.01$) in MIA offspring vs. controls. Trends towards significance were observed for i) increased total cluster size of clusters significantly correlated with PtP ($p = 0.057$) and ii) higher mean T-value of the FC map with PtA as seed in all MIA offspring vs. controls ($p = 0.081$).

Statistical difference maps (uncorrected, $p \leq 0.001$, $k \geq 10$) of the FC maps with PtP and TeA as seed regions revealed a difference between Poly I:C WL offspring and controls (Poly I:C WL > control, data not shown). When pooling all MIA offspring, a group difference with controls was only found for the FC maps with TeA as seed region. Statistical difference maps did not reveal any group difference between MIA and control offspring for the FC maps with Cg, RS or PtA as seed regions.

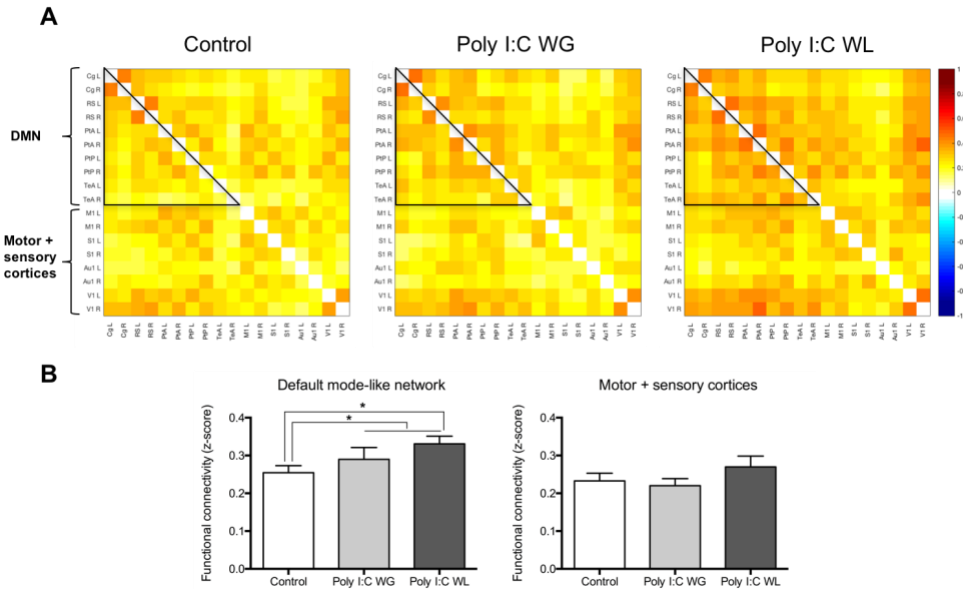


Fig.8-3. Region of interest-based analysis of resting-state functional MRI data reveals increased functional connectivity (FC) in the default mode-like network (DMN) of MIA offspring. A. Average group z-transformed FC matrices of DMN-like, motor and sensory cortical regions. From top to bottom: left and right anterior cingulate cortex, left and right retrosplenial cortex, left and right parietal association cortex, left and right posterior parietal cortex, left and right temporal association cortex, left and right primary motor cortex, left and right somatosensory cortex, left and right primary auditory cortex, left and right primary visual cortex. The black triangle indicates the correlations between DMN-like regions. The colour scale indicates the z-transformed correlation values. The values within the DMN-like network are higher (more red) in Poly I:C WL offspring compared to controls. Cg = cingulate cortex, RS = retrosplenial cortex, PtA = parietal association cortex, PtP = posterior parietal cortex, TeA = temporal association cortex, M1 = primary motor cortex, S1 = primary somatosensory cortex, Au1 = primary auditory cortex, V1 = primary visual cortex, L = left, R = right. **B.** The average zFC correlation values within the DMN-like network (left) and primary motor and sensory cortices (right). The average FC within the DMN-like network is significantly higher in Poly I:C WL offspring and all Poly I:C offspring vs. controls. Mean \pm SEM is shown. Control offspring: $n=11$, Poly I:C WG offspring: $n=10$, Poly I:C WL offspring: $n=15$. One-way ANOVA with Dunnett's multiple comparisons test (three groups) and unpaired t-test (two groups). * $p \leq 0.05$

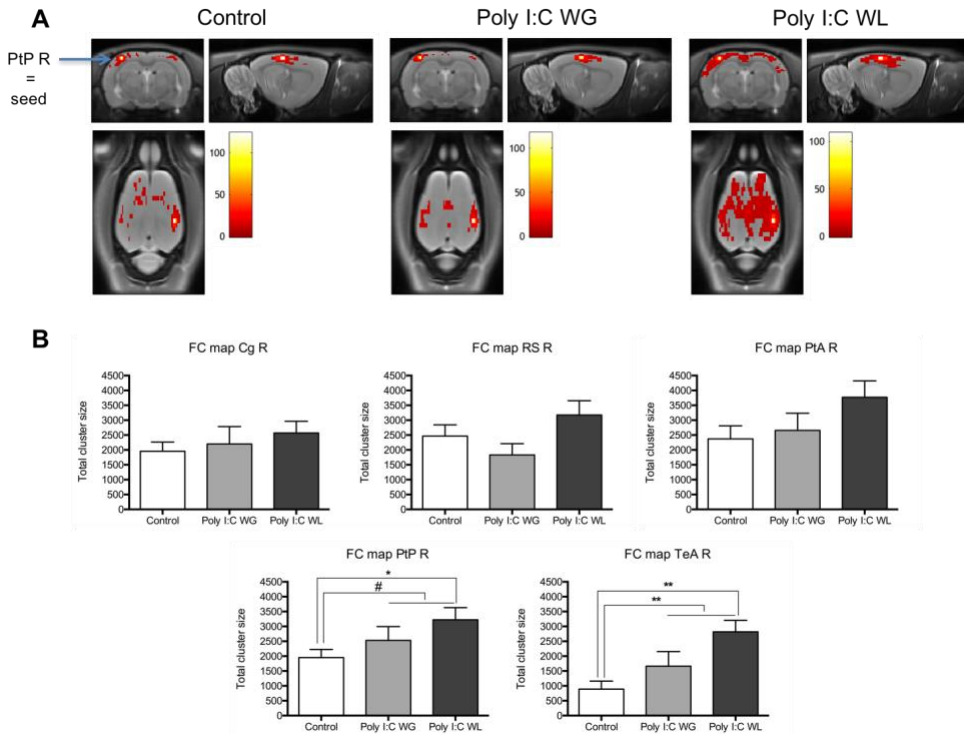


Fig.8-4. Seed-based analysis of resting-state functional MRI data reveals increased functional connectivity (FC) in the default mode-like network (DMN) of MIA offspring. **A.** Average group statistical seed-based FC maps with posterior parietal cortex as seed region (one-sample *t*-test, FWE corrected, $p < 0.05$, minimal cluster size $k \geq 10$). The colour scale indicates *T*-values. **B.** Total cluster size of all significantly correlated clusters (FWE corrected, $p < 0.05$, $k \geq 10$) with different seed regions of the DMN-like network: right cingulate cortex (Cg R), right retrosplenial cortex (RS R), right parietal association cortex (PtA R), right posterior parietal cortex (PtP R), and right temporal association cortex (TeA R). The total cluster sizes of the FC maps with PtP R and TeA R as seed regions are significantly higher in Poly I:C WL offspring vs. controls, as well as in all Poly I:C offspring for the FC maps with TeA R as seed. A trend was observed for a higher total cluster size of the FC maps with PtP R as seed region in all Poly I:C offspring vs. controls. Mean \pm SEM is shown. Control offspring: $n = 11$, Poly I:C WG offspring: $n = 10$, Poly I:C WL offspring: $n = 15$. One-way ANOVA with Dunnett's multiple comparisons test (three groups) and unpaired *t*-test (two groups). # $p < 0.1$, * $p \leq 0.05$, ** $p \leq 0.01$

4.3. No microstructural changes in adult MIA offspring

Whole-brain voxel-based analysis (VBA) did not reveal significant differences in fractional anisotropy, mean, axial and radial diffusivity between MIA and

control offspring (data not shown). VBA within the DMN did not reveal any significant group differences either (data not shown).

4.4. Attenuated response to NMDAR antagonist in adult MIA offspring

Administration of NMDAR antagonist MK-801 resulted in a decrease in blood-oxygen-level-dependent (BOLD) signal. The mean T-values of the pre>post contrast maps were significantly lower in striatum and thalamus of Poly I:C WG rats vs. controls ($p \leq 0.05$), i.e. there was a smaller drop in BOLD signal in Poly I:C WG offspring vs. controls (Fig.5). There were also trends for lower mean T-values in anterior cingulate ($p=0.088$) and motor cortices ($p=0.081$) of Poly I:C WG offspring vs. controls. The mean T-value in thalamus was also significantly lower in Poly I:C WL offspring compared to controls ($p \leq 0.05$). When taking all MIA offspring together, mean T-values were significantly lower in striatum ($p \leq 0.05$) and thalamus ($p \leq 0.01$) vs. controls. In addition, a trend for a lower mean T-value in hippocampus was observed in all MIA offspring vs. controls ($p=0.062$). No differences were observed in mean T-values for DMN and entire cortex between any of the groups.

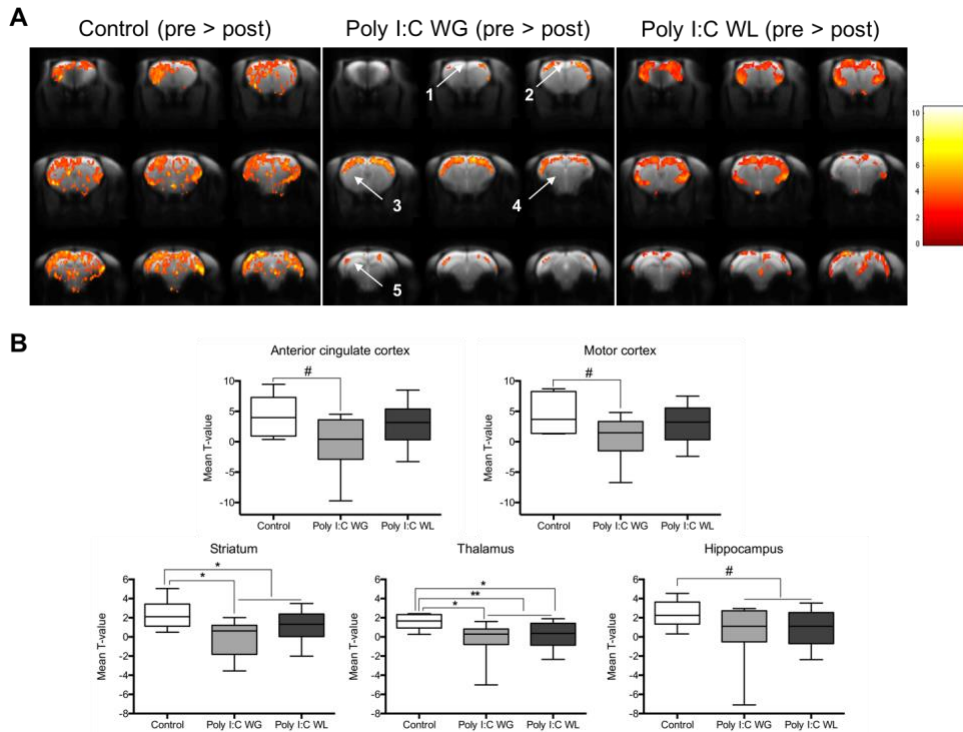


Fig.8-5. Pharmacological fMRI with the NMDA receptor antagonist MK-801 reveals altered NMDAR function in MIA offspring. **A.** Average group statistical difference maps of BOLD signal before – after (20-30 min post) MK-801 administration (uncorrected, $p < 0.01$, minimal cluster size $k \geq 10$). MIA offspring showed a significantly different response to the NMDAR antagonist in comparison with controls, which was most pronounced in Poly I:C WG offspring. The colour scale indicates T-values. 1: anterior cingulate cortex, 2: motor cortex, 3: striatum, 4: thalamus, 5: hippocampus. **B.** Mean T-values in anterior cingulate cortex, motor cortex, striatum, thalamus and hippocampus. Mean T-values were significantly lower in striatum of Poly I:C WG offspring and all MIA offspring vs. controls, and in thalamus of Poly I:C WG, Poly I:C WL and all MIA offspring. A trend was observed for lower mean T-values in frontal cortical regions (i.e., anterior cingulate cortex and motor cortex) of Poly I:C WG offspring and in hippocampus of all MIA offspring vs. controls. Data are presented as boxplots. Control offspring: $n=7$, Poly I:C WG offspring: $n=8$, Poly I:C WL offspring: $n=14$. Kruskal-Wallis test with Dunn's multiple comparisons test (three groups) and Mann-Whitney test (two groups). # $p < 0.1$, * $p \leq 0.05$, ** $p \leq 0.01$

4.5. Subtle behavioural deficits in adult MIA offspring

As expected, the % prepulse inhibition (PPI) increased significantly with prepulse intensity. Surprisingly, a trend towards significance for increased PPI with the 75 dB prepulse was observed in all MIA offspring vs. controls ($p=0.086$) (Fig.6A). No difference was observed in the magnitude of the startle reflex or PPI with the other prepulse intensities between the different groups.

Poly I:C WG offspring showed a trend for increased spontaneous locomotion during light phase ($p=0.074$) (Fig.6B). A weak trend was observed for decreased activity during dark phase in all MIA offspring vs. controls ($p=0.098$).

Poly I:C WL offspring showed trends for a decreased number of entries into the centre of the open field ($p=0.089$), decreased % time spent in centre ($p=0.072$) and decreased % distance travelled in centre ($p=0.063$) vs. controls (Fig.6C). When pooling all MIA offspring, there was a significantly decreased number of entries into centre ($p\leq 0.05$), decreased % time spent in centre ($p\leq 0.05$) and decreased % distance travelled in centre ($p\leq 0.05$), as well as a trend for increased latency to first entry into the centre of the open field vs. controls ($p=0.089$). There were no differences in total distance travelled or velocity between the groups.

There was no significant difference in % sucrose preference or total liquid consumption between the groups (Fig.6D). However, there was a non-significant higher proportion of animals with anhedonia (defined as sucrose preference $<90\%$) in Poly I:C WL and WG groups (both 25%, respectively 3/12 and 4/16 rats) than in controls (9%, 1/11 rats).

Poly I:C WG offspring initially showed a similar hyperlocomotive response to MK-801 as controls, but after approx. 85 min their responses started to deviate with the Poly I:C WG offspring exhibiting a reduced response to the drug vs. controls. This was significant at 95-100 min post-injection ($p \leq 0.05$) and a trend was observed at 125-130 min post-injection ($p = 0.073$) (Fig.6E). No difference was observed between Poly I:C WL offspring and controls or when comparing all MIA offspring vs. controls.

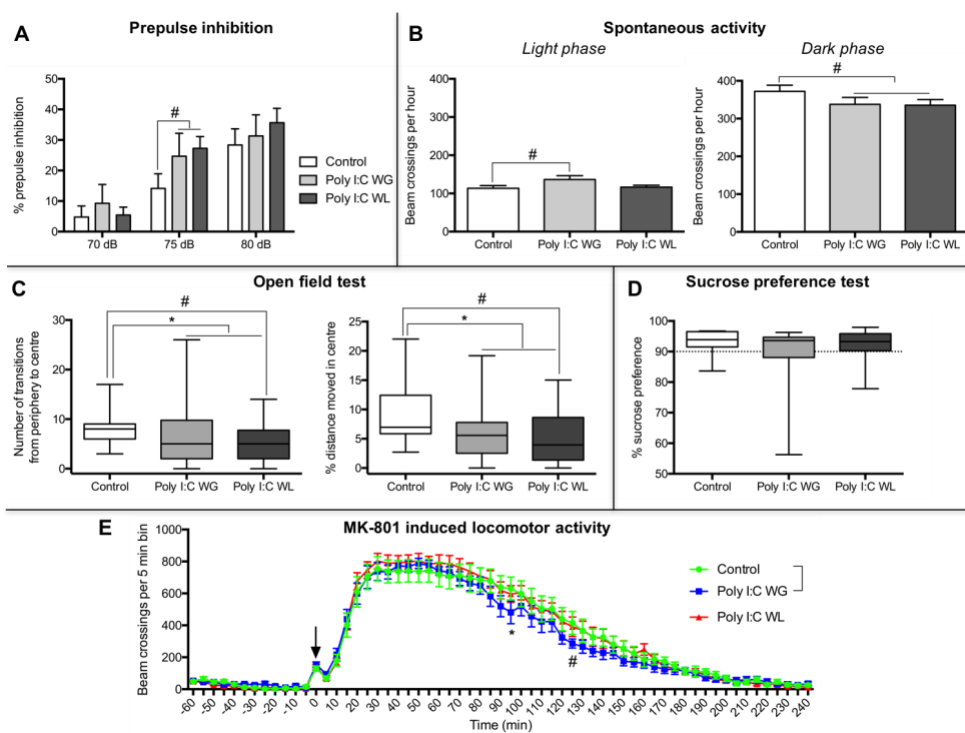


Fig.8-6. Subtle behavioural deficits in MIA offspring. **A.** All Poly I:C offspring exhibited an increased % prepulse inhibition with the 75 dB prepulse vs. controls, but not with the other prepulse intensities. **B.** Poly I:C WG offspring showed increased baseline locomotor activity (average beam crossings per hour) during the light phase compared to controls, and all Poly I:C offspring showed decreased activity during the dark phase. **C.** MIA offspring had a decreased number of entries into the centre of the open field and a lower % distance moved in the centre vs. controls, which was most pronounced in Poly I:C WL offspring. **D.** There was no significant difference in % sucrose preference between the three groups. **E.** Poly I:C WG offspring showed a slightly attenuated hyperlocomotive response to MK-801 compared to

controls. The arrow indicates the time-point of MK-801 administration. Mean \pm SEM is shown in panels A, B and E. Data in C and D are presented as boxplots. All behavioural tests: Control offspring: $n=11$, Poly I:C WG offspring: $n=12$, Poly I:C WL offspring: $n=16$. A, B: one-way ANOVA with Dunnett's multiple comparisons test (three groups) and unpaired t -test (two groups); C, D: Kruskal-Wallis test with Dunn's multiple comparisons test (three groups) and Mann-Whitney test (two groups), E: two-way repeated measures ANOVA with Dunnett's multiple comparisons test (three groups) and Sidak's multiple comparisons test (two groups). # $p<0.1$, * $p\leq 0.05$

4.6. No altered GluN1 protein levels in MIA offspring

There were no significant differences in the % area of GluN1 staining between the three groups in any of the investigated brain regions (data not shown).

4.7. FC in DMN correlates with behaviour in MIA offspring

Correlation analysis was performed between rsfMRI measurements (FC in DMN, total cluster sizes and mean T-values of seed-based FC maps with Cg, RS, PtA, PtP and TeA as seed regions) and phMRI measurements (mean T-values in anterior cingulate and motor cortices, striatum, hippocampus and thalamus) on the one hand and the following behavioural assessments in MIA offspring on the other hand: PPI with 75 dB prepulse, average locomotion during light and dark, latency to first entry in centre of open field, number of entries into centre, % time spent and % distance moved in centre, % sucrose preference and locomotion 95-100 min post-MK-801.

Correlation analysis revealed significant negative correlations between sucrose preference and i) average FC in DMN ($p\leq 0.01$, $r=-0.54$) (Fig.7), ii) total cluster size of the FC maps with Cg as seed region ($p\leq 0.01$, $r=-0.50$), iii) total cluster size ($p\leq 0.05$, $r=-0.46$) and mean T-value ($p\leq 0.05$, $r=-0.44$) of the FC maps with PtP as seed region, and iv) total cluster size of the FC maps

with TeA as seed ($p \leq 0.05$, $r = -0.45$). In addition, trends were observed for negative correlations between sucrose preference and i) mean T-value of the FC maps with Cg ($p = 0.065$, $r = -0.38$), ii) mean T-value of the FC maps with PtA ($p = 0.099$, $r = -0.34$), and iii) mean T-value of the FC maps with TeA as seed region ($p = 0.070$, $r = -0.37$).

Significant negative correlations were observed between total cluster size and mean T-value of the FC maps with Cg as seed region and number of entries into centre open field (both $p \leq 0.05$, $r = -0.42$). There were also trends for negative correlations between total cluster size ($p = 0.059$, $r = -0.38$) and mean T-value ($p = 0.057$, $r = -0.39$) of the FC maps with Cg as seed region and % distance moved in centre.

Positive correlations were observed between total cluster size and mean T-value of FC maps with TeA as seed region and MK-801-induced hyperlocomotion (both $p \leq 0.01$, $r = 0.51$) (Fig.7).

No significant correlations were observed between pHMRI measurements and behavioural assessments.

Forward stepwise regression analysis with all of the aforementioned FC measurements revealed that these parameters could predict some of the variability in i) PPI with 75 dB prepulse ($p \leq 0.01$, R^2 Adj=0.40), ii) number of entries into centre open field ($p \leq 0.05$, R^2 Adj=0.25), iii) sucrose preference ($p \leq 0.01$, R^2 Adj=0.43), and iv) MK-801-induced hyperlocomotion ($p \leq 0.05$, R^2 Adj=0.26) in MIA offspring.

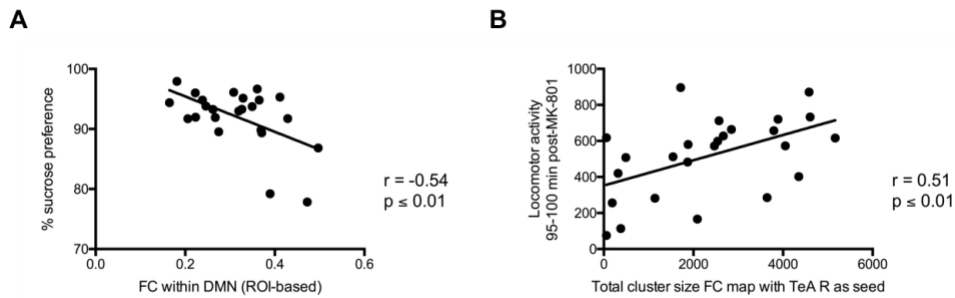


Fig.8-7. Correlation between functional connectivity (FC) in the default mode-like network (DMN) and behavioural outcome in MIA offspring. A. A negative correlation was observed between average FC in the DMN and sucrose preference in MIA offspring. **B.** A positive correlation was seen between the total cluster size of the FC maps with right temporal association cortex as seed region and MK-801 induced hyperlocomotion in MIA offspring. Red = Poly I:C WG offspring, blue = Poly I:C WL offspring. Pearson correlation.

5. Discussion

To our knowledge, we showed for the first time altered FC in MIA offspring. More precisely, we demonstrated increased FC in the DMN in adult offspring of dams that lost weight post-MIA. Furthermore, DMN FC correlated with behaviour in MIA offspring. Finally, we observed that MIA offspring have a different pathophysiology depending on the maternal response to the immune challenge. While Poly I:C WL offspring showed hypersynchronicity in the DMN, Poly I:C WG offspring exhibited more pronounced NMDAR dysfunction.

5.1. Maternal response to MIA

In line with our previous work (24), pregnant dams that lost weight following MIA seemed to display a slightly more pronounced inflammatory response in serum compared to dams that gained weight post-MIA. Hence, weight change may be a good surrogate marker of the severity of the immune

response. Accordingly, differential behavioural deficits in Poly I:C WL and Poly I:C WG offspring have been reported (18, 24-26).

5.2. Increased FC in DMN of MIA offspring in the absence of microstructural changes

We observed increased FC in the DMN of adult Poly I:C WL offspring, in agreement with most DMN studies in schizophrenia patients. This hypersynchronicity was most pronounced with posterior parietal and temporal association cortices of the DMN. Interestingly, these regions have been shown to comprise different modules of the rat DMN (29). However, little is known about the functional relevance of these different modules.

While FC was increased in the DMN, no microstructural changes could be observed in MIA offspring vs. controls. This is in contrast with previous studies of MIA offspring. However, these studies differ in many aspects from the current study. Beloosesky, Ginsberg and colleagues evaluated apparent diffusion coefficient in very young (postnatal day 25) female offspring of rats injected intraperitoneally with lipopolysaccharide, in which they found evidence for diffuse cerebral injury (11, 14). Fatemi and colleagues investigated FA in selected white matter structures of male mice prenatally exposed to human influenza virus and observed some alterations at different ages (ranging from birth to young adulthood), which were different depending on the exact timing of the prenatal immune challenge (12, 13). Only one study investigated FA throughout the entire brain of male adult mice exposed to Poly I:C during gestation and reported changes throughout fronto-striatal-limbic circuits, which were more pronounced when mice were exposed during early gestation (15). Differences in nature and timing

of the immune challenge, species and age of the offspring may explain the difference between our results and the results obtained in these studies.

5.3. Attenuated response to NMDAR antagonist in MIA offspring, but no change in NMDAR levels

Pharmacological fMRI with an NMDAR antagonist is ideally suited to investigate whole-brain NMDAR function. As expected, we observed an altered response to MK-801 in MIA offspring, which was most pronounced in Poly I:C WG offspring. The altered response was mostly detectable in subcortical structures, i.e. striatum, thalamus and hippocampus, which have all been implicated in schizophrenia (30, 31). However, a trend for an altered response could also be observed in frontal cortical regions in Poly I:C WG offspring. Frontal cortex abnormalities have also been widely reported in schizophrenia (32).

A slightly attenuated hyperlocomotive response to MK-801 was observed in Poly I:C WG offspring, but not Poly I:C WL offspring. The pharmacological fMRI response to MK-801 also showed the most pronounced difference in Poly I:C WG offspring compared to controls. Both assessments suggest that NMDAR function is most altered in Poly I:C WG offspring. In literature, both exaggerated (16, 17, 33) and attenuated (34) responses to MK-801 in MIA offspring have been reported as well as no difference vs. controls (35). Some authors have also described a difference in MK-801-induced hyperlocomotion depending on the maternal weight response to the immune challenge. A decreased response to MK-801 has been demonstrated in Poly I:C WL offspring, with either a similar but less pronounced response in Poly I:C WG offspring (26), a slightly increased response in Poly I:C WG offspring (18, 24) or a response comparable to

controls (25). It is clear that most studies have observed a disturbed NMDAR function using MK-801, but the responses are not consistent across studies and are likely dependent on the precise perturbation of the neurodevelopment.

Altered NMDAR function may potentially be explained by a change in total number of NMDARs. However, no difference was observed in GluN1 levels, the obligatory NMDAR subunit. While some studies have shown decreased GluN1 in MIA offspring (17, 19, 20), others have demonstrated increased GluN1 levels (36) or no change (37). Altered NMDAR function may also be explained by a differential subunit composition, i.e. a different contribution of GluN2A- or GluN2B-subunits, or a different phosphorylation level of the subunits. While some studies have shown no difference in GluN2A/B subunits (19, 20), others have reported increased GluN2B (38), decreased GluN2B levels (39) or no difference in GluN2B, but increased GluN2A levels (36). Clearly, the changes are not consistent across studies.

5.4. Subtle behavioural deficits in MIA offspring

The most prominent behavioural deficit was increased anxiety in the open field, which was most obvious in Poly I:C WL offspring. Anxiety symptoms and comorbid anxiety disorders have often been described in schizophrenia patients (40). Several other groups have also reported increased anxiety in open field in MIA offspring (41-44), while others reported no difference (25, 26, 45) or decreased thigmotaxis (46).

A trend for increased PPI was observed in the MIA offspring with 75 dB prepulse, but not with the other prepulse intensities. Interestingly, increased PPI has been observed in autistic children with a 76 dB prepulse

and not with a stronger prepulse (47). MIA offspring have also often been used as a model for autism. While many studies have shown decreased PPI in MIA offspring (48, 49), some failed to observe a difference (50) or showed increased PPI (26).

A trend for increased spontaneous locomotion during light phase and decreased activity during dark phase were observed in the MIA offspring, which suggests a disturbed rest-activity/sleep-wake rhythm. Circadian rest-activity/sleep-wake disruptions are a common problem in schizophrenia (51). Recently, a study has shown persistent sleep alterations in MIA offspring with increased locomotion during the light phase (52). Increased locomotion during the light phase has also been shown by others (34, 42, 53), but decreased locomotion has been observed as well (54).

Though there was a numerically higher proportion of subjects with anhedonia (defined as sucrose preference <90%) in the MIA offspring groups vs. controls, this difference was not significant. Again, anhedonia has not been consistently reported in MIA offspring (22, 24, 42, 55, 56).

5.5. Hypersynchronicity in the DMN is related to behaviour in MIA offspring

Interestingly, FC in the DMN of MIA offspring correlated with their behavioural outcome. Correlation and stepwise regression analyses showed that FC in the DMN could predict the variability in several behavioural parameters: PPI with 75 dB prepulse, sucrose preference, thigmotaxis in open field and MK-801-induced hyperlocomotion. Higher FC in DMN was related to higher PPI, lower sucrose preference and increased anxiety. Similarly, hypersynchronicity in the DMN of schizophrenia patients has been

related to psychopathological symptom severity (57, 58). Hypersynchronicity and hyperactivity of the DMN are thought to blur the line between internal thoughts/feelings and external perceptions in schizophrenia patients, resulting in exaggerated self-relevance of neutral events and aberrant integration of internal and external stimuli, ultimately leading to symptoms such as paranoia and hallucinations (58). On the other hand, higher FC in DMN was related to a higher (more normal) MK-801-induced hyperlocomotive response. Indeed, Poly I:C WG offspring with normal FC in DMN had a decreased MK-801-induced hyperlocomotive response while Poly I:C WL offspring with increased FC had a normal MK-801-induced hyperlocomotive response. The pharmacological fMRI response to MK-801 was not related to behaviour in the MIA offspring.

6. Conclusions and future perspectives

To our knowledge, our study is the first to show altered FC in a MIA model. We observed increased FC in the DMN of animals that were born to dams that lost weight following immune challenge. Moreover, FC in DMN was associated with behavioural outcome in MIA offspring. Since it has been shown that hypersynchronicity in the DMN of schizophrenia patients can be normalised by antipsychotic treatment, hypersynchronicity in the DMN of MIA models could be a potential biomarker to test novel therapies. While behavioural deficits were subtle in our study, the altered FC was clear and may be a more reliable read-out of the model than the behaviour. Finally, it remains to be seen if altered FC in the DMN of MIA offspring precedes the behavioural deficits and may be useful as a novel prognostic biomarker. All of these issues will need to be addressed in future studies. Finally, we showed that Poly I:C WL offspring exhibited DMN hypersynchronicity, while

Poly I:C WG offspring displayed a more attenuated response to an NMDAR antagonist. This underlines the importance of taking the individual maternal response into account in studying the long-lasting effects of disturbed neurodevelopment following prenatal immune activation.

Acknowledgments

We are very grateful for the technical assistance of Krystyna Szewczyk and Annemie Van Eetveldt. We thank UCB Biopharma and in particular Georges Mairet-Coello, Mathieu Schmitt and Tania Deprez for the use of the slide scanner. This study was supported by the Research Foundation Flanders (FWO) (G.0586.12). Stephan Missault had a PhD fellowship of the Research Foundation Flanders (11K3714N/11K3716N). The computational resources and services used in this work for making the 3D anatomical template were provided by the HPC core facility CalcUA of the Universiteit Antwerpen, the VSC (Flemish Supercomputer Center), funded by the Hercules Foundation and the Flemish Government – department EWI. The 7T PharmaScan MR system was purchased through Hercules foundation funding (Belgium) under the promotorship of Prof. Annemie Van der Linden. This work was also supported by the University of Antwerp (TTBOF/29267) and the Agency for Innovation by Science and Technology in Flanders (VLAIO O&O 150003).

Highlights

- Maternal immune activation (Poly I:C) results in Weight Loss or Weight Gain in dams
- Poly I:C WL offspring have hypersynchronicity in default mode-like network (DMN)

- Attenuated NMDA receptor function is most pronounced in Poly I:C WG offspring
- Poly I:C offspring exhibit increased anxiety
- Functional connectivity in DMN correlates with behaviour in Poly I:C offspring

7. References

1. Estes ML, McAllister AK (2016): Maternal immune activation: Implications for neuropsychiatric disorders. *Science*. 353:772-777.
2. Brown AS, Derkits EJ (2010): Prenatal infection and schizophrenia: a review of epidemiologic and translational studies. *Am J Psychiatry*. 167:261-280.
3. Balu DT (2016): The NMDA Receptor and Schizophrenia: From Pathophysiology to Treatment. *Adv Pharmacol*. 76:351-382.
4. Friston K, Brown HR, Siemerkus J, Stephan KE (2016): The dysconnection hypothesis (2016). *Schizophr Res*. 176:83-94.
5. Fornito A, Zalesky A, Pantelis C, Bullmore ET (2012): Schizophrenia, neuroimaging and connectomics. *Neuroimage*. 62:2296-2314.
6. Hu ML, Zong XF, Mann JJ, Zheng JJ, Liao YH, Li ZC, et al. (2017): A Review of the Functional and Anatomical Default Mode Network in Schizophrenia. *Neurosci Bull*. 33:73-84.
7. Smucny J, Wylie KP, Tregellas JR (2014): Functional magnetic resonance imaging of intrinsic brain networks for translational drug discovery. *Trends Pharmacol Sci*. 35:397-403.
8. Sambataro F, Blasi G, Fazio L, Caforio G, Taurisano P, Romano R, et al. (2010): Treatment with olanzapine is associated with modulation of the default mode network in patients with Schizophrenia. *Neuropsychopharmacology*. 35:904-912.
9. Surguladze SA, Chu EM, Marshall N, Evans A, Anilkumar AP, Timehin C, et al. (2011): Emotion processing in schizophrenia: fMRI study of patients treated with risperidone long-acting injections or conventional depot medication. *J Psychopharmacol*. 25:722-733.
10. Tregellas JR, Tanabe J, Rojas DC, Shatti S, Olincy A, Johnson L, et al. (2011): Effects of an alpha 7-nicotinic agonist on default network activity in schizophrenia. *Biol Psychiatry*. 69:7-11.
11. Beloosesky R, Ginsberg Y, Khatib N, Maravi N, Ross MG, Itskovitz-Eldor J, et al. (2013): Prophylactic maternal N-acetylcysteine in rats prevents maternal inflammation-induced offspring cerebral injury shown on magnetic resonance imaging. *Am J Obstet Gynecol*. 208:213 e211-216.
12. Fatemi SH, Folsom TD, Reutiman TJ, Abu-Odeh D, Mori S, Huang H, et al. (2009): Abnormal expression of myelination genes and alterations in white matter fractional anisotropy following prenatal viral influenza infection at E16 in mice. *Schizophr Res*. 112:46-53.
13. Fatemi SH, Reutiman TJ, Folsom TD, Huang H, Oishi K, Mori S, et al. (2008): Maternal infection leads to abnormal gene regulation and brain

atrophy in mouse offspring: implications for genesis of neurodevelopmental disorders. *Schizophr Res.* 99:56-70.

14. Ginsberg Y, Khatib N, Weiss B, Arison S, Ross MG, Weiner Z, et al. (2017): Magnesium sulfate (MG) prevents maternal inflammation induced offspring cerebral injury evident on MRI but not via IL-1beta. *Neuroscience.* 353:98-105.

15. Li Q, Cheung C, Wei R, Cheung V, Hui ES, You Y, et al. (2010): Voxel-based analysis of postnatal white matter microstructure in mice exposed to immune challenge in early or late pregnancy. *Neuroimage.* 52:1-8.

16. Zuckerman L, Weiner I (2005): Maternal immune activation leads to behavioral and pharmacological changes in the adult offspring. *J Psychiatr Res.* 39:311-323.

17. Meyer U, Nyffeler M, Yee BK, Knuesel I, Feldon J (2008): Adult brain and behavioral pathological markers of prenatal immune challenge during early/middle and late fetal development in mice. *Brain Behav Immun.* 22:469-486.

18. Bronson SL, Ahlbrand R, Horn PS, Kern JR, Richtand NM (2011): Individual differences in maternal response to immune challenge predict offspring behavior: contribution of environmental factors. *Behav Brain Res.* 220:55-64.

19. Escobar M, Crouzin N, Cavalier M, Quentin J, Roussel J, Lante F, et al. (2011): Early, time-dependent disturbances of hippocampal synaptic transmission and plasticity after in utero immune challenge. *Biol Psychiatry.* 70:992-999.

20. Forrest CM, Khalil OS, Pizar M, Smith RA, Darlington LG, Stone TW (2012): Prenatal activation of Toll-like receptors-3 by administration of the viral mimetic poly(I:C) changes synaptic proteins, N-methyl-D-aspartate receptors and neurogenesis markers in offspring. *Mol Brain.* 5:22.

21. Viviani B, Boraso M, Valero M, Gardoni F, Marco EM, Llorente R, et al. (2014): Early maternal deprivation immunologically primes hippocampal synapses by redistributing interleukin-1 receptor type I in a sex dependent manner. *Brain Behav Immun.* 35:135-143.

22. Bitanihirwe BK, Peleg-Raibstein D, Mouttet F, Feldon J, Meyer U (2010): Late prenatal immune activation in mice leads to behavioral and neurochemical abnormalities relevant to the negative symptoms of schizophrenia. *Neuropsychopharmacology.* 35:2462-2478.

23. Roenker NL, Gudelsky G, Ahlbrand R, Bronson SL, Kern JR, Waterman H, et al. (2011): Effect of paliperidone and risperidone on extracellular glutamate in the prefrontal cortex of rats exposed to prenatal immune activation or MK-801. *Neurosci Lett.* 500:167-171.

24. Missault S, Van den Eynde K, Vanden Berghe W, Fransen E, Weeren A, Timmermans JP, et al. (2014): The risk for behavioural deficits is determined by the maternal immune response to prenatal immune challenge in a neurodevelopmental model. *Brain Behav Immun.* 42:138-146.
25. Vorhees CV, Graham DL, Braun AA, Schaefer TL, Skelton MR, Richtand NM, et al. (2012): Prenatal immune challenge in rats: altered responses to dopaminergic and glutamatergic agents, prepulse inhibition of acoustic startle, and reduced route-based learning as a function of maternal body weight gain after prenatal exposure to poly IC. *Synapse.* 66:725-737.
26. Vorhees CV, Graham DL, Braun AA, Schaefer TL, Skelton MR, Richtand NM, et al. (2015): Prenatal immune challenge in rats: effects of polyinosinic-polycytidylic acid on spatial learning, prepulse inhibition, conditioned fear, and responses to MK-801 and amphetamine. *Neurotoxicol Teratol.* 47:54-65.
27. Lu H, Zou Q, Gu H, Raichle ME, Stein EA, Yang Y (2012): Rat brains also have a default mode network. *Proc Natl Acad Sci U S A.* 109:3979-3984.
28. Barbier M, Bottelbergs A, Nuydens R, Ebneith A, De Vos WH, Murphy R (2018): SliceMap: an algorithm for automated brain region annotation. *Bioinformatics.* 34:718-720.
29. Hsu LM, Liang X, Gu H, Brynildsen JK, Stark JA, Ash JA, et al. (2016): Constituents and functional implications of the rat default mode network. *Proc Natl Acad Sci U S A.* 113:E4541-4547.
30. Pergola G, Selvaggi P, Trizio S, Bertolino A, Blasi G (2015): The role of the thalamus in schizophrenia from a neuroimaging perspective. *Neurosci Biobehav Rev.* 54:57-75.
31. Heckers S (2001): Neuroimaging studies of the hippocampus in schizophrenia. *Hippocampus.* 11:520-528.
32. Mubarik A, Tohid H (2016): Frontal lobe alterations in schizophrenia: a review. *Trends Psychiatry Psychother.* 38:198-206.
33. Zavitsanou K, Lim CK, Purves-Tyson T, Karl T, Kassiou M, Banister SD, et al. (2014): Effect of maternal immune activation on the kynurenine pathway in preadolescent rat offspring and on MK801-induced hyperlocomotion in adulthood: amelioration by COX-2 inhibition. *Brain Behav Immun.* 41:173-181.
34. Howland JG, Cazakoff BN, Zhang Y (2012): Altered object-in-place recognition memory, prepulse inhibition, and locomotor activity in the offspring of rats exposed to a viral mimetic during pregnancy. *Neuroscience.* 201:184-198.

35. Meehan C, Harms L, Frost JD, Barreto R, Todd J, Schall U, et al. (2017): Effects of immune activation during early or late gestation on schizophrenia-related behaviour in adult rat offspring. *Brain Behav Immun.* 63:8-20.
36. Rahman T, Zavitsanou K, Purves-Tyson T, Harms LR, Meehan C, Schall U, et al. (2017): Effects of Immune Activation during Early or Late Gestation on N-Methyl-d-Aspartate Receptor Measures in Adult Rat Offspring. *Front Psychiatry.* 8:77.
37. Oh-Nishi A, Obayashi S, Sugihara I, Minamimoto T, Suhara T (2010): Maternal immune activation by polyriboinosinic-polyribocytidilic acid injection produces synaptic dysfunction but not neuronal loss in the hippocampus of juvenile rat offspring. *Brain Res.* 1363:170-179.
38. Khalil OS, Forrest CM, Pizar M, Smith RA, Darlington LG, Stone TW (2013): Prenatal activation of maternal TLR3 receptors by viral-mimetic poly(I:C) modifies GluN2B expression in embryos and sonic hedgehog in offspring in the absence of kynurenine pathway activation. *Immunopharmacol Immunotoxicol.* 35:581-593.
39. Connors EJ, Shaik AN, Migliore MM, Kentner AC (2014): Environmental enrichment mitigates the sex-specific effects of gestational inflammation on social engagement and the hypothalamic pituitary adrenal axis-feedback system. *Brain Behav Immun.* 42:178-190.
40. Muller JE, Koen L, Soraya S, Emsley RA, Stein DJ (2004): Anxiety disorders and schizophrenia. *Curr Psychiatry Rep.* 6:255-261.
41. Canetta S, Bolkan S, Padilla-Coreano N, Song LJ, Sahn R, Harrison NL, et al. (2016): Maternal immune activation leads to selective functional deficits in offspring parvalbumin interneurons. *Mol Psychiatry.* 21:956-968.
42. da Silveira VT, Medeiros DC, Ropke J, Guidine PA, Rezende GH, Moraes MF, et al. (2017): Effects of early or late prenatal immune activation in mice on behavioral and neuroanatomical abnormalities relevant to schizophrenia in the adulthood. *Int J Dev Neurosci.* 58:1-8.
43. Hsiao EY, McBride SW, Hsien S, Sharon G, Hyde ER, McCue T, et al. (2013): Microbiota modulate behavioral and physiological abnormalities associated with neurodevelopmental disorders. *Cell.* 155:1451-1463.
44. Nyffeler M, Meyer U, Yee BK, Feldon J, Knuesel I (2006): Maternal immune activation during pregnancy increases limbic GABAA receptor immunoreactivity in the adult offspring: implications for schizophrenia. *Neuroscience.* 143:51-62.
45. Schwendener S, Meyer U, Feldon J (2009): Deficient maternal care resulting from immunological stress during pregnancy is associated with a sex-dependent enhancement of conditioned fear in the offspring. *J Neurodev Disord.* 1:15-32.

46. Ozawa K, Hashimoto K, Kishimoto T, Shimizu E, Ishikura H, Iyo M (2006): Immune activation during pregnancy in mice leads to dopaminergic hyperfunction and cognitive impairment in the offspring: a neurodevelopmental animal model of schizophrenia. *Biol Psychiatry*. 59:546-554.
47. Madsen GF, Bilenberg N, Cantio C, Oranje B (2014): Increased prepulse inhibition and sensitization of the startle reflex in autistic children. *Autism Res*. 7:94-103.
48. Meyer U, Feldon J, Schedlowski M, Yee BK (2005): Towards an immuno-precipitated neurodevelopmental animal model of schizophrenia. *Neurosci Biobehav Rev*. 29:913-947.
49. Wolff AR, Bilkey DK (2008): Immune activation during mid-gestation disrupts sensorimotor gating in rat offspring. *Behav Brain Res*. 190:156-159.
50. Fortier ME, Luheshi GN, Boksa P (2007): Effects of prenatal infection on prepulse inhibition in the rat depend on the nature of the infectious agent and the stage of pregnancy. *Behav Brain Res*. 181:270-277.
51. Monti JM, BaHammam AS, Pandi-Perumal SR, Bromundt V, Spence DW, Cardinali DP, et al. (2013): Sleep and circadian rhythm dysregulation in schizophrenia. *Prog Neuropsychopharmacol Biol Psychiatry*. 43:209-216.
52. Missig G, Mokler EL, Robbins JO, Alexander AJ, McDougale CJ, Carlezon WA (2017): Perinatal Immune Activation Produces Persistent Sleep Alterations and Epileptiform Activity in Male Mice. *Neuropsychopharmacology*.
53. Zhu F, Zheng Y, Liu Y, Zhang X, Zhao J (2014): Minocycline alleviates behavioral deficits and inhibits microglial activation in the offspring of pregnant mice after administration of polyriboinosinic-polyribocytidilic acid. *Psychiatry Res*. 219:680-686.
54. Van den Eynde K, Missault S, Fransen E, Raeymaekers L, Willems R, Drinkenburg W, et al. (2014): Hypolocomotive behaviour associated with increased microglia in a prenatal immune activation model with relevance to schizophrenia. *Behav Brain Res*. 258:179-186.
55. Khan D, Fernando P, Cicvaric A, Berger A, Pollak A, Monje FJ, et al. (2014): Long-term effects of maternal immune activation on depression-like behavior in the mouse. *Transl Psychiatry*. 4:e363.
56. Labouesse MA, Langhans W, Meyer U (2015): Abnormal context-reward associations in an immune-mediated neurodevelopmental mouse model with relevance to schizophrenia. *Transl Psychiatry*. 5:e637.
57. Mingoia G, Wagner G, Langbein K, Maitra R, Smesny S, Dietzek M, et al. (2012): Default mode network activity in schizophrenia studied at resting state using probabilistic ICA. *Schizophr Res*. 138:143-149.

58. Whitfield-Gabrieli S, Thermenos HW, Milanovic S, Tsuang MT, Faraone SV, McCarley RW, et al. (2009): Hyperactivity and hyperconnectivity of the default network in schizophrenia and in first-degree relatives of persons with schizophrenia. *Proc Natl Acad Sci U S A*. 106:1279-1284.
1. Estes ML, McAllister AK (2016): Maternal immune activation: Implications for neuropsychiatric disorders. *Science*. 353:772-777.
 2. Brown AS, Derkits EJ (2010): Prenatal infection and schizophrenia: a review of epidemiologic and translational studies. *Am J Psychiatry*. 167:261-280.
 3. Balu DT (2016): The NMDA Receptor and Schizophrenia: From Pathophysiology to Treatment. *Adv Pharmacol*. 76:351-382.
 4. Friston K, Brown HR, Siemerkus J, Stephan KE (2016): The dysconnection hypothesis (2016). *Schizophr Res*. 176:83-94.
 5. Fornito A, Zalesky A, Pantelis C, Bullmore ET (2012): Schizophrenia, neuroimaging and connectomics. *Neuroimage*. 62:2296-2314.
 6. Hu ML, Zong XF, Mann JJ, Zheng JJ, Liao YH, Li ZC, et al. (2017): A Review of the Functional and Anatomical Default Mode Network in Schizophrenia. *Neurosci Bull*. 33:73-84.
 7. Smucny J, Wylie KP, Tregellas JR (2014): Functional magnetic resonance imaging of intrinsic brain networks for translational drug discovery. *Trends Pharmacol Sci*. 35:397-403.
 8. Sambataro F, Blasi G, Fazio L, Caforio G, Taurisano P, Romano R, et al. (2010): Treatment with olanzapine is associated with modulation of the default mode network in patients with Schizophrenia. *Neuropsychopharmacology*. 35:904-912.
 9. Surguladze SA, Chu EM, Marshall N, Evans A, Anilkumar AP, Timehin C, et al. (2011): Emotion processing in schizophrenia: fMRI study of patients treated with risperidone long-acting injections or conventional depot medication. *J Psychopharmacol*. 25:722-733.
 10. Tregellas JR, Tanabe J, Rojas DC, Shatti S, Olincy A, Johnson L, et al. (2011): Effects of an alpha 7-nicotinic agonist on default network activity in schizophrenia. *Biol Psychiatry*. 69:7-11.
 11. Beloosesky R, Ginsberg Y, Khatib N, Maravi N, Ross MG, Itskovitz-Eldor J, et al. (2013): Prophylactic maternal N-acetylcysteine in rats prevents maternal inflammation-induced offspring cerebral injury shown on magnetic resonance imaging. *Am J Obstet Gynecol*. 208:213 e211-216.
 12. Fatemi SH, Folsom TD, Reutiman TJ, Abu-Odeh D, Mori S, Huang H, et al. (2009): Abnormal expression of myelination genes and alterations in white matter fractional anisotropy following prenatal viral influenza infection at E16 in mice. *Schizophr Res*. 112:46-53.

13. Fatemi SH, Reutiman TJ, Folsom TD, Huang H, Oishi K, Mori S, et al. (2008): Maternal infection leads to abnormal gene regulation and brain atrophy in mouse offspring: implications for genesis of neurodevelopmental disorders. *Schizophr Res.* 99:56-70.
14. Ginsberg Y, Khatib N, Weiss B, Arison S, Ross MG, Weiner Z, et al. (2017): Magnesium sulfate (MG) prevents maternal inflammation induced offspring cerebral injury evident on MRI but not via IL-1beta. *Neuroscience.* 353:98-105.
15. Li Q, Cheung C, Wei R, Cheung V, Hui ES, You Y, et al. (2010): Voxel-based analysis of postnatal white matter microstructure in mice exposed to immune challenge in early or late pregnancy. *Neuroimage.* 52:1-8.
16. Zuckerman L, Weiner I (2005): Maternal immune activation leads to behavioral and pharmacological changes in the adult offspring. *J Psychiatr Res.* 39:311-323.
17. Meyer U, Nyffeler M, Yee BK, Knuesel I, Feldon J (2008): Adult brain and behavioral pathological markers of prenatal immune challenge during early/middle and late fetal development in mice. *Brain Behav Immun.* 22:469-486.
18. Bronson SL, Ahlbrand R, Horn PS, Kern JR, Richtand NM (2011): Individual differences in maternal response to immune challenge predict offspring behavior: contribution of environmental factors. *Behav Brain Res.* 220:55-64.
19. Escobar M, Crouzin N, Cavalier M, Quentin J, Roussel J, Lante F, et al. (2011): Early, time-dependent disturbances of hippocampal synaptic transmission and plasticity after in utero immune challenge. *Biol Psychiatry.* 70:992-999.
20. Forrest CM, Khalil OS, Pizar M, Smith RA, Darlington LG, Stone TW (2012): Prenatal activation of Toll-like receptors-3 by administration of the viral mimetic poly(I:C) changes synaptic proteins, N-methyl-D-aspartate receptors and neurogenesis markers in offspring. *Mol Brain.* 5:22.
21. Viviani B, Boraso M, Valero M, Gardoni F, Marco EM, Llorente R, et al. (2014): Early maternal deprivation immunologically primes hippocampal synapses by redistributing interleukin-1 receptor type I in a sex dependent manner. *Brain Behav Immun.* 35:135-143.
22. Bitanirwe BK, Peleg-Raibstein D, Mouttet F, Feldon J, Meyer U (2010): Late prenatal immune activation in mice leads to behavioral and neurochemical abnormalities relevant to the negative symptoms of schizophrenia. *Neuropsychopharmacology.* 35:2462-2478.
23. Roenker NL, Gudelsky G, Ahlbrand R, Bronson SL, Kern JR, Waterman H, et al. (2011): Effect of paliperidone and risperidone on extracellular

glutamate in the prefrontal cortex of rats exposed to prenatal immune activation or MK-801. *Neurosci Lett.* 500:167-171.

24. Missault S, Van den Eynde K, Vanden Berghe W, Fransen E, Weeren A, Timmermans JP, et al. (2014): The risk for behavioural deficits is determined by the maternal immune response to prenatal immune challenge in a neurodevelopmental model. *Brain Behav Immun.* 42:138-146.

25. Vorhees CV, Graham DL, Braun AA, Schaefer TL, Skelton MR, Richtand NM, et al. (2012): Prenatal immune challenge in rats: altered responses to dopaminergic and glutamatergic agents, prepulse inhibition of acoustic startle, and reduced route-based learning as a function of maternal body weight gain after prenatal exposure to poly IC. *Synapse.* 66:725-737.

26. Vorhees CV, Graham DL, Braun AA, Schaefer TL, Skelton MR, Richtand NM, et al. (2015): Prenatal immune challenge in rats: effects of polyinosinic-polycytidylic acid on spatial learning, prepulse inhibition, conditioned fear, and responses to MK-801 and amphetamine. *Neurotoxicol Teratol.* 47:54-65.

27. Lu H, Zou Q, Gu H, Raichle ME, Stein EA, Yang Y (2012): Rat brains also have a default mode network. *Proc Natl Acad Sci U S A.* 109:3979-3984.

28. Barbier M, Bottelbergs A, Nuydens R, Ebneith A, De Vos WH, Murphy R (2018): SliceMap: an algorithm for automated brain region annotation. *Bioinformatics.* 34:718-720.

29. Hsu LM, Liang X, Gu H, Brynildsen JK, Stark JA, Ash JA, et al. (2016): Constituents and functional implications of the rat default mode network. *Proc Natl Acad Sci U S A.* 113:E4541-4547.

30. Pergola G, Selvaggi P, Trizio S, Bertolino A, Blasi G (2015): The role of the thalamus in schizophrenia from a neuroimaging perspective. *Neurosci Biobehav Rev.* 54:57-75.

31. Heckers S (2001): Neuroimaging studies of the hippocampus in schizophrenia. *Hippocampus.* 11:520-528.

32. Mubarik A, Tohid H (2016): Frontal lobe alterations in schizophrenia: a review. *Trends Psychiatry Psychother.* 38:198-206.

33. Zavitsanou K, Lim CK, Purves-Tyson T, Karl T, Kassiou M, Banister SD, et al. (2014): Effect of maternal immune activation on the kynurenine pathway in preadolescent rat offspring and on MK801-induced hyperlocomotion in adulthood: amelioration by COX-2 inhibition. *Brain Behav Immun.* 41:173-181.

34. Howland JG, Cazakoff BN, Zhang Y (2012): Altered object-in-place recognition memory, prepulse inhibition, and locomotor activity in the offspring of rats exposed to a viral mimetic during pregnancy. *Neuroscience.* 201:184-198.

35. Meehan C, Harms L, Frost JD, Barreto R, Todd J, Schall U, et al. (2017): Effects of immune activation during early or late gestation on schizophrenia-related behaviour in adult rat offspring. *Brain Behav Immun.* 63:8-20.
36. Rahman T, Zavitsanou K, Purves-Tyson T, Harms LR, Meehan C, Schall U, et al. (2017): Effects of Immune Activation during Early or Late Gestation on N-Methyl-d-Aspartate Receptor Measures in Adult Rat Offspring. *Front Psychiatry.* 8:77.
37. Oh-Nishi A, Obayashi S, Sugihara I, Minamimoto T, Suhara T (2010): Maternal immune activation by polyriboinosinic-polyribocytidilic acid injection produces synaptic dysfunction but not neuronal loss in the hippocampus of juvenile rat offspring. *Brain Res.* 1363:170-179.
38. Khalil OS, Forrest CM, Pizar M, Smith RA, Darlington LG, Stone TW (2013): Prenatal activation of maternal TLR3 receptors by viral-mimetic poly(I:C) modifies GluN2B expression in embryos and sonic hedgehog in offspring in the absence of kynurenine pathway activation. *Immunopharmacol Immunotoxicol.* 35:581-593.
39. Connors EJ, Shaik AN, Migliore MM, Kentner AC (2014): Environmental enrichment mitigates the sex-specific effects of gestational inflammation on social engagement and the hypothalamic pituitary adrenal axis-feedback system. *Brain Behav Immun.* 42:178-190.
40. Muller JE, Koen L, Soraya S, Emsley RA, Stein DJ (2004): Anxiety disorders and schizophrenia. *Curr Psychiatry Rep.* 6:255-261.
41. Canetta S, Bolkan S, Padilla-Coreano N, Song LJ, Sahn R, Harrison NL, et al. (2016): Maternal immune activation leads to selective functional deficits in offspring parvalbumin interneurons. *Mol Psychiatry.* 21:956-968.
42. da Silveira VT, Medeiros DC, Ropke J, Guidine PA, Rezende GH, Moraes MF, et al. (2017): Effects of early or late prenatal immune activation in mice on behavioral and neuroanatomical abnormalities relevant to schizophrenia in the adulthood. *Int J Dev Neurosci.* 58:1-8.
43. Hsiao EY, McBride SW, Hsien S, Sharon G, Hyde ER, McCue T, et al. (2013): Microbiota modulate behavioral and physiological abnormalities associated with neurodevelopmental disorders. *Cell.* 155:1451-1463.
44. Nyffeler M, Meyer U, Yee BK, Feldon J, Knuesel I (2006): Maternal immune activation during pregnancy increases limbic GABAA receptor immunoreactivity in the adult offspring: implications for schizophrenia. *Neuroscience.* 143:51-62.
45. Schwendener S, Meyer U, Feldon J (2009): Deficient maternal care resulting from immunological stress during pregnancy is associated with a sex-dependent enhancement of conditioned fear in the offspring. *J Neurodev Disord.* 1:15-32.

46. Ozawa K, Hashimoto K, Kishimoto T, Shimizu E, Ishikura H, Iyo M (2006): Immune activation during pregnancy in mice leads to dopaminergic hyperfunction and cognitive impairment in the offspring: a neurodevelopmental animal model of schizophrenia. *Biol Psychiatry*. 59:546-554.
47. Madsen GF, Bilenberg N, Cantio C, Oranje B (2014): Increased prepulse inhibition and sensitization of the startle reflex in autistic children. *Autism Res*. 7:94-103.
48. Meyer U, Feldon J, Schedlowski M, Yee BK (2005): Towards an immuno-precipitated neurodevelopmental animal model of schizophrenia. *Neurosci Biobehav Rev*. 29:913-947.
49. Wolff AR, Bilkey DK (2008): Immune activation during mid-gestation disrupts sensorimotor gating in rat offspring. *Behav Brain Res*. 190:156-159.
50. Fortier ME, Luheshi GN, Boksa P (2007): Effects of prenatal infection on prepulse inhibition in the rat depend on the nature of the infectious agent and the stage of pregnancy. *Behav Brain Res*. 181:270-277.
51. Monti JM, BaHammam AS, Pandi-Perumal SR, Bromundt V, Spence DW, Cardinali DP, et al. (2013): Sleep and circadian rhythm dysregulation in schizophrenia. *Prog Neuropsychopharmacol Biol Psychiatry*. 43:209-216.
52. Missig G, Mokler EL, Robbins JO, Alexander AJ, McDougale CJ, Carlezon WA (2017): Perinatal Immune Activation Produces Persistent Sleep Alterations and Epileptiform Activity in Male Mice. *Neuropsychopharmacology*.
53. Zhu F, Zheng Y, Liu Y, Zhang X, Zhao J (2014): Minocycline alleviates behavioral deficits and inhibits microglial activation in the offspring of pregnant mice after administration of polyriboinosinic-polyribocytidilic acid. *Psychiatry Res*. 219:680-686.
54. Van den Eynde K, Missault S, Fransen E, Raeymaekers L, Willems R, Drinkenburg W, et al. (2014): Hypolocomotive behaviour associated with increased microglia in a prenatal immune activation model with relevance to schizophrenia. *Behav Brain Res*. 258:179-186.
55. Khan D, Fernando P, Cicvaric A, Berger A, Pollak A, Monje FJ, et al. (2014): Long-term effects of maternal immune activation on depression-like behavior in the mouse. *Transl Psychiatry*. 4:e363.
56. Labouesse MA, Langhans W, Meyer U (2015): Abnormal context-reward associations in an immune-mediated neurodevelopmental mouse model with relevance to schizophrenia. *Transl Psychiatry*. 5:e637.
57. Mingoia G, Wagner G, Langbein K, Maitra R, Smesny S, Dietzek M, et al. (2012): Default mode network activity in schizophrenia studied at resting state using probabilistic ICA. *Schizophr Res*. 138:143-149.

58. Whitfield-Gabrieli S, Thermenos HW, Milanovic S, Tsuang MT, Faraone SV, McCarley RW, et al. (2009): Hyperactivity and hyperconnectivity of the default network in schizophrenia and in first-degree relatives of persons with schizophrenia. *Proc Natl Acad Sci U S A*. 106:1279-1284.

9

Discussion and future perspectives

The main aim of this PhD thesis was to identify neuroimaging correlates of chronic behavioural outcome following discrete brain insults in experimental animal models, i.e. *status epilepticus* (SE) and traumatic brain injury (TBI) during young adulthood, and maternal immune activation (MIA) during prenatal development. In brief, we have successfully identified several *in vivo* imaging (or *in vitro* autoradiography) correlates of chronic behavioural alterations following distinct brain insults:

- *In vitro* autoradiography binding of the SPECT probe [¹¹¹In]MICA-401, which binds to active uPA/KLK8 (extracellular matrix proteases), in hippocampus in the chronic period following SE correlated with seizure burden in this period in a model of temporal lobe epilepsy (TLE).
- Subacute TSPO PET tracer uptake (neuroinflammation marker) and DTI metrics (FA, MD, AD and RD) in perilesional cortex and ipsilesional hippocampus was able to predict long-term behavioural outcome following experimental TBI (Controlled Cortical Impact (CCI) injury).
- Functional connectivity in the default mode-like network (DMN), assessed with resting-state fMRI, correlated with behaviour in adult offspring that were prenatally exposed to MIA, a model with relevance to schizophrenia.

Any kind of brain insult can have a major impact on the brain and affect different constituents of the brain, including neurons, glia and the extracellular matrix. Depending on the timing and the nature of the insult, brain insults can lead to altered neurodevelopment, neurodegeneration, neuroregeneration/plasticity, inflammation, and remodelling of the extracellular matrix. These processes interact and influence each other and

determine the long-term outcome following a brain insult. *In vivo* imaging of alterations in neurons, glia and extracellular matrix can be linked to the behavioural outcome of an insult and may provide insight in the neurobiological processes that underlie the behavioural changes. Since different constituents of the brain are altered following an insult, multimodal imaging of these alterations may prove to be necessary to provide the most accurate correlate of functional outcome. Several different potential *in vivo* imaging correlates of chronic outcome following brain insults were investigated in this thesis. This may lead to the identification of novel prognostic and predictive biomarkers.

We observed that alterations in extracellular matrix proteases (uPA/KLK8) were associated with seizure burden in a TLE model. Previous work from our lab has shown that upregulation of TSPO (i.e. inflammation) was also associated with seizure burden in this model (1). We found that subacute TSPO and DTI metrics could predict long-term TBI outcome, indicating that inflammation, neurodegeneration and/or regeneration play a role in the chronic TBI sequelae. Altered functional connectivity in the DMN was related to behaviour in adult MIA offspring. Alterations in inflammation and extracellular matrix have also been observed following MIA and in schizophrenia and may also be able to explain in part the functional deficits.

Our observations will be discussed in more detail below, especially in light of the outcome of other studies that were not implemented in this thesis, as well as more recent literature.

1. uPA/KLK8 activity correlates with seizure burden in a TLE model

In vitro autoradiography with the SPECT radiotracer [¹¹¹In]MICA-401 revealed decreased uPA/KLK8 activity in hippocampal subfield CA3 and temporal lobe in the subacute phase following *SE*, as well as in perilesional cortex and ipsilesional dentate gyrus in the subacute period following TBI. In the chronic phase following *SE*, when rats had developed spontaneous recurrent seizures, uPA/KLK8 activity was decreased in all investigated brain regions, and hippocampal uPA/KLK8 activity correlated with the seizure burden. A disadvantage of this radiotracer is its lack of specificity for a single protease, which is a common problem with radiotracers targeting enzymes. However, since both uPA and KLK8 had been shown to display similar responses to epileptogenic insults, i.e. a loss of uPA/KLK8 in degenerating neurons and an induction of uPA/KLK8 in glial cells, this was not deemed a problem (2-4). However, it puts some restraints on identifying the real culprit, i.e. the protease (or better: lack of protease) that is involved in the increased epileptic seizure burden. While uPA deficiency in knockout mice has been shown to result in increased neuronal loss and/or decreased neurogenesis following *SE* and TBI, as well as a worse neuromotor outcome following TBI, it did not affect chronic seizure susceptibility or epilepsy outcome following *SE* and TBI (5-8). Moreover, it resulted even in a decreased response to pilocarpine, a proconvulsant (8). However, KLK8 deficiency in knockout mice has been shown to result in an increased response to kainic acid (9, 10). Therefore, we hypothesise that a hippocampal decrease in KLK8, rather than uPA, may be involved in the increased frequency of spontaneous recurrent seizures that we observed following *SE*. It has been shown that KLK8 is involved in maintaining the

proper excitation-inhibition balance in hippocampus following kainic acid administration, which is dependent on NRG1/ErbB4 signalling towards parvalbumin-expressing GABAergic interneurons (10). A lack of KLK8 shifts the excitation-inhibition balance towards excitation, possibly explaining why rats with a more pronounced decrease in (uPA/)/KLK8 had a higher seizure burden in our study.

In another study, we applied the uPA/KLK8 inhibitor UAMC-01162, the compound from which [¹¹¹In]MICA-401 is derived, to cortical neuronal cell cultures (derived from postnatal rat neocortex). Electrophysiological analysis of the *in vitro* cortical neuronal networks using multielectrode arrays revealed that acute administration of the uPA/KLK8 inhibitor resulted in increased duration of network bursts (i.e. many neurons firing simultaneously), which might be explained by a shift of the excitation-inhibition balance towards excitation. The uPA/KLK8 inhibitor also resulted in an increased strength of functional connections in the networks. These observations are intriguing and give us insight into the electrophysiological characteristics of a neuronal network that has a compromised uPA/KLK8 activity. Increased burst duration and increased functional connectivity between excitatory neurons may underlie an increased seizure propensity. The results of this study have been submitted to PLOS ONE as “Van De Vijver S, Missault S, et al.: The effect on *in vitro* cortical neuronal networks electrophysiology of the acute pharmacological inhibition of urokinase type plasminogen activator and neuropsin extracellular proteases.”

Unfortunately, due to its incapacity to cross the intact blood-brain barrier (BBB), [¹¹¹In]MICA-401 could not be implemented in a longitudinal *in vivo* imaging study to investigate whether the early decrease in uPA/KLK8 could

predict the long-term outcome following *SE* and TBI. Hence, we explored other possible molecular targets that could serve as prognostic biomarkers of long-term outcome following brain injury.

2. MMP-9 following TBI

MMP-9 is a particularly attractive molecule that may serve as a prognostic and predictive biomarker for long-term outcome following TBI. MMP-9 is acutely upregulated in the brain, cerebrospinal fluid and blood of TBI patients (11-16). A more pronounced increase has been shown to correlate with more severe injury (15), lower score on the Glasgow Coma Scale (13) and poor short-term prognosis, i.e. longer length of stay and mortality in the intensive care unit (11, 14). Treatment with “MMP-9” inhibitors in experimental TBI models results in decreased BBB disruption, reduced oedema, smaller lesion volume, reduced neuronal loss, dendritic degeneration and synapse loss, attenuation of microgliosis and astrogliosis, and improved neurobehavioural outcome (including sensorimotor function and spatial learning and memory) (17-22). MMP-9 deficiency in knockout mice also results in reduced lesion size and improved motor outcome following TBI (23). Moreover, there is substantial evidence that MMP-9 is involved in epileptogenesis (24).

First of all, we evaluated two “MMP-9” PET tracers in a colorectal tumour model, i.e. Colo205 xenograft-bearing nude mice: published as “Vazquez N, Missault S, et al.: Evaluation of [¹⁸F]BR420 and [¹⁸F]BR351 as radiotracers for MMP-9 imaging in colorectal cancer. *J Labelled Comp Radiopharm.* 2017 Jan;60(1):69-79.” MMP-9 plays an important role in tumour progression: in angiogenesis, stromal remodelling and metastasis. In this study, we established that [¹⁸F]BR420 has a much higher metabolic stability than

[¹⁸F]BR351. In addition, [¹⁸F]BR351 has [¹⁸F]fluoroethanol as a prominent radiometabolite, which can mask the signal from [¹⁸F]BR351. Due to the much higher selectivity of [¹⁸F]BR420 towards MMP-9 (compared to [¹⁸F]BR351) and the much higher stability of this tracer, [¹⁸F]BR420 seems to be superior for MMP-9 imaging.

We evaluated MMP-9 activity in our TBI model using gel zymography at three different time points, i.e. 6 hours, 24 hours and 7 days post-injury. MMP-9 activity was increased at 6 and 24 hours post-injury in perilesional cortex and ipsilesional hippocampus, but not in contralateral cortex and contralesional hippocampus.

Both MMP PET radiotracers were first implemented in an *in vitro* autoradiography study of control brain sections. Both radiotracers showed a lot of aspecific binding. However, [¹⁸F]BR420 showed some specific binding in hippocampal subfield CA3.

[¹⁸F]BR420 was implemented in an *in vitro* autoradiography study of sham-operated and TBI-injured rats at 24 hours post-injury. No increased radiotracer binding could be observed in the perilesional areas. However, immunohistochemical staining of MMP-9 did reveal the presence of MMP-9 positive cells in these brain sections. Immunohistochemical staining of myeloperoxidase in consecutive sections revealed a very similar staining pattern, which suggests that the MMP-9 positive cells are neutrophils. The temporal profile of MMP-9 expression in the posttraumatic brain also matches closely with the temporal profile of neutrophil infiltration. Indeed, MMP-9 is known to be very acutely upregulated in the brain following TBI, and neutrophils are the first inflammatory cells to be massively activated and infiltrating the brain after TBI (preceding massive activation of microglia

and astrocytes). Moreover, neutrophils are unique in the fact that they are packed with TIMP-free MMP-9 (25). MMP-9 released by neutrophils is therefore very potent, since it is not co-released with its endogenous inhibitor TIMP1, as is the case in other cell types.

Due to the rather disappointing results with the MMP PET probes, we still explored other targets as possible prognostic biomarkers of long-term outcome following TBI.

In vivo imaging of extracellular matrix proteases in the brain is very challenging. Most ligands have low specificity and target different proteases of the same family. Moreover, low BBB permeability is a common issue for many of these ligands.

3. TSPO & DTI metrics as prognostic biomarkers for TBI outcome

Following TBI, an increased TSPO PET tracer ($[^{18}\text{F}]\text{PBR111}$) uptake was observed at 7 days post-injury in perilesional cortex and ipsilesional hippocampus, which significantly decreased over time. However, at 21 days post-injury, TSPO PET tracer uptake was still significantly increased in ipsilesional hippocampus. Fractional anisotropy (FA) was acutely decreased in these brain regions at 4 days post-injury and pseudo-normalised by 18 days post-injury. Mean, axial and radial diffusivity (MD, AD and RD) were acutely increased in these brain regions, which persisted or increased further by 18 days post-injury. Several of these measurements, and especially also the evolution over time in TSPO expression and DTI metrics, were predictive of long-term outcome following TBI, including disinhibition, behavioural seizure frequency at 9 months post-injury, convulsive seizure susceptibility and spatial learning deficit. This indicates that dynamic

changes in subacute brain inflammation, neurodegeneration and/or regeneration are valuable parameters for the prognosis of chronic TBI outcome. Importantly, we were able to build prognostic models for different TBI sequelae (disinhibition, seizure susceptibility, learning & memory), as opposed to currently existing prognostic models that only use overall unfavourable vs. favourable outcome as possible outcomes (26, 27). Prognostic models that use different aspects of chronic TBI outcome as outcome parameters will allow to make a more accurate prognosis of the patients.

In addition to *in vivo* PET scans, we also performed *in vitro* autoradiography with TSPO radioligands ($[^{18}\text{F}]$ PBR111 and $[^3\text{H}]$ PK11195) at 7 and 21 days post-injury. *In vitro* autoradiography showed a very similar binding profile of the TSPO radioligand as the *in vivo* PET scans. While the *in vivo* uptake of $[^{18}\text{F}]$ PBR111 may be influenced by local changes in perfusion (hyper- or hypoperfusion) and BBB disruption, the *in vitro* autoradiography results indicate that the *in vivo* radiotracer uptake is not merely reflecting altered perfusion or BBB integrity. However, some influence of these phenomena cannot be excluded.

Our results show that TSPO, and thus brain inflammation, is a valuable prognostic biomarker for long-term TBI outcome. However, a limitation of TSPO is the lack of cell specificity. While TSPO is highly expressed by activated microglia, it is also upregulated by other activated immune-competent cells, including macrophages, monocytes, astrocytes, neutrophils and lymphocytes. In order to explore which cell type(s) contribute more to the TSPO PET signal, immunohistochemistry with antibodies targeting CD11b (expressed on microglia, macrophages and

several other leukocytes) and glial fibrillary acidic protein (GFAP, expressed on astrocytes) was performed in separate cohorts at 7 and 21 days post-injury. The CD11b-immunoreactivity profile seemed to match the TSPO PET tracer profile more closely than the GFAP-immunoreactivity profile did. However, while activated microglia/macrophages probably contribute more to the TSPO signal than activated astrocytes, a contribution of astrocytes to the TSPO signal cannot be excluded, as previous studies in experimental TBI models have shown (28-31). However, a discrepancy between the CD11b-immunoreactivity profile and the TSPO PET profile was found in the thalamus of CCI-injured rats. While CD11b-immunoreactivity increased over time in the ipsilesional thalamus, the TSPO PET signal did not. An increased [¹⁸F]PBR111 uptake was observed in CCI-injured rats vs. sham-operated rats at 7 days post-injury, but not at 21 days post-injury. When comparing the ipsilesional and the contralesional thalami of CCI-injured rats, a significantly increased [¹⁸F]PBR111 uptake was observed in the ipsilesional thalamus vs. the contralesional thalamus, though it was more pronounced at 7 days ($p \leq 0.01$) than at 21 days ($p \leq 0.05$). This discrepancy might be explained by the fact that the activated microglia/macrophages in the ipsilesional thalamus at the later time-point have a different phenotype than the microglia/macrophages observed at earlier time-points. Microglia/macrophages can have different activation states, expressing different genes. Three major activation states have been described, i.e. classically activated M1 microglia/macrophages and M2 microglia/macrophages, which can be subdivided into alternative activation and acquired deactivation. Classically activated microglia are involved in tissue defence and produce a lot of pro-inflammatory cytokines. Alternatively activated microglia are involved in tissue repair and produce

anti-inflammatory cytokines. Acquired deactivated microglia exhibit immunosuppression and are associated with uptake of apoptotic cells (32). One has to keep in mind that this classification is probably a huge oversimplification and that many intermediate phenotypes exist. Some of these may be associated with high TSPO expression, while others may be not. One study of microglia in an experimental TBI model showed that activated microglia, which showed high TSPO gene expression, had increased gene expression of classical activation and acquired deactivation markers, but not of alternative activation (33). It is thus possible that TSPO is a marker of classically activated and acquired deactivated microglia, but not alternatively activated microglia, though more research is warranted. Several anti-inflammatory/immunomodulatory compounds are able to shift microglia/macrophages towards the beneficial M2 phenotype after TBI and have shown very promising results in experimental TBI models for improvement of the TBI outcome (reviewed in (34)). If TSPO is confirmed to be a marker of primarily the classically activated M1 microglia and not of the alternatively activated M2 microglia, then TSPO could potentially be used as a predictive biomarker for these treatments.

Antibodies that target microglia (CD11b, Iba1, CD68) also lack cell specificity. These antibodies also bind to macrophages, monocytes, and variably to neutrophils and lymphocytes. Hence, histological studies that have tried to determine the cell type that has the primary contribution to TSPO signal following TBI are essentially limited due to this lack of specific antibodies. Therefore, while it is commonly assumed that microglia are the major source of TSPO signal following TBI, it cannot be excluded that peripheral immune cells such as monocytes/macrophages and lymphocytes also contribute

significantly to the signal, in addition to astrocytes. Identification of the cell type or cell types that underlie the prognostic value of the TSPO PET signal for long-term TBI outcome could possibly aid in the search for more specifically targeted immunomodulatory treatments.

While TSPO is the most widely used *in vivo* imaging target for assessment of brain inflammation, clinical studies have revealed an important disadvantage of the second-generation TSPO PET tracers. A human gene polymorphism in *TSPO* (rs6971, resulting in Ala147Thr substitution in TSPO) determines the binding affinity of the PET tracers, resulting in a trimodal distribution in binding affinity amongst subjects (35, 36). There are low-affinity binders, high-affinity binders and mixed affinity binders. Knowledge of the individual binding status of the patient is therefore required to correctly interpret TSPO PET data.

Various other *in vivo* imaging techniques exist to study inflammation and can be used to study residential brain parenchymal cells that are involved in inflammation, peripheral immune cells, inflammatory mediators or metabolites that are altered during inflammation (reviewed in (37-39)). Another commonly used approach is the investigation of BBB breakdown using *in vivo* imaging, which is also involved in the inflammatory response following TBI. PET probes targeting cannabinoid receptor type 2 (CB2), which in the central nervous system is primarily expressed by microglia, can be used to study microgliosis. However, CB2 expression has also been reported in peripheral immune cells (monocytes, macrophages and lymphocytes). PET probes against monoamine oxidase B (MAO-B), which is upregulated in reactive astrocytes, may be used to study astrogliosis. Magnetic resonance spectroscopy (MRS) can be used to assess several metabolites that are highly

enriched in (activated) astrocytes, including myoinositol, glutathione, glutamine and lactate.

Different methods exist to track leukocytes. First of all, superparamagnetic iron oxide particles or perfluorocarbon emulsions can be administered intravenously, which are then taken up by peripheral immune cells with phagocytic capacity (monocytes, macrophages, neutrophils) (*in situ* labelling). However, iron nanocolloids may also possibly cross the disrupted BBB and be taken up by microglia. The iron oxide particles can be localised on T2*-weighted MR images. Perfluorocarbons can be assessed using ^{19}F MRI. A second method is to harvest leukocytes, label them with [$^{99\text{m}}\text{Tc}$]HMPAO, [^{111}In]oxinate or perfluorocarbon emulsions and to reinject them in order to monitor their *in vivo* circulation using SPECT imaging or ^{19}F MRI (*ex vivo* labelling). A third method is to conjugate ligands or antibodies directed towards leukocyte-specific receptors, adhesion molecules or enzymes to either paramagnetic contrast agents that shorten T1 and T2/T2* relaxation times (gadolinium or iron oxide particles) or radioactive PET/SPECT labels. However, there is usually a limited specificity to label specific leukocyte classes. Antibodies can also be directed towards adhesion molecules that are expressed on activated (inflammatory) endothelial cells. Activation of pro-inflammatory mononuclear phagocytes can also be assessed using MRS and increased hyperpolarised [^{13}C]pyruvate-to-lactate conversion.

Radiolabelled cytokines or cytokine inhibitors have also been employed to study inflammation. Radiolabelled inhibitors of the inducible isoform of cyclooxygenase, i.e. COX-2, which plays a major role in inflammation, are also promising tools for *in vivo* imaging of brain inflammation. Finally, BBB

dysfunction can be assessed using contrast agents such as gadolinium (MRI), ^{68}Ga (PET), ^{67}Ga (SPECT) or $^{99\text{m}}\text{Tc}$ (SPECT).

Our results also showed that DTI metrics had predictive value for the long-term prognosis of TBI. Alterations in diffusion MRI parameters can be explained by a variety of underlying pathophysiological changes, which fall into three main categories: neurodegeneration, neuroregeneration and inflammation. Hence, diffusion MRI measurements are rather unspecific and difficult to interpret. DTI metrics correlated strongly with TSPO PET SUVs in the lesion, which indicates that the observed alterations in DTI metrics in our study reflected at least partly the ongoing inflammatory processes. BBB injury leads to vasogenic oedema following TBI, which reduces FA and increases diffusivity measurements, and can likely also explain some of the observed changes in DTI metrics. Increases in diffusivity over time may be explained by delayed neuronal loss and the increase in FA over time (apparent normalisation) may be due to regeneration, maladaptive or otherwise. Given the diversity of neurobiological processes that might explain the observed alterations in diffusion MRI metrics, it is difficult to estimate which process (or all of them) underlies the prognostic value of the DTI metrics.

Magnetisation transfer MRI (based on the exchange of protons/energy between free water and macromolecules) can also be used to probe the tissue microenvironment, but is equally unspecific as diffusion MRI. On the other hand, chemical exchange saturation transfer (CEST) imaging is a MRI technique with which specific brain metabolites can be measured such as myoinositol and lactate.

Neuronal loss, dysfunction and regeneration can also be studied using other *in vivo* imaging techniques, such as [¹⁸F]FDG PET and assessment of N-acetyl-aspartate (NAA) using MRS. Neuronal loss and hypometabolism will result in a decreased [¹⁸F]FDG uptake by neurons. Regeneration of neurons might lead to increased [¹⁸F]FDG uptake. However, activated glia may also show an increased [¹⁸F]FDG uptake. Therefore, [¹⁸F]FDG PET results are also difficult to interpret when there is a combination of pronounced neuronal loss, neuronal regeneration and a strong inflammatory response. NAA is a marker of neuronal viability and is decreased upon neuronal loss or dysfunction. Neuronal regeneration may increase NAA levels. Finally, neuronal dysfunction and regeneration/plasticity can also be investigated using BOLD contrast-based functional MRI (fMRI). However, given the major changes in the vascular component of the central nervous system following TBI, fMRI changes would also be difficult to interpret and might reflect vascular changes rather than neuronal changes.

To summarise, TSPO and DTI metrics were shown to have prognostic value for long-term TBI outcome and more specifically for different chronic TBI sequelae (as opposed to a general TBI outcome score such as the Glasgow Outcome Scale, which was used as an outcome parameter for the currently existing prognostic models). However, limited specificity of the used (and most currently existing) *in vivo* imaging methods hampers the identification of the exact mechanisms (neurobiological processes and the cell types involved) that underlie their prognostic value.

4. Chronic inflammation after prenatal immune activation

We did not observe a difference in CD11b- or Iba1-immunostained microglial density and morphology between adult male MIA offspring and control offspring in the study described in chapter 5. However, we did observe an increase in CD11b-immunoreactive microglial density and altered microglial morphology in hippocampus, thalamus and corpus callosum of adult male and female MIA offspring in another study, which was published as “Van den Eynde K, Missault S, et al.: Hypolocomotive behaviour associated with increased microglia in a prenatal immune activation model with relevance to schizophrenia. *Behav Brain Res.* 2014 Jan 1;258:179-86.”. In the latter study, microglia of MIA offspring showed a thickening of the soma (i.e. cell body) and reduced arborisation (i.e. less processes), indicating a more activated state. However, these microglia did not express CD68, a marker of phagocytic cells.

Similarly, several studies have failed to observe microglial or astrocytic activation in adult MIA offspring (40-44) while others did observe gliosis (45-51). In one study, minocycline – a broad-spectrum tetracycline antibiotic that inhibits microglial activation, MMP-9, inducible nitric oxide synthase (iNOS), caspase-1 and -3 – was administered during puberty and was able to prevent the microgliosis and attenuate the behavioural deficits (51). While increased microglial activation has been reported during puberty in MIA offspring (52), others failed to observe this (41, 42). Interestingly, one group observed a strong M1-type microglial polarisation pattern during puberty in MIA offspring, which did not persist into adulthood when symptoms appeared (53). Another group observed increased microglial activation shortly following peripubertal stress in MIA offspring, which was no longer

present in adulthood (54). In this model, combination of MIA and peripubertal stress was necessary for the emergence of behavioural symptoms in adulthood. Administration of minocycline during peripubertal stress exposure prevented pubescent microgliosis and the expression of behavioural dysfunctions in adulthood (55). Several studies have investigated the sensitivity to a secondary insult in MIA offspring and reported exacerbated gliosis compared to control offspring that received the same insult (54, 56, 57). This may be due to microglial priming. Microglia may be primed following prenatal immune activation and respond in an exaggerated manner to a secondary immune stimulus.

Seemingly more consistently, several studies reported an increased expression of inflammatory cytokines or other inflammatory mediators in the brain of adult MIA offspring, both in the absence and presence of overt brain inflammation (i.e. gliosis) (40, 42, 47-49, 56, 58). Treatment with minocycline was able to revert these abnormalities and the accompanying behavioural deficits (47, 48). Treatment with paliperidone (an atypical antipsychotic) during young adulthood was also able to block the neuroinflammatory response and stimulated microglia towards the alternatively activated anti-inflammatory M2 phenotype. This also resulted in improved working memory (58). One study did not observe any changes in cytokine expression of isolated microglia from adult MIA offspring, though an increased microglial density and soma size was observed (46).

Several studies have investigated the peripheral immune system in adult MIA offspring and either reported altered blood cytokine levels (40, 45, 59) or no change in inflammatory cytokine expression (41, 42). Alterations in peripheral leukocytes have also been reported in MIA offspring (52, 60).

To summarise, most studies have observed some immunological disturbances in adult MIA offspring, often in the form of an increased expression of pro-inflammatory cytokines in the absence of overt brain inflammation (i.e. gliosis). This latent inflammation may become overt under certain conditions, e.g. following secondary insults or “second hits”, resulting in the emergence of behavioural deficits. Overt brain inflammation may be state-dependent and only be present during exacerbations and not throughout the course of the disorder. Several studies reveal an immunomodulatory effect of minocycline and antipsychotics, inhibiting brain inflammation and improving or altogether preventing behavioural deficits. This suggests an important role for inflammation in MIA-induced behavioural abnormalities.

A similar heterogeneity in data regarding microgliosis in schizophrenia patients has been described (recently reviewed in (61)). Alterations in peripheral immunological disturbances seem to be more consistent across several studies. Moreover, peripheral cytokines and oxidative stress markers can either be increased during an acute psychotic episode and normalise during remission following antipsychotic treatment (i.e. serve as state markers) or be elevated throughout the course of the disorder (i.e. be trait markers) (62, 63). Clinical trials of immunomodulatory compounds (especially minocycline and nonsteroidal anti-inflammatory drugs - NSAIDs) as add-on treatment have shown some improvement of symptoms in schizophrenic patients, pointing to a disease-modifying role of inflammation in schizophrenia (61).

5. Functional connectivity in the DMN correlates with behaviour in the MIA model

Hypersynchronicity in the default mode-like network (DMN) was observed in the offspring of dams that lost weight following MIA (Poly I:C WL offspring). An altered response to the NMDA receptor (NMDAR) antagonist MK-801, suggesting altered NMDAR function, was observed in all MIA offspring, but was much more pronounced in offspring of dams that gained weight following MIA (Poly I:C WG offspring). Hence, all MIA offspring replicated features of schizophrenia. Interestingly, the exact pathophysiology seemed to depend on the response of the mother to the immune challenge. It is possible that a more pronounced NMDAR malfunctioning in Poly I:C WG offspring interfered with the expression of increased functional connectivity within the DMN. Impaired functional connectivity in the DMN has been observed in patients with anti-NMDAR encephalitis, i.e. a disorder where antibody-mediated dysfunction of NMDARs causes severe neuropsychiatric symptoms (64). Administration of ketamine, an NMDAR antagonist, to healthy humans has been shown to reduce functional connectivity (65, 66). However, NMDAR dysfunction may also be involved in increased functional connectivity. Administration of ketamine has also been shown to increase functional connectivity in healthy humans. In these studies, hyperconnectivity correlated significantly with the psychotic, dissociative and negative symptoms elicited by ketamine. (67, 68). Moreover, ketamine administration has been shown to interfere with DMN deactivation during a working memory task in healthy subjects, the degree of which predicted task performance and transient ketamine-evoked symptoms characteristic of schizophrenia. (69). Similarly, schizophrenia

patients have been shown to display reduced task-related suppression of DMN activity during working memory tasks (70). More research is needed to elucidate the link between NMDAR function on the one hand and functional connectivity and anticorrelation of default-mode vs. task-positive networks on the other hand.

Both Poly I:C WL and Poly I:C WG offspring showed some subtle behavioural deficits. Functional connectivity in the DMN was able to explain the variability in the behavioural data in MIA offspring. The responsiveness to the NMDAR antagonist MK-801 could not explain the behavioural outcome. This could possibly be due to a lack of power, since fewer rats were included in this analysis than in the functional connectivity analysis due to head movement problems in some rats following administration of this drug in the scanner.

Similarly, several studies in schizophrenia patients have shown a correlation between increased functional connectivity in the DMN and symptom severity (reviewed in (71)).

As has been shown in this thesis, the behavioural outcome in this model is variable and inconsistent across studies, even studies performed by one research group (e.g. also (72-74)). To use behavioural outcome as the only indicator of drug efficiency in preclinical drug research of novel treatments for schizophrenia might be suboptimal. Identification of pathophysiological disturbances that underlie the symptoms and that are both present in schizophrenia and relevant animal models of schizophrenia and that can be used as a read-out of responsiveness to novel antipsychotic drugs would be extremely useful. Hypersynchronicity in the DMN is a very promising candidate. A few studies have shown that DMN functional

connectivity/activation alters with antipsychotic treatment with a concomitant amelioration of symptoms in schizophrenia patients (75-77).

Studies have shown that DMN connectivity has a strong genetic basis. Heritability of DMN connectivity has been estimated to be 0.54 (78). DMN hyperconnectivity has been suggested to be an endophenotype of schizophrenia. Endophenotypes are quantitative biological traits that can be reliably measured, are heritable and associated with a specific (neuropsychiatric) disorder. As such, endophenotypes lie on the causal pathway between genes (genotype) and disease (phenotype). Indeed, altered DMN connectivity/activation has not only been shown in schizophrenia patients, but also in unaffected first-degree relatives (70), suggesting its usefulness as an endophenotype of schizophrenia. However, true endophenotypes are state-independent. The few studies that showed that DMN connectivity/activity altered with antipsychotic treatment disprove the idea of altered DMN connectivity/activity as a true endophenotype.

6. Changes in extracellular proteases in schizophrenia

A polymorphism in the *MMP-9* gene, which modulates synaptic MMP-9 protein levels, has been linked to the severity of symptoms in schizophrenia patients (79). KLK8 acts on NRG1 and may also be involved in schizophrenia (10). *NRG1* is one of the most important susceptibility genes for schizophrenia. Radiotracers for MMP-9 and KLK8 may therefore be useful to investigate the precise role of these extracellular matrix components in schizophrenia in the future.

7. Future perspectives

Further development of radiotracers for uPA/KLK8 is needed in order to get BBB permeable tracers with higher specificity towards respectively uPA and KLK8. Further development of radiotracers for MMP-9 is also warranted to get more selective probes for MMP-9 that have low non-specific binding and that are metabolically stable. These could then be implemented in a preclinical longitudinal *in vivo* imaging study to investigate whether KLK8, uPA and MMP-9 could be useful prognostic biomarkers of long-term outcome following epileptogenic insults and brain injury in general.

Preclinical studies should confirm the prognostic value of TSPO and DTI metrics for the long-term outcome following TBI, as suggested by our work. Clinical neuroimaging studies can then be performed in order to confirm the prognostic value of these measurements in TBI patients.

Finally, future studies in the MIA model need to establish whether DMN hyperconnectivity is a more consistent and reproducible pathophysiological feature of the model than the behavioural deficits. Future studies should also investigate whether functional connectivity in the DMN in the MIA model is responsive to antipsychotic treatment and may be used as a predictive biomarker for therapeutic responsiveness. Finally, future research should explore whether DMN hyperconnectivity might be present early in life following MIA and may have value as a prognostic biomarker for MIA-induced neuropathology and ultimately for schizophrenia. It will also be interesting to investigate whether MIA offspring exhibit a similar reduced task-related suppression of DMN activity as observed in schizophrenia patients.

8. References

1. Amhaoul H, Hamaide J, Bertoglio D, Reichel SN, Verhaeghe J, Geerts E, et al. (2015): Brain inflammation in a chronic epilepsy model: Evolving pattern of the translocator protein during epileptogenesis. *Neurobiol Dis.* 82:526-539.
2. Cho E, Lee KJ, Seo JW, Byun CJ, Chung SJ, Suh DC, et al. (2012): Neuroprotection by urokinase plasminogen activator in the hippocampus. *Neurobiology of disease.* 46:215-224.
3. He XP, Shiosaka S, Yoshida S (2001): Expression of neuropsin in oligodendrocytes after injury to the CNS. *Neuroscience research.* 39:455-462.
4. Tomizawa K, He X, Yamanaka H, Shiosaka S, Yoshida S (1999): Injury induces neuropsin mRNA in the central nervous system. *Brain research.* 824:308-311.
5. Bolkvadze T, Rantala J, Puhakka N, Andrade P, Pitkanen A (2015): Epileptogenesis after traumatic brain injury in Plau-deficient mice. *Epilepsy Behav.* 51:19-27.
6. Lahtinen L, Nnode-Ekane XE, Barinka F, Akamine Y, Esmaeili MH, Rantala J, et al. (2010): Urokinase-type plasminogen activator regulates neurodegeneration and neurogenesis but not vascular changes in the mouse hippocampus after status epilepticus. *Neurobiol Dis.* 37:692-703.
7. Morales D, McIntosh T, Conte V, Fujimoto S, Graham D, Grady MS, et al. (2006): Impaired fibrinolysis and traumatic brain injury in mice. *J Neurotrauma.* 23:976-984.
8. Rantala J, Kempainen S, Nnode-Ekane XE, Lahtinen L, Bolkvadze T, Gurevicius K, et al. (2015): Urokinase-type plasminogen activator deficiency has little effect on seizure susceptibility and acquired epilepsy phenotype but reduces spontaneous exploration in mice. *Epilepsy Behav.* 42:117-128.
9. Davies B, Kearns IR, Ure J, Davies CH, Lathe R (2001): Loss of hippocampal serine protease BSP1/neuropsin predisposes to global seizure activity. *J Neurosci.* 21:6993-7000.
10. Kawata M, Morikawa S, Shiosaka S, Tamura H (2017): Ablation of neuropsin-neuregulin 1 signaling imbalances ErbB4 inhibitory networks and disrupts hippocampal gamma oscillation. *Transl Psychiatry.* 7:e1052.
11. Copin JC, Rebetez MM, Turck N, Robin X, Sanchez JC, Schaller K, et al. (2012): Matrix metalloproteinase 9 and cellular fibronectin plasma concentrations are predictors of the composite endpoint of length of stay and death in the intensive care unit after severe traumatic brain injury. *Scand J Trauma Resusc Emerg Med.* 20:83.

12. Grossetete M, Phelps J, Arko L, Yonas H, Rosenberg GA (2009): Elevation of matrix metalloproteinases 3 and 9 in cerebrospinal fluid and blood in patients with severe traumatic brain injury. *Neurosurgery*. 65:702-708.
13. Liu CL, Chen CC, Lee HC, Cho DY (2014): Matrix metalloproteinase-9 in the ventricular cerebrospinal fluid correlated with the prognosis of traumatic brain injury. *Turk Neurosurg*. 24:363-368.
14. Simon D, Evaldt J, Nabinger DD, Fontana MF, Klein MG, do Amaral Gomes J, et al. (2017): Plasma matrix metalloproteinase-9 levels predict intensive care unit mortality early after severe traumatic brain injury. *Brain Inj*. 31:390-395.
15. Zheng K, Li C, Shan X, Liu H, Fan W, Wang Z, et al. (2013): Matrix metalloproteinases and their tissue inhibitors in serum and cerebrospinal fluid of patients with moderate and severe traumatic brain injury. *Neurol India*. 61:606-609.
16. Guilfoyle MR, Carpenter KL, Helmy A, Pickard JD, Menon DK, Hutchinson PJ (2015): Matrix Metalloproteinase Expression in Contusional Traumatic Brain Injury: A Paired Microdialysis Study. *J Neurotrauma*. 32:1553-1559.
17. Ding JY, Kreipke CW, Schafer P, Schafer S, Speirs SL, Rafols JA (2009): Synapse loss regulated by matrix metalloproteinases in traumatic brain injury is associated with hypoxia inducible factor-1alpha expression. *Brain Res*. 1268:125-134.
18. Hadass O, Tomlinson BN, Gooyit M, Chen S, Purdy JJ, Walker JM, et al. (2013): Selective inhibition of matrix metalloproteinase-9 attenuates secondary damage resulting from severe traumatic brain injury. *PLoS One*. 8:e76904.
19. Higashida T, Kreipke CW, Rafols JA, Peng C, Schafer S, Schafer P, et al. (2011): The role of hypoxia-inducible factor-1alpha, aquaporin-4, and matrix metalloproteinase-9 in blood-brain barrier disruption and brain edema after traumatic brain injury. *J Neurosurg*. 114:92-101.
20. Jia F, Yin YH, Gao GY, Wang Y, Cen L, Jiang JY (2014): MMP-9 inhibitor SB-3CT attenuates behavioral impairments and hippocampal loss after traumatic brain injury in rat. *J Neurotrauma*. 31:1225-1234.
21. Lee M, Chen Z, Tomlinson BN, Gooyit M, Heseck D, Juarez MR, et al. (2015): Water-Soluble MMP-9 Inhibitor Reduces Lesion Volume after Severe Traumatic Brain Injury. *ACS Chem Neurosci*. 6:1658-1664.
22. Shigemori Y, Katayama Y, Mori T, Maeda T, Kawamata T (2006): Matrix metalloproteinase-9 is associated with blood-brain barrier opening

and brain edema formation after cortical contusion in rats. *Acta Neurochir Suppl.* 96:130-133.

23. Wang X, Jung J, Asahi M, Chwang W, Russo L, Moskowitz MA, et al. (2000): Effects of matrix metalloproteinase-9 gene knock-out on morphological and motor outcomes after traumatic brain injury. *J Neurosci.* 20:7037-7042.

24. Wilczynski GM, Konopacki FA, Wilczek E, Lasiecka Z, Gorlewicz A, Michaluk P, et al. (2008): Important role of matrix metalloproteinase 9 in epileptogenesis. *J Cell Biol.* 180:1021-1035.

25. Ardi VC, Kupriyanova TA, Deryugina EI, Quigley JP (2007): Human neutrophils uniquely release TIMP-free MMP-9 to provide a potent catalytic stimulator of angiogenesis. *Proc Natl Acad Sci U S A.* 104:20262-20267.

26. Collaborators MCT, Perel P, Arango M, Clayton T, Edwards P, Komolafe E, et al. (2008): Predicting outcome after traumatic brain injury: practical prognostic models based on large cohort of international patients. *BMJ.* 336:425-429.

27. Steyerberg EW, Mushkudiani N, Perel P, Butcher I, Lu J, McHugh GS, et al. (2008): Predicting outcome after traumatic brain injury: development and international validation of prognostic scores based on admission characteristics. *PLoS Med.* 5:e165; discussion e165.

28. Raghavendra Rao VL, Dogan A, Bowen KK, Dempsey RJ (2000): Traumatic brain injury leads to increased expression of peripheral-type benzodiazepine receptors, neuronal death, and activation of astrocytes and microglia in rat thalamus. *Exp Neurol.* 161:102-114.

29. Venneti S, Wagner AK, Wang G, Slagel SL, Chen X, Lopresti BJ, et al. (2007): The high affinity peripheral benzodiazepine receptor ligand DAA1106 binds specifically to microglia in a rat model of traumatic brain injury: implications for PET imaging. *Exp Neurol.* 207:118-127.

30. Wang Y, Yue X, Kiesewetter DO, Niu G, Teng G, Chen X (2014): PET imaging of neuroinflammation in a rat traumatic brain injury model with radiolabeled TSPO ligand DPA-714. *Eur J Nucl Med Mol Imaging.* 41:1440-1449.

31. Yu I, Inaji M, Maeda J, Okauchi T, Nariai T, Ohno K, et al. (2010): Glial cell-mediated deterioration and repair of the nervous system after traumatic brain injury in a rat model as assessed by positron emission tomography. *J Neurotrauma.* 27:1463-1475.

32. Colton CA (2009): Heterogeneity of microglial activation in the innate immune response in the brain. *J Neuroimmune Pharmacol.* 4:399-418.

33. Cao T, Thomas TC, Ziebell JM, Pauly JR, Lifshitz J (2012): Morphological and genetic activation of microglia after diffuse traumatic brain injury in the rat. *Neuroscience*. 225:65-75.
34. Donat CK, Scott G, Gentleman SM, Sastre M (2017): Microglial Activation in Traumatic Brain Injury. *Front Aging Neurosci*. 9:208.
35. Mizrahi R, Rusjan PM, Kennedy J, Pollock B, Mulsant B, Suridjan I, et al. (2012): Translocator protein (18 kDa) polymorphism (rs6971) explains in-vivo brain binding affinity of the PET radioligand [(18)F]-FEPPA. *J Cereb Blood Flow Metab*. 32:968-972.
36. Owen DR, Yeo AJ, Gunn RN, Song K, Wadsworth G, Lewis A, et al. (2012): An 18-kDa translocator protein (TSPO) polymorphism explains differences in binding affinity of the PET radioligand PBR28. *J Cereb Blood Flow Metab*. 32:1-5.
37. Ory D, Celen S, Verbruggen A, Bormans G (2014): PET radioligands for in vivo visualization of neuroinflammation. *Curr Pharm Des*. 20:5897-5913.
38. Quarantelli M (2015): MRI/MRS in neuroinflammation: methodology and applications. *Clin Transl Imaging*. 3:475-489.
39. Wu C, Li F, Niu G, Chen X (2013): PET imaging of inflammation biomarkers. *Theranostics*. 3:448-466.
40. Garay PA, Hsiao EY, Patterson PH, McAllister AK (2013): Maternal immune activation causes age- and region-specific changes in brain cytokines in offspring throughout development. *Brain Behav Immun*. 31:54-68.
41. Giovanoli S, Notter T, Richetto J, Labouesse MA, Vuillermot S, Riva MA, et al. (2015): Late prenatal immune activation causes hippocampal deficits in the absence of persistent inflammation across aging. *J Neuroinflammation*. 12:221.
42. Giovanoli S, Weber-Stadlbauer U, Schedlowski M, Meyer U, Engler H (2016): Prenatal immune activation causes hippocampal synaptic deficits in the absence of overt microglia anomalies. *Brain Behav Immun*. 55:25-38.
43. Nyffeler M, Meyer U, Yee BK, Feldon J, Knuesel I (2006): Maternal immune activation during pregnancy increases limbic GABAA receptor immunoreactivity in the adult offspring: implications for schizophrenia. *Neuroscience*. 143:51-62.
44. Piontkewitz Y, Bernstein HG, Dobrowolny H, Bogerts B, Weiner I, Keilhoff G (2012): Effects of risperidone treatment in adolescence on hippocampal neurogenesis, parvalbumin expression, and vascularization following prenatal immune activation in rats. *Brain Behav Immun*. 26:353-363.

45. Borrell J, Vela JM, Arevalo-Martin A, Molina-Holgado E, Guaza C (2002): Prenatal immune challenge disrupts sensorimotor gating in adult rats. Implications for the etiopathogenesis of schizophrenia. *Neuropsychopharmacology*. 26:204-215.
46. Hadar R, Dong L, Del-Valle-Anton L, Guneykaya D, Voget M, Edemann-Callesen H, et al. (2017): Deep brain stimulation during early adolescence prevents microglial alterations in a model of maternal immune activation. *Brain Behav Immun*. 63:71-80.
47. Mattei D, Djodari-Irani A, Hadar R, Pelz A, de Cossio LF, Goetz T, et al. (2014): Minocycline rescues decrease in neurogenesis, increase in microglia cytokines and deficits in sensorimotor gating in an animal model of schizophrenia. *Brain Behav Immun*. 38:175-184.
48. Mattei D, Ivanov A, Ferrai C, Jordan P, Guneykaya D, Buonfiglioli A, et al. (2017): Maternal immune activation results in complex microglial transcriptome signature in the adult offspring that is reversed by minocycline treatment. *Transl Psychiatry*. 7:e1120.
49. O'Loughlin E, Pakan JMP, Yilmazer-Hanke D, McDermott KW (2017): Acute in utero exposure to lipopolysaccharide induces inflammation in the pre- and postnatal brain and alters the glial cytoarchitecture in the developing amygdala. *J Neuroinflammation*. 14:212.
50. Ratnayake U, Quinn TA, Castillo-Melendez M, Dickinson H, Walker DW (2012): Behaviour and hippocampus-specific changes in spiny mouse neonates after treatment of the mother with the viral-mimetic Poly I:C at mid-pregnancy. *Brain Behav Immun*. 26:1288-1299.
51. Zhu F, Zheng Y, Liu Y, Zhang X, Zhao J (2014): Minocycline alleviates behavioral deficits and inhibits microglial activation in the offspring of pregnant mice after administration of polyriboinosinic-polyribocytidilic acid. *Psychiatry Res*. 219:680-686.
52. Juckel G, Manitz MP, Brune M, Friebe A, Heneka MT, Wolf RJ (2011): Microglial activation in a neuroinflammatory animal model of schizophrenia--a pilot study. *Schizophr Res*. 131:96-100.
53. Esslinger M, Wachholz S, Manitz MP, Plumper J, Sommer R, Juckel G, et al. (2016): Schizophrenia associated sensory gating deficits develop after adolescent microglia activation. *Brain Behav Immun*. 58:99-106.
54. Giovanoli S, Engler H, Engler A, Richetto J, Voget M, Willi R, et al. (2013): Stress in puberty unmasks latent neuropathological consequences of prenatal immune activation in mice. *Science*. 339:1095-1099.
55. Giovanoli S, Engler H, Engler A, Richetto J, Feldon J, Riva MA, et al. (2016): Preventive effects of minocycline in a neurodevelopmental two-hit model with relevance to schizophrenia. *Transl Psychiatry*. 6:e772.

56. Krstic D, Madhusudan A, Doehner J, Vogel P, Notter T, Imhof C, et al. (2012): Systemic immune challenges trigger and drive Alzheimer-like neuropathology in mice. *J Neuroinflammation*. 9:151.
57. Zager A, Peron JP, Menecier G, Rodrigues SC, Aloia TP, Palermo-Neto J (2015): Maternal immune activation in late gestation increases neuroinflammation and aggravates experimental autoimmune encephalomyelitis in the offspring. *Brain Behav Immun*. 43:159-171.
58. MacDowell KS, Munarriz-Cueva E, Caso JR, Madrigal JL, Zabala A, Meana JJ, et al. (2017): Paliperidone reverts Toll-like receptor 3 signaling pathway activation and cognitive deficits in a maternal immune activation mouse model of schizophrenia. *Neuropharmacology*. 116:196-207.
59. Romero E, Guaza C, Castellano B, Borrell J (2010): Ontogeny of sensorimotor gating and immune impairment induced by prenatal immune challenge in rats: implications for the etiopathology of schizophrenia. *Mol Psychiatry*. 15:372-383.
60. Ponzio NM, Servatius R, Beck K, Marzouk A, Kreider T (2007): Cytokine levels during pregnancy influence immunological profiles and neurobehavioral patterns of the offspring. *Ann N Y Acad Sci*. 1107:118-128.
61. De Picker LJ, Morrens M, Chance SA, Boche D (2017): Microglia and Brain Plasticity in Acute Psychosis and Schizophrenia Illness Course: A Meta-Review. *Front Psychiatry*. 8:238.
62. Flatow J, Buckley P, Miller BJ (2013): Meta-analysis of oxidative stress in schizophrenia. *Biol Psychiatry*. 74:400-409.
63. Miller BJ, Buckley P, Seabolt W, Mellor A, Kirkpatrick B (2011): Meta-analysis of cytokine alterations in schizophrenia: clinical status and antipsychotic effects. *Biol Psychiatry*. 70:663-671.
64. Peer M, Pruss H, Ben-Dayana I, Paul F, Arzy S, Finke C (2017): Functional connectivity of large-scale brain networks in patients with anti-NMDA receptor encephalitis: an observational study. *Lancet Psychiatry*. 4:768-774.
65. Kraguljac NV, Frolich MA, Tran S, White DM, Nichols N, Barton-McArdle A, et al. (2017): Ketamine modulates hippocampal neurochemistry and functional connectivity: a combined magnetic resonance spectroscopy and resting-state fMRI study in healthy volunteers. *Mol Psychiatry*. 22:562-569.
66. Scheidegger M, Walter M, Lehmann M, Metzger C, Grimm S, Boeker H, et al. (2012): Ketamine decreases resting state functional network connectivity in healthy subjects: implications for antidepressant drug action. *PLoS One*. 7:e44799.

67. Dandash O, Harrison BJ, Adapa R, Gaillard R, Giorlando F, Wood SJ, et al. (2015): Selective augmentation of striatal functional connectivity following NMDA receptor antagonism: implications for psychosis. *Neuropsychopharmacology*. 40:622-631.
68. Driesen NR, McCarthy G, Bhagwagar Z, Bloch M, Calhoun V, D'Souza DC, et al. (2013): Relationship of resting brain hyperconnectivity and schizophrenia-like symptoms produced by the NMDA receptor antagonist ketamine in humans. *Mol Psychiatry*. 18:1199-1204.
69. Anticevic A, Gancsos M, Murray JD, Repovs G, Driesen NR, Ennis DJ, et al. (2012): NMDA receptor function in large-scale anticorrelated neural systems with implications for cognition and schizophrenia. *Proc Natl Acad Sci U S A*. 109:16720-16725.
70. Whitfield-Gabrieli S, Thermenos HW, Milanovic S, Tsuang MT, Faraone SV, McCarley RW, et al. (2009): Hyperactivity and hyperconnectivity of the default network in schizophrenia and in first-degree relatives of persons with schizophrenia. *Proc Natl Acad Sci U S A*. 106:1279-1284.
71. Hu ML, Zong XF, Mann JJ, Zheng JJ, Liao YH, Li ZC, et al. (2017): A Review of the Functional and Anatomical Default Mode Network in Schizophrenia. *Neurosci Bull*. 33:73-84.
72. Bronson SL, Ahlbrand R, Horn PS, Kern JR, Richtand NM (2011): Individual differences in maternal response to immune challenge predict offspring behavior: contribution of environmental factors. *Behav Brain Res*. 220:55-64.
73. Vorhees CV, Graham DL, Braun AA, Schaefer TL, Skelton MR, Richtand NM, et al. (2012): Prenatal immune challenge in rats: altered responses to dopaminergic and glutamatergic agents, prepulse inhibition of acoustic startle, and reduced route-based learning as a function of maternal body weight gain after prenatal exposure to poly IC. *Synapse*. 66:725-737.
74. Vorhees CV, Graham DL, Braun AA, Schaefer TL, Skelton MR, Richtand NM, et al. (2015): Prenatal immune challenge in rats: effects of polyinosinic-polycytidylic acid on spatial learning, prepulse inhibition, conditioned fear, and responses to MK-801 and amphetamine. *Neurotoxicol Teratol*. 47:54-65.
75. Sambataro F, Blasi G, Fazio L, Caforio G, Taurisano P, Romano R, et al. (2010): Treatment with olanzapine is associated with modulation of the default mode network in patients with Schizophrenia. *Neuropsychopharmacology*. 35:904-912.
76. Surguladze SA, Chu EM, Marshall N, Evans A, Anilkumar AP, Timehin C, et al. (2011): Emotion processing in schizophrenia: fMRI study of patients

treated with risperidone long-acting injections or conventional depot medication. *J Psychopharmacol.* 25:722-733.

77. Tregellas JR, Tanabe J, Rojas DC, Shatti S, Olincy A, Johnson L, et al. (2011): Effects of an alpha 7-nicotinic agonist on default network activity in schizophrenia. *Biol Psychiatry.* 69:7-11.

78. Xu J, Yin X, Ge H, Han Y, Pang Z, Liu B, et al. (2017): Heritability of the Effective Connectivity in the Resting-State Default Mode Network. *Cereb Cortex.* 27:5626-5634.

79. Lepeta K, Purzycka KJ, Pachulska-Wieczorek K, Mitjans M, Begemann M, Vafadari B, et al. (2017): A normal genetic variation modulates synaptic MMP-9 protein levels and the severity of schizophrenia symptoms. *EMBO Mol Med.* 9:1100-1116.

Acknowledgments/Dankwoord

These past five years have been a unique, thrilling and very rewarding experience. I have learned a great deal during this time and have worked with some wonderful people. Coming to the end of this chapter in my life, and the end of this thesis, I would like to express my heartfelt gratitude to those who stood by me during this journey.

Allereerst wil ik mijn promotoren bedanken. Stefanie, bedankt om me de kans te geven om eerst een masterthesis en vervolgens een doctoraatsthesis in jouw lab te mogen doen. Het was het perfecte lab om mij te ontplooiën als wetenschapper en ik ben enorm blij dat ik deel mocht zijn van jouw team. Het gaf me ook de kans om deel uit te maken van een internationaal consortium met onze Finse en Poolse partners en interessante internationale ervaringen op te doen. Ik wil je ook bedanken voor de vrijheid die je mij gegeven hebt tijdens mijn doctoraat om aan verschillende projecten te kunnen werken en zo een maximum aan ervaring op te doen. Ik denk met veel plezier terug aan de jaarlijkse BBQ bij jouw thuis en de vele etentjes en terrasjes die we deden als er een nieuw persoon in ons team kwam of iemand vertrok, of als we Poolse/Finse gasten op bezoek hadden. Merci voor alles!

Marleen, hoewel je pas later betrokken geraakte bij mijn doctoraat, heb ik heel veel aan jou gehad in de afgelopen twee jaar. Ik kon eender wanneer binnenlopen in jouw bureau en je maakte altijd meteen tijd vrij om feedback of advies te geven of simpelweg om een babbeltje te doen. ☺ Bedankt

hiervoor! Ik wil jou en Annemie en Georgios ook bedanken dat ik deel mocht uitmaken van het Bio-Imaging Lab. Ik ben enorm blij dat ik hier een thuis heb mogen vinden nadat het Experimenteel Lab TNW ermee stopte.

Steven, ik wil jou graag bedanken voor de uitstekende samenwerking met het MICA en dat ik ook altijd op jouw team kon rekenen.

I thank the jury for reading my PhD thesis and providing some useful feedback: Prof. Dr. Mathias Hoehn, Dr. Nadja Van Camp, Prof. Dr. Patrick Cras and Prof. Dr. Sebastiaan Engelborghs.

I would like to thank all my colleagues from the Experimental Laboratory of Translational Neuroscience and the Bio-Imaging Lab for the great times and their support. Bedankt Krystyna om altijd klaar te staan om mij te helpen bij dierproeven als het nodig was. Ik heb genoten van onze babbels, cinema's en ijsjes en hoop dat er nog veel mogen volgen. ☺ Merci Annemie voor je hulp bij autoradiografie en het snijden en kleuren van grote hoeveelheden hersenen als ik er zelf geen tijd voor had. Je bent een geweldige, veelzijdige en heel efficiënte laborante en ik vond het tof om met je samen te werken. Thank you Naiara, your enthusiasm and willingness to work very hard were contagious and inspiring. I will remember the late nights that we had to wait for radiotracers to decay so we could capture good images on imaging plates and films. Thank you also for taking me into the radiopharmacy clean room, so I could experience the radiotracer productions at first hand. Thank you Marion, your joyful presence was truly uplifting. I enjoyed working with you and regretted that it was only for such a short time. I remember with pleasure the coffees, beers and cocktails that we had together. ☺ Dank je

Karliën, deel van het werk beschreven in deze thesis hebben we samen uitgevoerd tijdens mijn masterthesis en is dus ook mede te danken aan jou. Ik vond het heel leuk om met jou samen te werken en vond het spijtig dat je ons zo snel verliet. Een enorme dank u aan alle masterstudenten die een steentje hebben bijgedragen aan het onderzoek beschreven in deze thesis: Lore, Soumaya, Glenn, Stephanie, Nora, Jeroen, Anagha en Barbara. Ik vond het heel plezant om met jullie samen te werken en sommigen onder jullie zijn goede vrienden geworden. Mogen er nog veel dinertjes volgen! 😊 Merci Cynthia, Ines en Disha voor jullie hulp bij MRI acquisities en analyses. Ik heb veel geleerd van jullie en vond het tof om samen te werken. Thank you Halima, Joery, Krystyna, Annemie, Karliën, Daniele, Marion, Lore, Rukun and Cynthia, for being the best office mates one could wish for! I enjoyed our conversations, coffee/tea/lunch breaks and outside-of-the-office activities enormously, as well as with many other people including Karin, Kristof, Monica, Sara, Inès, Serena, Aneta and many others. Dank je Halima voor de vele babbels. Ik vond het heel leuk dat we samen naar Tübingen geweest zijn voor EMIM 2015, ook al was je geen 100% toen ;) Bedankt Joery voor de leuke momenten tijdens onze masterthesis en ook daarna nog. Door jou ontdekte ik de beste cocktailbar van België, merci :p Dank u Lore, Rukun en Cynthia voor de toffe tijden in het BIL en daarbuiten en een ongelooflijk leuk EMIM 2018 in San Sebastian. 😊

Thank you Georgios and Annemie for giving me the opportunity to start a postdoc at the Bio-Imaging Lab and to be able to be part of this great lab for a little while longer.

Merci Philippe en Caroline om de PET experimenten zo vlot te laten verlopen. Bedankt Steven en Jeroen voor jullie hulp bij PET analyses. Thank you Ann-Marie for your assistance with biodistributions if we needed an extra pair of hands. En dank je Christel voor je hulp bij de Colo205 experimenten.

Bedankt Leonie voor de goede samenwerking met de radiofarmacie en je feedback bij verschillende PET experimenten. Thank you David for making [¹¹¹In]MICA-401 and for your help during the MMP-9 PET experiments.

I would also like to express my gratitude to all other people that I collaborated with during my PhD, especially Debby and Femke for their help with the Morris water maze test, Michaël and Winnok for their help with immunohistochemistry analyses, Kenny and Samir for doing the multiplex cytokine assay, Sebastiaan and Michele for doing the multi electrode array experiments, Peter for allowing me to make use of his lab equipment and the fluorescence microscope for the *in situ* zymography experiments, Roos and Lesley for their help with the gel zymography experiment, and Jurgen and Pieter for the uPA inhibitors and other chemical compounds.

Thank you Tamuna, you taught me several valuable things during my stay in Finland and it was a great pleasure working with you. You will remain a dear friend. I would also like to thank Asla for allowing me to stay in her lab for a few months and for her valuable feedback on the uPA paper.

I have met several interesting people during stays abroad and it was always a joyful experience to meet those people again at conferences to exchange

PhD troubles or to have a nice drink or a party. 😊 I thank especially Jenni, Melissa, Maria Elisa (Melisa), Shweta and Jennifer for a good time.

Ik bedank ook mijn vrienden voor hun steun tijdens de afgelopen jaren: Linde, Dana, Seline, Amélie, Jolien, Rida, An en Lina. Ik kan altijd terecht bij jullie en ben hier enorm dankbaar voor.

Tot slot wil ik ook graag mijn familie bedanken voor hun onvoorwaardelijke steun en om er altijd te zijn voor mij, in het bijzonder mijn ouders en mijn broer en zussen.

Stephan, april 2018

Curriculum vitae

Personal details

- Surname Missault
- Name Stephan
- Date of birth 03/09/1990
- Nationality Belgian
- Place of birth Antwerp (Merksem)
- Telephone number +32 3 265 8818
+32 494 729509
- E-mail address Stephan.Missault@uantwerpen.be
stephanmissault@hotmail.com

Education

- 2002-2008 Vita et Pax-College
Ancient Greek-Mathematics-Sciences
- 2008-2011 University of Antwerp
Bachelor of Science in Biomedical Sciences
- 2011-2013 University of Antwerp
Master of Science in Biomedical Sciences:
Neuroscience
- 2012-2013 University of Antwerp
FELASA C

Work experience

- Nov-Dec 2013 Internship at the Nencki Institute of Experimental Biology, Warsaw, Poland
 - Laboratory of Molecular and Systemic Neuromorphology (Head: Grzegorz Wilczynski)
 - Laboratory of Neurobiology (Head: Leszek Kaczmarek)

- Jan-Apr 2014 Internship at the A.I. Virtanen Institute for Molecular Sciences, Kuopio, Finland
 - Epilepsy Research Laboratory (Head: Asla Pitkänen)

- Oct 2013-now PhD at the University of Antwerp (FWO aspirant): Doctorate in Medical Sciences
 - Experimental Laboratory of Translational Neurosciences, Dept of Translational Neurosciences, Faculty of Medicine and Health Sciences (Head: Stefanie Dedeurwaerdere)
 - Bio-Imaging Lab, Dept of Biomedical Sciences, Faculty of Pharmaceutical, Biomedical and Veterinary Sciences (Head: Annemie Van der Linden)

Teaching experience

Supervision of Master theses:

- Master dissertation of Nora Barriche (Master in Biomedical Sciences - Neuroscience) 2016-2017: "Spatiotemporal Evaluation of Inflammation and Evaluation of Chronic Behavioural Deficits in a Controlled Cortical Impact Injury Rat Model"
- Master dissertation of Barbara Favier & Anagha Thakur (Master in Medical Sciences) 2013-2017: "Evaluation of extracellular matrix proteases in traumatic brain injury"
- Master dissertation of Soumaya Ahmadoun (Master in Biomedical Sciences - Neuroscience) 2015-2016: "Evaluation of the NMDAR function in a maternal immune activation model, a neurodevelopmental model with relevance for schizophrenia"
- Master dissertation of Glenn De Pauw (Master in Biomedical Sciences - Neuroscience) 2015-2016: "Traumatic Brain Injury: Assessment of Acute and Long-term Behavioural Deficits with a Focus on Seizure Susceptibility in the Controlled Cortical Impact Rat Model"
- Master dissertation of Lore Peeters (Master in Biomedical Sciences - Neuroscience) 2014-2015: "Characterisation of a rat model of traumatic brain injury: the controlled cortical impact model in terms of behaviour, extracellular matrix changes, neurodegeneration, microglia activation and blood-brain barrier alterations"
- Master dissertation of Jeroen Kerstens (Master in Medical Sciences) 2012-2016: "De rol van herseninflammatie in een ratmodel met relevantie voor schizofrenie (The role of brain inflammation in a rat model with relevance for schizophrenia)"

Grants and Awards

- Grant for participation in a conference abroad from FWO for the Joint Annual Meeting ISMRM-ESMRMB 2018
- Best oral presentation award at the 10th annual meeting of ISMRM Benelux Chapter (2018)
- Trainee (Educational) Stipend from the ISMRM for the Joint Annual Meeting ISMRM-ESMRMB 2018
- Travel grant for the 4th Annual Conference of COST Action BM1001 (2014)
- Travel grant for a long stay abroad from FWO (2013-2014)
- Grant for a Short Term Scientific Mission from COST Action BM1001 (2013)
- Fellowship of the Research Foundation – Flanders (FWO) (+ renewal) (2013/2015)
- Award for most excellent student (Bachelor of Biomedical Sciences, 2011)

Publications

- **Missault S**, Anckaerts C, Ahmadoun S, Blockx I, Barbier M, Bielen K, Shah D, Kumar-Singh S, De Vos W, Van der Linden A, Dedeurwaerdere S, Verhoye M: Hypersynchronicity in the default mode-like network is correlated with behavioural outcome in a neurodevelopmental model with relevance for schizophrenia. *Submitted to Brain, Behavior, and Immunity.*
- **Missault S**, Anckaerts C, Blockx I, Deleye S, Van Dam D, Barriche N, De Pauw G, Aertgeerts S, Valkenburg F, De Deyn PP, Verhaeghe J, wyffels L,

- Van der Linden A, Staelens S, Verhoye M, Dedeurwaerdere S: Neuroimaging of subacute brain inflammation and microstructural changes predicts long-term functional outcome after experimental traumatic brain injury. *Submitted to Journal of Neurotrauma*.
- Van De Vijver S, **Missault S**, Van Soom J, Van Der Veken P, Augustyns K, Joossens J, Dedeurwaerdere S, Giugliano M: The effect on in vitro cortical neuronal networks electrophysiology of the acute pharmacological inhibition of urokinase plasminogen activator and neuropsin extracellular proteases. *Submitted to PeerJ*.
 - Peeters L, Hinz R, Detrez J, **Missault S**, De Vos W, Verhoye M, Van der Linden A, Keliris GA: Functional MRI reveals resting state network alterations upon DREADD-induced silencing of the right dorsomedial prefrontal cortex in mice. *In preparation*
 - **Missault S**, Peeters L, Amhaoul H, Thomae D, Van Eetveldt A, Favier B, Thakur A, Van Soom J, Pitkänen A, Augustyns K, Joossens J, Staelens S, Dedeurwaerdere S: Decreased levels of active uPA and KLK8 assessed by [¹¹¹In]MICA-401 binding correlate with the seizure burden in an animal model of temporal lobe epilepsy. *Epilepsia*. 2017 Sep;58(9):1615-1625.
 - van der Werf IM, Van Dam D, **Missault S**, Yalcin B, De Deyn PP, Vandeweyer G, Kooy RF: Behavioural characterization of AnkyrinG deficient mice, a model for ANK3 related disorders. *Behav Brain Res*. 2017 Jun 15;328:218-226.
 - Vazquez N, **Missault S**, Vangestel C, Deleye S, Thomae D, Van der Veken P, Augustyns K, Staelens S, Dedeurwaerdere S, Wyffels L: Evaluation of [¹⁸F]BR420 and [¹⁸F]BR351 as radiotracers for MMP-9 imaging in colorectal cancer. *J Labelled Comp Radiopharm*. 2017 Jan;60(1):69-79.

- Amhaoul H, Ali I, Mola M, Van Eetveldt A, Szewczyk K, **Missault S**, Bielen K, Kumar-Singh S, Rech J, Lord B, Ceusters M, Bhattacharya A, Dedeurwaerdere S: P2X7 receptor antagonism reduces the severity of spontaneous seizures in a chronic model of temporal lobe epilepsy. *Neuropharmacology*. 2016 Jun;105:175-85.
- **Missault S**, Van den Eynde K, Vanden Berghe W, Fransen E, Weeren A, Timmermans JP, Kumar-Singh S, Dedeurwaerdere S: The risk for behavioural deficits is determined by the maternal immune response to prenatal immune challenge in a neurodevelopmental model. *Brain Behav Immun*. 2014 Nov;42:138-46.
- Van den Eynde K, **Missault S**, Fransen E, Raeymaekers L, Willems R, Drinkenburg W, Timmermans JP, Kumar-Singh S, Dedeurwaerdere S: Hypolocomotive behaviour associated with increased microglia in a prenatal immune activation model with relevance to schizophrenia. *Behav Brain Res*. 2014 Jan 1;258:179-86.

Abstracts

- **Missault S**, Anckaerts C, Ahmadoun S, Blockx I, Bielen K, Shah D, Kumar-Singh S, Van der Linden A, Dedeurwaerdere S, Verhoye M: Hypersynchronicity in the default mode-like network and altered NMDA receptor function in a maternal immune activation model. Joint Annual Meeting ISMRM-ESMRMB 2018. Paris, France. 16-21.06.2018.
- Peeters L, Hinz R, **Missault S**, Verhoye M, Van der Linden A, Keliris GA: Functional MRI reveals resting state network alterations upon DREADD-induced silencing of the right dorsomedial prefrontal cortex in mice. Joint Annual Meeting ISMRM-ESMRMB 2018. Paris, France. 16-21.06.2018.

- **Missault S**, Anckaerts C, Blockx I, Deleye S, Van Dam D, Barriche N, De Pauw G, Aertgeerts S, Valkenburg F, De Deyn PP, Verhaeghe J, wyffels L, Van der Linden A, Staelens S, Verhoye M, Dedeurwaerdere S: Neuroimaging of subacute brain inflammation and microstructural changes predicts long-term functional outcome after experimental traumatic brain injury. 13th European Molecular Imaging Meeting 2018. San Sebastian, Spain. 20-23.03.2018. **(Talk)**
- **Missault S**, Anckaerts C, Ahmadoun S, Blockx I, Bielen K, Shah D, Kumar-Singh S, Van der Linden A, Dedeurwaerdere S, Verhoye M: Increased functional connectivity in the default mode-like network is related to behavioural outcome in a neurodevelopmental model with relevance for schizophrenia. 13th European Molecular Imaging Meeting 2018. San Sebastian, Spain. 20-23.03.2018. **(Talk)**
- Peeters L, Hinz R, **Missault S**, Verhoye M, Van der Linden A, Keliris GA: DREADD-MRI reveals functional connectivity changes upon inactivation of the right dorsomedial prefrontal cortex in mice. 13th European Molecular Imaging Meeting 2018. San Sebastian, Spain. 20-23.03.2018.
- **Missault S**, Anckaerts C, Ahmadoun S, Blockx I, Bielen K, Shah D, Kumar-Singh S, Van der Linden A, Dedeurwaerdere S, Verhoye M: Hypersynchronicity in the default mode-like network and altered NMDA receptor function in a maternal immune activation model. 10th annual meeting of the International Society for Magnetic Resonance in Medicine Benelux Chapter. Antwerp, Belgium. 26.01.2018. **(Talk)**
- Peeters L, Hinz R, **Missault S**, Verhoye M, Van der Linden A, Keliris GA: Functional MRI reveals resting state network alterations upon DREADD-induced silencing of the right dorsomedial prefrontal cortex in mice. 10th

annual meeting of the International Society for Magnetic Resonance in Medicine Benelux Chapter. Antwerp, Belgium. 26.01.2018.

- **Missault S**, Anckaerts C, Ahmadoun S, Blockx I, Shah D, Van der Linden A, Verhoye M, Dedeurwaerdere S: Hypersynchronicity in the default mode-like network and altered NMDAR function in a maternal immune activation model. 18th Bio-NMR Workshop & ISMRM Nordic Chapter meeting 2018. Kuopio, Finland. 08.09.06.2017. **(Talk)**
- **Missault S**, Anckaerts C, Ahmadoun S, Blockx I, Shah D, Van der Linden A, Verhoye M, Dedeurwaerdere S: A decreased response to the NMDAR antagonist MK-801 is shown by pharmacological MRI in a maternal immune activation model. 12th National Congress of the Belgian Society for Neuroscience 2017. Ghent, Belgium. 22.05.2017.
- **Missault S**, Ahmadoun S, Blockx I, Shah D, Van der Linden A, Verhoye M, Dedeurwaerdere S: A decreased response to the NMDAR antagonist MK-801 is shown by pharmacological MRI in a maternal immune activation model. 3rd Belgian Molecular Imaging Congress 2017. Brussels, Belgium. 16.05.2017.
- **Missault S**, Ahmadoun S, Blockx I, Shah D, Van der Linden A, Verhoye M, Dedeurwaerdere S: A decreased response to the NMDAR antagonist MK-801 is shown by pharmacological MRI in a maternal immune activation model. 12th European Molecular Imaging Meeting 2017. Cologne, Germany. 5-7.04.2017.
- **Missault S**, Amhaoul H, Thomae D, Van Eetveldt A, Van Der Veken P, Joossens J, Staelens S, Dedeurwaerdere S: Evaluation of a novel extracellular matrix radiotracer: expression of proteases uPA and KLK8 is correlated with seizure outcome in an animal model of acquired

- epilepsy. 29th European Association of Nuclear Medicine Congress 2016. Barcelona, Spain. 15-19.10.2016.
- **Missault S**, Chomet M, Vázquez N, Thomae D, Deleye S, Blockx I, Van Der Veken P, Van Der Linden A, wyffels L, Staelens S, Dedeurwaerdere S: Evaluation of [18F]BR420 and [18F]BR351 as potential PET ligands for in vivo imaging of MMP-9 activity in an animal model of traumatic brain injury. 29th European Association of Nuclear Medicine Congress 2016. Barcelona, Spain. 15-19.10.2016.
 - Van De Vijver S, **Missault S**, Van Soom J, Van Der Veken P, Joossens J, Dedeurwaerdere S and Giugliano M: Electrophysiological Effect of uPA Inhibition on Synaptic Plasticity Through Modulation of the Extracellular Matrix. Front. Neurosci. Conference Abstract: MEA Meeting 2016 | 10th International Meeting on Substrate-Integrated Electrode Arrays. Reutlingen, Germany. 28.06-01.07.2016.
 - Vázquez N, **Missault S**, Vangestel C, Thomae D, Van Der Veken P, Staelens S, Dedeurwaerdere S, wyffels L: Evaluation of [18F]BR420 and [18F]BR351 as potential PET radiotracers for MMP-9 imaging in a colorectal cancer tumor model. 28th Annual Congress of the European Association of Nuclear Medicine 2015. Hamburg, Germany. 10-13.10.2015.
 - **Missault S**, Thomae D, Deleye S, Blockx I, Vázquez N, Van Eetveldt A, Amhaoul H, Van Der Veken P, Joossens J, Van Der Linden A, Staelens S, Dedeurwaerdere S: Assessment of faulty brain repair in animal models of acquired epilepsy: evaluation of a novel extracellular matrix radiotracer. World Molecular Imaging Congress 2015. Honolulu, Hawaii. 2-5.09.2015.

- **Missault S**, Vázquez N, Thomae D, Deleye S, Blockx I, Van Der Veken P, Van Der Linden A, wyffels L, Staelens S, Dedeurwaerdere S: Evaluation of [18F]BR420 and [18F]BR351 as potential PET ligands for in vivo imaging of MMP-9 activity in an animal model of traumatic brain injury. World Molecular Imaging Congress 2015. Honolulu, Hawaii. 2-5.09.2015.
- Vázquez N, **Missault S**, Vangestel C, Thomae D, Van Der Veken P, Staelens S, Dedeurwaerdere S, wyffels L: Evaluation of [18F]BR420 as a potential radiotracer for MMP-9 imaging in a colorectal cancer tumor model. 17th Symposium of Belgian Society of Nuclear Medicine 2015. Maastricht, the Netherlands. 09-10.05.2015.
- **Missault S**, Anckaerts C, Van Eetveldt A, Amhaoul H, Thomae D, Van Der Veken P, Joossens J, Dedeurwaerdere S: Evaluation of a novel radiotracer for the assessment of serine proteases in the brain: 111In-MICA-401. 10th European Molecular Imaging Meeting 2015. Tübingen, Germany. 18-20.03.2015.
- **Missault S**, Anckaerts C, van Eetveldt A, Amhaoul H, Thomae D, van der Veken P, Joossens J, Staelens S, Dedeurwaerdere S: Evaluation of a novel radiotracer for the assessment of serine proteases in the brain: 111In-MICA-401. SWO Midwinter Meeting 2015. Amsterdam, the Netherlands. 11.03.2015.
- **Missault S**, Bolkvadze T, Dedeurwaerdere S, Pitkänen A: Evaluation of spontaneous epileptiform activity, seizure susceptibility and matrix metalloproteinase activity in rat after controlled cortical impact injury. 4th Annual Conference of COST Action "Brain Extracellular Matrix in Health and Disease". Antalya, Turkey. 29.09-03.10.2014.
- Vázquez N, **Missault S**, Vangestel C, Waldron AM, Van Der Veken P, Staelens S, Dedeurwaerdere S, wyffels L: Evaluation of [18F]BR420 as a

potential MMP-9 tracer for brain injury by in vitro autoradiography and in vivo PET study in tumor model. 9th European Molecular Imaging Meeting 2014. Antwerp, Belgium. 04-06.06.2014.

